FIXED BED COUNTER CURRENT GASIFICATION OF MESQUITE AND JUNIPER BIOMASS USING AIR-STEAM AS OXIDIZER

A Dissertation

by

WEI CHEN

Submitted to the Office of Graduate Studies of
Texas A&M University
in partial fulfillment of the requirements for the degree of

DOCTOR OF PHILOSOPHY

Approved by:

Co-Chairs of Committee,	Kalyan Annamalai
	Jim Ansley
Committee Members,	Eric Petersen
	Devesh Ranjan
Head of Department,	Jerald Caton

December 2012

Major Subject: Mechanical Engineering

ABSTRACT

Thermal gasification of biomass is being considered as one of the most promising technologies for converting biomass into gaseous fuel. Here we present results of gasification, using an adiabatic bed gasifier with air, steam as gasification medium, of mesquite and juniper. From Thermo-gravimetric analyses the pre-exponential factor (B) and activation energy of fuels for pyrolysis were obtained using single reaction models (SRM) and parallel reaction model (PRM). The single reaction model including convention Arrhenius (SRM-CA) and maximum volatile release rate model (SRM-MVR). The parallel reaction model fits the experimental data very well, followed by MVR. The CA model the least accurate model. The activation energies obtained from PRM are around161,000 kJ/kmol and 158,000 kJ/kmol for juniper and mesquite fuels, respectively. And, the activation energies obtained from MVR are around100,000 kJ/kmol and 85,000 kJ/kmol for juniper and mesquite fuels, respectively.

The effects of equivalence ratio (ER), particle size, and moisture content on the temperature profile, gas composition, tar yield, and higher heating value (HHV) were investigated. For air gasification, when moisture increased from 6% to 12% and ER decreased from 4.2 to 2.7, the mole composition of the dry product gas for mesquite varied as follow: 18-30% CO, 2-5% H_2, 1-1.5% CH_4, 0.4-0.6% C_2H_6, 52-64% N_2, and 10-12% CO_2.

The tar yield shows peak value (150 g/Nm^3) with change in moisture content between 6-24%. The tar collected from the gasification process included light tar and

heavy tar. The main composition of the light tar was moisture. The chemical properties of heavy tar were determined.

For air-steam gasification, H_2 rich mixture gas was produced. The HHV of the mesquite gas increased first when S: F ratio increased from 0.15 to 0.3 and when the S: F ratio increased to 0.45, HHV of the gas decreased.

Mesquite was blended with the Wyoming Powder River Basin (PRB) coal with ratio of 90:10 and 80:20 in order to increase the T_{peak} and HHV. It was found that the T_{peak} increased with the increase of PRB coal weight percentage (0% to 20%).

DEDICATION

I want to thank to my parents and my older brother for their support and providing me with the opportunity, means, and desire to pursue all of my dreams.

ACKNOWLEDGEMENTS

I would like to express my gratitude to Dr. Kalyan Annamalai and Dr. Jim Ansley for the support and guidance which they have given to me during my graduate studies at Texas A&M University. Also, I would like to thank Dr. Eric Petersen, Dr. Devesh Ranjan for taking the time to serve on my committee, and for the advice they have given me during this undertaking.

Thanks to all of the graduate students who have worked with me in Coal and Biomass Energy Laboratory, in particular, Siva Thanapal, Aubrey Spear, Dustin E. Eseltine, and Benjamin Lawrence. It was precious time and fun to discuss and chat with them, and it gave me so much energy.

I wish to acknowledge the financial support from Texas AgriLife Research State Bioenergy Initiative Funding and U.S. Department of Energy-NREL, Golden, Colorado.

NOMENCLATURE

Symbol	Definition and units
a	Stoichiometric moles of oxygen
B	pre-exponential factor
b	Stociometric moles of CO_2
C	Celluloses (C)
C_i	Oxidizer concentration (kmol/m^3)
c	Stochiometric moles of H_2O
CEA	Chemical equilibrium application model
$CAFO_s$	Concentrated feeding operations
CA	Convectional arrhenius
D	Inner diameter of gasifier (m)
DAF	Dray ash free
DTA	Temperature difference between sample and reference
EES	Engineering equation solver code
ECE	Energy conversion efficiency
EIA	Energy information administration
ER	Equivalence ratio
e	Actual air coefficient (mol)
f	Actual moles steam supplied as reactant
FC	Fixed carbon

HC	Hemicelluloses
$h_{k,p}$	Enthalpy of the products
$h_{k,R}$	Enthalpy of the reactants
HHV	High heating value of gases
HHV_{Gases}	High heating value of gases (kj/m3)
HHV_i	High heating value of products (kj/m3)
HRSG	Heat recovery steam generation
i	Actual moles of CH_4
IEO	International energy outlook
IGCC	Integrated gasification combined cycle
K_1	Kinetics constant of pyrolysis reaction (kg/m^3 s)
K_5	Kinetics constant of the reaction of CO with O_2
K_7	Kinetics constant of shift reaction
K_E	Equilibrium constant of shift reaction
K_j	Constant kinetics of heterogeneous reactions (m/s), j=2, 3, 4, 6, and 8
K_m	Diffusion constant (m/s)
l	Actual moles of H_2
m_A	Mass of air (kg)
M	Moisture
MS	Mass spectrometer
MVR	Maximum volatile release

N	Nitrogen
S: A	Steam to air ratio
SATP	Standard ambient temperature (25°C) and pressure (100 kPa)
S: F	Steam to fuel ratio (mole basis)
SCFH	Standard feet cubic per hour
STDEV	Standard deviation
T_p	Adiabatic temperature
T_{peak}	Peak temperature
Ts	Surface temperature of the particle
Tx,t	Temperature along gasifier axis (K)
$T\infty$	Ambient temperature (K)
U	Global heat transfer coefficient of the gasifier (kW/ m2. K)
W_j	Rate of reaction (kmol/m^3 s)
W_5	Reaction rate of $CO+O_2$ reaction
W_7	Reaction rate of shift reaction
X_i	Moles fraction of each fuel product
Y_i	Mass fraction of oxidizer
ΔH_R	Enthalpy of reaction
$\eta_{Gas,E}$	Energy conversion efficiency
ρ	Air density (kg/m3)
λ	Latent heat of the water (kj/Kg)
ε	Bed porosity or void fraction

$\rho_{biomass}$	Biomass density (kg/m^3)
Subscripts	Definition
Fuel	fuel
FC	Fixed carbon
gas	gas
gas max	gas maximun
h	H atoms
i	Species and char oxidizer (O_2, CO_2, H_2O, and H_2)
j	Reaction number (2, 3, 4, 6, and 8)
n	N atoms
l	Liquid
$O_{2,in}$	Oxygen moles entering
PRB	Powder river basin
PRM	Parallel reaction model
VM	Volatile matter

TABLE OF CONTENT

Page

LIST OF FIGURES

Page

LIST OF TABLES

Page

1 INTRODUCTION

The total global energy consumption is around 515 quadrillion Btu in 2010 (Figure 1). The demand of the energy is expected to increase by 43% from 2010 to 2035 according to U.S. Energy Information Administration (EIA). This projection is based on the assumption that there is no global economics recession and world economics will continue to grow. The most rapid growth in energy demand occurs in the developing countries such as China and India. International energy outlook (IEO) projects similar consumption of energy from all full sources over the 2010- 2035 period (Figure 2). From Figure 2, it is observed that the demand for all the fuel sources continue to growth and fossil fuels are expected to supply majority of energy worldwide. Although liquid fuels remain the largest energy source from 2010 to 2035, the share percentage of the renewables energy seems to increase from 8% to 14% in 2035. The continued high liquid fuel price would lead many of the energy users to switch away liquid fuel and more renewable energy sources are expected to replace the fossil fuels. Further, the pollutions such as NO_x, $SO_{x,}$ and greenhouse gas (CO_2) are released to the atmosphere by combustion of the fossil fuel. The total CO_2 emission is expected to increase from 30 to 42 billion tons over 2010-2030 periods (Figure 3). The elevated CO_2 levels contribute to additional absorption and emission of thermal infrared in the atmosphere, which results in net warming. According to the latest assessment report from the Intergovernmental Panel on Climate Change: "most of the observed increase in globally averaged temperatures since the mid-20th century is very likely due to the observed increase in anthropogenic greenhouse gas concentrations"[1].

Figure 1. World marketed energy consumption 1990-2035(Quadrillion Btu), adopted from [2]

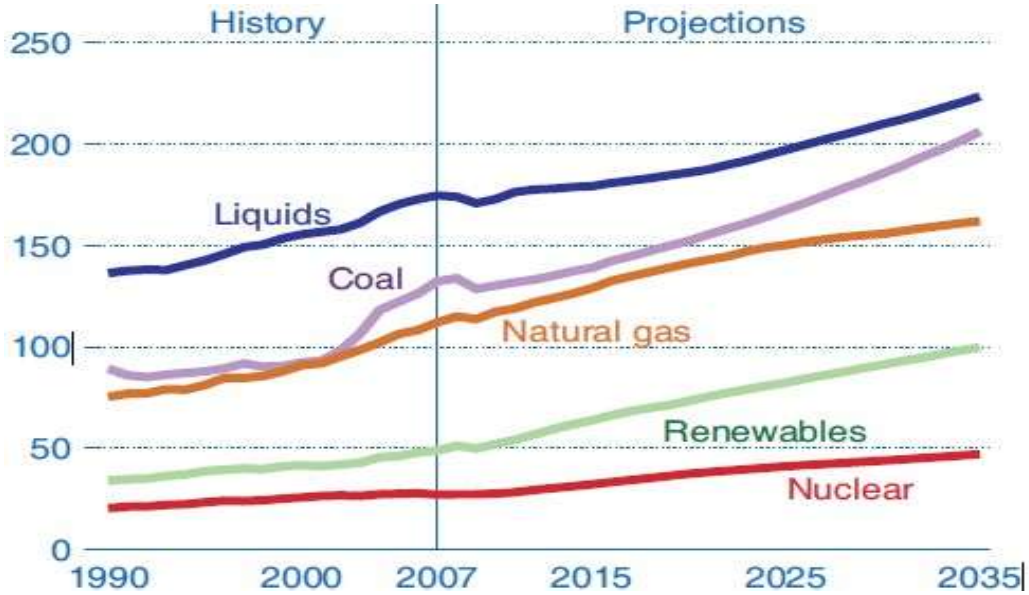

Figure 2. Global projection on annual energy consumption (Quadrillion Btu), by fuel type, adopted from [2]

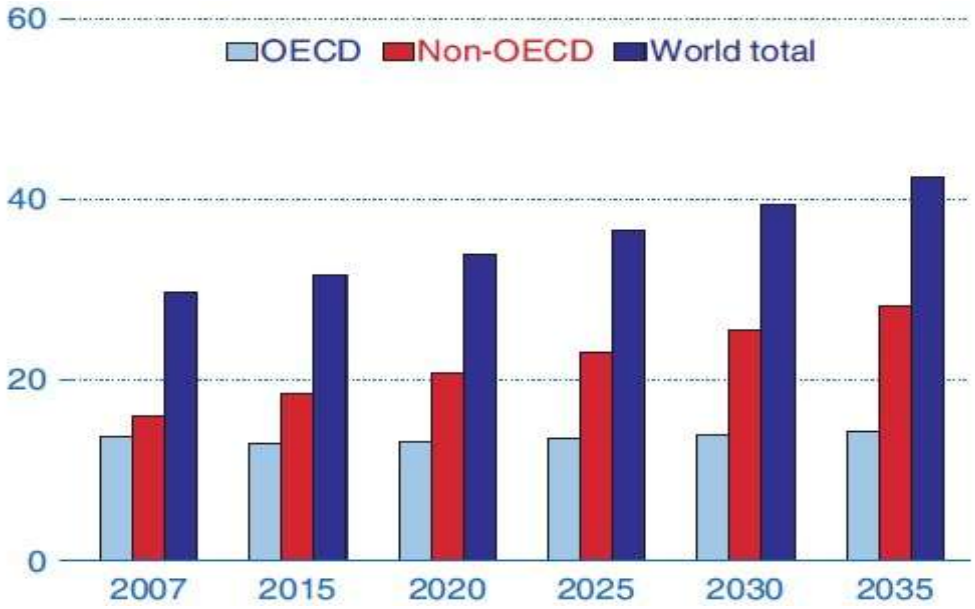

Figure 3. World energy-related carbon dioxide emissions 2007-2035, adapted from[2]

In order to reduce the emission of NOx, SOx, and CO_2 and mitigate the dependence on the fossil fuel, the exploration of renewable energy and increase its share percentage in the total energy consumption would be essentially in the next 25 years. Renewable energy comes from natural resources that includes biomass, hydropower, geothermal, wind, and solar. According to EIA, about 8% of the energy used in the United States was supplied by renewable energy in 2010 (Figure 4). Among the renewable energy sources, biomass share more than 50% of the total renewable energy consumption in Unite States. Biomass includes a wide range of material such as agriculture and forest waste, animal waste, landfill gas, and biogas, ethanol, and biodiesel. Since biomass absorbs carbon dioxide when it grows, and releases carbon back into the atmosphere during combustion or gasification process, it is a carbon neutral fuel.

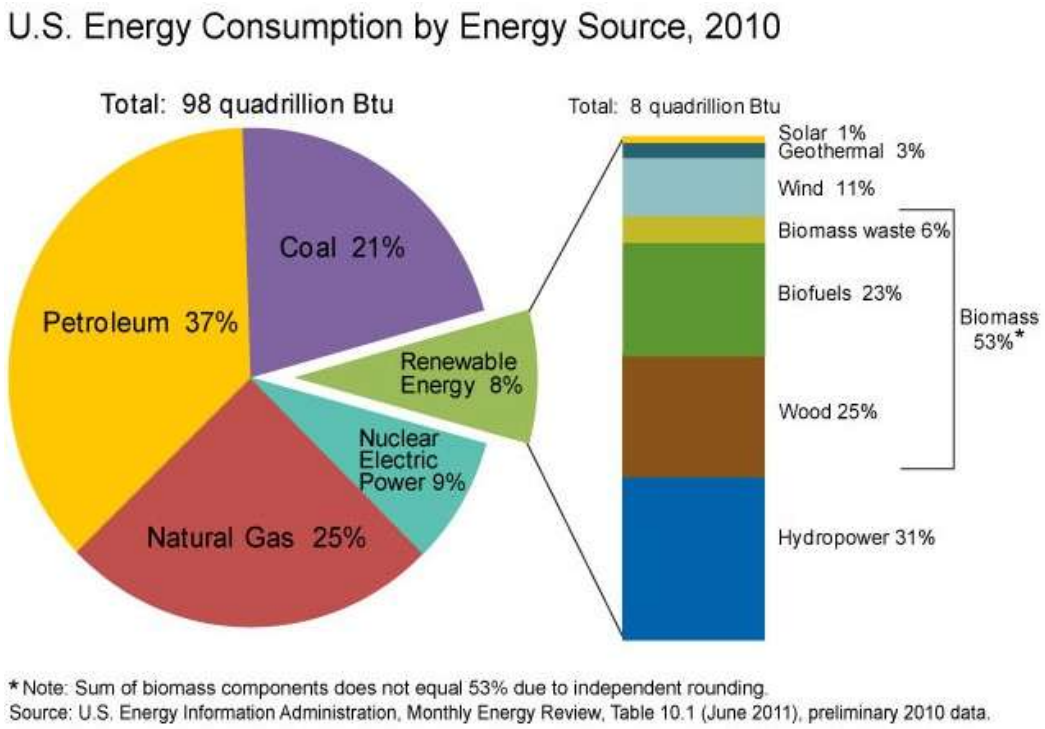

Figure 4.U.S. Energy consumption by energy source, 2010. Adapted from [3]

Fuel constituents rather than C, H, and O are undesired elements since they are related to pollutant and deposit formation, corrosion, and ash. The SOx and NOx emissions from biomass combustion are mainly caused by the nitrogen in the fuel which contribute to the formation of acid rain and photochemical smog[4, 5].

Gasification is a thermal-chemical process where a solid fuel was converted into gaseous species through a series of chemical reactions and physical transformation. Air, steam, and pure oxygen are three mainly gasifying media or blasts, although other agents like CO_2 or H_2 are also being studied. The main product gas from a combustion process is CO_2 and H_2O, whose amounts depend directly on the fuel composition. Gasification process end product gas includes more complex mixture; CO, H_2, CO_2, CH_4, H_2O, and

C_2H_6 are known as the synthesis gas. Because air contains high percentage of Nitrogen, the heating value of the gasification gas is very low. The oxygen-blow gasification produce a syngas with medium heating value and steam blow gasification lead to the production of a syngas with an acceptable HHV value 10-16 MJ/Nm^3[6].

The gasification gas after cleaning, purification , and drying can be sent to gas turbines to generate electricity and heat or used as feedstock for synthesis, using catalyzed techniques like the Ficher-Tropsch process or methanol synthesis[7]. The liquid, mainly tar, can be used as fuel or in chemical industries. The emerging biomass gasification energy technologies are expected to play an important role in the future development of energy systems.

Figure 5 shows a schematic flow diagram of an integrated Gasification Combined Cycle (IGCC) plan. Coal, heavy petroleum residues, or biomass is gasified in the gasifier using air or steam media to generate syngas under high temperature and pressure. The syngas was first cooled to lower temperature and the slag and water in the syngas was separated and disposed. The clean syngas was sent into the combustion chamber to produce electrical power.

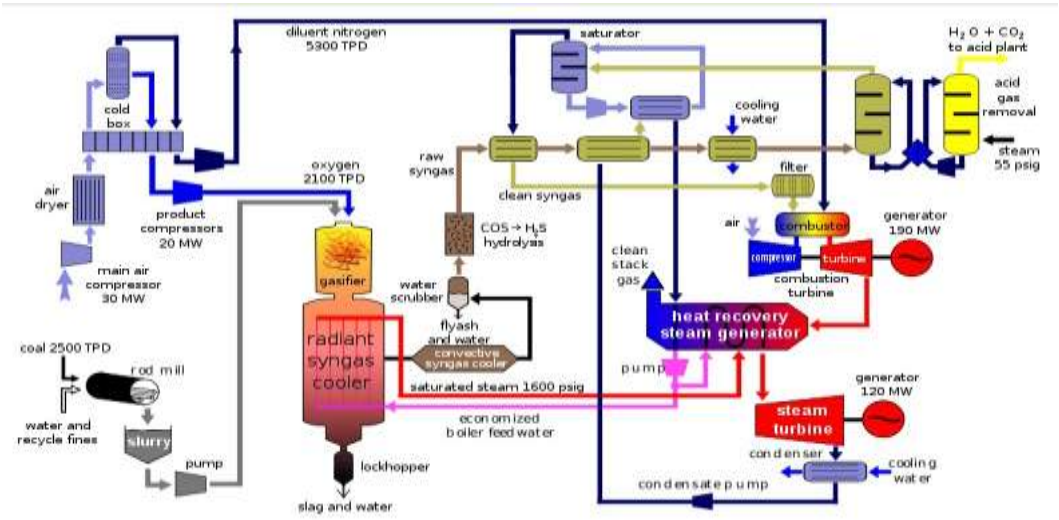

Figure 5. A schematic of an integration gasification combined cycle Power plan. Adapted from[8]

The utilization of wastes as a renewable energy source in a thermal-chemical process to generate electricity or heat has been wildly used. The U.S. independent biomass energy industry today provides for the disposal of approximately 22 million tons/yr of solid biomass waste[9]. Brian et al [10] reported that approximately 60% of biomass energy consumption occurs in the forest products industry in U.S. The forest products industry produces its own sources of biomass such as bark, sawdust, wood scraps/shavings, and waste water treatment sludge.

Due to limitations of land area for growing biomass for large bio-fuel conversion facilities in the upper Midwest and the high cost of feedstock transportation in regions that have lower biomass density, it would be beneficial to develop a small scale, less expensive, and localized conversion facilities that require less feedstock and have lower feedstock transportation costs. Woody species (brush) growing on semi-arid non-

cultivated lands (rangelands), such as mesquite *(Prosopis glandulosa)* and juniper *(Juniperus spp.),* may have potential as bioenergy feedstock. These species occur on over 20 million ha in Texas alone and can achieve standing biomass of 50 metric tons ha-1[11] . They are perceived as noxious plants that are detrimental to rangeland ecosystems and their removal and use as a bioenergy feedstock would result in improvements in ecosystem quality as well as services from these lands such as increased income from livestock grazing[12]. These species may be ideal candidates to produce syngas and bio-oil in small scale gasification units that can be located near the fuel source to reduce feedstock transport costs.

1.1 Scope of the Proposed Work

In the present study, a10 kW batch-type, counter-current, fixed-bed gasification facility consists of a reactor, steam generator, pre-heat system, gas sampling unit, control panel, and data acquisition system. The gasifier contains a fuel-feeding system, ash removal, temperature monitor, and a real-time gas composition monitor via mass spectrometry. This gasification facility was modified by installing a gas condensing system to collect the liquid yield from the produce gas.

This counter current adiabatic fixed gasification facility was employed to investigate the effect of oxidizing source, enriched air or air-steam on the temperature profile and properties of gasification product gas and bio-oils. Because moisture content play an important role in auto-gasification process, mesquite and juniper woody fuel

with different moisture will be evaluated to determine optimum moisture content for gasification. Woody fuels at different particle size will also be studied to investigate the gasification performance.

Pyrolysis studies using TGA will be performed to study wood fuel decomposition under inert atmosphere. The TGA will be used to determine required temperatures and rates of decomposition of cellulose, hemi-cellulose and lignin. The temperature for the maximum volatile releasing rate will also be determined. A single and a parallel reaction model were applied to predict and study the pyrolysis kinetics of different size mesquite and juniper fuels. The predictions obtained from these models were compared to the results of actual experiments.

In order to produce H_2 rich gasification gas, air-steam gasification will be carried out to investigate the effect of the steam: fuel (S: F) ratio on the temperature profile, gas concentration, and gas HHV.

Co-gasification of mesquite and PRB coal will be performed. Mesquite fuel will be mixed with different weight% PRB coal. The gas gasification temperature, gas concentration, and HHV will also be studied and the results will be compared to those obtained from air gasification.

2 LITERATURE REVIEW

In this section, the gasification background would be introduced and a number of earlier studies on the biomass gasification are presented.

2.1 Types of Gasifier

The main types of gasification reactors can be classified into three main groups according to the flow condition [8]**.**

1. Entrained flow gasifiers
2. Fluidied bed gasifiers including bubbling (BFB) and circulating (CFB) beds
3. Fixed bed gasifiers including counter-current (updraft), Co-current (downdraft), and cross-current moving beds.

Some of the fixed bed gasifier configurations are presented in Figure 6. It can be obtained that the name of the gasifiers was defined according to the movement of fuel and air in the gasifier. In this research, an adiabatic fixed bed counter current facility is used for woody biomass gasification study.

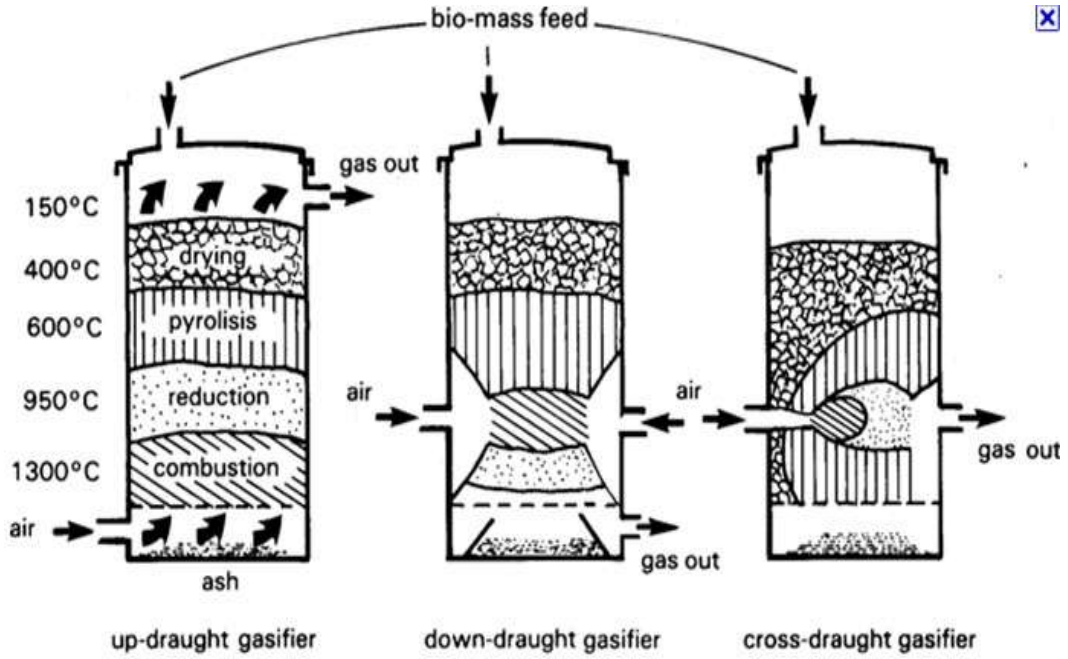

Figure 6. Types of fixed gasifiers. Adapted from[13]

The major advantages of the counter current gasifier are its simplicity, high charcoal burn-out and high gasification efficiency. The hot gas generated in the combustion and reduction zone would move up through the pyrolysis and drying zone to heat up the fuel and lower the produce gas temperature.

Figure 7 shows a schematic of an updraft fixed bed gasifier. This figure shows the different reaction zones, temperature profiles, and product gas for the biomass gasification. For this gasifier, the fuel was fed at the top while the air or steam was injected into the gasifier at the bottom. Because gases from pyrolysis zone do not pass through the high temperature zone such as combustion and reduction zone, the major drawback of this gasifier is the high amounts of tar in the produce gas which need to be moved before sending to internal engine or gas turbine.

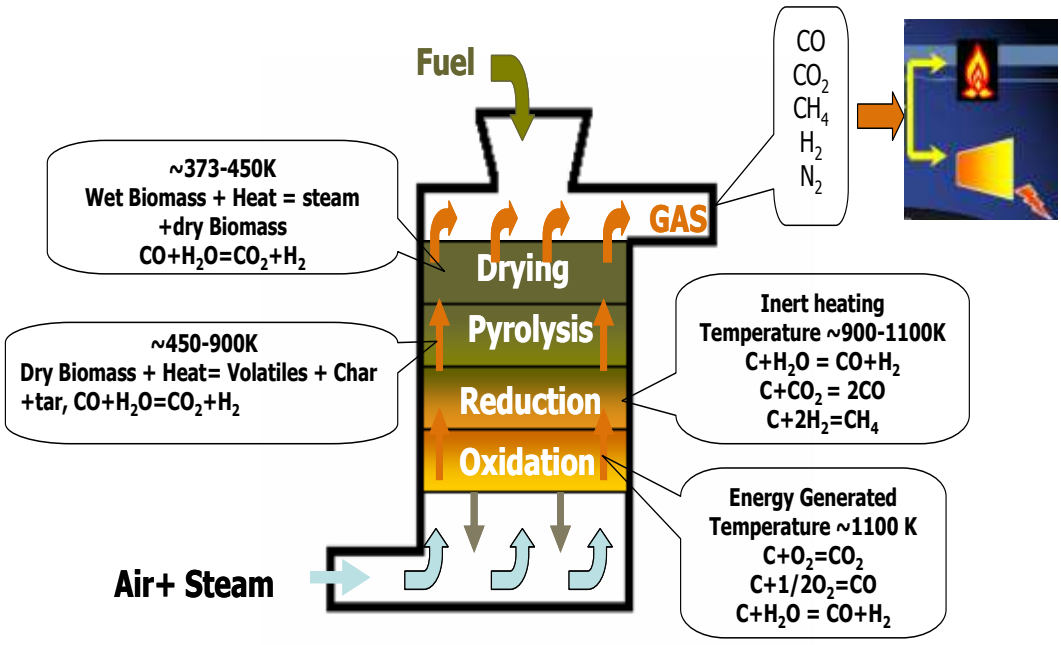

Figure 7. Schematic of a fixed bed gasifier. Adapted from[14]

Fluidized bed and entrained bed gasification require high velocity air flow. These gasifiers have high specific capacity and can be fast heat-up and they tolerate wide variations in fuel quality and a broad particle-size distribution [8, 15]. However, there is high dust content in the gas phase and the conflict between high reaction temperature with good conversion efficiency and low melting points of ash components[15] .

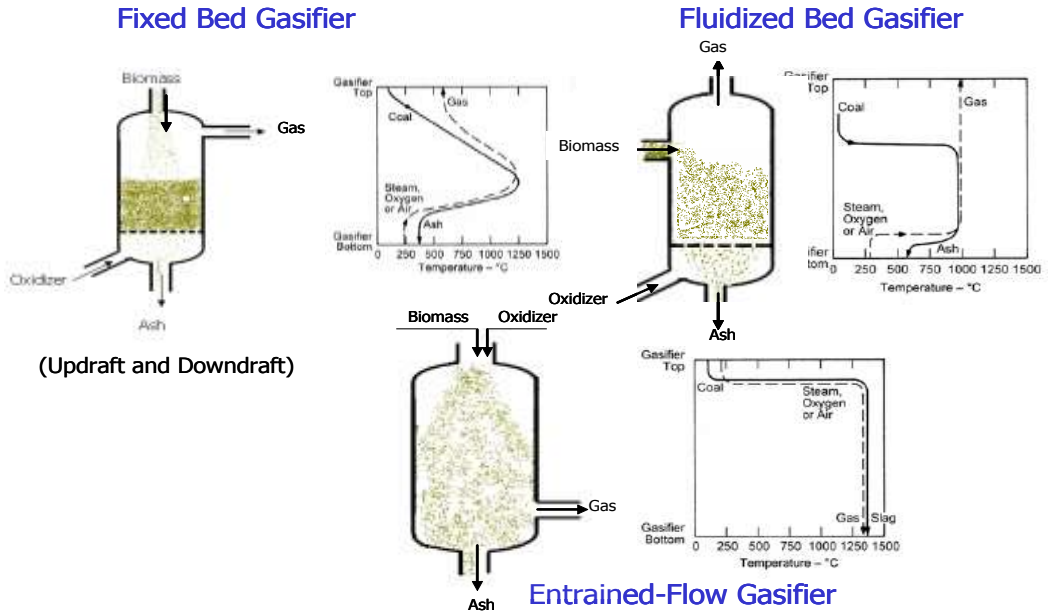

Figure 8. Temperature profiles for the different gasifiers. Adapted from[14]

As discussed before, gasifiers are named according to the fuel and gas movement inside the reactor. For updraft gasifier, fuel move down and gases move up and heat transfer occurred between the hot gases and cool fuel, while both the fuel and gases move down in the down draft gasifier. Thus, the temperature of the existing gas from the updraft gasifer is much lower than those leaving from a down draft gasifer[8]. Fixed bed gasifiers have a wide temperature distribution, while fluidized bed and entrained gasifiers have good heat and material transfer between the gas and solid phases with the almost constant temperature distribution. Also, the temperature of the produce gases is much higher than that leaving the fixed bed gasifiers.

Fluidized bed and entrained bed gasification require high velocity air flow. These gasifiers have high specific capacity and can be fast heat-up and they tolerate wide variations in fuel quality and a broad particle-size distribution [8, 15]. However, there is

high dust content in the gas phase and the conflict between high reaction temperature with good conversion efficiency and low melting points of ash components[15]. Table 1 gives the properties of the produce gas for updraft, downdraft, and fluidized bed using air as gasification media. Downdraft gasifier produce the highest HHV gases and H_2 volume% can reach 17% because the tar passed through a high temperature zone leading to the tar cracking in to H_2 or H_2O , or other short chain hydrocarbons[8]. The updraft gasifier produces more CO and high content of tar in the produce gas and fluidized produces more CH_4.

Table 1.Typical specie production from the most common gasifiers. Adapted from[8]

	Gaseous products (Vol.% dry)						Gas quality	
Gasifier Type	H2	CO	CO2	CH4	N2	HHV (MJ/m3)	Tars (g/m3)	Dusts
Air-blown Updraft	11	24	9	3	53	5.5	~50	Low
Air-blown Downdraft	17	21	13	1	48	5.7	~1	Medium
Air-blown Fluidized bed	9	14	20	7	50	5.4	~10	High

Table 2 gives the composition of gas produced from various biomass sources. It also can be found that the gases composition is also affected by gasifier design. The calorific value of gases is different when the same fuel is used in different gasifer.

Table 2. Composition of producer gas from various fuels

Fuel	Gasification method	volume percentage					Calorific value MJ/m^3	Ref
		CO	H_2	CH_4	CO_2	N_2		
Dairy biomass	updraft	4.77-11.73	13.5-25.5	0.43-1.73	11-25.2	54-60	3.3-4.3	[16]
Olive husk	updraft	26.2-28.5	6.4-8	1.4-1.6	7.5-6.2	56	4.8-8.5	[17]
Beachwood	updraft	28.6-30	7	1.8	-	55.6	5-5.5	[17]
charcoal	updraft	30	19.7	-	3.6	46	5.98	[18]
Wheat straw pellet	downdraft	14-17	17-19	-	11-14	-	4.5	[19]
Coconut shells	downdraft	19-24	10-15	-	11-15	-	5.8	[19]
Coconut husks	downdraft	19-24	10-15	-	10-15	55-60	5-5.86	[19]
Pressed sugarcane	downdraft	15-18	15-18	-	12-14	-	5.3	[19]
Rice hulls pelleted	downdraft	16.1	9.6	0.95	-	-	3.25	[20]
Charcoal	downdraft	28-31	5-10	1-2	1-2	55-60	4.6-5.65	[20]
Feedlot biomass	fluidized bed	27-30	7-10	1-3	2-6		4.8	[21]
Dairy biomass	fluidized bed	26.9	17.1		6.1	49.9	5.1	[22]

2.2 Gasification Reactions

Gasification process includes a number of complex reactions, and different types of gas components in the products, because these reactions and end-product are very sensitive to equivalence ratio or other experimental conditions.

Table 3.Main gasification reactions. Adapted from [6, 27]

Reaction	Equation	ΔH(298K) KJ/K-mol	Reactions
Pyrolysis	Solid biomass +Heat →VM+Char	-	(1)
Partial Combustion	$C+0.5\ O_2 \leftrightarrow CO$	-111	(2)
Combustion	$CO+0.5\ O_2 \leftrightarrow CO_2$	-254	(3)
Combustion	$H_2+0.5\ O_2 \leftrightarrow H_2O$	-242	(4)
Water –gas-shift	$CO+H_2O \leftrightarrow CO_2+H_2$	-41	(5)
Methanation	$C+H_2 \leftrightarrow CH_4$	-75	(6)
Methanation	$CO+3H_2 \leftrightarrow CH_4+H_2O$	-206	(7)
Steam carbon reaction	$C+H_2O \leftrightarrow CO+H_2$	+131	(8)
Boundouard	$C+CO_2 \leftrightarrow 2CO$	+172	(9)

When the enthalpy of reaction $\Delta H_R<0$, reaction is an exothermic process. Otherwise, $\Delta H_R>0$ indicates endothermic reaction. From Table 3, it can observed that the most relevant equations for carbon conversion are (2), (8),and (9) , which also yield the much of the syngas compounds (H_2 and CO)[23]. For reaction (2) and (3), oxidization of carbon can either produce CO and CO_2, or both. Reaction (2) dominated when T > 800K, whereas reaction (3) dominated for T< 800 K[24]. Reaction (2) and (3) are found to be much faster than other reaction according to Smoot and Smith [25].

Siva and Gerardo[8, 26] found that the production of the hydrogen increased with the rise of the steam-to-fuel ratio. Since water-gas-shift reaction is an endothermic reaction, the temperature would come down when steam was injected into the reactor.

Gerardo [8] concluded the rate of reaction of the heterogeneous reactions of O_2, H_2O, CO_2, and H_2 for single particle model and accounting the simultaneous effects of diffusion and intrinsic chemical kinetics.

$$\overset{\circ}{W}_j = \frac{[C_i]}{\frac{1}{K_m} + \frac{1}{K_j}} A_p \nu_p \tag{10}$$

$$K_j = A_j \exp(-\frac{E_j}{R_u T_s}) \tag{11}$$

$$A_p \nu_p = \frac{6\,(1-\varepsilon)}{d_p} \tag{12}$$

$$K_m = \frac{2.06 U_G}{\varepsilon} R_E^{-0.575} S_C^{-2/3} \tag{13}$$

Where $\overset{\circ}{W}$ j is the rate of reaction (kmol m-3 s-1) per unit char mole consumed, j the reaction number (2, 3, 4, 6, and 8), i the oxidizer (O_2, CO_2, H_2O, and H_2), dp the diameter of the particle (m), C_i the oxidizer concentration (kmol m-3), K_j the kinetics

constant (m s-1), Km the diffusion constant (m s-1), ε the bed porosity (fraction) or void fraction, Re the particle Reynolds number, and SC the particle Schmidt number.

For the homogenous equation of CO with O_2 and H_2O, the reaction rate of the can be estimated by using the following equations[8] .

$$\overset{\circ}{W}_5 = \varepsilon K_5 [CO][O_2][H_2O]^{-0.5} \tag{14}$$

$$\overset{\circ}{W}_7 = \varepsilon K_7 \{[CO][H_2O] - \frac{[CO_2][H_2]}{K_E}\} \tag{15}$$

In Equation (14) K_5 is the kinetics constant of the reaction of CO with O_2 while K_7 and K_E correspond to kinetics and equilibrium constants of the water shift reaction respectively. The chemical reaction kinetics constants of the global reactions (2-10) are summarized in Table 4.

Table 4. Chemical reaction kinetics constants of the gasification reaction

Kinetics Constants	K	Source
K_1	$1.516x10^3$ exp (-75549/T_s) (s^{-1})	Di Blasi et al. [27]
K_2	2.3 exp(-11100/T_s) (m s^{-1})	Hobbs ML et al. [28]
K_3	$1.6x10^5$ exp(-20000/T_s) (m s^{-1})	Annamalai et al. [29]
K_4	$10x10^{14}$ exp(-5052/T_s) (m s^{-1})	Gerun et al. [30]
K_5	2.78 x exp(-1513/T_G) (m^3 mol s^{-1})	Di Blasi et al. [27]
K_6	589 exp(-26800/T_s) (m s^{-1})	Hobbs ML et al. [28]
K_7	$3x10^5$T exp(-1508/T)(m s^{-1})	Giltrap DL et al.[31]
K_8	$589x10^{-3}$ exp(-26800/T_s) (m s^{-1})	Hobbs ML et al. [28]
K_9	$589x10^{-3}$ exp(-26800/T_s) (m s^{-1})	Hobbs ML et al. [28]

The main product of combustion and gasification of oxidization of char are CO and CO_2. High temperature favors the exothermic reactions and prohibits them in endothermic reaction[32]. The CO/CO2 reaction rate ratio increase with the temperature. It is estimated that the relationship of CO/CO2 between the temperature 730 K and 1170 K[8].

$$\frac{\dot{m}_{CO}}{\dot{m}_{CO2}} = 2500 \exp(-6240 / T_s) \qquad (16)$$

Where, T_s is the char particle surface temperature which can be estimated with equation 16 for a char particle burning under diffusion controlled conditions and without the inclusion of radiative losses [8].

$$\frac{c_P(T_S - T_\infty)}{h_C} = B \tag{17}$$

$$B = \frac{Y_{O2_\infty}}{\nu_{O2,3}} \tag{18}$$

Where, T_s is the surface temperature of the particle (K), c_p the specific heat of the oxidizer, Y_{O2_∞} mass fraction of the oxidizer, $\nu_{O2,3}$ =1.33, and h_c reaction enthalpy (kJ/ kg of C burned to produce CO) of the reaction (3).

2.3 Previous Studies on Gasification

In this section some relevant previous research on gasification and pyrolysis of wood chips including mesquite and juniper are presented.

Singe and parallel kinetics are the most common models predicting the pyrolysis behavior. Antal *et al* [33] applied a simple, first order, high activation energy (ca. 238 kJ/mol) model to accurately describes the pyrolytic decomposition of a variety of cellulosic substrates.

Teng *et al* [34] simulated the rice hull pyrolysis by using a combination of four independent parallel reactions corresponding to moisture, hemicellulose, cellulose, and lignin. In this model a single activation energy and pre-exponential factor have been assigned to each reaction.

Puigjaner *et al* [35] have developed a three independent parallel model for sugarcane bagasse and waste wood samples. The three independent parallel decomposition reactions proceeding in parallel corresponding to the hemicellulose, cellulose, and lignin. The weight loss associated with the pyrolysis process is simulated and the result showed a good agreement between simulated and experimental data.

Orfao *et al* [36] also supplied a first-order three independent reaction for pine, eucalyptus woods and pine bark. In this model, the first and the second pseudo-components correspond to the fractions of hemicellulose, cellulose and the third includes lignin and the remaining fractions of the carbohydrates. Reasonable agreements were obtained with actual data.

Besides, two-parallel reactions model have been developed by Junpirom *et al* [37] for two different components: hemicellose and lignin of longan seed biomass. Both reactions were assumed to proceed simultaneously. The activation energies and pro-exponential factors decreased with increasing particle size from 500 to 2000 μm at heating rates ranging from 100 ^{o}C to 600 ^{o}C and mass of samples approximately 15 mg due to lesser heat transfer resistance in smaller particle sizes compared to larger sizes.

Anthony *et al* [38] developed a more general parallel reaction model (PRM) (also known as distributed reaction model) for lignite and bituminous coals in order to account

for varying bond energies for chemical compounds within coal. Thus the activation energies are assumed to follow Gaussian distribution law described by mean activation energy (E_m) and standard deviation (σ). They found that the model can predict well the pyrolytic behavior of these two fuel types. The mean activation energies for the coals were 236,000 kJ/kmol and 212,000 kJ/kmol with standard deviations of 46,000 kJ/kmol and 29,000 kJ/kmol, respectively.

Tsamba *et al* [39] reviewed the literature and summarized the kinetic parameters values of biomass components from the literatures and their studies as follows: E_{min} (hemicellulose) =147.24±38.52 kJ/mol, E_{max} (hemicellulose) =172.75±39.44 kJ/mol, E_{min}(cellulose) =176.92±42.41 kJ/mol and E_{max} (cellulose) = 248.64±25.75 kJ/mol.
Brandon [40] studied the degradation of coal and, cattle and coal /cattle biomass blends pyrolysis in an inert (N_2) environment. They used a single as well as a parallel reaction to predict the pyrolysis kinetics of biomass and coal fuels. They found that PRM provided a more accurate result than the single reaction for the feedlot biomass and blends of feedlot biomass with coal. The current study used Mesquite and Juniper biomass samples with relatively low ash content.

Toshiaki *et al* [41] have used Japanese oak and red pine barks as a feedstock to study air-steam gasification gas components in a downdraft fixed-bed gasifier at 1117*K* under atmosphere pressure. They found that the product gas composition (mol%) for Japanese oak was 39.9% CO, 23.4% CO_2, 22% H_2,10.4% CH_4 , and 3.1% C_2H_4 and the product gas composition (mol%) for red pine bark was 25.6% CO, 34.7% CO_2, 31% H_2, 5.5% CH_4 and 2.5% C_2H_4.

Sommas *et al* [42] have carried out experiments of rubber wood chip gasification in a 100-kW bubbling fluidized bed gasifier to investigate the equivalence ratio (ER) on the yield and properties of synthesis gas. They found that increasing the ER resulted in a decrease of syngas product and lower product gas heating value. The product gas had low heating value (9.41 MJ/Nm^3) at 950 ^oC and with ER of 0.42. Ulich *et al* [9] performed the ultimate analysis of mesquite with moisture content of 19.0%. The results based upon weight percent of weight were as follows: carbon 53.49%, oxygen 36.33%, hydrogen 6.45%, nitrogen (N) 1.065%, and sulfur 0.086%.

In 1989, Kurkela et al [43] used peat and biomass as a fuel to gasifier in a bioneer updraft fixed-bed gasifier. Peat pellet with 16% moisture content were used as fuel. Air flow and steam flow were set to be 25-50Nm^3h^{-1} and 7-10kg h^{-1}, respectively. Cracking air was preheated to 360-380^oC. It was found that the compositions of dry raw gas was as follows: CO, 25-27%; H_2, 13-15%; CH_4, 2.4-2.8%; CO_2, 8-10%;N_2,47-50% 。It also found that tar concentration in the raw gas exhausted from the updraft gasifier is around 50-150 g $(Nm^3)^{-1}$ tar concentration decrease with the increase of temperature. Blasi et al [17] carried out the gasification experiment using Beachwood, nutshells, olive husks, and grape residues biomass as a fuel in a laboratory- scale countercurrent fixed-bed gasification plan. He found out that the gas molar composition of the producer gas consists of 28-30% CO, 5-7% CO_2, 6-8% H_2, 1-2% CH_4, and minor fractions of C_2 species (apart from nitrogen). The heating value of the gas is in a rangeof 5-5.5 MJ/Nm^3. The heating value of the producer gas increases with the increase of air to fuel ratio.

Blasi also performed the pyrolysis experiments of the beechwood and agricultural residues at 730 K. The results are given in the following Table 5:

Table 5. Product yields (% on moisture-free (mf) Initial Mass) from fixed-bed pyrolysis (bench scale) of beachwood and agricultural residues for Tb =730 K. Adapted from[17]

biomass	char [wt %]	gas [wt %]	liquids [wt %]
beechwood	29	16.03	55.52
nutshells	36.82	17.91	41.66
olive husks	34.13	19.6	46.01
grape residues	44.84	17.44	35.72
straw pellets	34.63	20.1	41.05

Hightower [44] used the mesquite as feedstock in a fluidized bed gasifer under different air- fuel- stream ratio condition. The mass, heat, carbon and nitrogen balance were calculated in this report. The gas composition from mesquite was reported under different gasification condition and it was found that heating values range from 2370 to 5573 Btu/lb DAF feed and show a definite increase with increasing reactor temperature.

Thannapal et al [45] carried out air-stream gasification of dairy biomass in a 10 kw fixed bed updraft bed gasifier. It was found that the amount of hydrogen in the end product gas increased with the presence of steam, however, the HHV of the gasification gas on mass based is less due to lower molecular weight of H_2.

Lucas et al [46] gasified 12 mm diameter wood pellets in a countercurrent and updraft fixed bed gasifier using preheated air and steam. It was found that increasing the molar percentage of the steam in the feed gas resulting in higher the

hydrogen in the produced gas. Also, higher the molar fraction of the steam in the feed gas would lower the temperature in the bed and that of the exit gas. The steam did not have significant effects on the heating value of the produce gas.

It is apparent that there is no literature on air and steam gasification using Mesquite and Juniper as biomass fuels and updraft gasifiers; further there is no previous study on extracting kinetics at low heating rate using maximum volatile release (MVR) method. The present work is expected to fill that void.

3 OBJECTIVE AND TASKS

The overall objective of the current research is to conduct a gasification study with mesquite and juniper woody biomass as a feedstock in an updraft fixed bed gasifier. In order to achieve the overall objective, the following tasks must be carried out.

1. Perform global modeling studies on gasification to determine operating conditions
2. Modify the gasification facility
   a. Build a gas condensing system to collect liquid yield from the gas
   b. Fabricate three of the condensers and helix cooper and connect them to the gasifier
   c. Install a gas exhaust bypass system in order to avoid tar condensing in the condensers before the gasifier reaches steady state.
3. Conduct thermogravimetric analysis (TGA) study and develop single and parallel reaction model for fuels to simulate pyrolysis process.
4. Perform the proximate and ultimate analyses for mesquite and juniper fuels
5. Conduct experiments on gasification with air, air-steam, and catalyst and obtain data on temperature profile, gas composition, and liquid yield under various operating conditions.

4 MODELING

In this section gasification models were built for the gasification process. Thermodynamic equilibrium model was built by EES and CEA (chemical equilibrium application model) developed by NASA was used to predict the gasification performance.

4.1 Thermodynamic Equilibrium Model

In this section, an equilibrium model (developed by using EES) based on equilibrium constant to predict the gas compositions for juniper and mesquite biomass. This model is based on the model proposed by Jarungthamamachote et al[47]. In order to simulate and simplify the gasification process some of the assumptions were made:

(1) Gasifier is an adiabatic facility;

(2) The temperature in the gasification zone is set to be a fixed temperature, and the air is supplied at 298K and producer gas also be exhausted at 298K;

(3) Gasification is in a steady state process.

Biomass has a general empirical formula of $CH_xO_yN_z$. The main gasification gas products include CO, H_2, CO_2, CH_4, N_2 and H_2O. The following is the global chemical reaction in a gasifier:

$$CH_xO_yN_z+wH_2O+m(O_2+3.76N_2)\rightarrow n_{H2}H_2+n_{co}CO+n_{CO2}CO_2+n_{CH4}CH_4+n_{H2O}H_2O+(z/2+3.76m)N_2 \quad (19)$$

Where x, y, z represent the numbers of H, O, N for a single atom of carbon in the feedstock, respectively; w is the mole amount of the moisture or steam; m is the number of mole of air; n_i is the number of mole of species *i* in the product, which is unknown. Equation (18) presents a global chemical reaction in a gasifier but a number of competing reactions are taking place at the same time in the process[48]. The temperature for the reactants in the left side of the equation is set to be 298.15K.

4.1.1 Mass Balance

On the left side of the equation (19), five unknown species of product gases need to be determined. Therefore, five equations are required to solve these unknown species. Three equations can be obtained from the element balance of the C, H, and O.

$$C: \ n_{co} + n_{CO2} + n_{CH4} = 1 \tag{20}$$

$$H: \ 2n_{H2} + 2n_{H2O} + 4n_{CH4} = x + 2w \tag{21}$$

$$O: \ n_{CO} + 2n_{CO2} + n_{H2O} = y + w + 2m \tag{22}$$

4.1.2 Thermodynamic Equilibrium

In a fixed bed updraft gasifier, there are four different zones existing in the gasifier known as combustion, gasification, pyrolysis, and drying[14]. In this section, only the chemical reactions occurring in the gasification zone were simulated by the thermodynamic equilibrium model. Chemical equilibrium is usually explained either by the minimization of Gibbs free energy or by using equilibrium constants[48]. Due to the complex mathematical theories of Gibbs free energy model, the present thermodynamic equilibrium model is developed based on the equilibrium constants and it is assumed that all the reactions are in thermodynamic equilibrium. Hence, another two equations can be obtained from equilibrium constants. The reactions for the equilibrium constants are shown as follows:

$$C + CO_2 \leftrightarrow 2CO \quad (23)$$

$$C + H_2O \leftrightarrow CO + H_2 \quad (24)$$

$$C + 2H_2 \leftrightarrow CH_4 \quad (25)$$

Equation(23) and (24) can be combined together to form the water –gas shift reaction [49]:

$$CO + H_2O \leftrightarrow CO_2 + H_2 \quad (26)$$

All gases in these reactions are considered as ideal gas and at 1 atm.

The equilibrium constant for the water-gas shift reaction equation $K_2=\frac{n_{CH_4} n_{total}}{(n_{H_2})^2}$

(28) is:

$$K_1 = \frac{n_{CO_2} n_{H_2}}{n_{CO} n_{H_2O}} \tag{27}$$

The equilibrium constant for the methane formation equation $C + 2H_2 \leftrightarrow CH_4$

(25) is:

$$K_2=\frac{n_{CH_4} n_{total}}{(n_{H_2})^2} \tag{28}$$

Where n_i is the fraction of specie i in the mix gas. n_{total} is the total mole of product gas.

For ideal gas mixture

$$\ln(K)=-\frac{\Delta G_T^0}{RT} \tag{29}$$

$$\Delta G_T^0 = \sum_i v_i \Delta \bar{g}_{f,T,i} \tag{30}$$

Where R is the universal gas constant, v_i is the stoichiometric number. $\Delta G^0{}_T$ is the standard Gibbs function of reaction, and $\Delta\bar{g}_{f,T,i}$ is the standard Gibbs function of formation of the gas species *i* at a given temperature T. $\Delta\bar{g}_{f,T,i}$ can be expressed by the empirical equation shown as below:

$$\Delta\bar{g}_{f,T,i} = \bar{h}_f{}^o - a'TlvT - b'T^2 - \frac{c'}{2}T^3 - \frac{d'}{3}T^4 + \frac{e'}{2T} + f' + g'T \tag{31}$$

Where enthalpies of formation of the gas and coefficients $a' - g'$ can be obtained from Table 6.

Table 6.The value of $\bar{h}^o_f$ and coefficients of the empirical equation for $\Delta g^o_{f,T}$. Adapted from [50]

Compound	$\bar{h}^o_f$	d	b'	c'	d'	e'	f'	g'
CO	-110.5	$5.619\text{x}10^{-3}$	$-1.190\text{x}10^{-5}$	$6.383\text{x}10^{-9}$	$-1.846\text{x}10^{-12}$	-4.891x102	$8.684\text{x}10^{-1}$	$-6.131\text{x}10^{-2}$
CO_2	-393.5	$-1.949\text{x}10^{-2}$	$3.122\text{x}10^{-5}$	$-2.448\text{x}10^{-8}$	$6.946\text{x}10^{-12}$	-4.891x102	5.270	$-1.207\text{x}10^{-1}$
H_2O	-241.8	$-8.95\text{x}10^{-3}$	$-3.672\text{x}10^{-6}$	$5.209\text{x}10^{-9}$	$-1.478\text{x}10^{-12}$	0.0	2.868	$1.722\text{x}10^{-2}$
CH_4	-74.8	$-4.62\text{x}10^{-2}$	$1.130\text{x}10^{-5}$	$1.319\text{x}10^{-8}$	$-6.647\text{x}10^{-2}$	-4.891x102	$1.411\text{x}10^{1}$	$-2.234\text{x}10^{-1}$

4.1.3 Energy Balance

The gasification process in the well-insulated gasifer can be assumed to be an adiabatic process which means there is no heat loss to the environment. The enthalpy balance for this process can be written as:

$$\sum n_{r,j}\bar{h}^0_{f.j} = \sum n_{p.j}(\bar{h}^0_{f.j} + \Delta\bar{h}^0_{T.j}) \tag{32}$$

Where $\bar{h}^0_f$ is the enthalpy of formation in kJ/kmol and its value is zero for all chemical elements such as C, H_2, and O_2. $\Delta\bar{h}^0_T$ is the enthalpy difference between a given state and at reference state. It can be calculated by:

$$\Delta\bar{h}^0_T = \int_{298}^{T} c_p dT \tag{33}$$

Where C_p is the specific heat at constant pressure in *kJ/kmol-K* and it is a function of temperature. It can be defined by empirical equation shown as below:

$$C_p(T) = a + bT + cT^2 + dT^3 \tag{34}$$

The coefficients *a-d* can be obtained from Table 7.

Table 7. Coefficients of a-d. Adapted from[51]

gas species	a	b	c	d	Temperature range (K)
Hydrogen	29.11	-0.1916x10^{-2}	0.4003x10^{-5}	-8.8704x10^{-9}	273-1800
carbon monoxide	28.16	0.1675x10^{-2}	0.5372x10^{-5}	-2.22x10^{-9}	273-1800
carbon dioxide	22.26	5.981x10^{-2}	-3.501x10^{-5}	-7.469x10^{-9}	273-1800
water vapor	32.24	0.1923x10^{-2}	1.055x10^{-5}	-3.595x10^{-9}	273-1800
methane	19.89	5.201x10^{-2}	1.269x10^{-5}	-11.01x10^{-9}	273-1800
nitrogen	28.9	-5.1571x10^{-2}	0.8084x10^{-5}	-2.873x10^{-9}	273-1800

The enthalpy of formation for solid fuel in the reaction is written as follow[52]:

$$\bar{h}^0_{f.fuel} = \text{LHV} + \sum_{prod} n_k (\bar{h}^0_f)_k \tag{35}$$

Where $(\bar{h}^0_f)_k$ is the enthalpy of formation of product *k* under complete combustion of the solid fuel. LHV is the lower heating value of the solid fuel in kJ/kmol. Once the temperature in the gasification zone is given, the mole fraction of the producer gas species *i* can be determined by using the above equations.

4.1.4 Result and Discussions

Figure 9 shows the effect of the adiabatic temperature on gas composition for mesquite and juniper. The fuel moisture content was set to be 12% and adiabatic temperature can be changed by varied the air supply to the gasifier. Increasing the adiabatic temperature implies decreasing ER or increasing oxygen (more air) supplied to the gasifier. Hence, the oxidation of char takes place in a sufficient O_2 environment, more CO_2 was produced and less CO generated. In addition, the H_2 mole content decreased with the increase of the adiabatic temperature due to less char was available to react with H_2O under O_2 sufficient environment. There was a very small amount of CH_4 content (less 1%) in the end product gas.

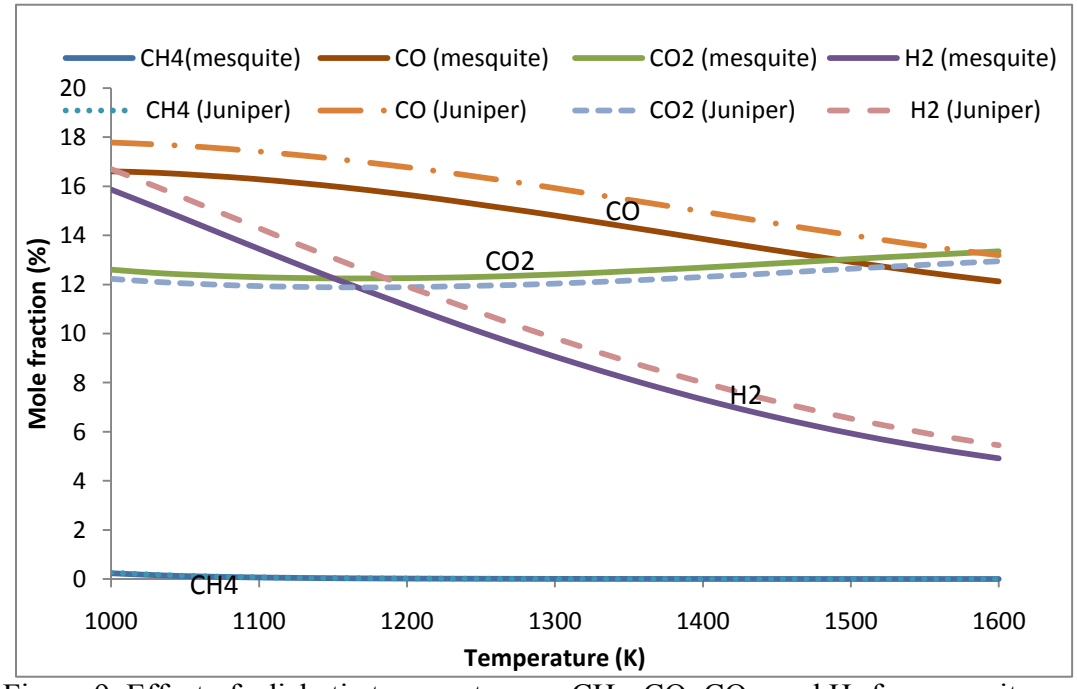

Figure 9. Effect of adiabatic temperature on CH_4, CO, CO_2, and H_2 for mesquite and juniper fuel with 12% moisture content.

The fuel moisture content is an important parameter that effects on the gasification performance. In this model, the gasification adiabatic temperature was fixed at 1000 ^{o}C and the gas yield as a function of moisture content would be investigated. From Figure 10 and Figure 11 give the gas composition of H_2, CO, CO_2, and CH_4. It can be seen that H_2 and CO_2 content increased with the increasing of moisture content, and CO content decrease. Higher moisture content promoted the water-carbon reaction resulting in more H_2 and CO formation. Also, With the increase of the [H_2O] in the fuel, the equilibrium of the water gas shift reaction (equation 36) would move to the right side of the reaction, which resulted in increase of the CO_2 and H_2 content and decrease of the CO concentration.

$$CO + H_2O \leftrightarrow CO_2 + H_2 \qquad \Delta H = 935 \text{ kJ/kg of } CO_2 \qquad (36)$$

The CH_4 mole fraction increases slightly with the moisture increase because under higher moisture condition, more H_2 generated to react with the fixed carbon to form CH_4.

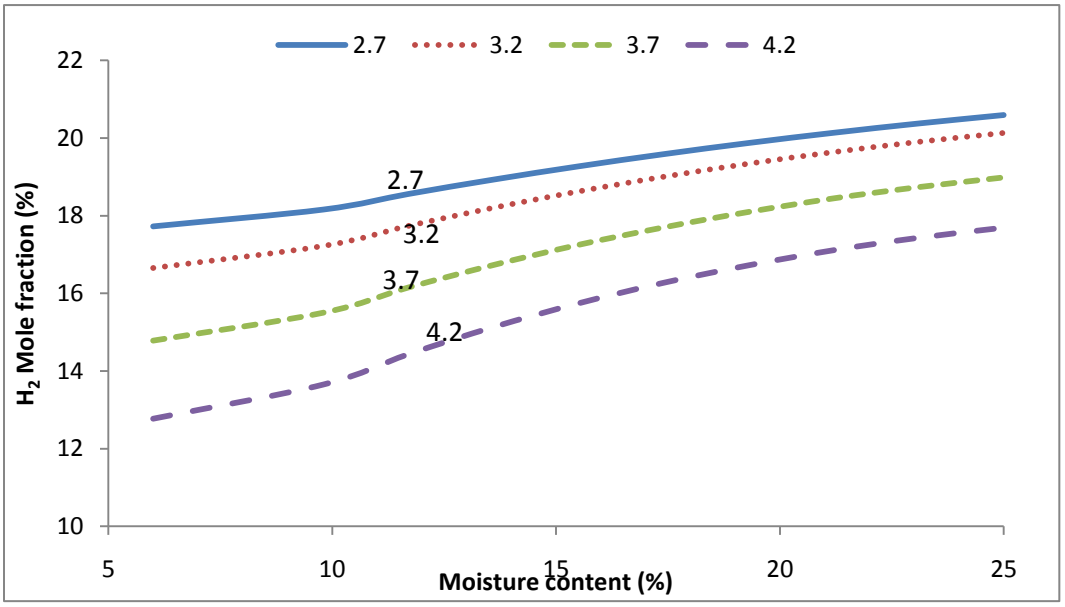

Figure 10. Effect of moisture content on H_2 mole fraction under different ER for juniper biomass

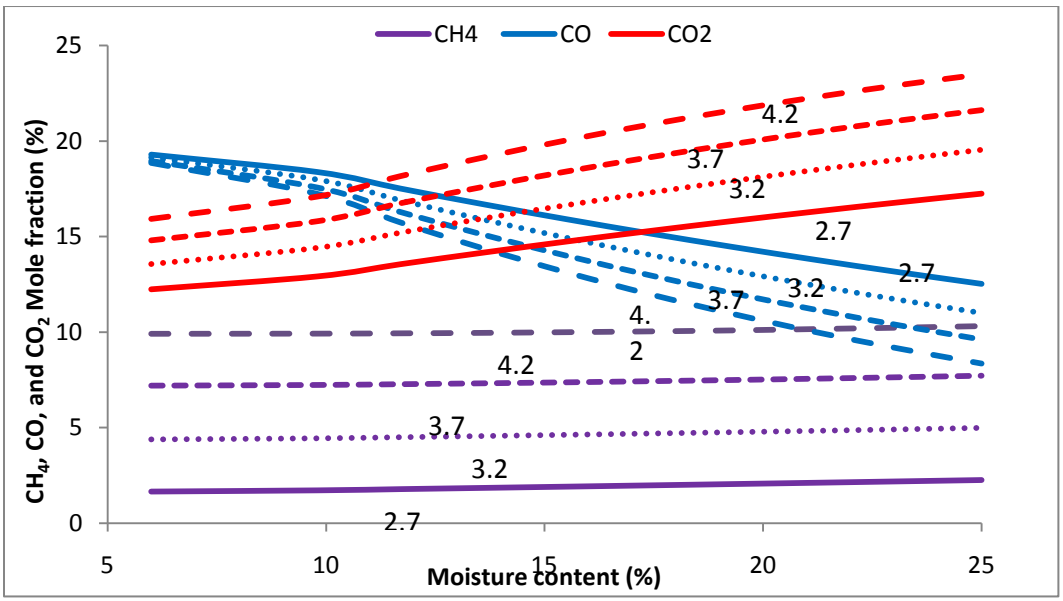

Figure 11. Effect of moisture content on CH_4, CO, and CO_2 mole fraction under different ER for juniper biomass

Figure 12 and Figure 13 show the effect of the moisture on the H_2, CO, CO_2 and CH_4 mole fraction for mesquite fuel. The same trend was for the mesquite fuel.

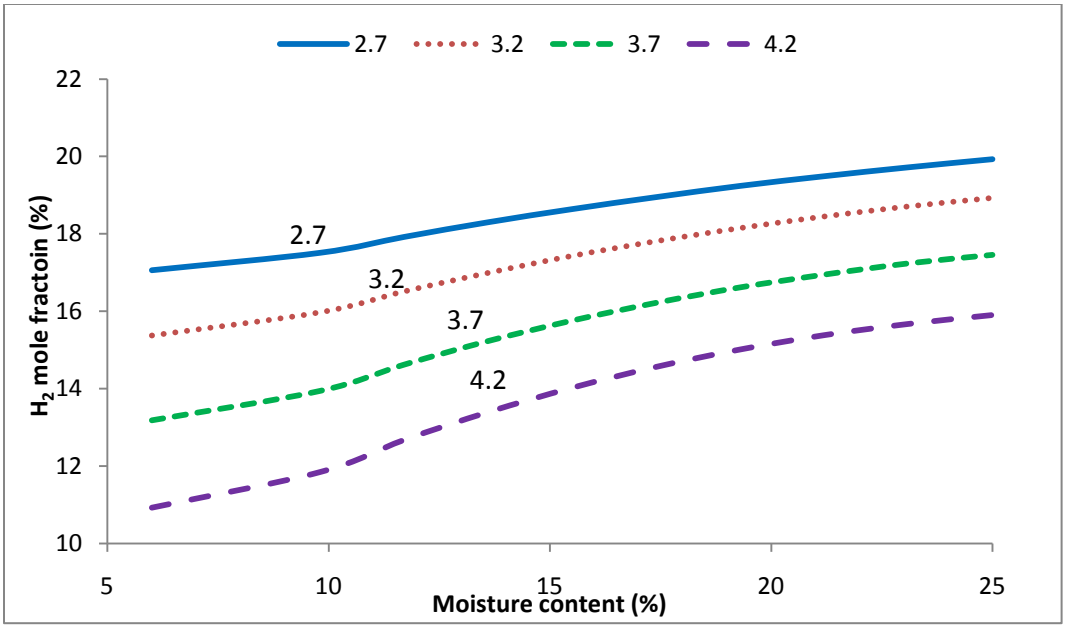

Figure 12. Effect of moisture on H_2 mole fraction under different ER for mesquite biomass

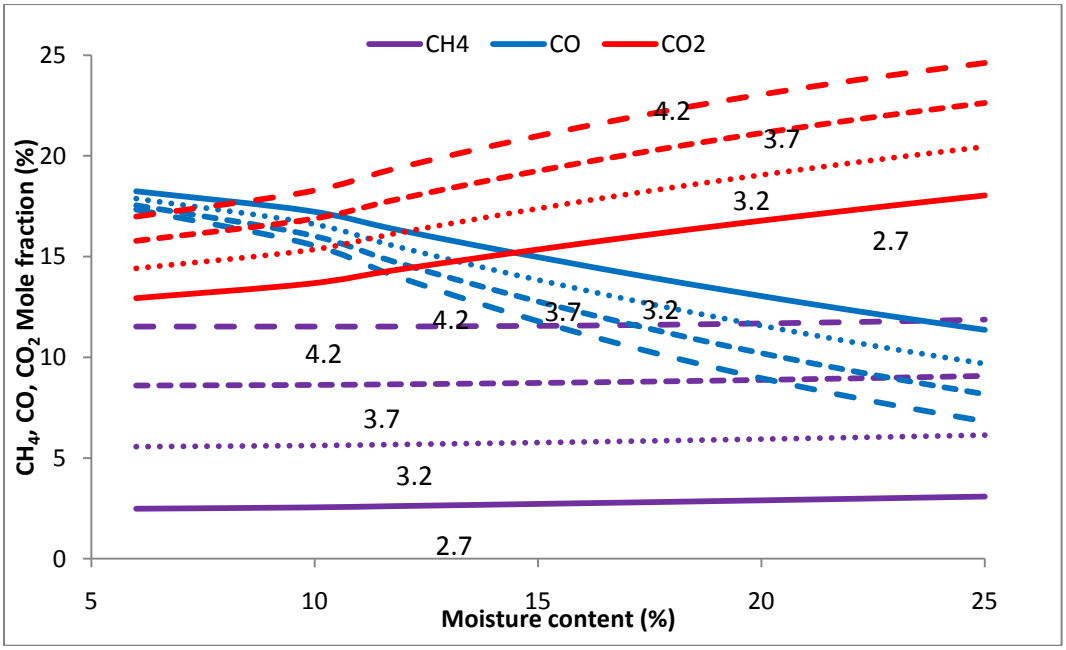

Figure 13. Effect of moisture content on CH_4, CO, and CO_2 mole fraction for mesquite biomass

4.1.5 The Effect of the Adiabatic Temperature on the HHV

Figure 14 give the HHV of the juniper and mesquite fuel with moisture content of 12%. It was found that with the increase of the adiabatic temperature (e.g. Lower ER and more air supply), the HHV of the mesquite and juniper decreased because more incombustible gas produced such as CO_2. Juniper gas had a slighter higher HHV than that of mesquite under same condition due to higher HHV of the juniper fuel.

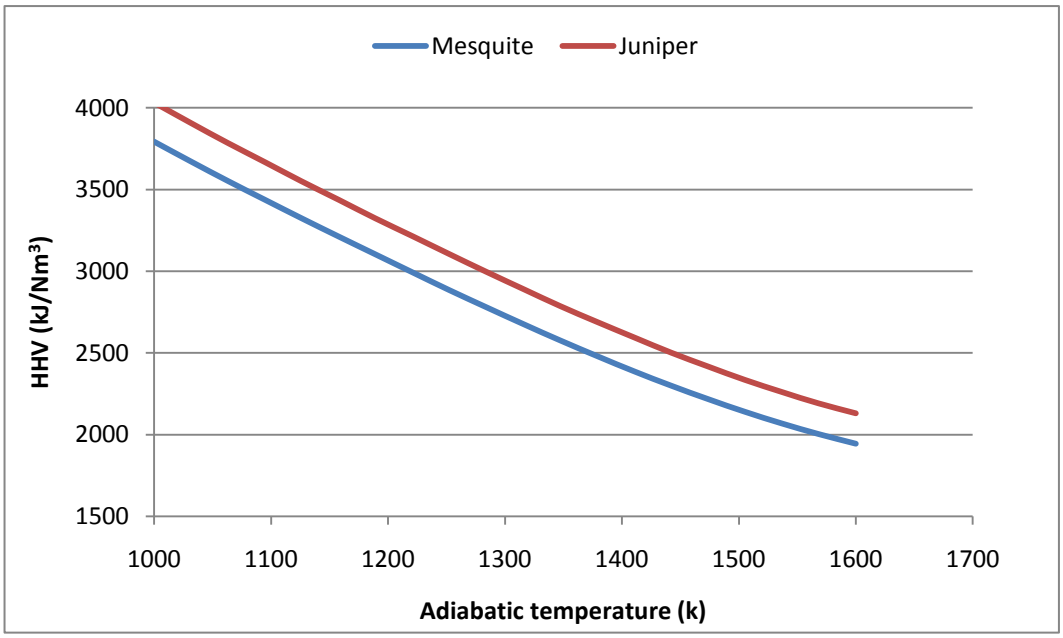

Figure 14. HHV of the mesquite and juniper gas from EES model

4.2 NASA Chemical Equilibrium with Applications (CEA) Model

The NASA CEA calculates chemical equilibrium compositions and properties of complex mixture. There are over 2000 species are contained in the thermodynamic

database and 150 species in the product gas. Thus, this model was employed to estimate the adiabatic temperature and end product gas composition. In this study, the NASA CEA PC version was applied to predict the mesquite and juniper gasification including gas species and adiabatic temperature.

4.2.1 Modeling Procedure

As discussed earlier, the mixture end product gasification gas composted of CO, CO_2, CH_4, H_2 and N_2 with air, steam and CO_2 as gasification media[26]. The molar fraction and adiabatic temperature under ideal kinetic gasification conditions can be predicted using a) mass and energy conversation equation b) atom balance and c) chemical equilibrium.

For complete combustion, all the combustible components in the fuel are burned completely and the main products are CO_2 and H_2O. Following is a typical completely biomass combustion reactions:

$$CH_hO_oN_nS_s + aO_2 \rightarrow bCO_2 + cH_2O + dSO_2 \quad (37)$$

The conventional equivalence ratio was expressed as: $ER = \frac{stochiometric\ air\ moles}{actual\ air\ moles} = \frac{a}{e}$

Because the fuel usually contains moisture and steam was some time used as gasification media. The general gasification reaction can be wrote as follow equation

$$CH_hO_oN_nS_s + e(O_2 + 3.76N_2) + fH_2O \rightarrow gCO_2 + hCO + iCH_4 + jH_2S + kN_2 + lH_2 \quad (38)$$

The ratio of steam to fuel can be expressed as:

$$S:F = \frac{mass\ of\ steam}{mass\ of\ biomass(as-received)} = f \quad (39)$$

Under adiabatic gasification condition, the total energy in the reactants is equal to the total energy in the products. The energy conservation can be expressed as follow:

$$\sum_k N_{k,P} h_{k,P}(T_P) = \sum_k N_{k,R} h_{k,R}(T_R) \quad (40)$$

Where $N_{k,p}$ and $h_{k,p}$ are the moles and enthalpies of the products at temperature T_P and $N_{k,R}$ and $h_{k,R}$ are the moles and enthalpies of the reactants at temperature T_R. The major objective of gasification is to convert solid fuel into combustible fuel gas, while tar and char are the byproducts. And thus, the recover energy in the combustible gases is lower than that in the reactants, and the energy conversion efficiency in the gasification process is always less than 100% [13]. Table 8 gives the simulation constions.

Table 8.Condition used in modeling studies

Parameter	Value
Pressure (kPa)	100
Equivalence ratio (ER)	2.7-4.2
Steam to fuel ratio (S:F)	0.15-0.45
Steam temperature (K)	373
Inlet air and fuel temperature (K)	298
Temperature of products (K)	873-1473

4.2.2 Model Results

In these section results of the modeling studies are presented. The effects of the fuel moisture content, ER, S: F ratios on the adiabatic temperature, gas compositions, and gas HHV were investigated.

4.2.3 Effect of the Moisture Content on Gas Composition

Figure 15 and Figure 16 shows the CO and CO_2 mole percentage under different ER for juniper fuel with moisture content of 6%, 12%, and 24%. It was found that the CO mole percentage increased with the increasing of ER while CO_2 percentage decreased with the increase of ER. At lower ER, air was abundant for the carbon oxidization and the main product are CO_2. With the increase of the ER, less air was supplied into the gasifier and CO_2 concentration decreased and CO percentage increased

correspondingly. With the increase of the moisture of fuel, CO_2 concentration increased while CO percentage decreased due to the fact that the higher moisture content fuel lowered the gasification temperature and shifted the equilibrium of the water-gas shift reaction ($CO+H_2O \leftrightarrow CO_2+H_2$) to the formation of product direction. In addition, high moisture content fuel promoted the steam carbon reaction results in increasing of the H_2 and CO concentration. Generally, fuel with higher moisture content produced more H_2 and CO, while less CO_2.

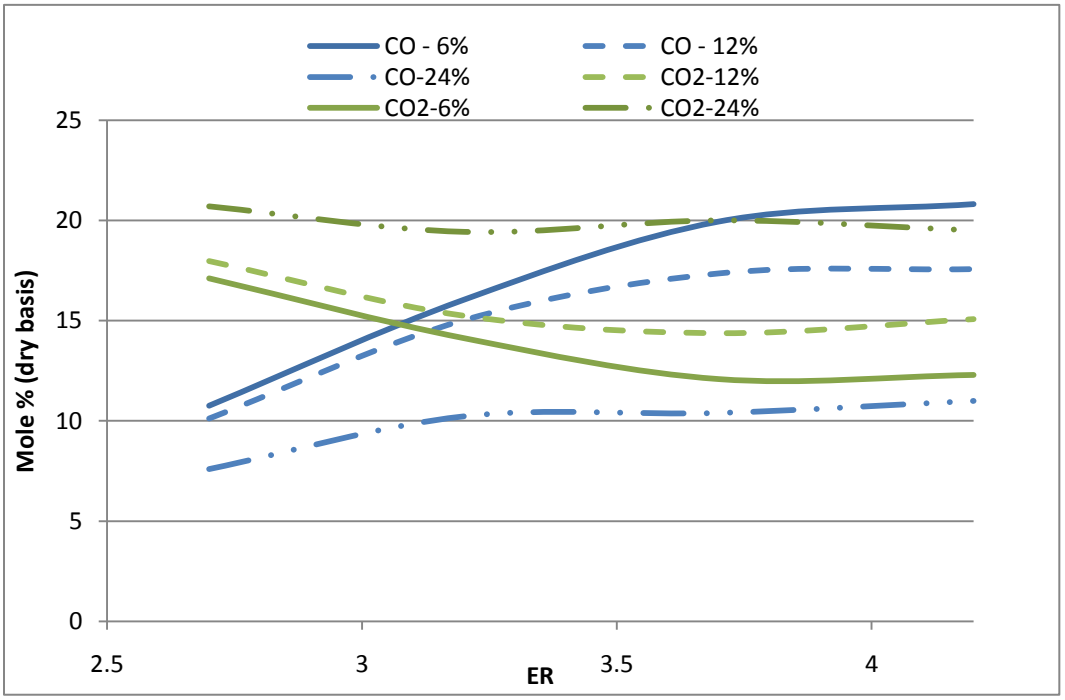

Figure 15. CO and CO_2 mole fraction vs. ER for juniper fuel

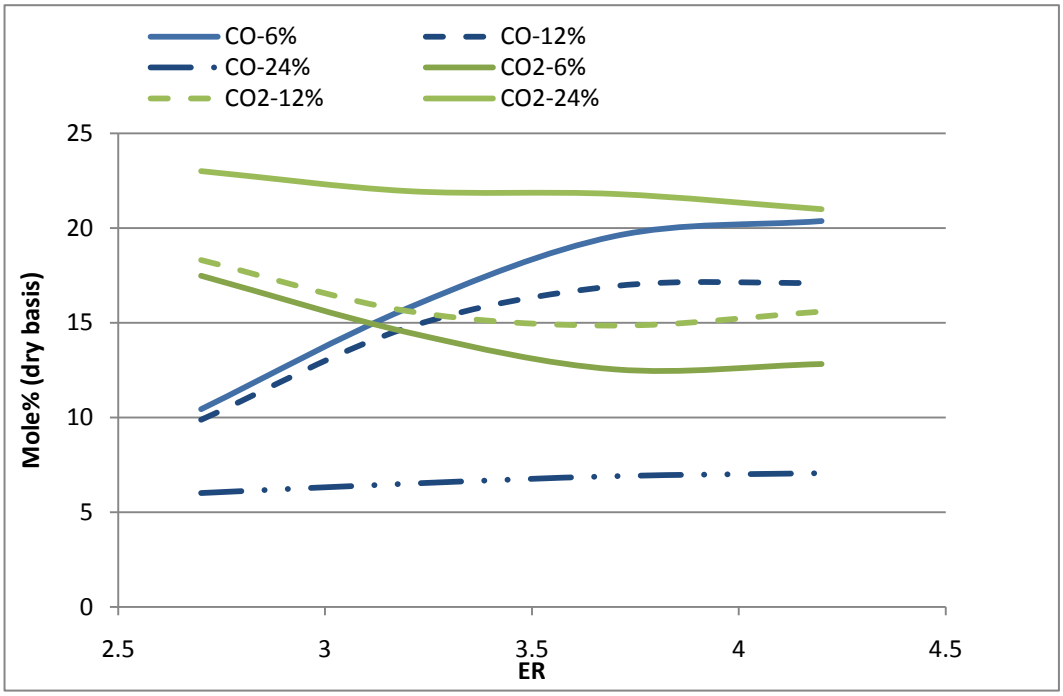

Figure 16. CO and CO_2 mole fraction vs. ER for mesquite fuel

Figure 17 and Figure 18 show the H_2 concentrations for juniper and mesquite fuels with moisture content of 6%, 12%, and 24%. It is seen that H_2 content was between 21%-32% and 21%-31% for juniper and mesquite gas, respectively, when moisture content increased from 6% and 24%. As discussed early, the H_2 concentration increased with increase of the moisture content.

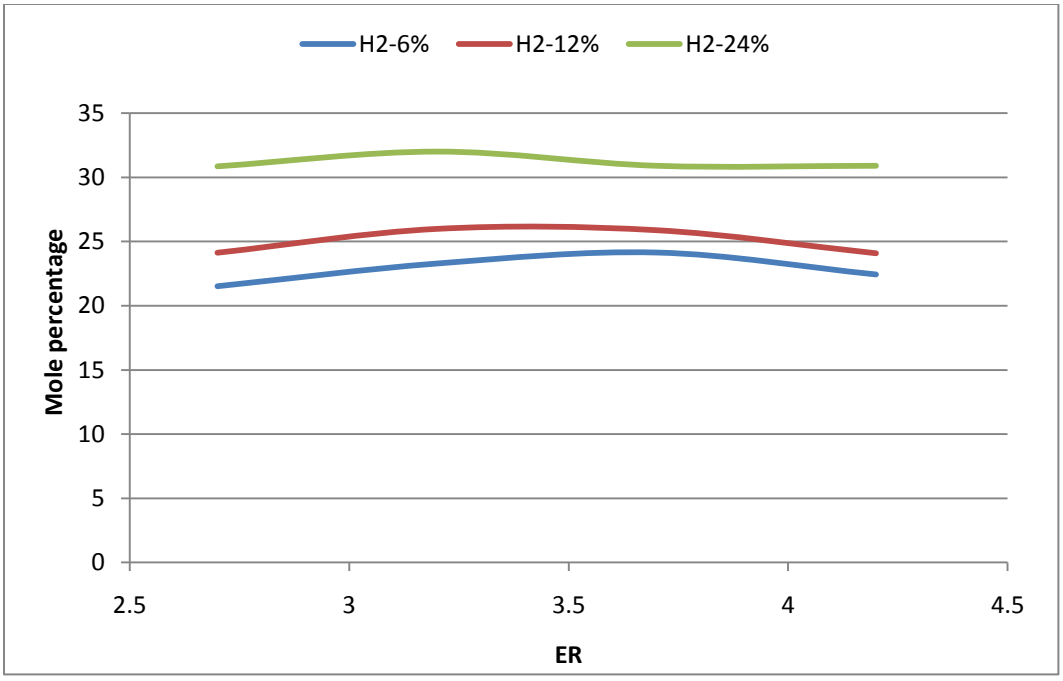

Figure 17. H_2 mole fraction vs. ER for juniper fuel

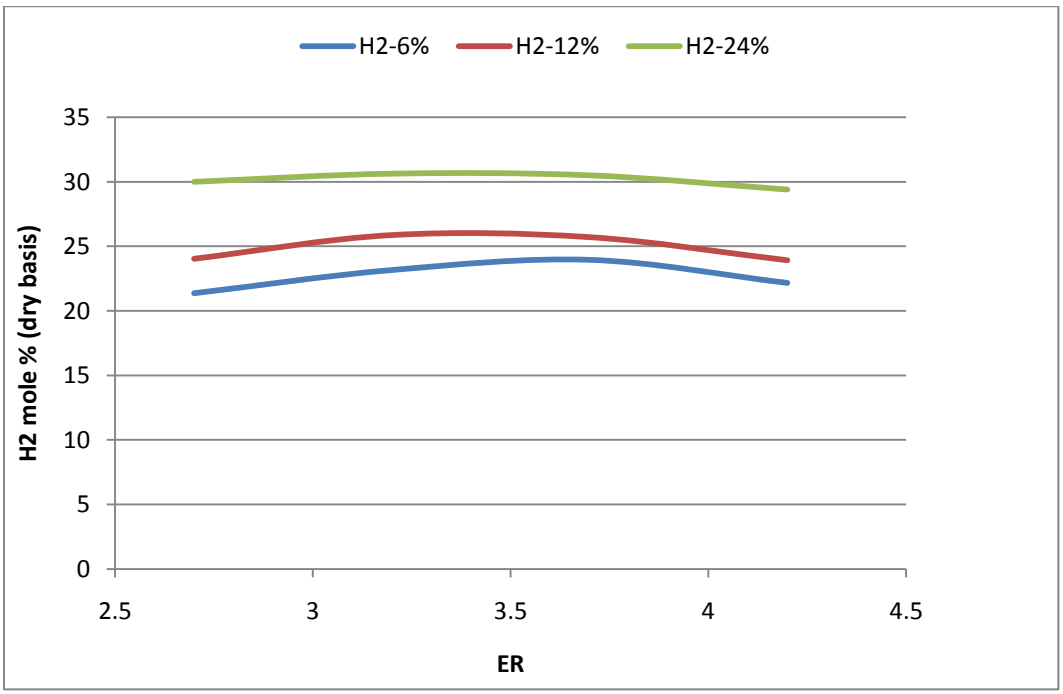

Figure 18. CO_2 mole fraction vs. ER for mesquite fuel

Figure 19 and Figure 20 give the CH_4 percentage vs. ER. It was found that the CH_4 percentage is negligible (< 1%) when ER< 3.2 for juniper while it increased to 2.5% and 3.5% for juniper fuel with 6% and 12% at ER=4.2, respectively. At lower ER, more carbon was oxidized to be CO_2 and less carbon was available to react with H_2 to generate CH_4. When fuel moisture content increased from 6% to 12%, more H atom is available to from the CH_4 and thus the fuel with higher moisture content product more CH_4. However, when the moisture content went up further (24%), CH_4 concentration decreased due to the gasification temperature was not high enough for H_2 and C to form CH_4.

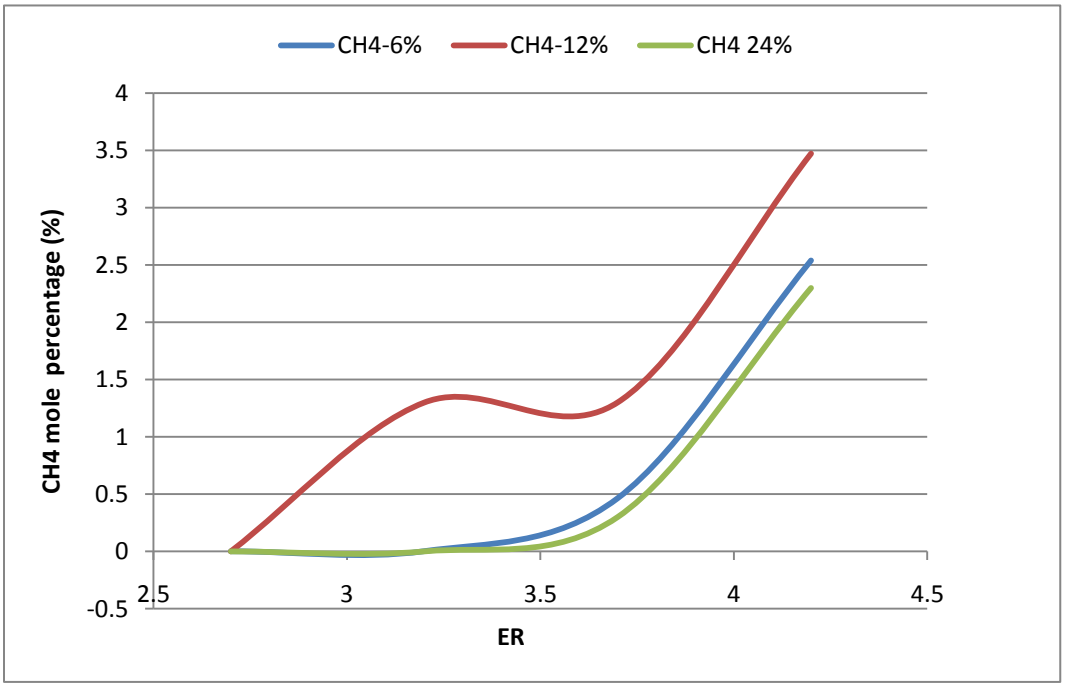

Figure 19. CH_4 mole fraction vs. ER_m for juniper fuel

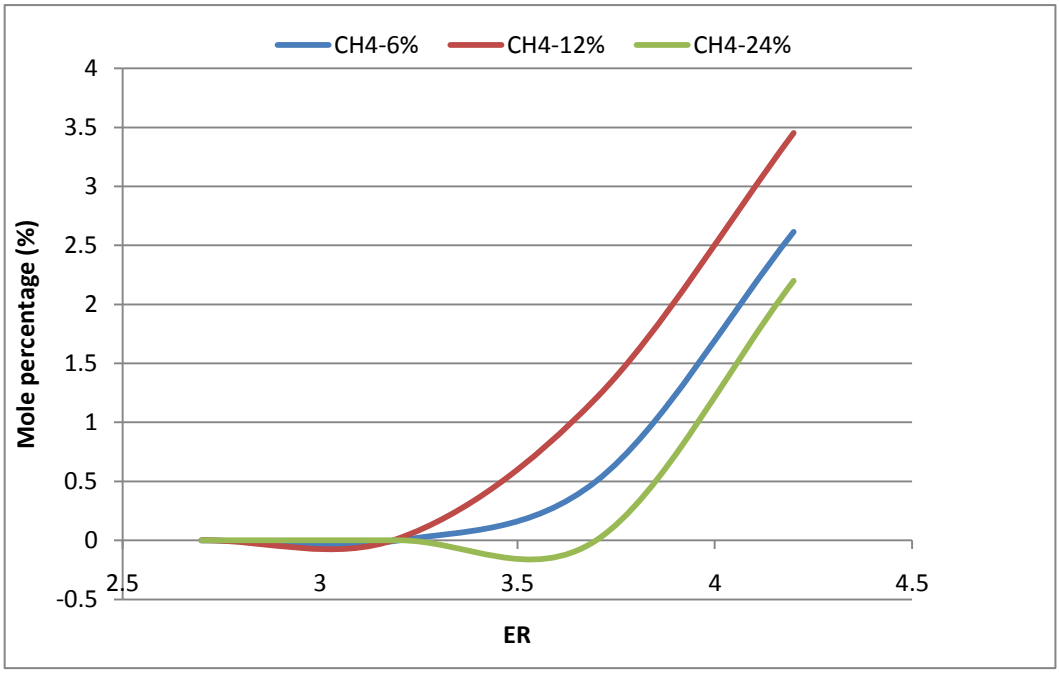

Figure 20. CH_4 percentage vs. ER for mesquite fuel.

4.2.4 Effect of the Moisture Content on Adiabatic Temperature

Figure 21 and Figure 22 show the adiabatic temperature at different ER conditions for the juniper and mesquite. It was found that the adiabatic temperature of the both fuels decreased with the increase of the ER. In addition, increasing of the fuel moisture content would lower the adiabatic temperature. For instance, the adiabatic temperature can go up to 1370 K and 1270 K for juniper with moisture content of 6% and 12%, respectively. When the ER increased to 4.2, adiabatic temperature dropped to 880 K and 900 K, respectively.

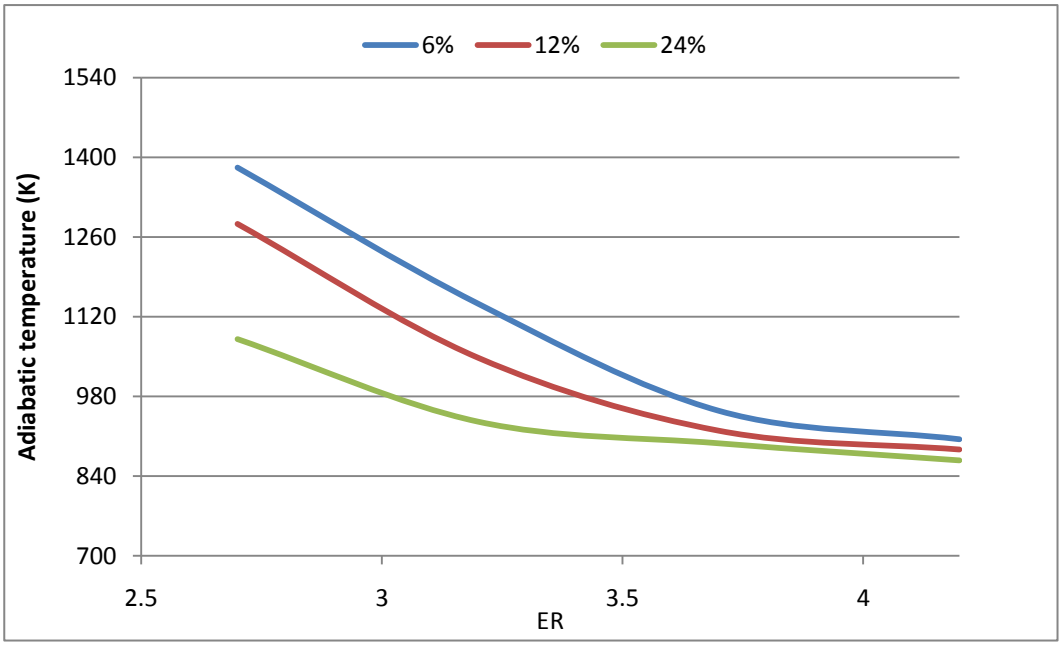

Figure 21. The adiabatic temperature for juniper fuel under different ER

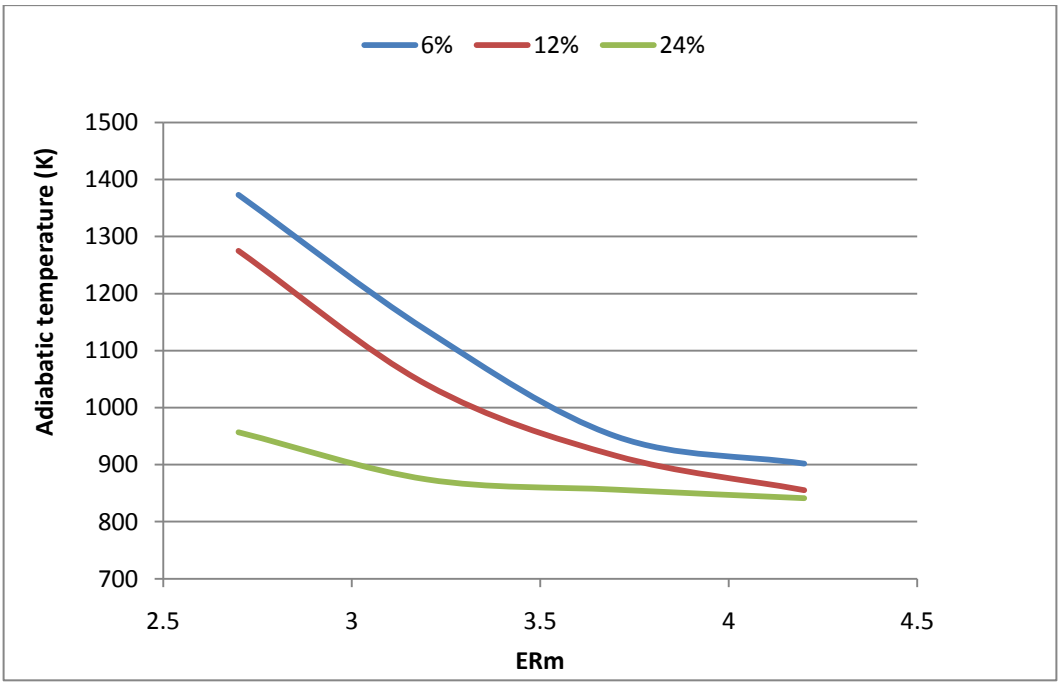

Figure 22. Adiabic temperature of the mesquite fuel vs. ER

4.2.5 The Effect of Moisture Content on Gas HHV

Figure 23 and Figure 24 give the HHV of the juniper and mesquite samples with different moisture contents. It can be seen that the HHV of the gases increased first when moisture increased from 6% to 12%, and then it decreased as the moisture content increased to 24%. It is because when moisture content increased from 6% to 12%, more combustible gas such as H_2 was produced in the end product gas. While when moisture content increased further, H_2 concentration increased but CO and CH_4 percentage significantly resulting in lowering the gas HHV. As ER increased The HHV of the gas increased as well. This is because higher ER (less air available) more CO and CH_4 were produced in the end product gas.

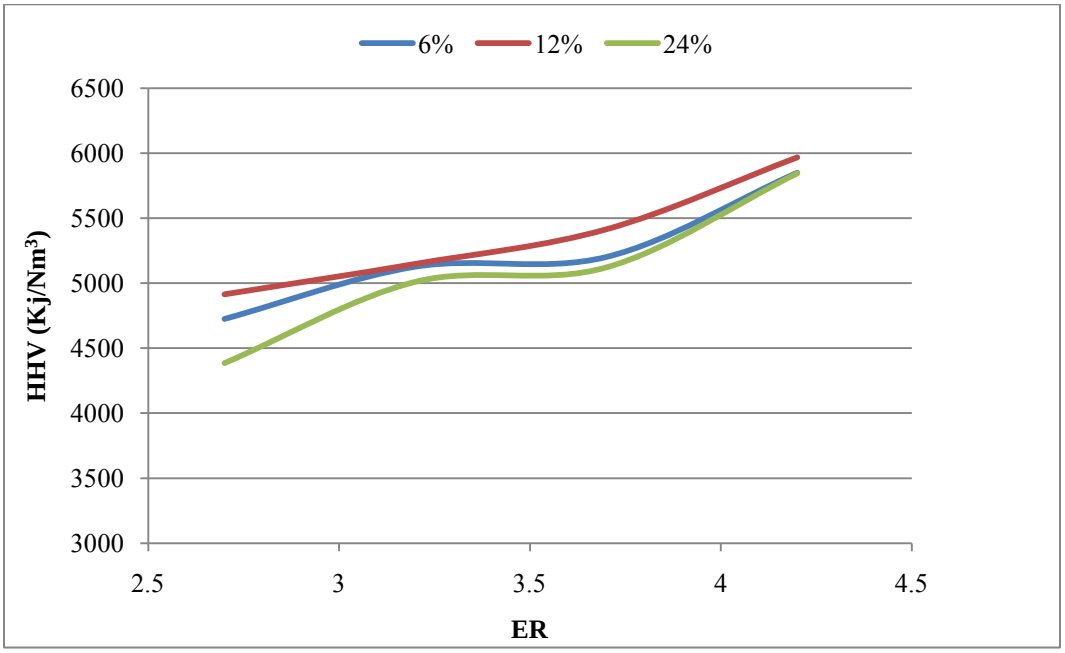

Figure 23. Gas HHV of juniper fuel with different moisture

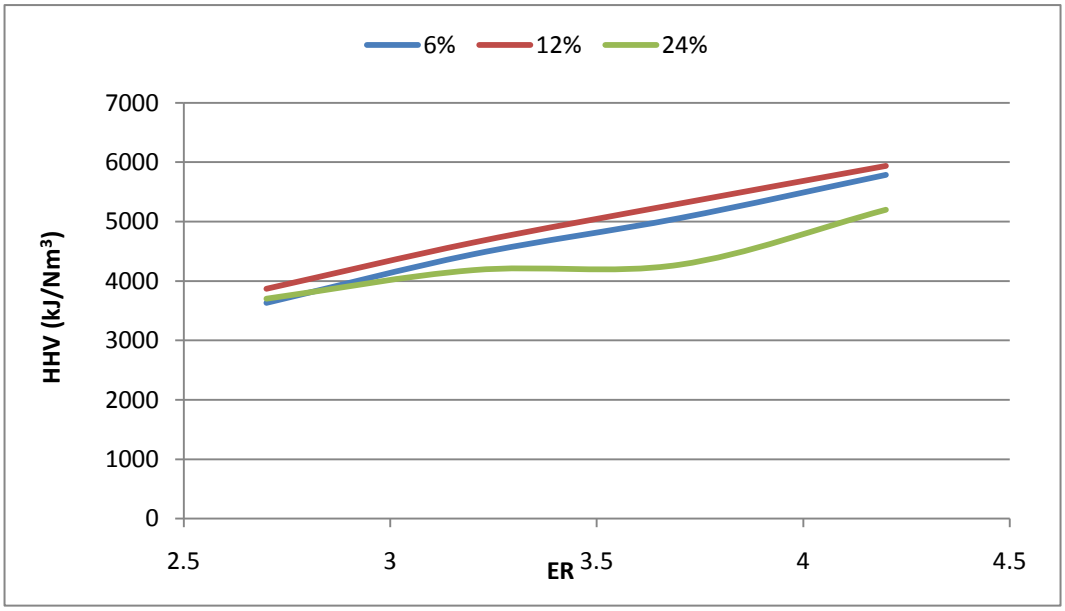

Figure 24. Gas HHV of mesquite fuel with different moisture content

4.2.6 The Effect of Air-Steam Ratios on Gas Composition and Adiabatic Temperature

In this section, the gas concentrations and adiabatic temperature at three S:F ratios (0.15, 0.3, and 0.45) were simulated by using the CEA software. Figure 25 and Figure 26 show the CO_2 concentration for the juniper and mesquite fuel. It is seen that CO_2 concentration increased with the increase of S: F ratio and ER. This is because higher S: F ratio and ER shifted the equilibrium of the water gas reaction (i.e.$CO+H_2O \leftrightarrow CO_2+H_2$) to the direction of formation of CO_2 and thus CO_2 concentration increased. The CO_2 percentage is in a range of 18% - 28% when S: F was between 0.15 and 0.45.

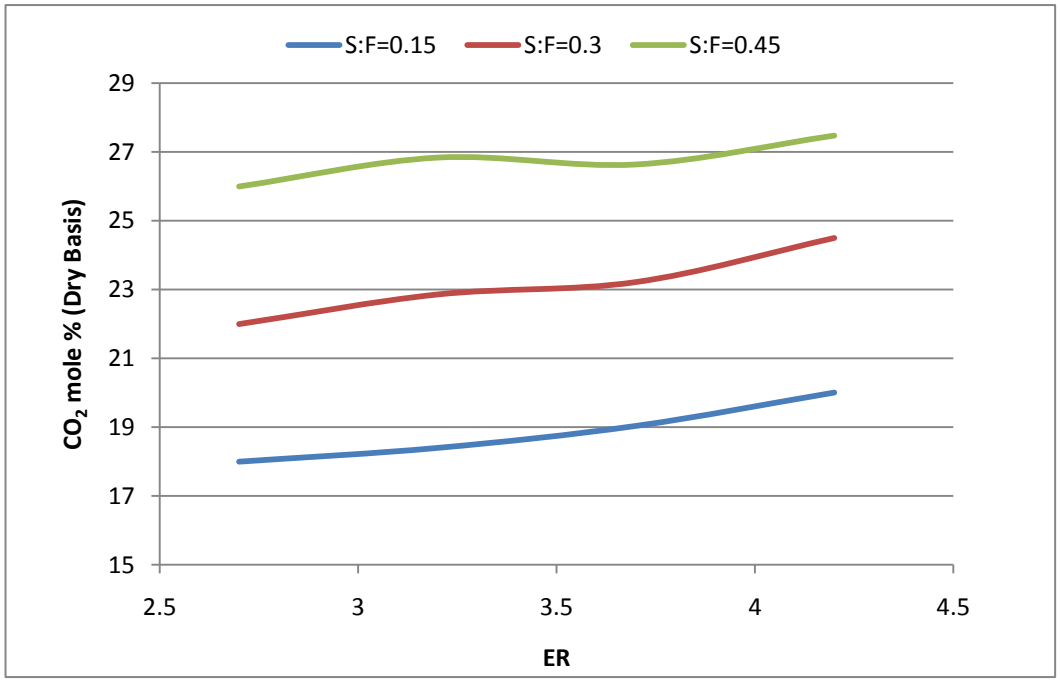

Figure 25. CO_2 mole % vs. ER for juniper fuel at several S: F ratio

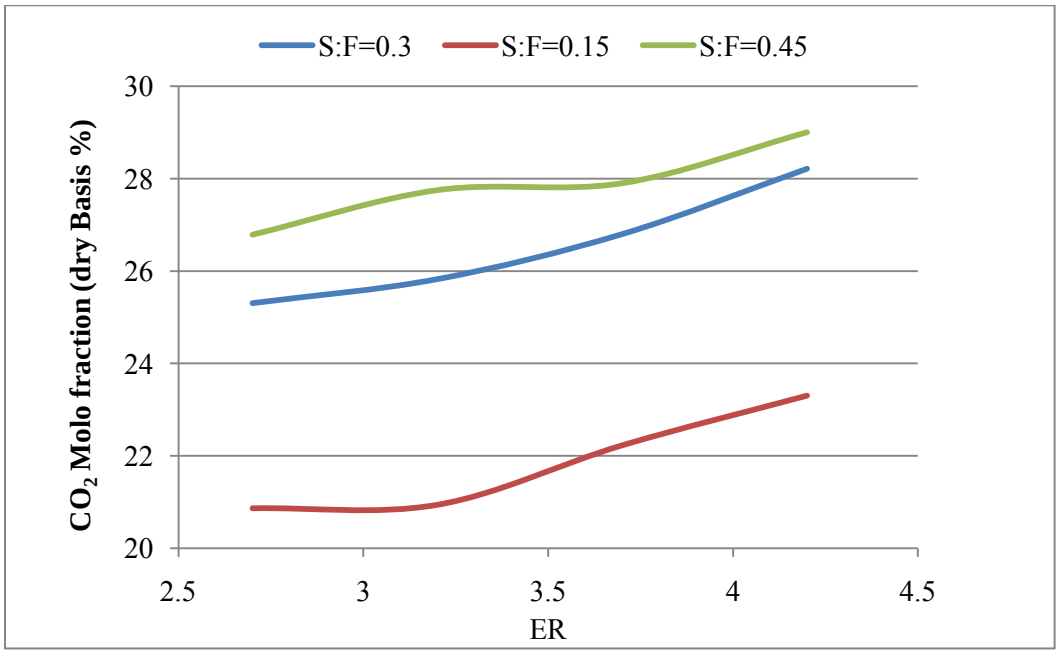

Figure 26. CO_2 mole % vs. ER for mesquite fuel at several S: F ratio

Figure 27and Figure 28 show the CO concentration VS ER at several S:F ratios. It was found that CO% increased with the decrease of S:F due to the water gas shift reaction. At a constant moisture content , CO % increased first when ER<3.3. When ER > 3.3, CO % decreased slightly due to fact that under steam rich environment CO react with H_2O to form CO_2 and H_2.

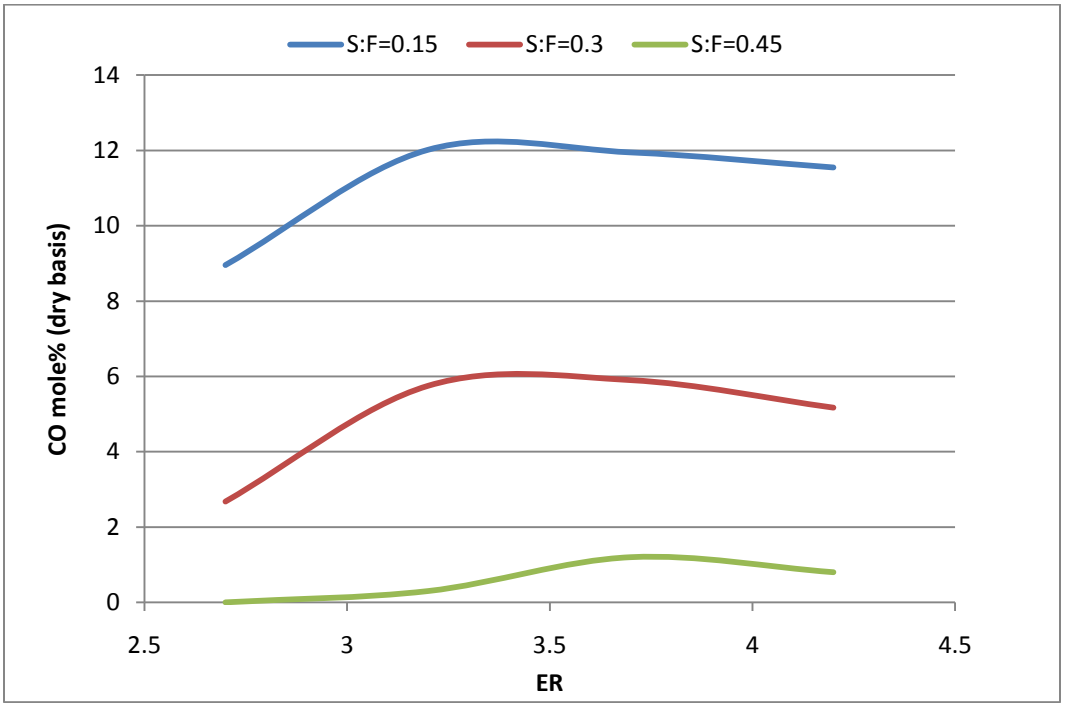

Figure 27.CO mole % vs. ER for juniper fuel at several S:F ratio

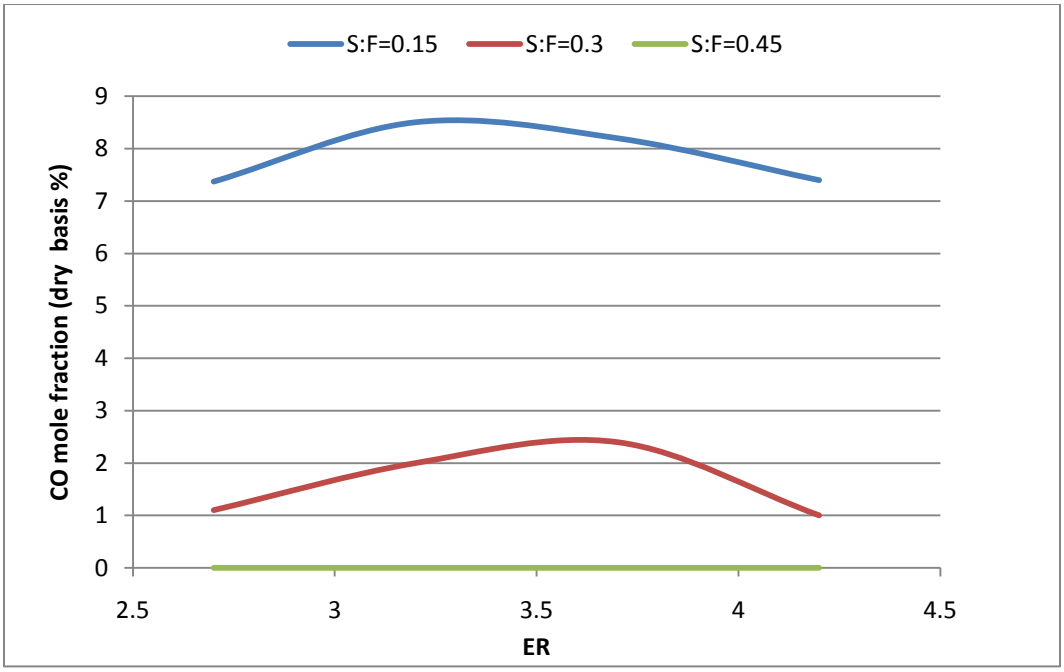

Figure 28. CO mole % vs. ER for mesquite fuel at several S:F ratio

Figure 29 and Figure 30 show the H_2% VS ER at several S: F ratios. It was seen that higher S: F ratio resulted in higher H_2 % because more H was extracted from steam. The H_2 mole % can go up to 35% when the S: F= 0.45. At a constant S: F ratio, the H_2% increased with the increase in ER.

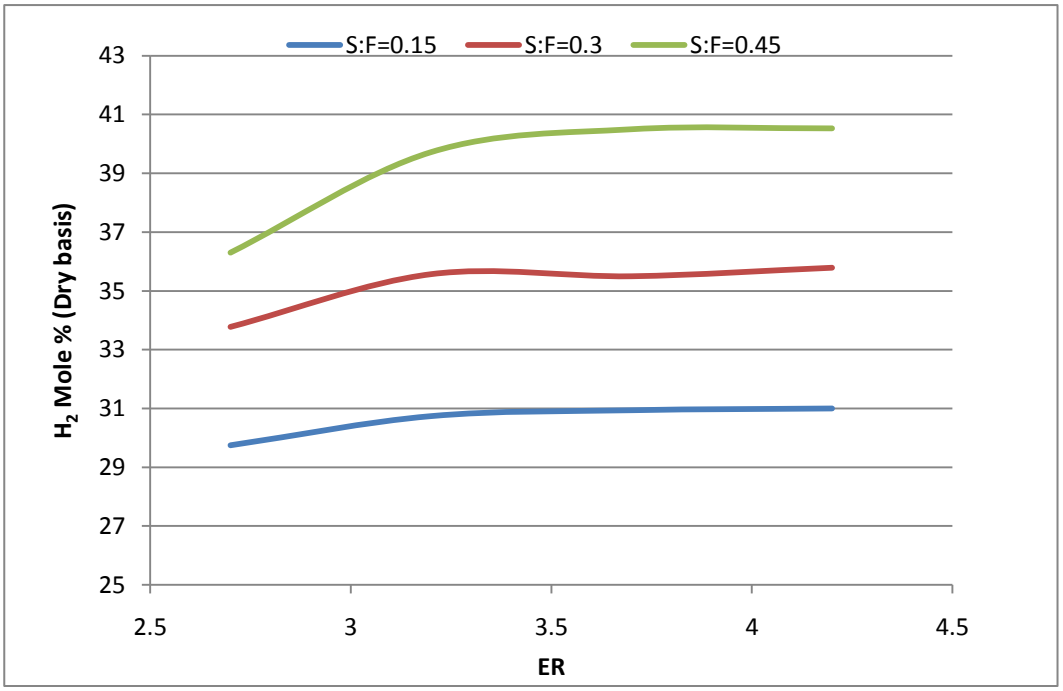

Figure 29. H_2 mole % vs. ER for juniper fuel at several S: F ratio

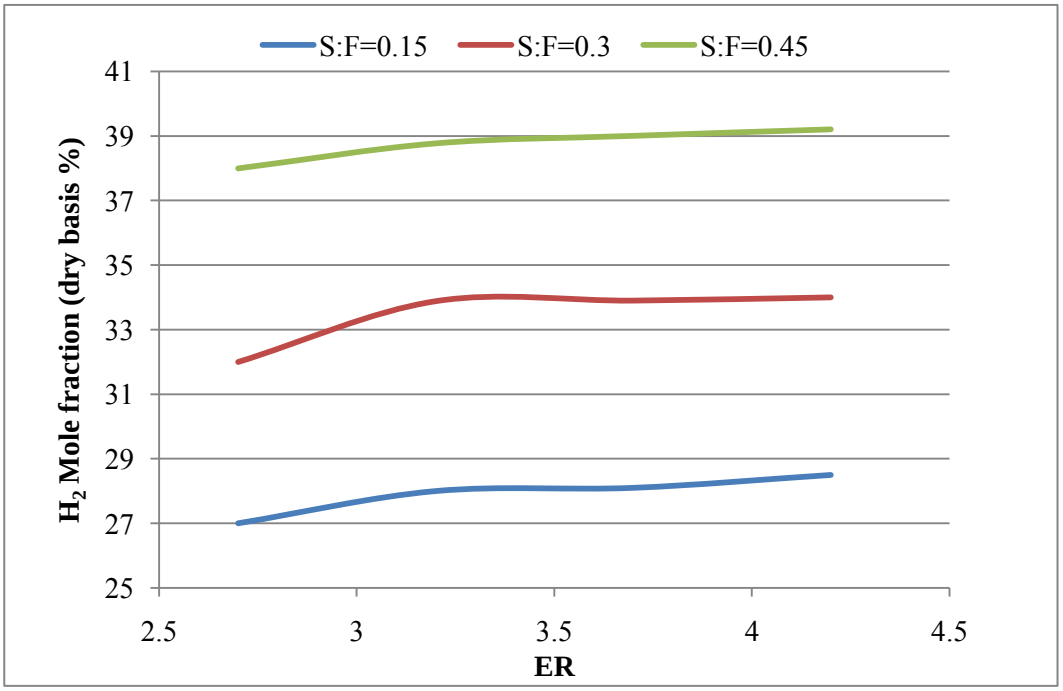

Figure 30. H_2 mole % vs.ER for mesquite fuel at several S:F ratio

Figure 31 and Figure 32give the CH_4 concentration at S:F ratios of 0.15, 0.3, and 0.45. It was found that CH_4 concentration decreased with the increase of S:F ratio for juniper and mesquite fuels. As discussed in the next section, rising of the S:F ratio would lower the adiabatic temperature, and thus CH_4 concentration decreased.

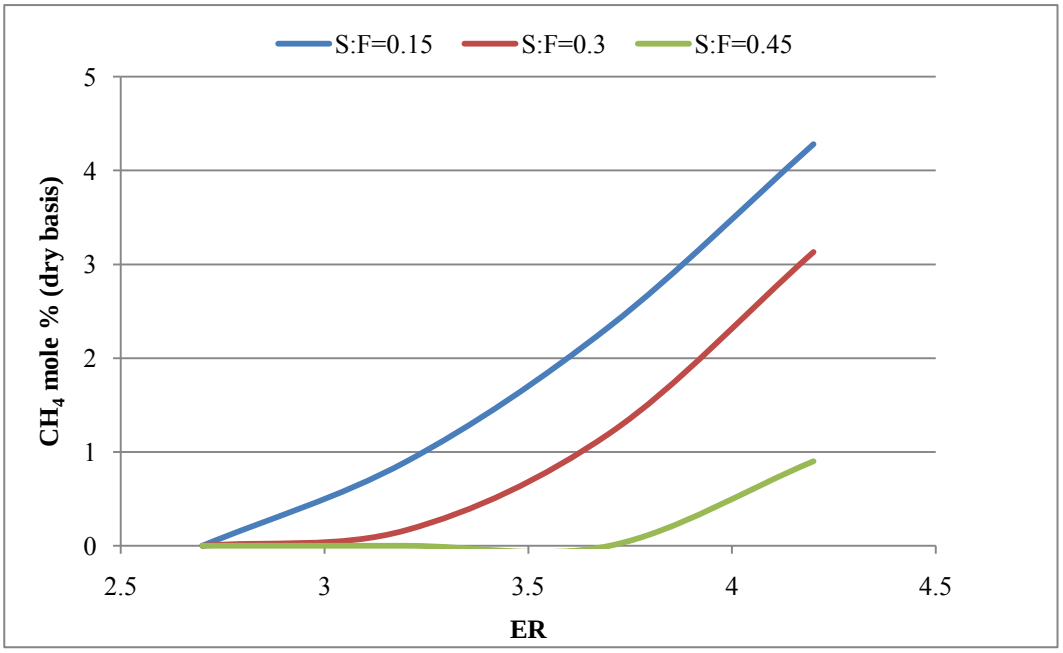

Figure 31. CH_4 of the juniper gas at several S: F ratio

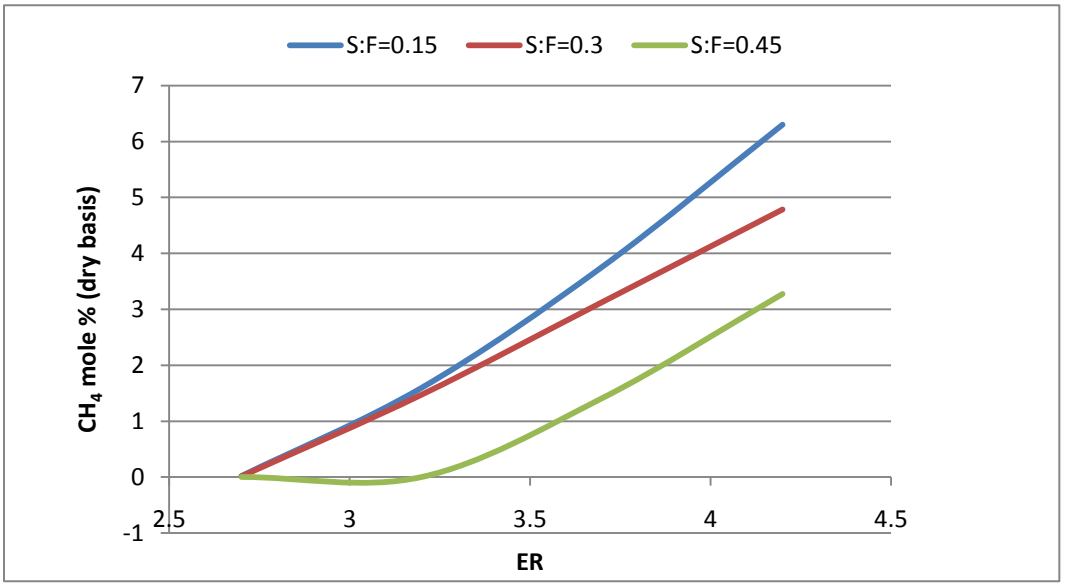

Figure 32. CH_4 of the mesquite gas at several S: F ratio

4.2.7 The Effect of Air-Steam Ratio on Gasification on Adiabatic Temperature

Figure 33 and Figure 34 show the adiabatic temperature for the mesquite and juniper fuel at different S: F ratio. It is seen that the adiabatic temperature decreased with the increase of the S: F because the reaction of the H_2O with char is an endothermic process which would lower the gasification temperature. In addition, the adiabatic temperature decreased with the increase of ER due to less air supplied into the gasifier.

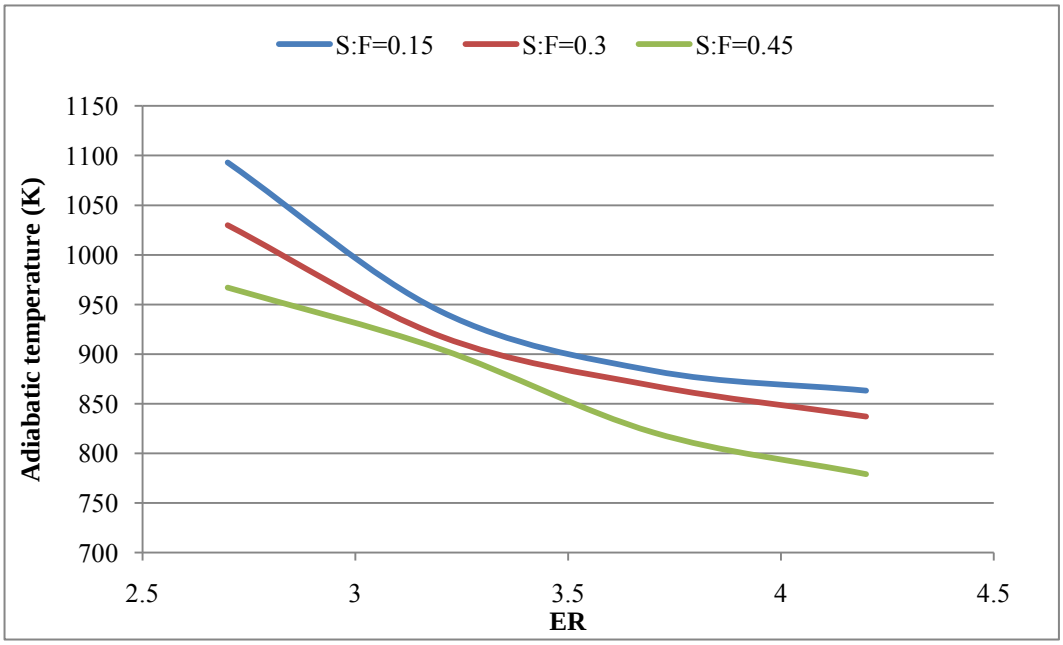

Figure 33. Adiabatic temperature vs. ER for juniper fuel at several S: F ratio

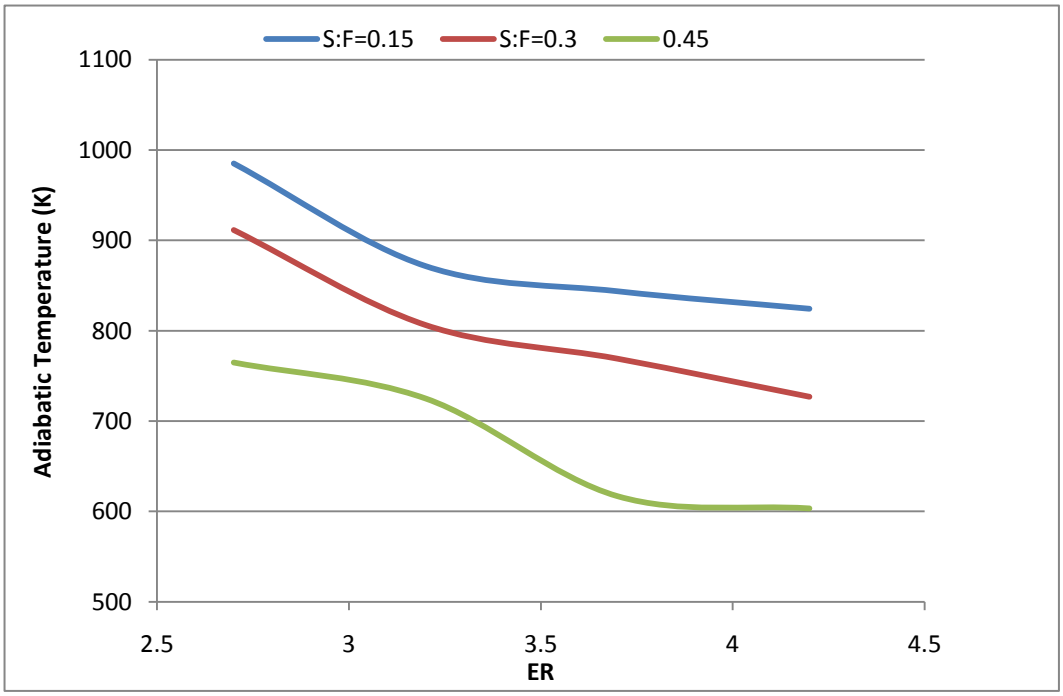

Figure 34. Adiabatic temperature vs. ER for mesquite fuel at several S: F ratio

4.2.8 The Effect of Air-Steam Ratio on Gas HHV

Figure 35 and Figure 36 give the HHV of the juniper and mesquite gas from air-steam gasification at S: F of 0.15, 0.3, and 0.45. It was seen that with the increase of the S: F ratio m HHV of the juniper and mesquite gas decrease. This is because even though the H_2 concentration increases at high S: F, CO percentage decreased significantly and CO_2 percentage increased resulting in reduce of HHV. In addition, at a constant S: F, HHV for both fuel increased due to more combustible gas generated, especially CH4.

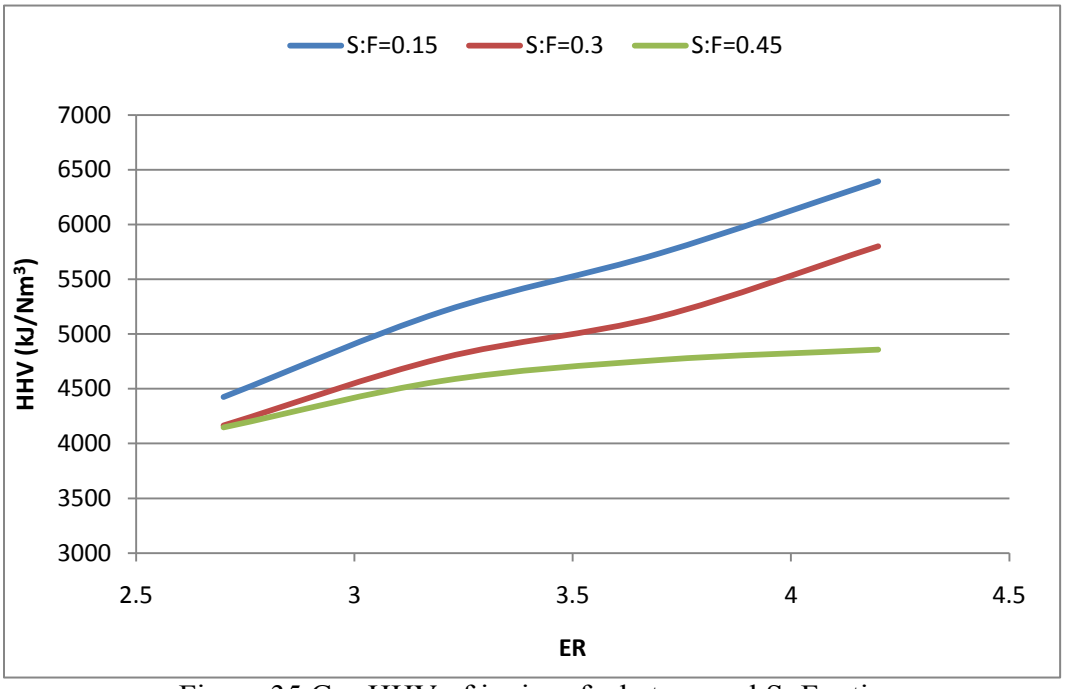

Figure 35.Gas HHV of juniper fuel at several S: F ratio

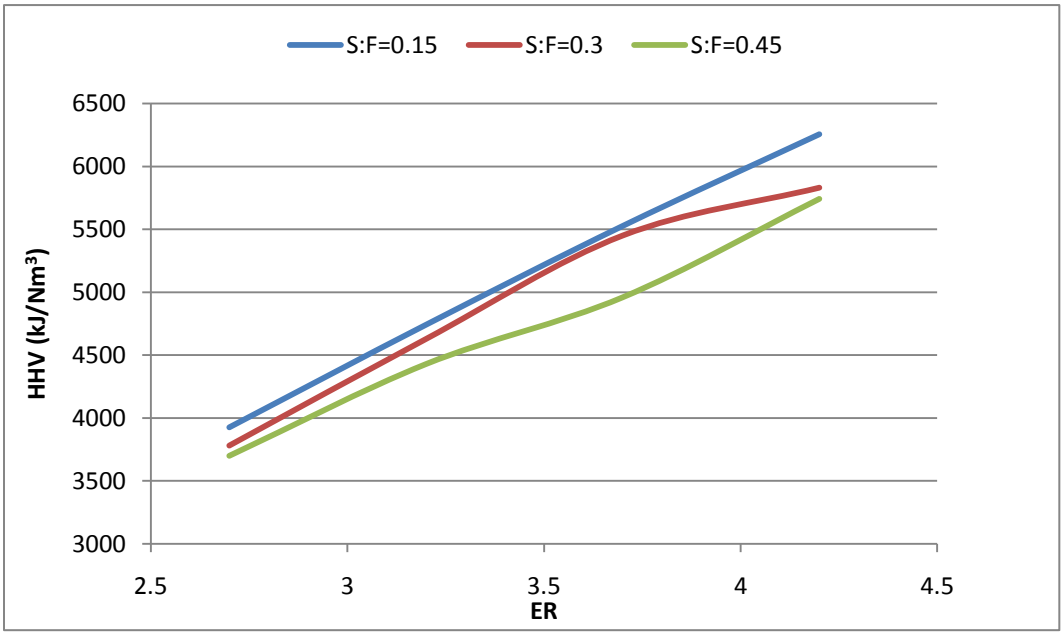

Figure 36.Gas HHV of mesquite fuel at several S: F ratio

5 EXPERIMENTS AND PROCEDURE

5.1 Mesquite and Juniper Harvest

Mesquite and juniper samples were harvested from native rangeland areas in north central Texas near Vernon (annual precipitation 665 mm). Trees were 3-4 m tall and had multiple basal stems. Basal stem diameter ranged from 5-15 cm. Tree ring counts indicated that aboveground portions of these trees were 15 to 35 years old. Tree branches (5-10 cm diameter) were chain sawed down and then passed through a Vermeer wood chipper. Leaf and small twigs were removed from branches before chipping. Chipped material was then passed through a motorized sieve system to separate into different particle sizes. No attempt was made to separate heartwood, sapwood and bark in either species. At the time of harvest, fresh wood moisture content was between 35-45 % [Ansley, unpublished data]. During the chipping and sieving process, wood moisture content declined to between 10-20 %. Wood chips were subsequently stored in cellulose bags and transferred to College Station for gasification experiments.

5.2 TGA/DSC Facility and Procedure

All thermal decomposition tests were performed using a TA Instruments Q600 thermal analyzer. Thermogravimetric Analysis (TGA), ± 1% accuracy, as well as

Differential Scanning Calorimetry (DSC) measurements can be conducted using the Q 600 thermal analyzer.

Setup of the thermal analyzer was show in Figure 37. A 120 V, 60 hz power connection was required as well as an ethernet connection to a computer. Other required connections were for carrier gases and purge gas. N_2 was used as carrier gases for pure pyrolysis and air for oxidation and kinetics studies, regulated below 20 psi as required by the manufacturer. The purge gas used was air, which is used to cool the furnace after testing[53].

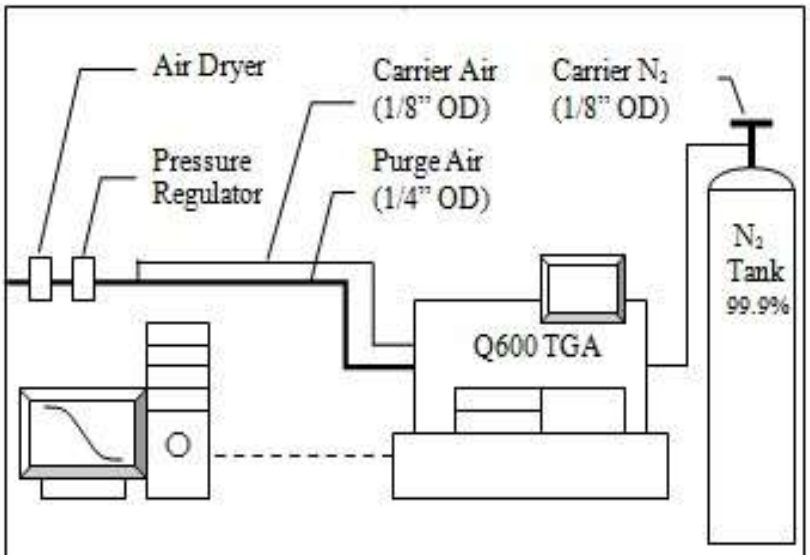

Figure 37. Schematic of TGA and connections[53]

Measurements were made using TA Instruments software, and equipment calibration was performed by TA instruments personnel during the software installation prior to the beginning of testing. The Q600 has a wide range of test parameters that can be tuned for a particular test or adjusted as independent variables during testing[53]. For

the tests being conducted, temperature, time, particle size, and sample composition are considered independent variables, while weight and heat flow are dependent variables[53]. Other possible variables include initial temperature, final temperature, heating rate, carrier gas flow rate, and sample size, which were held fixed during testing [53].

5.2.1 Test Procedure

The test procedure for the mesquite and juniper pyrolysis is the same as that given in Martin thesis for coal and animal waste analysis[53].

Software

The software package included with the thermal analyzer was a windows based program that allowed for easy changes to the test procedure. A typical test procedure was as follows:

1. Select Gas (1 for N_2)
2. Set Gas Flow Rate to 100 ml/min (0 – 1050 ml/min)
3. Heat at 20 K/min (0 – 100 K/min)

Hardware

The TGA had to be preheated if it had been an idle; this was done by heating the furnace to 1273 K and cooling without a sample[53]. The sample cups were alumina and had a 90 μl capacity (Figure 38). To begin testing, the furnace was opened, and the

sample cups checked for any residual material and cleaned if necessary. The furnace was then closed to tare the balances. The Q600 had a dual beam balance capable of measuring up to 350 mg each. After tarring, the furnace was opened and the test cup was removed, noting the orientation before removal. The test cup was nearest the front of the machine; the other cup was a reference cup used for heat flow calculations (DSC).

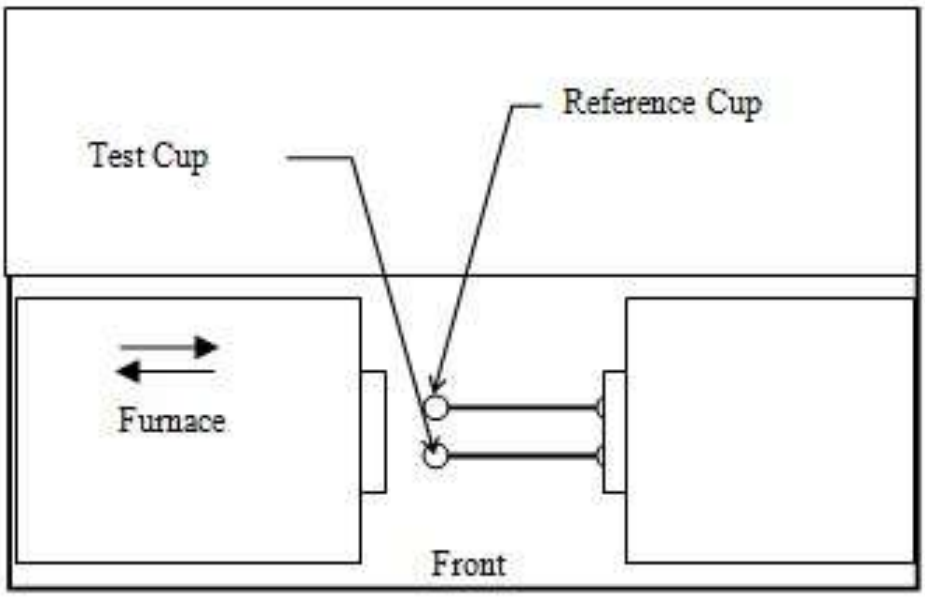

Figure 38. Balance of schematic. Adapted from[53]

Once removed, around 10-12 mg of the fuel sample was added to the cup, ensuring that no excess material was on the top or exterior of the sample cup. These could damage the platinum thermocouples embedded in the balance at the bottom surface of the cups. The sample cup was replaced in the same orientation, and the furnace closed to begin testing.

5.2.2 Sample Preparation

About 60 g mesquite and juniper samples (as received) were first crushed into small size powder by using the grinder as shown in Figure 39. These powders were then sieved by six standard screens corresponding to sieve opening size of 150, 300, 580, 1191, 2000 and 2300 µm. Five different sized particles (150-300 ***µ***m, 300-580 ***µ***m, 580-1190 ***µ***m, 1190-2000 ***µ***m, and 2000-2300 ***µ***m) were collected for TGA study.

Figure 39. Wood chip grinder

In each experiment, about 10-12 mg fuel sample was heated at a rate of 20 ^{o}C/min from ambient temperature to 1500 ^{o}C in an inert (N_2) environment. The mass of the fuel as a function of temperature was recorded for the trace.

5.2.3 Procedures for TGA Study of Dolomite and Mesquite and Juniper Mixtures

Mesquite and juniper wood chips were first ground into small size. These powders were sieved by a standard screens with open size of 150 micro. The wood powder with size less than 150 μm were collected and mixed with the catalyst for the TGA study.

In these experiments, mesquite and juniper fuels were mixed with, 5%, 10% and 15 wt % dolomite powder. For each TGA experiment, approximately 10 mg of the mixture fuel was heated up to a finial temperature of 1000 ^{o}C at a heating rate 20 ^{o}C/min in an inert atmosphere of nitrogen (500 ft^3/min). The mass of the fuel as a function of temperature was recorded. The liberated gases from the fuel were mixed with the carrying gas nitrogen and sent to a FTIR (MutilGas 2030) through a heated gas transfer line. The heated gas transfer line was maintained at 200^{o}C by an external heater which covers by an insulated stainless steel core flexible house. The liberated gases such as CO, CO_2, NH_3, H_2O, and CH_4 were record to measure their compositions every 20 second by FTIR.

5.3 Gasification Experiments and Procedure

5.3.1 Fixed Bed Adiabatic Updraft Gasifier

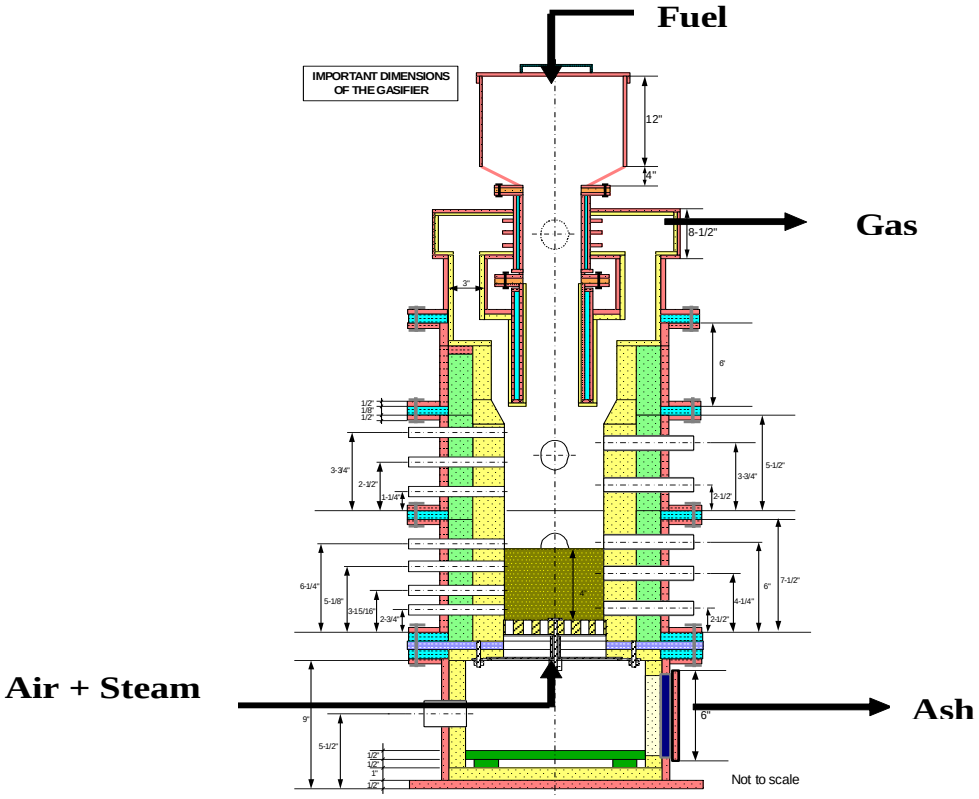

Figure 40. 10 kw fixed bed gasifier.Adopted from [7]

Figure 40 presents a schematic of 10 kW gasifier located at the coal and biomass energy laboratory in mechanical engineering at Texas A&M university [8]. This gasifier as developed by Gerardo [13] did not have tar condensing system. In order to measure to the tar yield from the gasification process, the gasifier facility was modified by fabricating and connecting the three condensers to the gas exhausting system.

Modifications include the following:

a. Three stainless steel condensers were built and connected together
b. Helix shape copper coils were created and inserted into the condensers
c. A thermocouple was mounted at the outlet of the condenser to record the temperature of exhausting gases.

A steam generator was built by Gerardo to obtain vapor required by the gasifier [7]. The steam generator supplied vapor at 373 k and under 1 bar. A release valve was provided to prevent excess pressure and water lever visor was installed to prevent the overpressure and to control the water level. The steam generator was calibrated to determine the rate of evaporation as a function of the power [8].

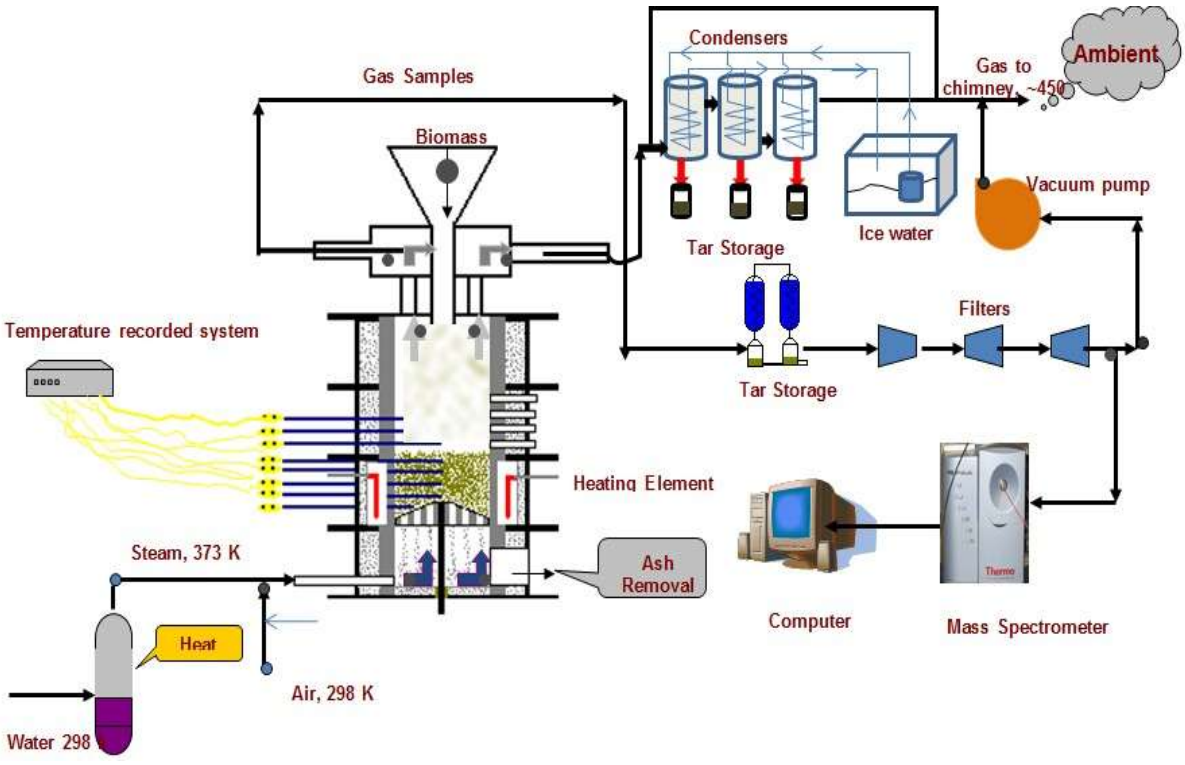

Figure 41.Schematic of gasifier, modified and adapted from [13]

The gasifier (72 cm tall) was divided into four sections which are joined by using ring type flanges of 12.7 x 35.6 x 50.8 mm (Figure 41). The gasifier was constructed of castable alumina refractory tube. The inner and outer diameters of tube are 13.9 cm and 24.5cm, respectively. The tube was surrounded by 4.45 cm insulating blanket in order to minimize heat losses. The layer was then surrounded by a steel outer tube with an inner diameter of 34.3 cm. An ash disposal system is installed to maintain quasi-steady operation. A conical gyratory cast iron grate drilled with large number holes with diameter of 6.4 mm is coupled to a pneumatic vibrator of variable frequency that vibrates the grate in order to dispose the ash continuously from the bed. The rate of ash removed can be controlled by changing the vibration frequency in the vibrator.

5.3.2 Gasification Procedure

5.3.2.1 Experimentation

i) At the beginning of the experiment, the empty bed was preheated to 600 ^{o}C using a propane torch. ii) After the temperature reached 600 ^{o}C, the torch was turned off and biomass samples were gradually added to the gasifier. This addition continued until the bed height of the gasifier reach to 22 cm (8.5 in). iii) Afterwards, the fuel port was closed and air or the mixture of air and steam was sent into this system at the desired rate. iv) Because mesquite and juniper have low ash content (< 3%), the vibrator operated for < 1 minute to dispose the ash from the plenum before it reached steady state. Afterwards, the grate was vibrated over a short period of 5 to 10 s to dispose of the

ash, maintain a constant bed height, and obtain a steady temperature profile within the reactor. v) Air was used as the source of oxygen for gasification. vi) The desired ER can be reached by varying the air flow rate. Fuel was fed at the top of the gasifier while air was supplied from the bottom. As fuels gasified in the reactor chamber, negative pressure was maintained using vacuum fan in order to exhaust the gases from the gasifier.

5.3.2.2 Temperature Measurement

Eight K type thermocouples were located at 2 cm, 4 cm, 7 cm, 10 cm, 13 cm, 20 cm, 24 cm, and 28 cm from the bottom along the gasifier axis to measure the temperature in the gasification chamber. The temperature inside the gasifier was recorded every 60 s into a flash card.

5.3.2.3 Tar Measurement

At the beginning of the tar yield experiments, the gas condensing system valve was first closed and the gases were sucked trough the bypass system. After the experiments reached steady state, the valve of the condensing system was opened and the gas bypass system valve was closed correspondingly. For the condensing system, three condenser units were connected in sequence to ensure the condensation of most of the tar. Helix shaped copper coils were inserted into the condensers, and then the cold water (0 ^{o}C) was pumped into the condensers through the copper coil to cool the high

temperature gas. The gas from gasifer was first passed through a bypass line system. After the experiment reached a steady state condition, the bypass gas line was closed and the producer gas was then passed through the condensers. The gas temperature was measured after the condensing units to make sure that the producer gas was cooled down enough (13-17 ^{o}C) to condense most of the tar. Tar condensed out at the bottom of the condensers, was measured and reported in per Nm^3 (Nm^3, normal, 20 ^{o}C and 101 kpa) of gas produced. Figure 42 gives the detail drawing of the gas condensing system.

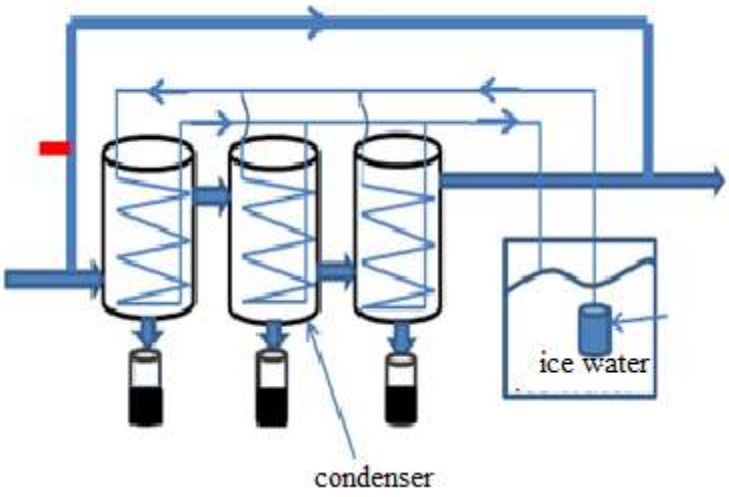

Figure 42.Tar condensing of the gasification system

5.3.2.4 Gas Composition Measurement

A mass spectrometer was used to measure the concentrations of the composition of the product gases. The gas was first passed through a condenser to remove tar and condensable vapors, and then passed through a series of filters to capture associated particles. A small amount of gas was supplied into the gas analyzer. The mass

spectrometer was precalibated using a standard mixture of gas (N_2, CO, CO_2, H_2, C_2H_6 and CH_4) and inert gas (Helium) every three days in order to improve its accuracy.

5.3.2.5 Calibration of Steam Generation

Gerardo[8] have installed a steam generator to supply the steam to the gasifier. The steam generator was first calibrated make sure that the desired flow was supplied to the gasifier. Figure 43 gives the rate of the water evaporated by steam generator vs. the percentage of power supplied to the heater element surrounding the steam generator pipe. In an addition, a transparent glass pipe visor was installed to monitor permanently the level of water in the steam generator. The rate of the steam leaving the steam generator was equal to the rate of water entering during the experimentation. The rate of the water entering the generator and the power supplied to the heater were controlled by using flow meter and a power controller, respectively. Before each experiment, the steady state of the steam generator was verified.

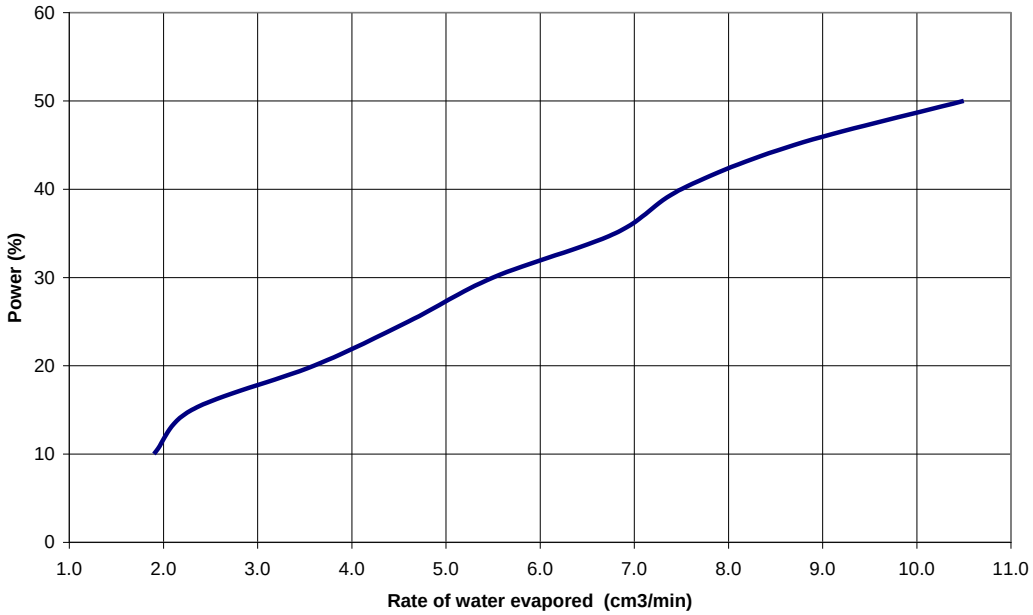

Figure 43.Power supplied in the steam generator vs. vapor produced, adopted from [8]

5.3.2.6 Verification of Adiabaticity of the Gasifier

It is assumed that the system has a uniform temperature distribution. Gerardo [8] have used a lumped capacitance method to estimate the global heat transfer coefficient along the gasifier axis. Taking the the gasifier as control volume and neglecting the temperature gradients within the gasifier, the global heat transfer coefficient of the gasifier was estimated by solving following equation [8]:

$$m_s c_{Ps} \frac{dT_{(X,t)}}{dt} = -UA_S(T_{(X,t)} - T_\infty) \tag{41}$$

Where $T_{x,t}$ denote air temperature along of the gasifier axis, T_{∞} ambient temperature, m_s and $C_{P,s}$ correspond to mass and specific heat of the gasifier respectively, U global heat transfer coefficient, and A_s gasifier surface area.

It was found that the global heat transfer coefficient of the gasifier was very low and it was expressed as: U=3E-0.8 T-9E-06 kw/m^2 K

and thus it was reasonable to assume gasification was under the adiabatic operating conditions [13].

5.3.3 Fuel Proximate Analysis Testing Procedure

A solid fuel is generally comprised of combustibles, ash, and moisture; the combustibles contain fixed carbon (FC) and volatile matter (VM). Proximate analysis provides the composition of a material in terms of moisture, VM, FC, mineral matter and ash, as well as a heating value[24]. Ultimate analysis gives elemental-mass-based compositions including C, H, N, O, S, moisture and mineral matter[24].

In order to test the effect of the sample size on the fuel physical properties, mesquite and juniper fuels were cut into four different sizes: < 2 mm, 2-4 mm, 4-6 mm, and 6-9.5 mm. The proximate analysis was conducted in a 1 kW muffle furnace. This procedure includes four steps.

1. The first step was the sample preparation and moisture content (MC) determination (ASTM D 3173). First, samples were well grounded in a hammer mill and then passed through 2, 4, 6, and 9.5 mm sieves and different sized fuels were collected.

Then, around 5 to 6 g samples of each size were placed the oven with automatic temperature controller set at 105+1 ^{o}C for a minimum of 12 hours until a constant weight (a 0.001g difference) achieved. The initial and final weight of the aluminum pan and fuel were measured using an analytical balance with a sensitivity of 0.1 mg. The moisture content (wet basis) was determined from the following equation:

$$MC_{wb}(\%) = \frac{Initial\ \ Weight - Final\ \ Weight}{Initial\ \ Weight} x100\% \tag{42}$$

2. The second step was to perform the volatile combustible matter analysis (ASTM E 3175). First, muffle furnace were heated to 950 ^{o}C, the preheated crucible containing the dry samples sent into the furnace, then the muffle furnace was purged with nitrogen gas in order to obtain an inert environment. The dry sample was kept in the furnace for 15 minutes. After that, the sample was removed from the furnace 15 minutes after turn off the muffle furnace. The samples were cooled in the desecrator for another 15 minutes and weighed.

3. The third step was ash analysis (ASTM E 1755). At first, recorded the weight of the uncovered crucibles and samples used in volatile matter determination. Then, the crucible was placed in the muffle furnace at 575 ^{o}C for the minimum of 4 hours. Finally, the sample was removed from the furnace and cooled in the desiccator for 15 minutes before weighing.

4. The final step was the fixed carbon calculations. The fixed carbon content can be obtained by subtracting the ash % (d.b) and VM % (d.b.) from100.

6 RESULTS AND DISCUSSION

In this section, fuel properties including proximate and ultimate analyses, TGA testing results, chemical kinetics from the single and parallel reaction model, and gasification results are discussed.

6.1 Fuel Properties

In this section, the proximate and ultimate analyses of the mesquite and juniper as well as the PRB coal fuel are discussed.

6.1.1 Proximate Analysis of the Mesquite and Juniper from ASTM Testing

By using the ASTM testing methods as Hazen laboratory, the proximate analysis of the different sized mesquite and juniper were listed in Table 9 to 11:

Table 9. Moisture content (%) of the mesquite and juniper

Size	< 2 mm	2-4 mm	4-6 mm	6-9.5 mm
Mesquite	7.6	11.2	12.4	13.3
Juniper	9.2	14	13.2	12.6

Table 10. Mesquite proximate analysis % (Dry Basis)

Size	< 2 mm	2-4 mm	4-6 mm	6-9.5 mm
Ash	1.31	1.16	1.38	2.07
Volatile	76.81	78.14	83.91	78.62
Fix Carbon	21.88	20.7	14.71	19.31
Total	100	100	100	100

Table 11. Juniper proximate analysis % (Dry Basis)

Size	< 2 mm	2-4 mm	4-6 mm	6-9.5 mm
Ash	1.1	2.58	1.9	1.8
Volatile	80.83	82.91	76.54	83.64
Fix Carbon	18.07	14.51	21.56	14.56
Total	100	100	100	100

As we can see from the Table 9, the moisture content (M) increases with the sample size for both mesquite and juniper fuels. This is because the ratio of the wood particles surface area to its mass decreases with increase in size. That means, smaller the particle, the easier it was for the M to come out to the surface from the center of the particle. The ash, VM and FC did not vary with fuel sizes. For mesquite, ash content was very low, usually less than 2%, VM was around 78% and FC was close to 19%. This matches the data obtained from the Hazen research Lab. However, fixed carbon and volatile content were different for mesquite and juniper. Mesquite has higher FC while less VM.

6.1.2 Proximate and Ultimate Analysis of the Mesquite and Juniper

There are two types of mesquite fuels (West walker and Agrilife) and two types of juniper fuel (west ranch and copper break). These fuels were cut into small size (less than 2 mm) and sent to Hazen research laboratory for the analyses. Table 12 and Table 13 present proximate and ultimate analysis of mesquite and juniper samples collected from different regions of north Texas. It can be seen from Table 12 that the physical and chemical properties of the two mesquite fuels did not vary much. On dry, ash free basis, Agrilife mesquite may have a slightly higher VM content and less oxygen content. However, the FC content and HHV are almost the same for two fuels.

Table 12.Mesquite fuels proximate and ultimate analysis

	West walker (As received)	Agrilife (As received)
Moisture	10.57	10.86
Ash	3.14	3.19
VM	69.76	70.63
FC	16.53	15.32
Carbon	47.94	47.7
Oxygen	33.57	32.28
Hydrogen	5.11	5.17
Nitrogen	0.71	0.72
Sulfur	0.07	0.08
HHV (kJ/kg)	17422	20191
	Dry, Ash Free	
Moisture	0	0
Ash	0	0
VM	80.84	82.17
FC	19.16	17.83
Carbon	55.56	55.51
Oxygen	37.61	37.54
Hydrogen	5.92	6.02
Nitrogen	0.83	0.84
Sulfur	0.08	0.09
HHV (kJ/kg)	20191	19902
Volatile HHV (kJ/kg)$^{+}$	17210	17111
Chemical formula	$CH_{1.2675}O_{0.5256}N_{0.0127}S_{0.0005}$	$CH_{1.2888}O_{0.5080}N_{0.0129}S_{0.0006}$

From Table 13, It was found that the west ranch juniper have higher VM content while less FC content than copper break juniper. Other elemental analysis was almost the same for both juniper samples. Copper break juniper has a higher HHV than west ranch juniper due to the higher FC content.

Table 13. Juniper proximate and ultimate analysis

	West ranch (As received)	Copper break (As received)
Moisture	22.99	16.91
Ash	1.16	1.12
VM	65.33	67.87
FC	10.52	14.1
Carbon	43.16	46.22
Oxygen	27.89	30.73
Hydrogen	4.65	4.89
Nitrogen	0.11	0.08
Sulfur	0.04	0.05
HHV (kJ/kg)	15687	16998
	Dry, Ash Free	
Moisture	0	0
Ash	0	0
VM	86.12	82.80
FC	13.88	17.20
Carbon	56.89	56.38
Oxygen	36.79	37.54
Hydrogen	6.12	6.02
Nitrogen	0.14	0.1
Sulfur	0.05	0.05
HHV (kJ/kg)	20676	20771
Volatile HHV (kJ/kg)[+]	18728	18279
Chemical formula	$CH_{1.2811}O_{0.4851}N_{0.0022}S_{0.0003}$	$CH_{1.2581}O_{0.4991}N_{0.0015}S_{0.0004}$

[+] Computed using $HV_{vm} \approx (HV - (1-VM)*HV_{FC})/VM$ [24]

In generally, for both mesquite and juniper, the fuel growing areas did not have significant effects on the fuel properties. On a dry ash free (DAF) basis the HHV of mesquite and juniper can reach 20,191 kJ/kg (west walker) and 20,771 kJ/kg (copper break). This is typically constant with DAF heating value of most biomass fuels and animal waste. From the chemical formulas of mesquite and juniper fuels it can be

observed that juniper has a slightly lower O/C ratio than mesquite and as a result, and its HHV is slightly higher. Mesquite and juniper are better quality fuels with higher HHV compared to cattle manure FB which has more than 14.5%-45% (depending on collection methods) ash content and low HHV (12843 kJ/kg) [54]. The nitrogen (N) in juniper is significantly lower compared to mesquite, thus juniper is expected to release less NOx compared to mesquite. Mesquite is a legume that fixes its own N and would be expected to have higher N. Juniper is known to accumulate nutrients from grass areas in interstitial spaces between juniper plants [55] but this process did not increase wood N content over that of mesquite. Bituminous coal has approximately 30%-40% VM and lignite has approximately 40%-50% VM. However, both mesquite and juniper have almost twice the VM of coal, but HHV of both is less than that of coal. From the above information, under pure pyrolysis almost 80% of the DAF biomass of both mesquite and juniper is released as gases while coal can only release 40-50% as gas. Gas yield during gasification is typically higher for woody biomass compared to coal.

In this project, the Agrilife mesquite and Copper breaker juniper were used for gasification study.

6.1.3 Wyoming Powder River Basin (PRB) Coal Properties

The mesquite fuel with size of 2-6 mm was blended with 10% and 20% Wyoming Powder River Basin (PRB) coal for gasification experiments. Table 14 gives the proximate and ultimate analysis of the agrilife mesquite and Wyoming PRB coal. From

Table 14, It can be found that the mesquite fuel had very high VM content (>80%) while volatile matter of the PRB coal was less 50% under DAF basis, which means less gas would liberate from PRB coal during the gasification process. However, the FC (DAF basis) for the Wyoming coal is significantly higher than that of mesquite. Higher C element means more C is available to fom the gas such as CO_2, CO and CH_4 which can lead to high T_{peak}, and thus HHV of the gasification gas is correspondingly higher. It can be also seen from Table 14 that C/O ratio for the PRB coal is 4.12 while only 1.48 for mesquite fuel, and thus the HHV of the PBR coal is much higher than that of mesquite.

Table 14. Mesquite fuels and Wyoming PRB coal proximate and ultimate analysis

As received	PRB	Mesquite
Moisture	32.88	10.86
Ash	5.64	3.19
VM	28.49	70.63
FC	46.52	15.32
Carbon	47.94	47.7
Oxygen	33.57	32.28
Hydrogen	2.73	5.17
Nitrogen	0.66	0.72
Sulfur	0.27	0.08
HHV (kJ/kg)	18193	20191
	Dry, Ash Free	
Moisture	0	0
Ash	0	0
VM	46.34	82.17
FC	53.66	17.83
Carbon	75.67	55.51
Oxygen	18.36	37.54
Hydrogen	4.44	6.02
Nitrogen	1.07	0.84
Sulfur	0.45	0.09
HHV (kJ/kg)	29593	19902

6.1.4 Properties of Dolomite

The dolomite was ordered from C.B Chrystal.inc. The chemical and physical properties of dolomite were listed as in Table 15.

Table15. Chemical composition (wt. %) and physical properties of dolomite[provided by C.B Chrystal.inc]

Chemical specification :		
CaCO3	55.00%	
MgCO3	43.00%	
SiO2	0.70%	
Al2O3	0.20%	
Fe2O3	0.30%	
Moisture	0.10%	
Physical Specification		
+140 Mesh	425 Micron	0.10%
+100 Mesh	150 Micron	1.50%
+200 Mesh	75 Micron	17.00%
+ 325 Mesh	44 Micron	40.00%
Thru 325		60%
Density	70-80 lb/cu ft	

6.2 Kinetics of Pyrolysis TGA/DSC for Mesquite and Juniper Fuel

6.2.1 Theory of the Reaction Models

In this section, three different models would be employed to simulate the mesquite and juniper pyrolysis process and the chemical kinetics would be obtained from these models.

6.2.1.1 Single Reaction Model

The first-order one step single-reaction model offers a simple mathematical description of pyrolysis (or thermal decomposition) of biomass. The rate of devolatilization for a first order pyrolysis can be expressed as

$$\frac{dm}{dt}_{v} = -Bm_{v} \quad \exp\left(\frac{-E}{RT}\right) \tag{43}$$

Where: m_v = mass of volatiles remaining in sample (kg)

B = Pre-exponential rate constant (1/min)

E= Activation energy (kJ/kmol)

R= Ideal gas constant (8.314 kJ/kmol-K)

Since that the heating rate (dT/dt=β) is constant, and the equation (43) can be rewritten as follows:

$$\frac{d\ln(m_v)}{dt} = \left(\frac{B}{dT/dt}\right)\exp\left(\frac{-E}{RT}\right) \tag{44}$$

Let: $X = \frac{C}{T}$ Where: $C = \frac{E}{R}$

Then equation (44) becomes:

$$\int_{mo}^{m} d\ln(m_v) = \int_{xo}^{x}\left(\frac{BC}{dT/dt}\right)\frac{e^{-x}}{X^2}dX \tag{45}$$

Integrating and using the following initial conditions:

$$\ln\left(\frac{(m - m_{char} - m_{ash} - m_{H2O})}{m_o - m_{char} - m_{ash} - m_{H2O}}\right) = \left(\frac{BC}{dT/dt}\right)\left[\int_{Xo}^{\infty}\frac{e^{-x}}{X^2}dX - \int_{X}^{\infty}\frac{e^{-x}}{X^2}dX\right] \tag{46}$$

Using a formula to approximate the integral:

$$\ln\left(\frac{\left(m-m_{char}-m_{ash}-m_{H2O}\right)}{m_o-m_{char}-m_{ash}-m_{H2O}}\right)=\left(\frac{BC}{dT/dt}\right)\left[\frac{E_2\left(X_0\right)}{X}-\frac{E_2\left(X\right)}{X}\right] \tag{47}$$

Exponential integrals can be evaluated using the following expressions and approximations in terms of polynomials [24, 56]

$$\mathrm{E}_2\left(X\right)=\left\{\exp\left(-X\right)-X\cdot\mathrm{E}_1\left(X\right)\right\} \tag{48}$$

$$\mathrm{E}_1\left(X\right)=\frac{1}{X\cdot\exp\left(X\right)}\cdot\left(\frac{X^2+a_1\cdot X+a_2}{X^2+b_1\cdot X+b_2}\right) \tag{49}$$

$$where: a_1=2.334733, a_2=0.250621, b_1=3.330657, b_2=1.681534$$

Using the expression for $E_1(X)$, the $E_2(X)$ can also be expressed as:

$$\mathrm{E}_2\left(X\right)=\exp\left(-X\right)\left\{\frac{(b_1-a_1)\cdot X+(b_2-a_2)}{X^2+b_1\cdot X+b_2}\right\} \tag{50}$$

6.2.1.1.1 Single Reaction Model -Conventional Arrhenius Method (SRM-CA)

Equation (47) presents the exact relation between m_v, volatiles remaining at temperature T and heating rate for SRM. The conventional Arrhenius plot of ln (m_v/m_{v0}) vs 1/T for extraction of E and B for the whole domain of pyrolysis is based on further approximations of equation (45) If T>> T_0 (pyrolysis start temperature), then, X<< X_0, and $E_2(X)/X >>>> E_2(X_0)/X_0$ and with equation (48), equation (47) becomes:

$$-\ln\left(\frac{m-m_{char}-m_{ash}-m_{H2O}}{m_o-m_{char}-m_{ash}-m_{H2O}}\right)\approx\left\{\frac{B\,(E/R)}{dT/dt}\right\}\left[\frac{E_2(X)}{X}\right]\approx\left\{\frac{B\,C(X)\;\;(E/R)}{(dT/dt)}\right\}\exp(-X) \tag{51}$$

$$where\;\; C(X)=\left\{\frac{(b_1-a_1)X+b_2-a_2}{X\left(X^2+b_1X+b_2\right)}\right\}$$

$$\ln\left\{-\ln\left(\frac{m-m_{char}-m_{ash}-m_{H2O}}{m_o-m_{char}-m_{ash}-m_{H2O}}\right)\right\}\approx\ln\left\{\frac{(E/R)B\{C(X)\}}{(dT/dt)}\right\}-\frac{E}{\bar{R}T}$$

Let

$$A=\ln\left\{\frac{(E/R)B\{C(X)\}}{\beta}\right\}=\ln\left\{\frac{(E/R)B}{\beta}\right\}+\ln\left\{\frac{(b_1-a_1)X+b_2-a_2}{X\left(X^2+b_1X+b_2\right)}\right\} \tag{52}$$

$$\ln\left\{-\ln\left(\frac{m-m_{char}-m_{ash}-m_{H2O}}{m_o-m_{char}-m_{ash}-m_{H2O}}\right)\right\}\approx A-\frac{E}{\bar{R}T} \tag{53}$$

Figure 44 to Figure 53 show the expected plot of ($\ln(-\ln(m_v/m_o))$) vs 1/T for mesquite and juniper. This approximation works well when $T >> T_o$ or $E_2(x)/X >>> E(x)/X_o$. It is seen that the linearity breaks down at low T. The activation energy E and pre-exponential factor B thus can be determined from the slope and intercept of the of the linear plot $\ln(-\ln(m_v/mv_o)$. The coefficients of the regression (R^2) are between 0.9 and 0.95. Higher R^2 means these linear plots can accurately predict the pyrolysis behavior.

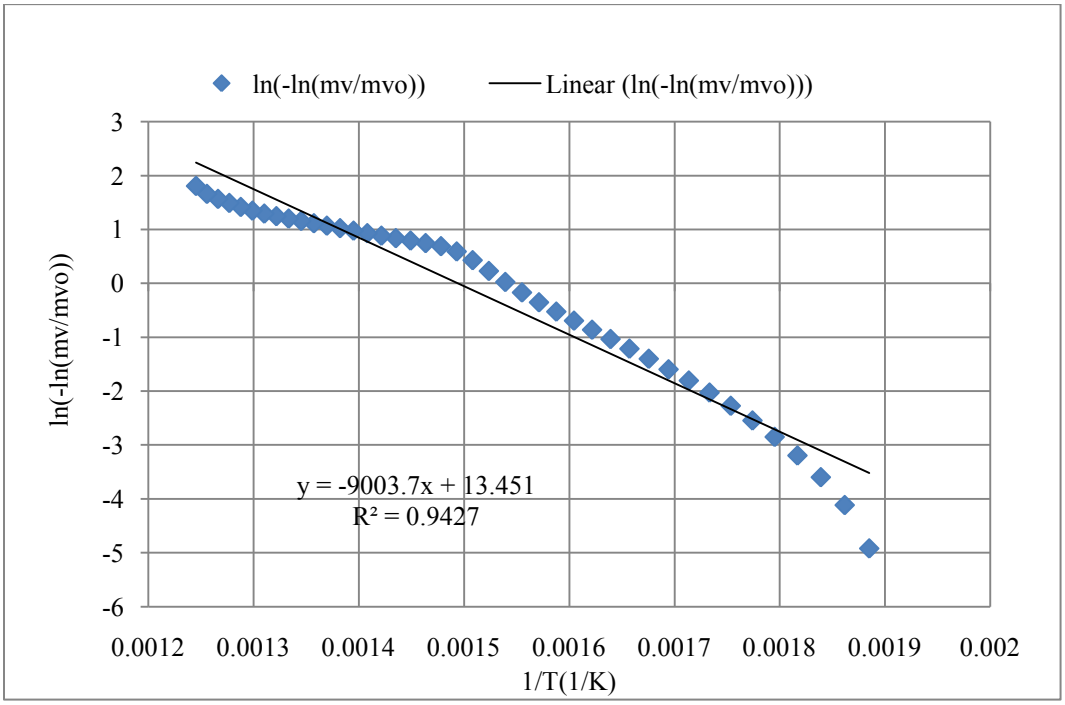

Figure 44. Experiment data vs. linear plot for ln(-ln(mv/mvo)) for juniper fuel of size 150-300µm

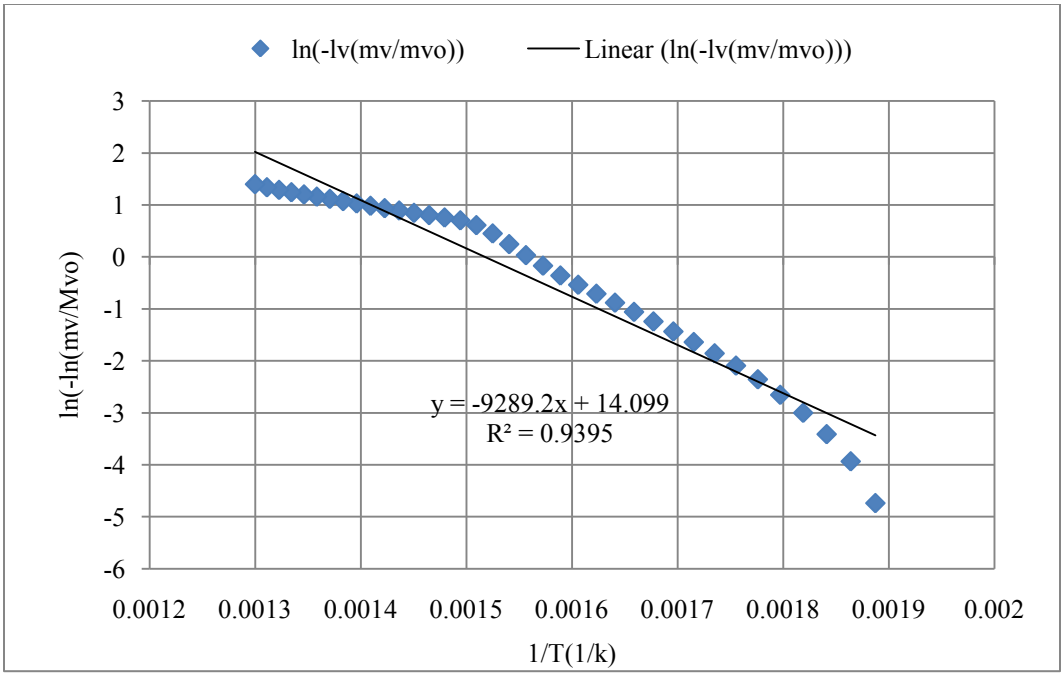

Figure 45. Experiment data vs. linear plot for ln(-ln(mv/mvo)) for juniper fuel of size 300-580µm

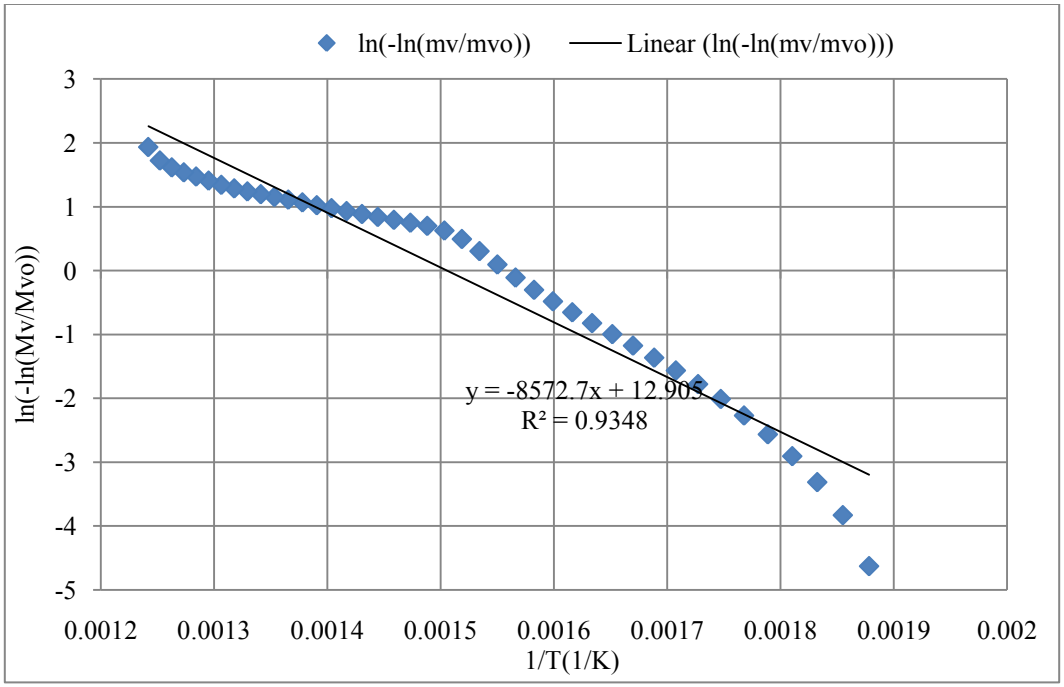

Figure 46. Experiment data vs. linear plot for ln(-ln(mv/mvo)) for juniper fuel of size 580-1190µm

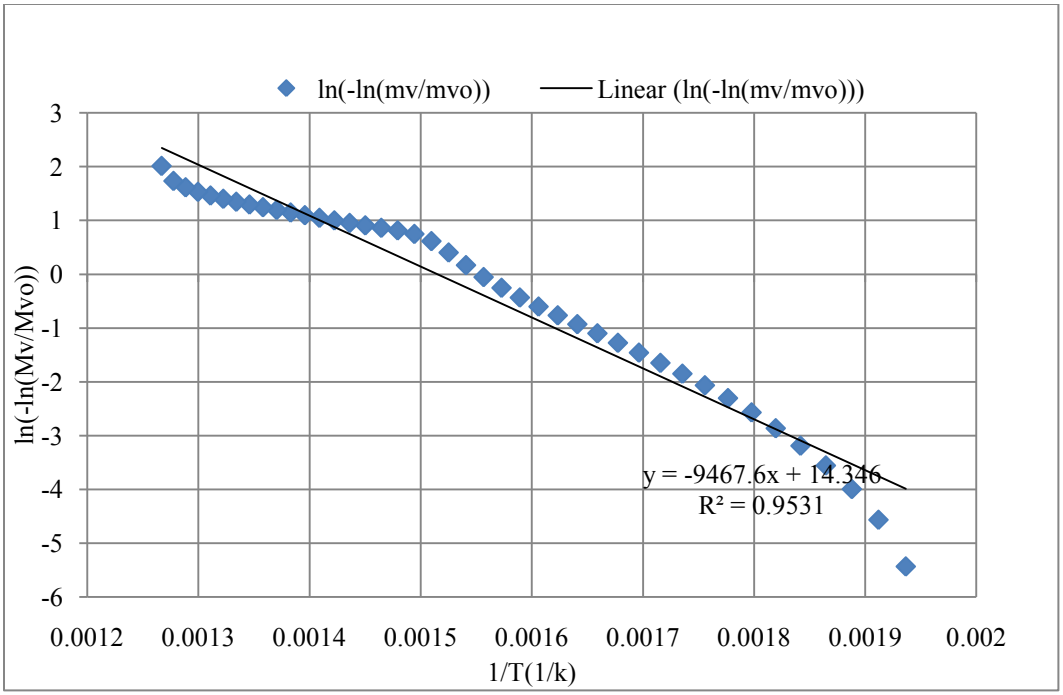

Figure 47.Experiment data vs. linear plot for ln(-ln(mv/mvo)) for juniper fuel of size 1190-2000µm

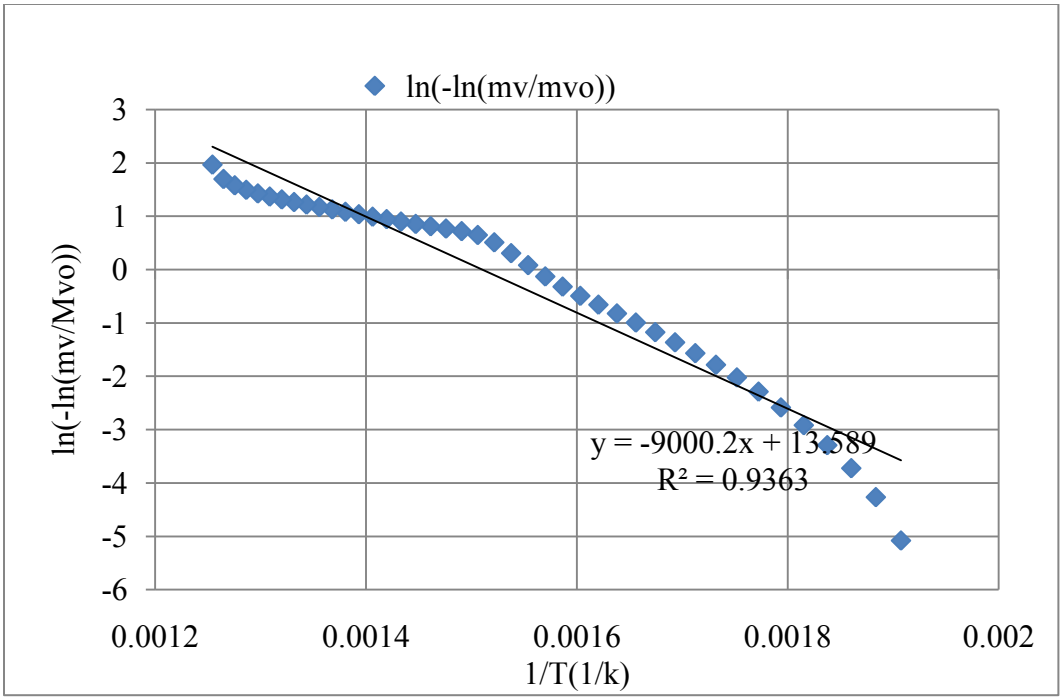

Figure 48.Experiment data vs. linear plot for ln(-ln(mv/mvo)) for juniper fuel of size 2000-2300µm

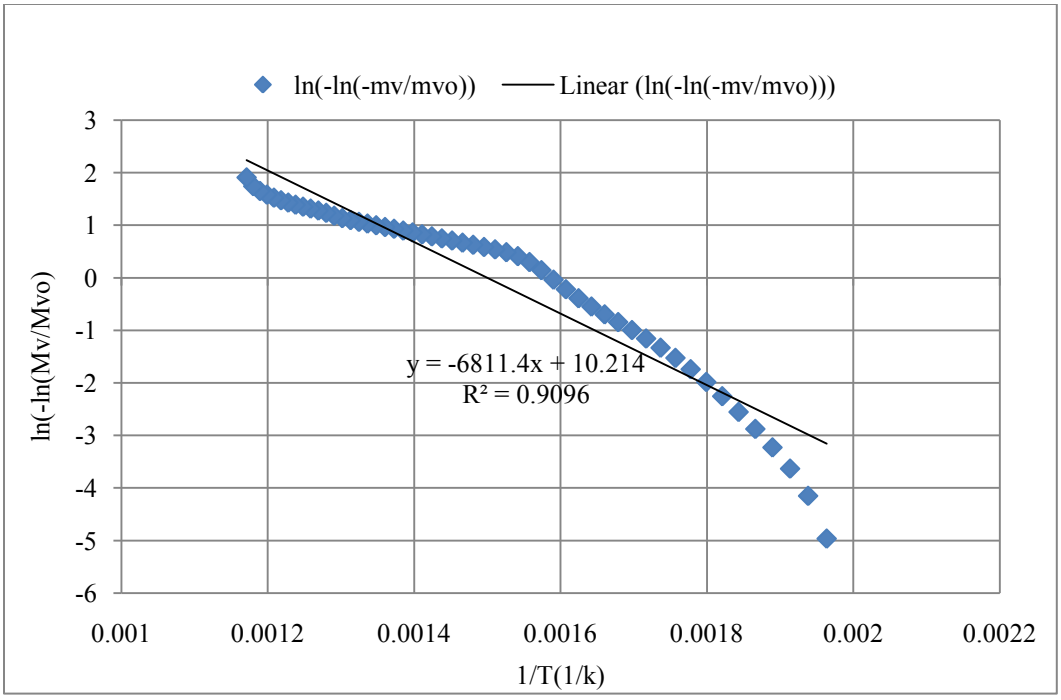

Figure 49.Experiment data vs. linear plot for ln(-ln(mv/mvo)) for mesquite fuel of size 150-300µm

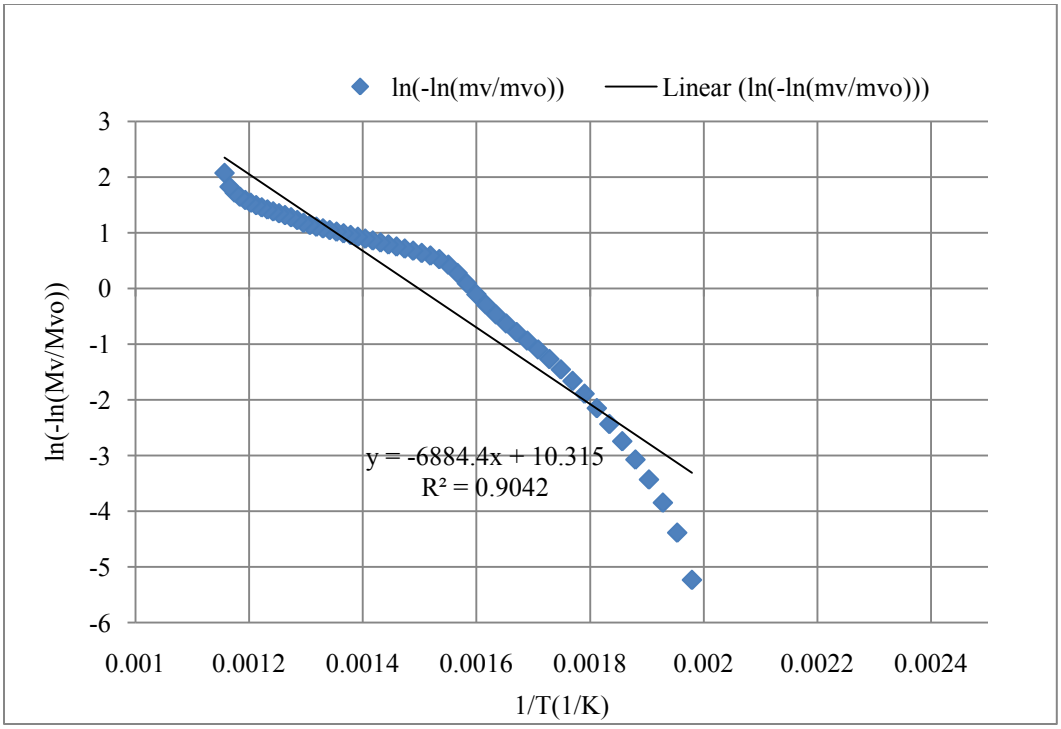

Figure 50. Experiment data vs. linear plot for ln(-ln(mv/mvo)) for mesquite fuel of size 300-580µm

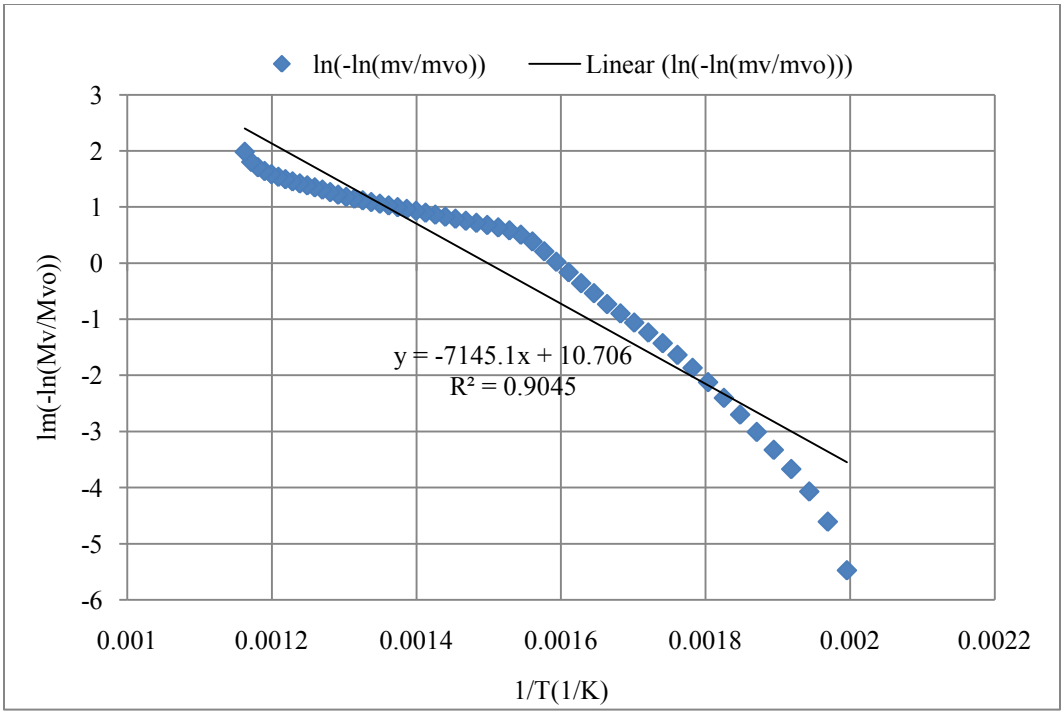

Figure 51.Experiment data vs. linear plot for ln(-ln(mv/mvo)) for mesquite fuel of size 580-1190µm

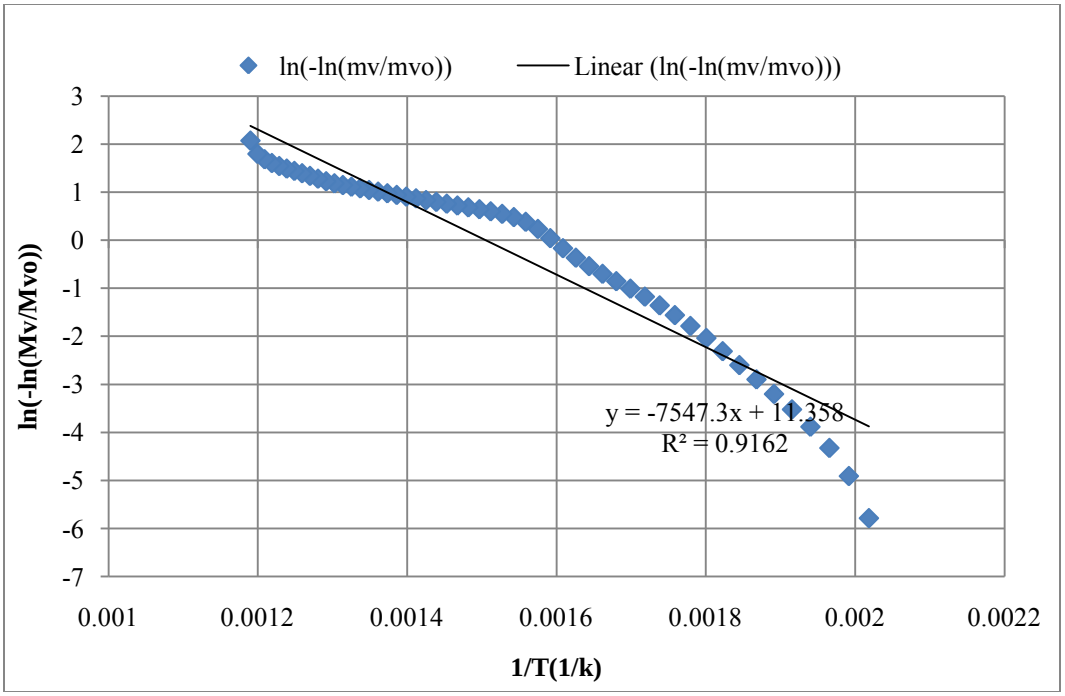

Figure 52.Experiment data vs. linear plot for ln(-ln(mv/mvo)) for mesquite fuel of size 1190-2000 µm

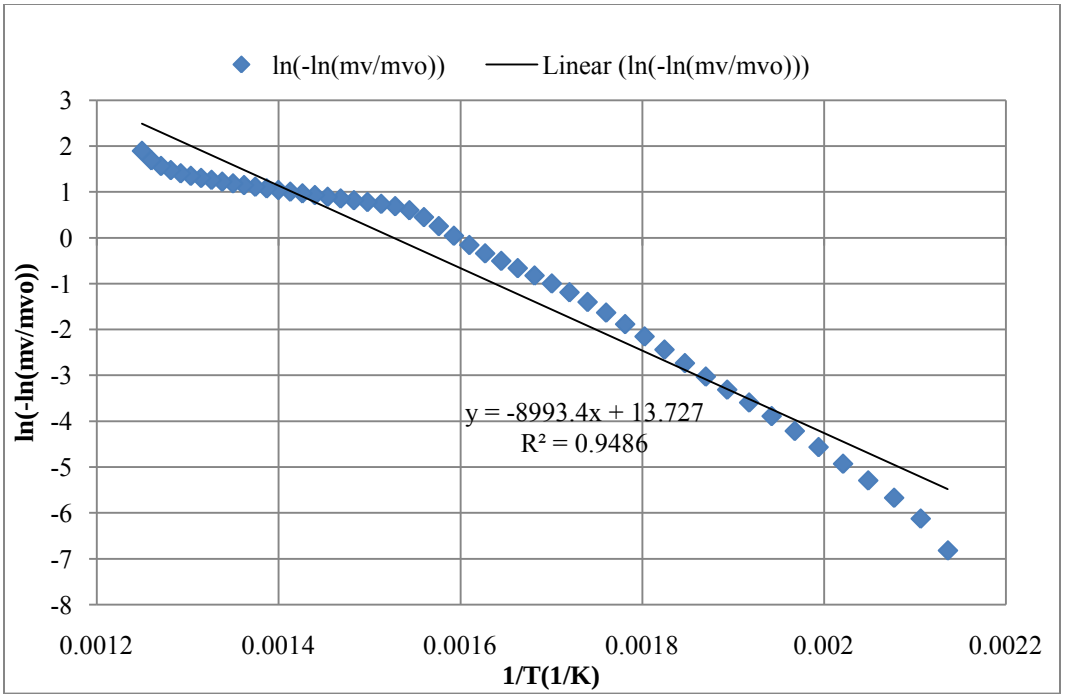

Figure 53.Experiment data vs. linear plot for ln(-ln(mv/mvo)) for mesquite fuel of size 2000-2300µm

6.2.1.1.2 Single Reaction-Maximum Volatile Release Method (SR-MVR)

It is seen from equation (43) that $dm_v/dt \approx 0$ at low temperature since at low T, $E/RT \rightarrow \infty$ and thus $dm_v/dt \rightarrow 0$. At high T, volatile matters $m_v \rightarrow 0$, then $dm_v/dt \rightarrow 0$. Thus, volatile release rate shows a maximum at a particular T_{max}. Considering equation (44) the maximum volatile release rate of volatiles and corresponding temperature T_{max} can also be determined by differentiating equation (43) with T and setting to 0. On simplification,

$$B = \left(\frac{E \cdot \beta}{R \cdot T_{max}^{\ 2}} \right) \cdot \exp\left(\frac{E}{R \cdot T_{max}} \right) \tag{54}$$

Substituting equation (54) into (44) yields:

$$\left(\frac{df}{dt}\right)_{\max} = -\frac{E \cdot \beta \cdot f_{\max}}{R \cdot T_{\max}^{\ 2}} \tag{55}$$

Where $f = \frac{m_v}{m_{v,0}}$ and $m_v = m - m_{char} - m_{ash} - m_{H2O}$

With $X_{max} = E/RT_{max}$, equation (47) can be rewritten as:

$$f_{\max} = \exp\left[\left(\frac{BC}{\beta}\right)\left(\frac{E_2(X_0)}{X_0} - \frac{E_2(X_{\max})}{X_{\max}}\right)\right] \tag{56}$$

Substituting equation (56) into (55) yields:

$$\left(\frac{df}{dt}\right)_{\max} = -\frac{E \cdot \beta}{R \cdot T_{\max}^{\ 2}} \exp\left[\left(\frac{BE}{R^2 \cdot T_{\max}^{\ 2}}\right)\left(\frac{E_2(X_0)}{X_0} - \frac{E_2(X_{\max})}{X_{\max}}\right)\right] \tag{57}$$

Knowing T_{max} and $\left(\frac{df}{dt}\right)_{\max}$ from TGA data, the two unknowns, E and B can be solved from two equations (54) and (57).

6.2.1.2 Parallel Reaction Model (PRM)

The parallel reaction model of Anthony *et al* [38] will be called as the distributed activation energy model in order to avoid confused with the three single reactions proceeding in parallel. The distributed model was employed to determine the kinetics of pyrolysis for mesquite and juniper. Since the activation energy is related to the bound energy, it can be assumed that the pyrolysis process consists of a series of reactions proceeding in parallel [38]. Mesquite and juniper biomass sample are assumed to consist of a series of components with activation energy E ranging from 0 to infinity. If $\delta m_{V,E}$ is the mass change within a short period of time dt having an activation energy between E and E + dE, the rate of liberation of volatiles can be written as:

$$-\frac{d\{\delta m_{v,E}\}}{dt} = k_E \cdot \left(\delta m_{v,E}\right), \tag{58}$$

Where k_E is given by the Arrhenius expression:

$$k_E = k_{0,E} \cdot \exp\left(-\frac{E}{R \cdot T}\right) \tag{59}$$

Where $k_{0,E}$ and E are the pre-exponential factor and activation energy, respectively. R is the gas constant, and T is the absolute temperature. Assuming linear heating rate $\beta = dT/dt$ and rewriting:

$$-\frac{d\{\ln \delta m_{v,E}\}}{dT} = -\frac{k_{0,E}\exp\left(-\frac{E}{\bar{R}\cdot T}\right)}{\beta} \tag{60}$$

Integrating equation (60) with T and with initial condition $\delta m_{v,E,0}$ which represents the initial elemental mass of volatiles having an activation energy between E and E + dE at $T= T_0$.

$$\ln\left(\frac{\delta m_{v,E}}{\delta m_{v,E,0}}\right) = -\int_{T_0}^{T}\frac{k_{0,E}}{\beta}\cdot\exp\left(-E/\bar{R}T\right)\cdot dT \tag{61}$$

Solving for mass loss of those volatile shaving activation energy E,

$$\delta m_{v,E} = \delta m_{v,E,0}\ \ E\exp\left\{-\int_{T_0}^{T}\frac{k_{0,E}}{\beta}\cdot\exp\left(-E/\bar{R}T\right)\cdot dT\right\} \tag{62}$$

Initially the solid fuel consists of volatiles with distributed activation energy. Assuming Gaussian distribution, the fraction of initial total volatiles mass:

$$\frac{\delta m_{v,E,0}}{m_{v,0}} = f\left(E\right)dE \tag{63}$$

Where

$$f(E) = \frac{1}{\sigma\sqrt{2\pi}} \exp\left(-\frac{(E - E_m)^2}{2 \cdot \sigma^2} \right) \tag{64}$$

Where E_m is the mean activation energy, and ζ is the standard deviation of activation energy. For the Gaussian distribution function:

$$\int_0^\infty f(E) dE = 1 \tag{65}$$

The Gaussian distribution indicates that 1 % mass has activation energy within E< Em-2.3σ and 10 % mass lies with E < Em-1.3σ; these values correspond to low activation energy components of the volatiles; The average activation energy at low end is E_{low}= Em-1.8 σ; similarly between 1 to 10 % of mass correspond to high activation energy components with Em+1.3 σ < E < Em+2.3 σ with an average activation energy of E_{high} = Em+1.8 σ. About 99.9% of the mass located within Em-3σ< E< Em+3σ.

Using equation (62) in (63), assuming pre-exponential factors k_0, E are same for all volatiles having activation energy 0 < E< ∞ and equal to k_0, and integrating over all possible value of E will give us the volatile fraction:

$$\frac{(m - m_{char} - m_{ash} - m_{H2O})}{m_o - m_{char} - m_{ash} - m_{H2O}} = \int_0^\infty \exp\left\{ -\int_{T_0}^{T} \frac{k_0}{\beta} \cdot \exp\left(-E/\overline{R}T\right) \cdot dT \right\} f(E) dE \tag{66}$$

Substituting equation (64) into equation (66) yields:

$$\frac{\left(m-m_{char}-m_{ash}-m_{H2O}\right)}{m_o-m_{char}-m_{ash}-m_{H2O}}=\frac{1}{\sigma\cdot\sqrt{2\pi}}\cdot\int_0^{\infty}\exp\left\{-\int_{T_0}^{T}\frac{k_0}{\beta}\cdot\exp\left(-E/\overline{R}T\right)\cdot dT\right\}\cdot\exp\left\{-\frac{\left(E-E_m\right)^2}{2\cdot\sigma^2}\right\}dE, \tag{67}$$

The inner integral of equation (67) can be written in terms of the exponential integrals [54]:

$$\int_{T_0}^{T}\exp\left(-E/\overline{R}T\right)\cdot dT=\left(\frac{E}{\overline{R}}\right)\cdot\left\{\frac{\mathrm{E}_2(X)}{X}-\frac{\mathrm{E}_2(X_0)}{X_0}\right\} \tag{68}$$

$$\mathrm{E}_2(X)=\left\{\exp(-X)-X\cdot\mathrm{E}_1(X)\right\}\cdot$$

$$\mathrm{E}_1(X)=\frac{1}{X\cdot\exp(X)}\cdot\left(\frac{X^2+a_1\cdot X+a_2}{X^2+b_1\cdot X+b_2}\right)$$

Where: $X=\left(\frac{E}{\overline{R}\cdot T}\right), X_0=\left(\frac{E}{\overline{R}\cdot T_0}\right)$ (69)

$$a_1=2.334733, a_2=0.250621$$

$$b_1=3.330657, b_2=1.681534$$

$$\mathrm{E}_2(X)=\exp(-X)\left\{\frac{X^2+(b_1-a_1)\cdot X+(b_2-a_2)}{X^2+b_1\cdot X+b_2}\right\} \tag{70}$$

Substituting equation (68) into equation (67) and rearranging, the mass fraction is now a function of temperature:

$$\frac{m_v(T)}{m_{v,0}} = \frac{1}{\sigma \cdot \sqrt{2\pi}} \cdot \int_0^{\infty} \exp\left\{ -\frac{k_0}{\beta} \cdot \left(\frac{E}{\overline{\overline{R}} \cdot T}\right) \cdot \left\{ \frac{\mathrm{E}_2\left(\frac{E}{\overline{\overline{R}} \cdot T}\right)}{\frac{E}{\overline{\overline{R}} \cdot T}} - \frac{\mathrm{E}_2\left(\frac{E}{\overline{\overline{R}} \cdot T_0}\right)}{\frac{E}{\overline{\overline{R}} \cdot T_0}} \right\} - \frac{(E - E_m)^2}{2 \cdot \sigma^2} \right\} dE \qquad (71)$$

With further rearranging, equation (71) becomes:

$$\frac{m_v(T)}{m_{v,0}} = \frac{1}{\sigma \cdot \sqrt{2\pi}} \cdot \int_{E_m - 3\sigma}^{E_m + 3\sigma} \exp\left\{ -\frac{k_0}{\beta} \cdot \left[T \cdot \mathrm{E}_2\left(\frac{E}{\overline{\overline{R}} \cdot T}\right) - T_0 \cdot \mathrm{E}_2\left(\frac{E}{\overline{\overline{R}} \cdot T_0}\right) \right] - \frac{(E - E_m)^2}{2 \cdot \sigma^2} \right\} dE \qquad (72)$$

Note: the limits of integration have been changed from 0, ∞ to Em ± 3δ [38] which covers 99.9 % of total mass.

$$G(E,T) = \exp\left\{ -\frac{k_0}{\beta} \cdot \left\{ T \cdot \mathrm{E}_2\left(\frac{E}{\overline{\overline{R}} \cdot T}\right) - T_0 \cdot \mathrm{E}_2\left(\frac{E}{\overline{\overline{R}} \cdot T_0}\right) \right\} - \frac{(E - E_m)^2}{2 \cdot \sigma^2} \right\} \qquad (73)$$

G will be represented as a matrix for values of E between Em-3σ and Em+3σ and values of T between T_0 and Tn (beginning and ending of pyrolysis respectively).

$$G(E,T)=\begin{vmatrix} G(E_m-3\sigma,T_0) & \cdots & \cdots & \cdots & G(E_m-3\sigma,T_n) \\ \vdots & & & & \vdots \\ \vdots & & & & \vdots \\ \vdots & & & & \vdots \\ G(E_m+3\sigma,T_0) & \cdots & \cdots & \cdots & G(E_m+3\sigma,T_n) \end{vmatrix} \tag{74}$$

Where $T = T_0, T_0+ \Delta T, T_0+ 2\Delta T, T_0+ 3\Delta T, \ldots. T_n=T_0+ n \Delta T,$

Note that total number of terms in the G matrix will increase as the temperature T is increased. The value for B was set at 1.67×10^{13} (1/sec) from transition state theory [57]. Assuming Em and σ, volatile mass fraction $m_v(T) /m_{v0}$ can now be calculated at a selected T by using G (E,T). Let the error between the calculated and measured $m_v(T)/m_{v0}$ from TGA be ε_j at selected $T= T_j$. The values for E_m and σ were calculated by minimizing the summed squared error $\Sigma_j \varepsilon_j^{\ 2}$ at all selected data points within the domain of pyrolysis.

A spreadsheet program was developed to determine the values of E_m and σ for the most minimum $\Sigma_j \varepsilon_j^{\ 2}$. In the spreadsheet, first the value of E_m is fixed and σ is varied. For a fixed value of Em, there is a value of sigma that will produce the minimum amount of error $\Sigma_j \varepsilon_j^2$. Then E_m is varied and the combination of E_m and σ that produces the minimum error can be determined.

6.2.2 TGA Results

Figure 54 and Figure 55 show the experimental mass loss characteristics of juniper and mesquite for different sized particles. It was seen that weight loss curves did not vary appreciably when the particle size increased from 150-300 μm to 2000 -2300 μm since a low heating rate of 20 ^{o}C/min resulted in lesser temperature gradient within the particles. Juniper started pyrolyzing around 240 ^{o}C and mesquite started at 250 ^{o}C (10 % mass loss). The rapid pyrolysis occurred at the temperatures between 280-500 ^{o}C at which almost 65% weight loss occurred for both samples. These weight losses typically correspond to volatile matter liberation form hemicellulose and cellulose. The volatiles matter continues to be released from the fuel as temperature increases. Pyrolysis of juniper and mesquite ended approximately at 1000 ^{o}C. Only ash and fixed carbon left in the pan after pyrolysis and the weight remained constant.

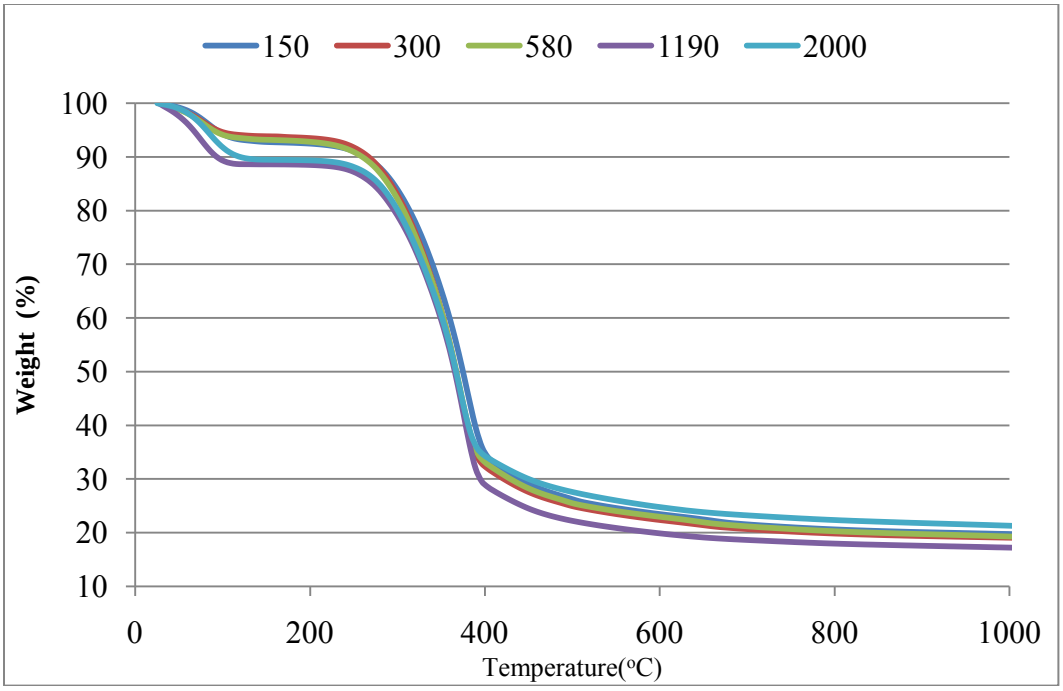

Figure 54. Pyrolysis tracing curves of dry juniper fuels with different sizes (µm).

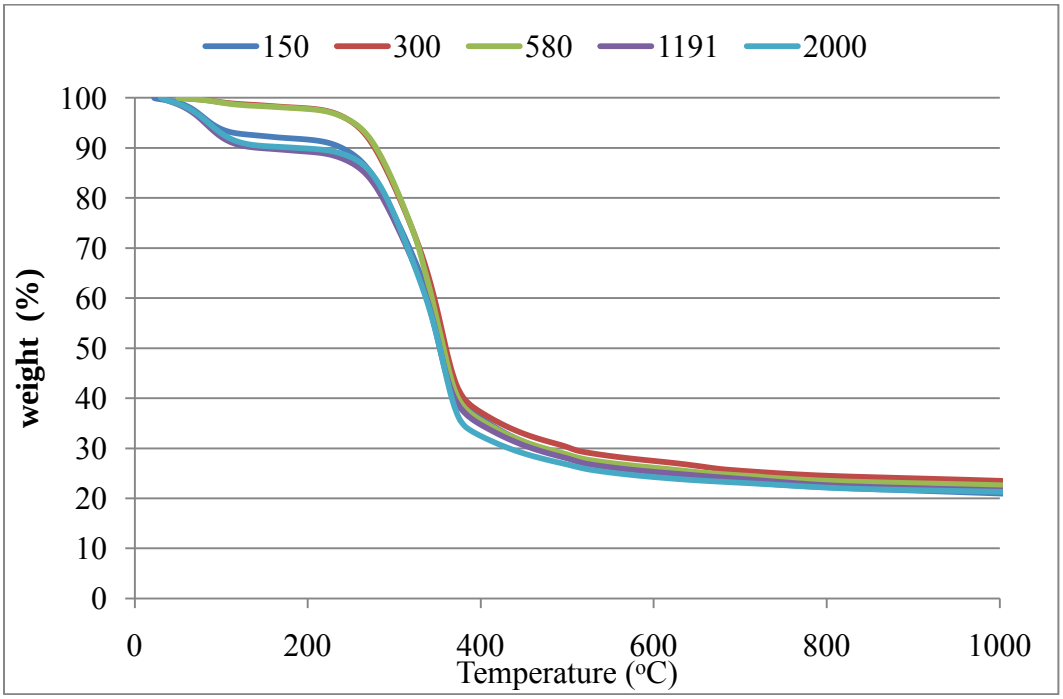

Figure 55. Pyrolysis tracing curves of dry mesquite fuels with different sizes (µm).

Figure 56 and Figure 57 show the mass lost rate (dm/dt) as a function of temperature for juniper and mesquite. It can be found that there were two peaks in the thermal decomposition for both mesquite and juniper samples. The first peak occurred between 30 ^{o}C to 110 ^{o}C. In this process, there was a 10%-12% weight loss for both mesquite and juniper sample which can be attributed to the loss of moisture. Paul et al[58] found that hemicellulose began to thermally decompose at about 250 ^{o}C and main weight loss occurred between 250-350 ^{o}C; Cellulose began to decompose at 325 ^{o}C and main weight loss occurred between about 325-400 ^{o}C ; lignin decomposed at a wide temperature range of 200 -720 ^{o}C [58]. The second weight loss peak occurred between 200 ^{o}C and 400 ^{o}C within which hemicelluloses (HC) and celluloses (C) decomposed and the lighter volatiles released from the samples resulting in almost 50% weight loss.

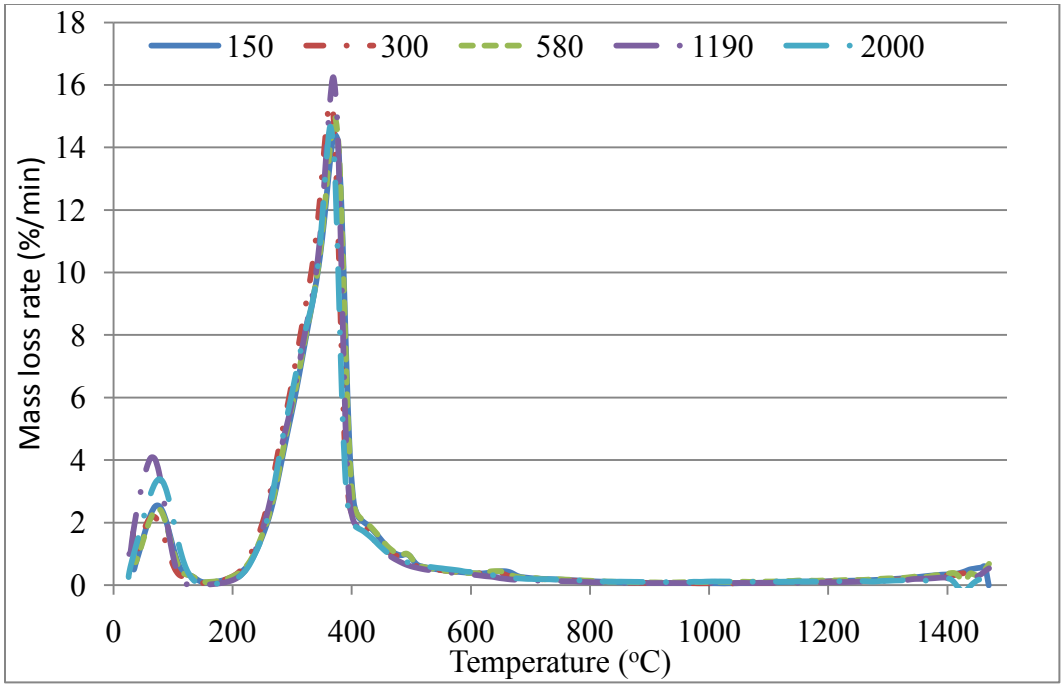

Figure 56. Weight loss rate of different size (**μ**m) juniper samples on N_2 environment

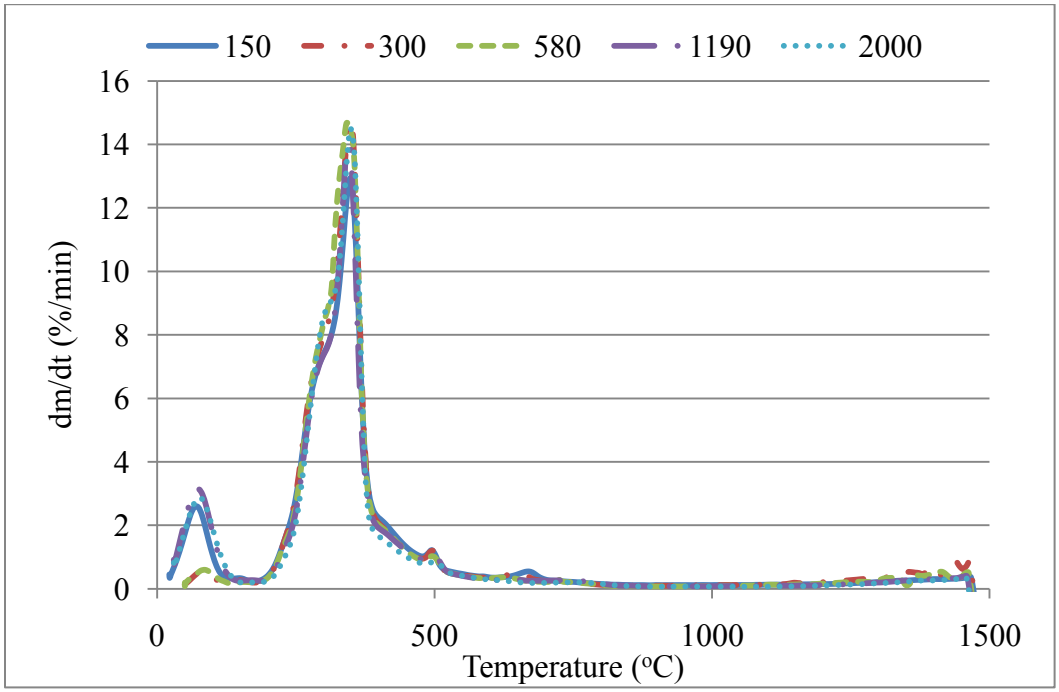

Figure 57. Weight loss rate of different size (**μ**m) mesquite samples on N_2 environment

Figure 58 shows the TGA and DTA traces for juniper fuel with size 1190 µm. The DTA trace presents the temperature difference between the sample in the sample pan and the reference pan ($\Delta T=T_{sample}-T_{reference}$). It is apparent that moisture loss is an endothermic process (phase change from liquid to vapor) from 30 ^{o}C to 110 ^{o}C since DTA curve reveals $\Delta T<0$ (i.e. $T_{sample} <T_{reference}$). When DTA was plotted vs. time (not shown) the area under DTA yields enthalpy change. From 110 ^{o}C to 660 ^{o}C, the DTA curve indicates $\Delta T>0$ implying that heat was released from the fuel due to thermal decomposition of biomass. As the temperature of sample increased beyond 660 ^{o}C, the pyrolysis reactions became endothermic.

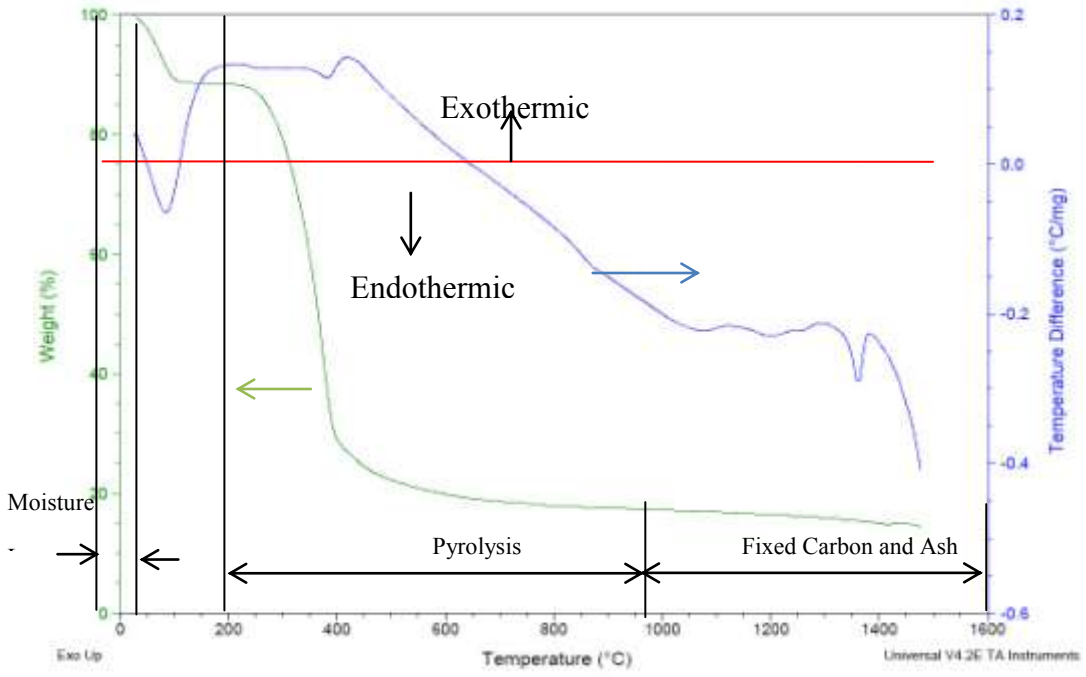

Figure 58. TGA and DTA trace for juniper sample with size of 1190 µm

6.2.3 Kinetics Data

6.2.3.1 Kinetics Data from Single Reaction Model-Convention Arrhenius (SRM-CA)

The SRM-CA method is based on approximation that most of the pyrolysis loss occurs at $T >> T_0$ (initial pyrolysis temperature) and the exponential terms dominate in the second exponential integral. Figure 44 to Figure 53 show the expected plot of ($\ln(-\ln(m_v/m_o))$ vs 1/T for different sized mesquite and juniper fuels. As seen in these figures that the linearity breaks down at low T since the approximation $E_2(X)/X >>> E(X_0)/X_0$ breaks down. The activation energy E and pre-exponential factor B can be determined from the slope and intercept of the of the linear plot $\ln(-\ln(m_v/mv_o)$. The values obtained from the Arrhenius plot are shown in Figure 59 for the mesquite and juniper as a function of T of biomass fuel. The activation energies E for juniper were between 70,000 and 80,000 kJ/kmol, and between 57,000 and 75,000 kJ/kmol for mesquite, depending on the particle size. In addition, juniper samples have higher activation energies than those of mesquite. This is because mesquite is deciduous wood while Juniper belongs to coniferous wood[59, 60]; deciduous wood was found to be much more reactive than coniferous wood because the xylan in hemicellulose of deciduous wood is more sensitive to temperature than the manna found in coniferous wood[61]. The activation energies obtained from Arrhenius plot are much lower than those obtained from parallel reaction model as discussed in detail in the following section. From equation (43) it was found that at a constant weight loss rate (dm/dt), if E is higher and value of B is higher; B is lower if E is lower.

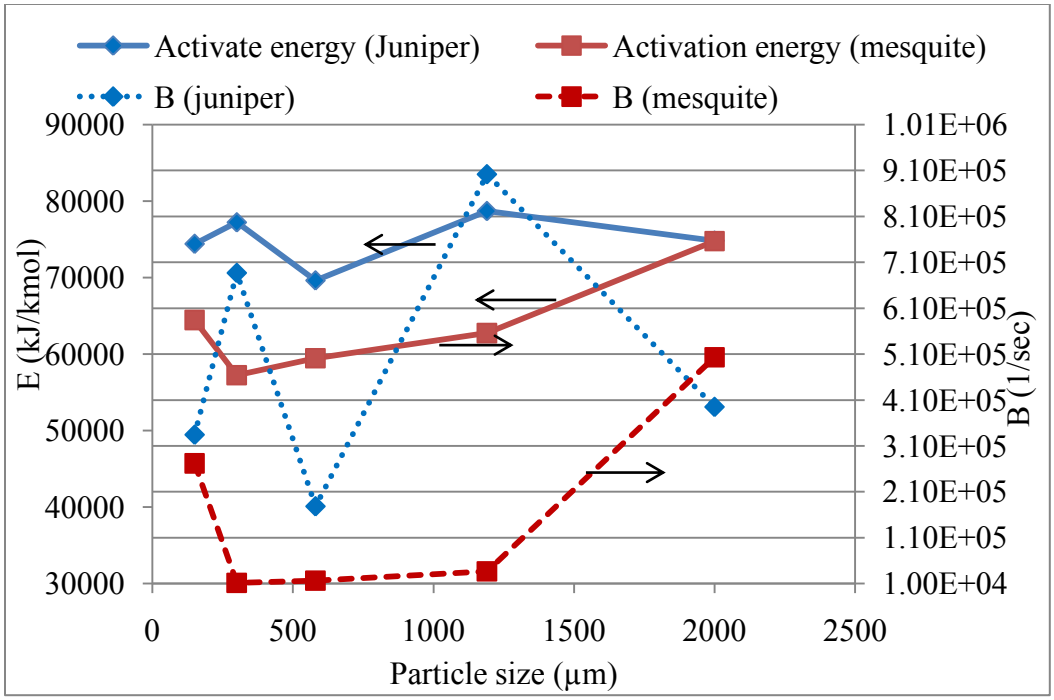

Figure 59. Activation energy and pre-exponential factor obtained from SRM-CA method

6.2.3.2 Kinetics Data from Single Reaction-Maximum Volatile Release Method (SR-MVR)

The T_{max} and weight % (=f_{max}*100) at which the maximum volatile release rate occurs are shown in Figure 60 as a function of particle size d_p. It shows that T_{max} occurred at a lower temperature 625±5 K for mesquite fuel compared to 645 ±5 K for juniper. However, the TGA data shows that juniper lost more mass at T_{max} compared to mesquite. For the mesquite sample, pyrolysis began at 520 K and ended around 800 K where dm/dt=0. The rapid pyrolysis occurred at temperatures ranging from 600 K to 700 K. It is found that the size of the particle has little influence on these processes for the current heating rate of 20 K/min. The SRM-MVR method is simple for the evaluation of

E and B and thus TGA instrument could be automated to yield B and E, once data on "f" vs. T (or time t) data is available. The predictions from SRM-MVR will be useful in determining the temperature of torrefaction which involves partial pyrolysis. The torrefaction temperature T_{torr} must keep blow T_{max} in order to enhance heat value of torrefied biomass. If the torrefaction temperature approaches or passes T_{max}, high mass release rate would occur. A large amount of volatile matter would be liberated from the fuel and hence torrefaction biomass would have lower heating value. More than 55% and 60% of mass was lost for mesquite and juniper when the pyrolysis temperature approached $T_{max,}$ respectively (Figure 60). Although juniper has higher VM content, it also has higher $T_{max.}$ Thus, when juniper samples were heated up to a higher T_{max}, it lost more VM and hence less mass remaining. Figure 61 presents the variation of the activation energies and pre-exponential factors for different sized mesquite and juniper samples. The activation energies of juniper samples are also higher than those of mesquite samples. This result is consistent with the data obtained from the SRM-CA.

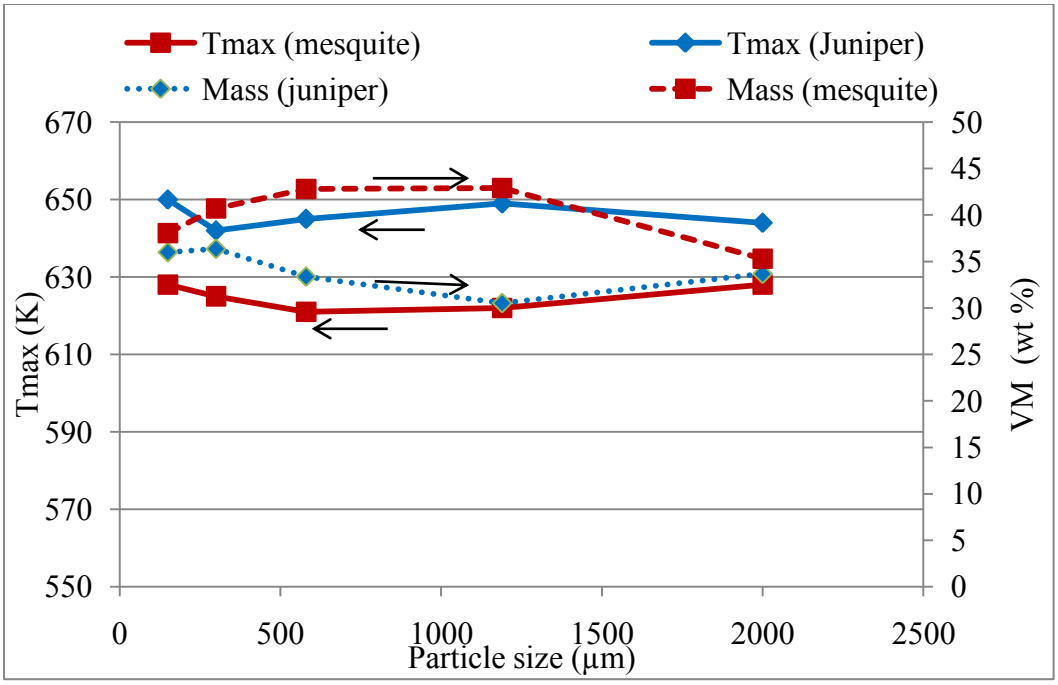

Figure 60. Experimental data T_{max} and VM (wt %) at maximum volatile release point from TGA study for different sized fuels

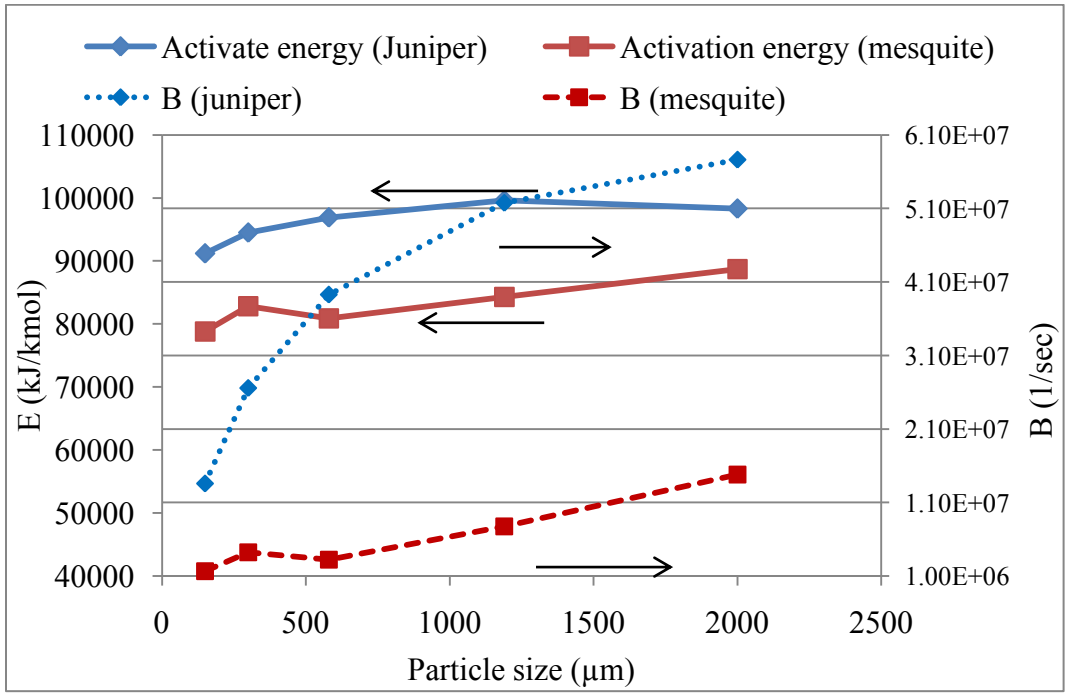

Figure 61. Kinetics constants E and B estimated from SRM-MVR.

6.2.3.3 Kinetics Data from Parallel Reaction Model

This method was presented in chapter 6.2.1. The mean activation energy "E_m" and standard deviation "ζ" were determined by using the following procedure. Taking mesquite of size 150-300 μm as an example, the pre-exponential factor B was set to be $1.67x10^{13}$ 1/sec [8]. The E_m was originally set to a fixed value of 155,000 kJ/kmol and ζ was increased from 10,000 to 14,000 in steps of 400 kJ/kmol, then the sum of the square errors (i.e. different between the measured mass and the computed mass were compared at the temperature range of 500 -800 K) was summarized and plotted in Figure 62 . It can be seen from Figure 62 that the sum of squared errors value decreased first and reached a minimum value, then began to increase again. The minimum value of sum of squared errors was 0.1453 when ζ set to 12,800 kJ/kmol at fixed E_m of 155000 kJ/kmol. By increasing E_m at same ζ the sum of squared errors decreased first with the increase of E_m (155,000 to 158,000 kJ/kmol) and then started to increase when E_m was further increased to 160,000 kJ/kmol. For mesquite fuel with particle size of 150-300 μm the minimum value squared errors occurred when E_m =158000 kJ/kmol and ζ= 12800 kJ/kmol. By applying the same methodology to other fuels and carefully selecting E_m and ζ, the parallel can accurately simulate for the whole domain of pyrolysis. The effect of particle size on E_m and ζ are shown in Figure 63. As seen in Figure 63 the size of the fuel particle did not have a significant influence on the activation energy. The "σ" represents the degree of heterogenity within the fuel. Juniper fuel has higher activation energies and a lower standard deviation compared to mesquite fuel probably indicating higher energy bonds but less heterogeneity. A higher standard deviation value indicates a

wider activation energy distribution for mesquite fuel. Compared to SRM, juniper still has higher activation energies than those of mesquite by using PRM.

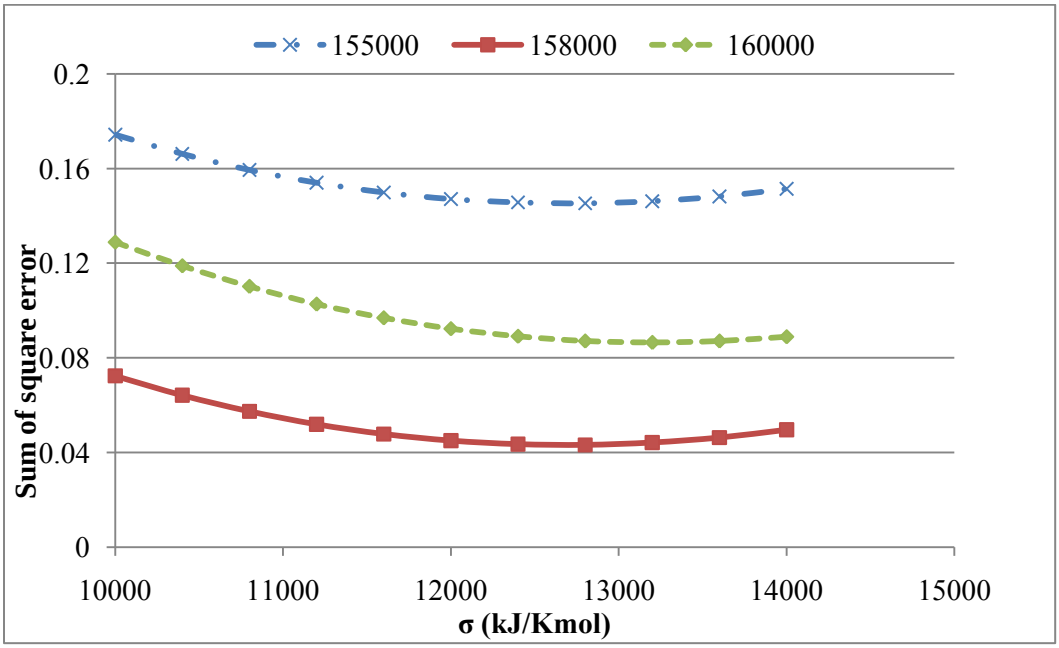

Figure 62. Sum of squared errors for various values of E_m and ζ for mesquite (150-300 μm)

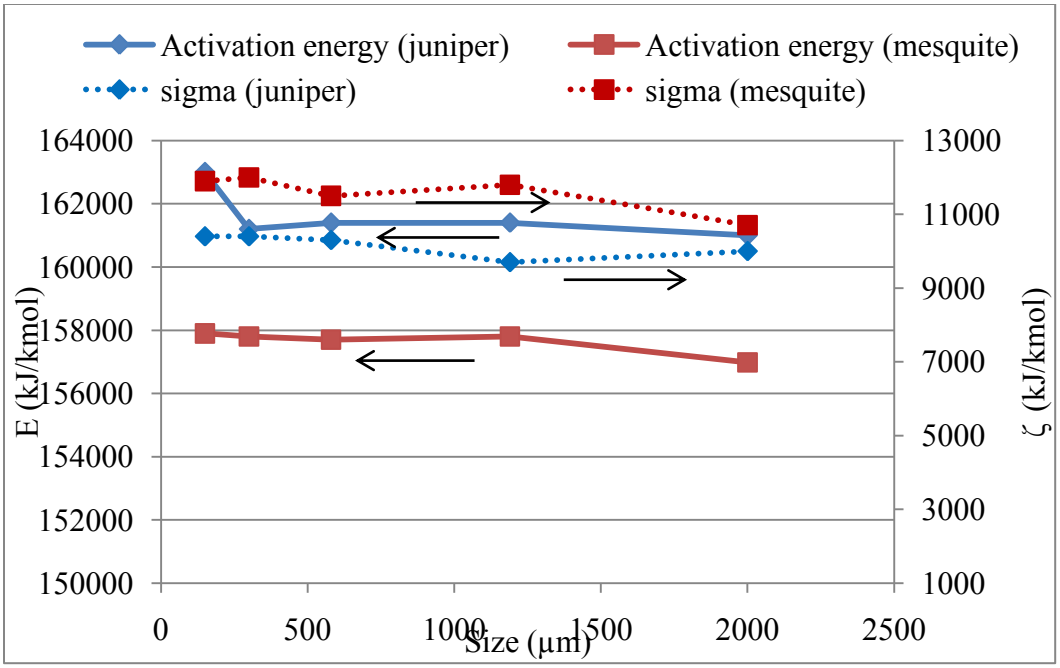

Figure 63. Mean activation energies (E_m) and σ for the parallel reaction model of mesquite and juniper

6.2.4 Comparison of Different Methods

In order to evaluate the accuracy of the three methods (SMR-CA, SMR-MVR, PRM), the volatile fraction m_v/m_{v0} and $d(m_v/m_{v0})/dt$ were computed with extracted kinetics by each method and compared with TGA data.

6.2.4.1 Volatile Content Fraction mv/mv0 vs. Temperature

Figure 64 and Figure 65 show the comparison of experimental data and theoretical prediction for juniper and mesquite with particle sizes ranging from 580 to1190 µm. The root mean square error for three methods is shown in Table 16. It was

found that the PRM provided the most accurate assessment of the pyrolysis behavior since it accounts for different activation energies of chemical components within the biomass and agreed well with those obtained from the experimental data, especially, within the temperatures from 510 K to 750 K. The PRM fitted the experimental curve well and the maximum error never exceeded 4%. However, The SRM-CA exhibited a maximum error (more than 30%) at a peak point based on initial mass.

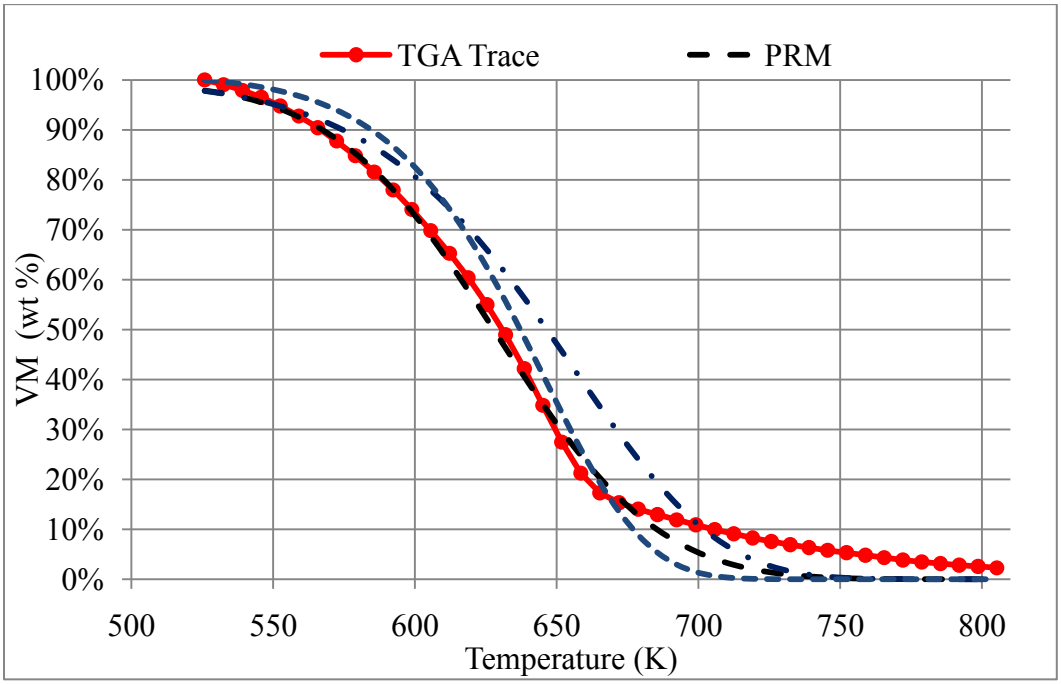

Figure 64. Comparison of the model results for VM (wt %) with experimental data for Juniper fuel of size 580-1190 µm.

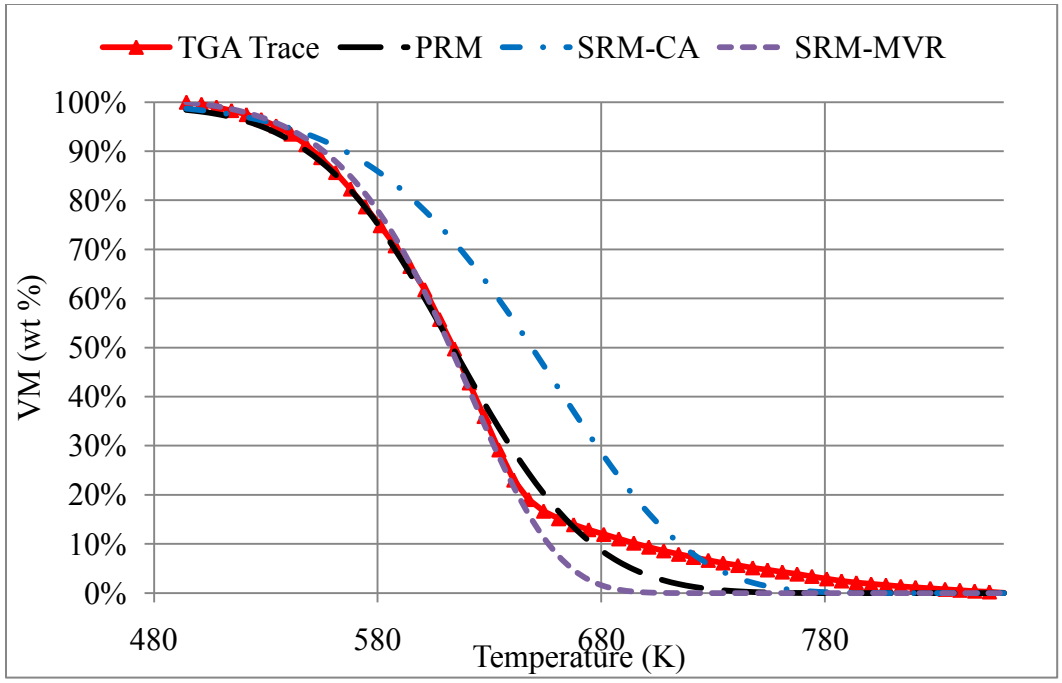

Figure 65. Comparison of the model results for (VM %) with experimental data for Mesquite fuel of size 580-1190 µm.

The largest error was 5.9% for mesquite samples with particle sizes between1190 and 2000 µm at the pyrolysis temperature of 640 K using PRM. Consistently, PRM predicted the mass loss behavior better than the SRM. The SRM-MVR shows lesser error compared to SRM-CA method (Table 16).

Table 16. Error (%) of different methods for VM remaining (wt. %)

	Root mean square error for whole domain of pyrolysis (1%-99% mass loss)	maximum error (%) at a point	Root mean square error for whole domain of pyrolysis (1%-99% mass loss)	maximum error (%) at a point
	Mesquite		Juniper	
PRM	3.17	5.91	3.01	5.8
SRM-CA	13.5	32.5	7.95	18.87
SRM-MVR	4.58	10.50	6.16	9.17

6.2.5 Volatiles Liberation Rate

Figure 66 and Figure 67 show the comparison of predicted volatile matter loss rate with experimental data vs. T for both SRM and PRM. As expected, the prediction using SRM-MVR agreed very well with experimental data around peak point since constants B and E were selected to match the peak point data. Typically the activation energies obtained from this methodology were much higher than those from the SRM-CA.

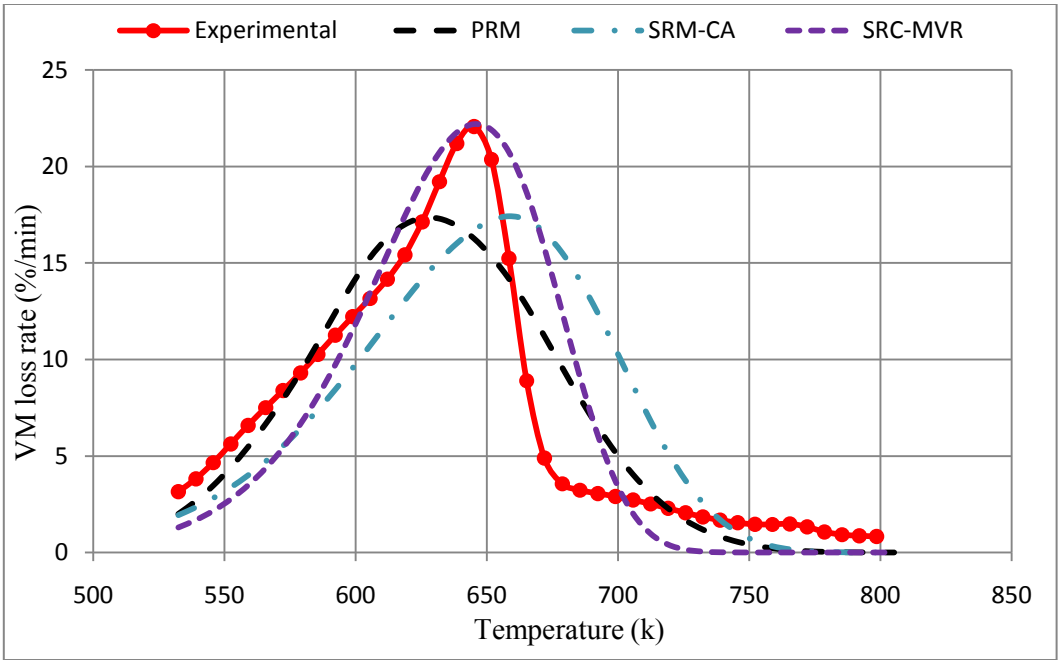

Figure 66. Comparison of experimental data for specific weight loss rate (% per min) vs. temperature with predictions from single and parallel reaction models for juniper

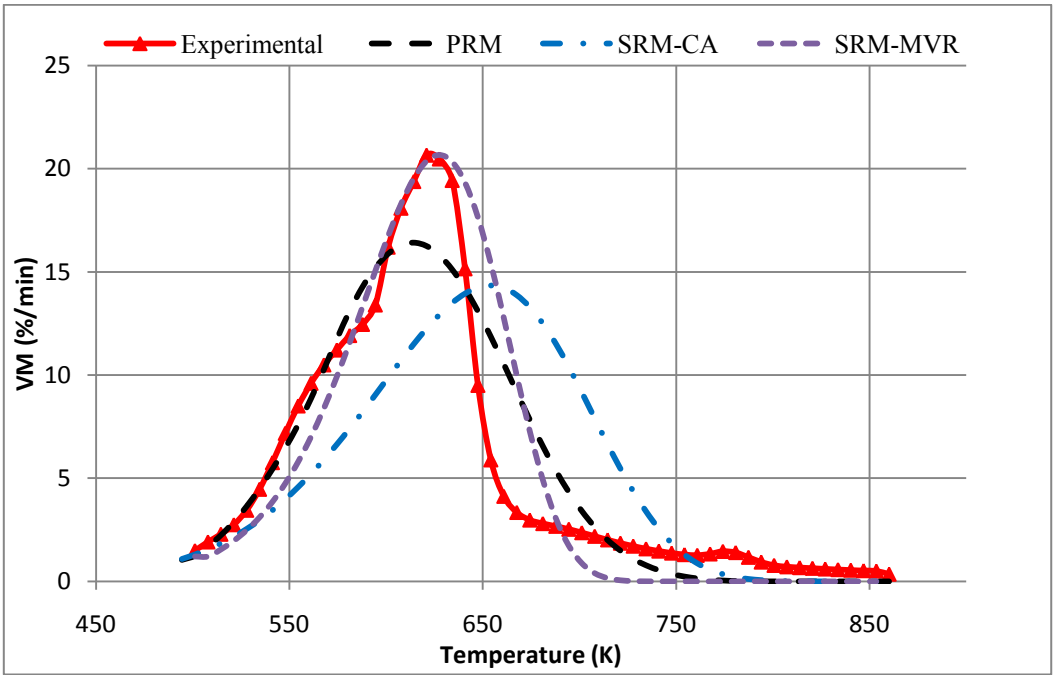

Figure 67. Comparison of experimental data for specific weight loss rate (% per min) vs. temperature with predictions from Single and parallel reaction models for Mesquite

The error between the $(dm/dt)_{experiment}$ and the $(dm/dt)_{estimate}$ was computed as a function of T, and then the error was squared and summed up. The root mean square error was evaluated as shown in Table 17. It was found that the mass loss rate curves for the SRM-MVR and PRM method showed an almost similar deviation while SRM-CA showed higher deviation compared to PRM.

Table 17. Error (%) of different methods for VM mass loss rate (wt%/min)

	Root mean square error for whole domain of pyrolysis (1%-99% mass loss)	error% at peak point	Root mean square error for whole domain of pyrolysis (1%-99% mass loss)	error (%) at peak point
	Mesquite		Juniper	
PRM	2.23	4.4	2.41	5.8
SRM-CA	5.27	9.2	4.49	5.4
SRM-MVR	2.00	0.00	3.12	0.00

6.2.6 Volatiles Mass at Maximum Volatile Liberation Rate

Kinetics from SRM-MVR are important in predicting the volatile content and Tmax at which it occurs. Figure 68 shows the comparison of TGA data with SRM-MVR method for the volatile content mass remaining in the fuel at the peak point for different particle size. It was found that the prediction of the volatile content mass remaining in the fuel by using MVR can generally match the data obtained from TGA. For Juniper, it was predicted that less than 40% volatile matter remaining at T_{max} and the largest

deviation was approximately 6% based on original mass. While, for mesquite the error was only 4%. Thus, the SRM-MVR method reasonably predicted the volatile content in the pyrolysis of biomass fuel, particularly, around the peak points.

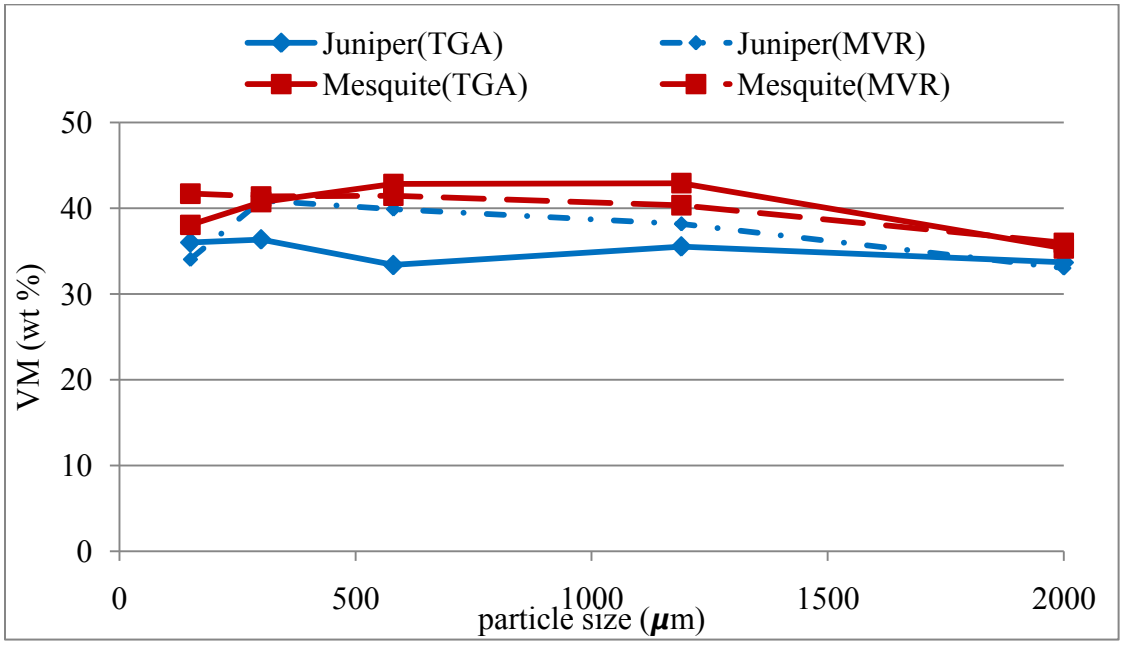

Figure 68. Comparison of remaining VM (wt %) at T_{max} with those of predictions from SRM-MVR method

6.3 TGA Studies of the Dolomite and Woody Biomass Mixture

6.3.1 TGA Trace of Mesquite and Juniper

In these experiments, mesquite and juniper fuels were mixed with, 5%, 10%, and 15 wt % dolomite powder. For each TGA experiment, approximately 10 mg of the mixture fuel was heated up to a finial temperature of 1000 ^{o}C at a heating rate 20 ^{o}C/min in an inert atmosphere of nitrogen (500 ft^3/min). The mass of the fuel as a function of

temperature was recorded. The liberated gases from the fuel were mixed with the carrying gas nitrogen and sent to a FTIR (MutilGas 2030) through a heated gas transfer line. The heated gas transfer line was maintained at 200 ^{o}C by an external heater which covers by an insulated stainless steel core flexible house. The liberated gases such as CO, CO_2, NH_3, H_2O, and CH_4 were record to measure their compositions every 20 second by FTIR.

Figure 69 and Figure 70 and give the relationship of the weight loss of the mixed fuel as a function of temperature. It can be found that the catalyst did not have significant effect on the pyrolysis in the temperature range from 30 ^{o}C to 350 ^{o}C. Above the 350 ^{o}C, the TGA tracing curves start deviating for different wt% catalyst blended mixture. The fuel without catalyst lost more weight compared to others with catalyst when fuels were heated from 350 ^{o}C to 750 ^{o}C. In addition, increase of the catalyst wt% in the fuel result in less weight losses in this temperature zone. This is because catalyst do not decomposed under low temperature; only biomass devolatiled. After temperature went up to 750 ^{o}C, the catalyst started decomposing and the tracing curves for the different catalyst blend merged together. So in the gasification experiments, it is important to maintain the temperature above 750 ^{o}C to make dolomite catalyst to react with the biomass.

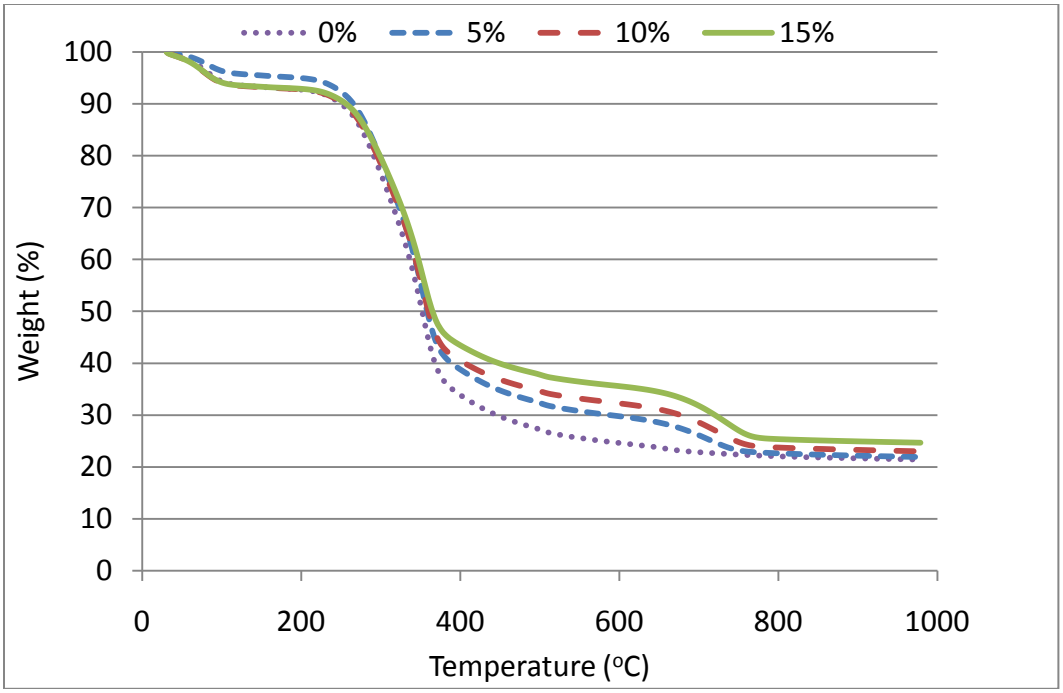

Figure 69. Pyrolysis tracing curves of mesquite fuels with dolomite catalyst.

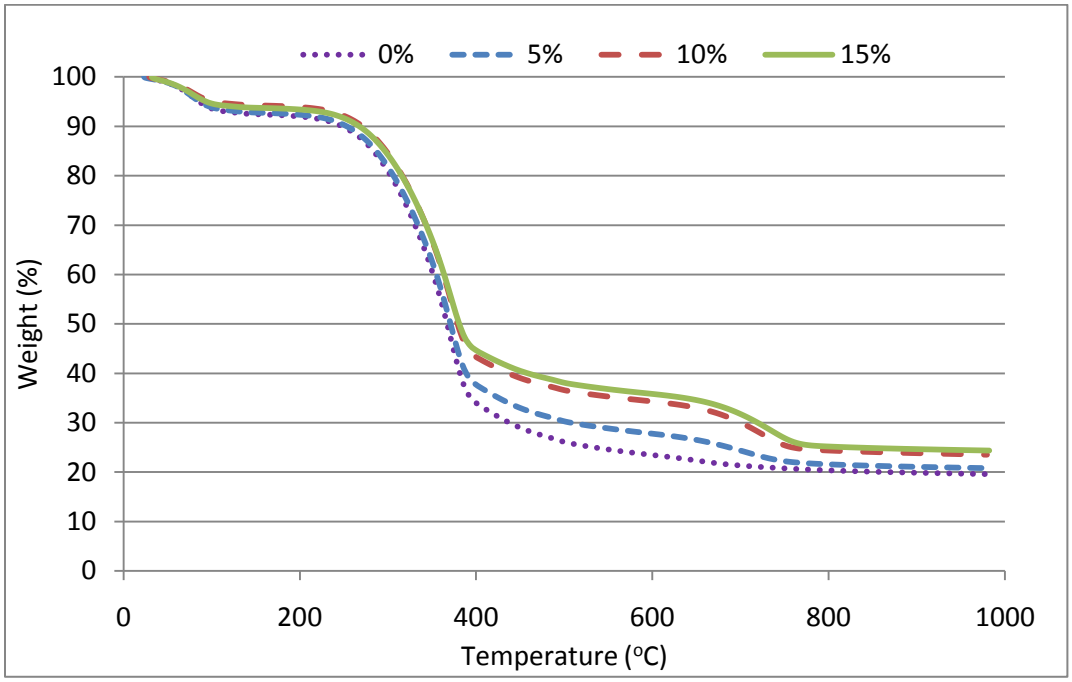

Figure 70. Pyrolysis tracing curves of juniper fuels with dolomite catalyst.

Figure 71 and Figure 72 show the weight loss rate vs. temperature for mesquite and juniper with and without catalyst. Form these two figures, It was observed that three weight loss peak existed in the pyrolysis process. The first weight loss peak was due to the moisture evaporation. The second weight loss peak casued by gas releasing from the hemicellolose and cellolose. It was seen that the fuel without catalyst exhibited highest weight loss rate at temperature of 360-380 ^{o}C, and the weight loss rate decreased with increase of the wt% catalyst in the fuel due to the fact that catalysis is inactive and did not decompond at low temperature. The third weight lost peak may correspond to the activities of the catalyst on the biomass. Ngamcharussrivichai et al.[62] concluded that the decomposition of the carbonate in $MgCO_3$, giving MgO in the temperature range of 600-700 ^{o}C and the thermal decomposition of $CaCO_3$ in dolomite occurred at temperature of 750-800 ^{o}C . Ngamcharussrivichai et al.[62] also found that the high temperature DTG peak occurred at 754 ^{o}C and 774 ^{o}C for non-calcined dolomite and hydrated DM-800, respectively. From Figure 71 and Figure 72 , it can be found that the the weight loss rate of the fuels increased with increase of the catalyst wt% in the temperature range of 650-800 ^{o}C due to the decomposion of the dolomite. For example, the weight loss rate increased significatly with 5 wt% catalyst in the fuel compared to the fuel withot catalyst for mesquite and the weight loss rate increase slightly catalyst wt% inceseased from 5% to 15%. Also, the temperature of the DTG peak curve swifted to higher temperature with the increase of catalyst content in the fuel.

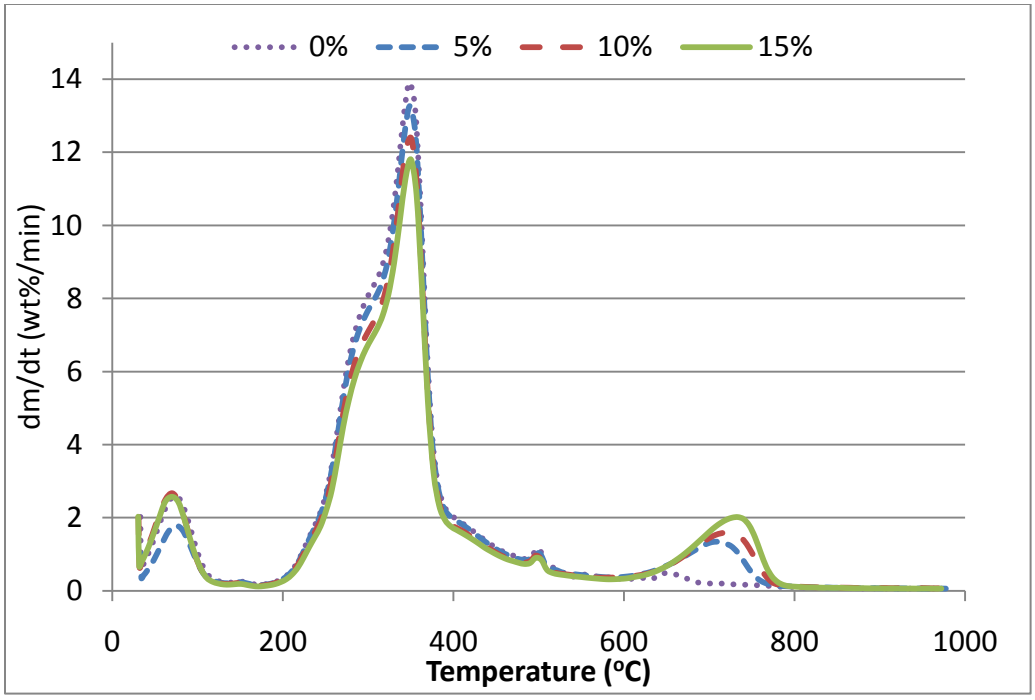

Figure 71.Weight loss rate of different size mesquite samples with dolomite catalyst on N_2 environment

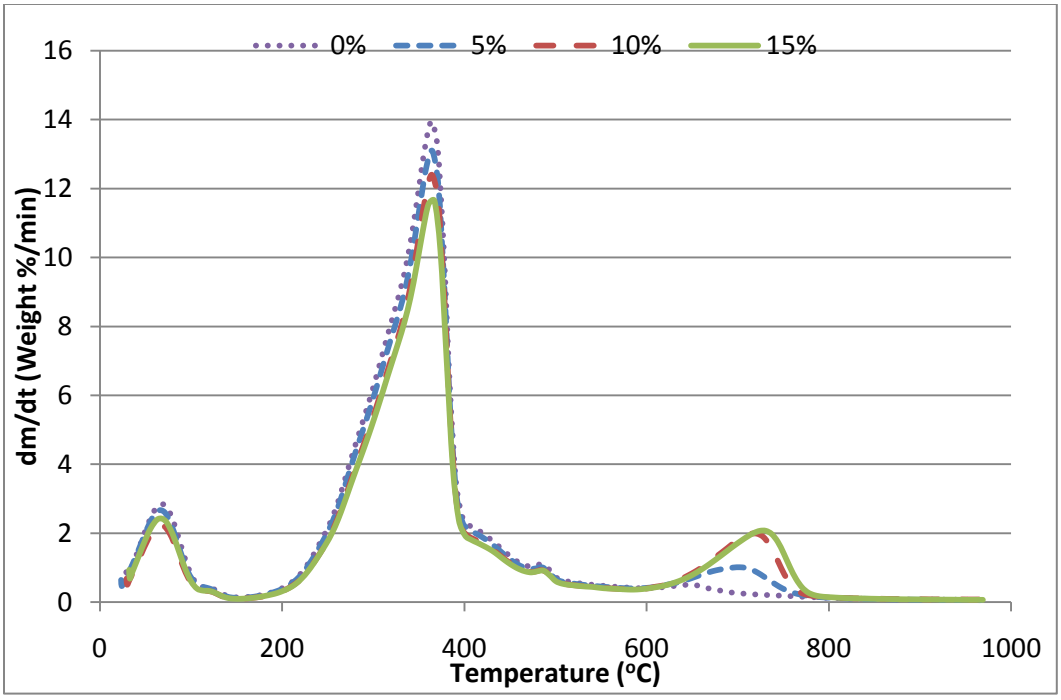

Figure 72. Weight loss rate of different size juniper samples with dolomite catalyst on N_2 environment

6.3.2 Gas Emission from The Blend Mixture

Figure 73 and Figure 74 present the CO emission in the pyrolysis process for mixtures of mesquite: catalyst and juniper: catalyst pyrolysis process, respectively. For mesquite, CO emission mainly occurred between temperature 250 ^{o}C-400 ^{o}C while the CO emission mainly happened in the temperature range of 650-820 ^{o}C for juniper. For both mesquite and juniper, the CO emission concentration increase with the catalyst wt% at temperature zone from 650 ^{o}C to 820 ^{o}C because of catalyst decomposition.

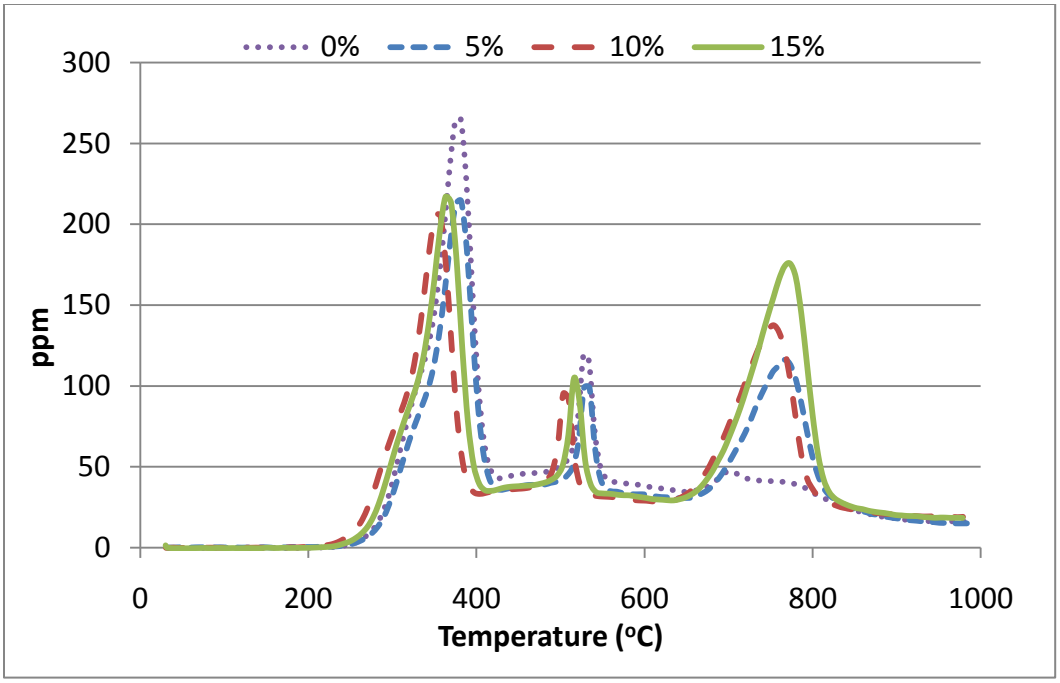

Figure 73. CO concentration vs. temperature for mesquite fuel with dolomite catalyst

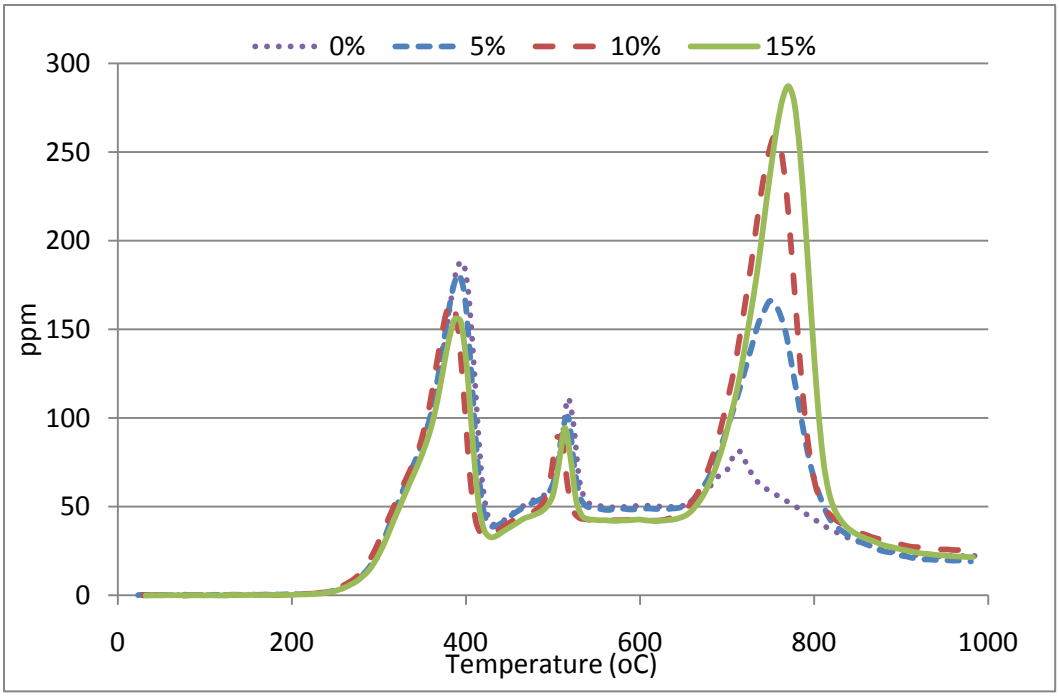

Figure 74. CO concentration vs. temperature for juniper fuel with dolomite catalyst

Figure 75and Figure 76 show the CO_2 liberation from mixtures of mesquite: catalyst and juniper: catalyst pyrolysis process, respectively. These figures exhibit two CO_2 emission peak during the pyrolysis process for both mixtures. The first peak may due to the long chain hydrocarbon cracking resulted in CO_2 liberating from volatile in the temperature range of 250-500 ^oC. The second peak corresponds to the decomposition of the catalyst on the pyrolysis process. Similar to CO, the CO_2 emission increased with the catalyst wt% increase within the temperature range of 650- 820 ^oC.

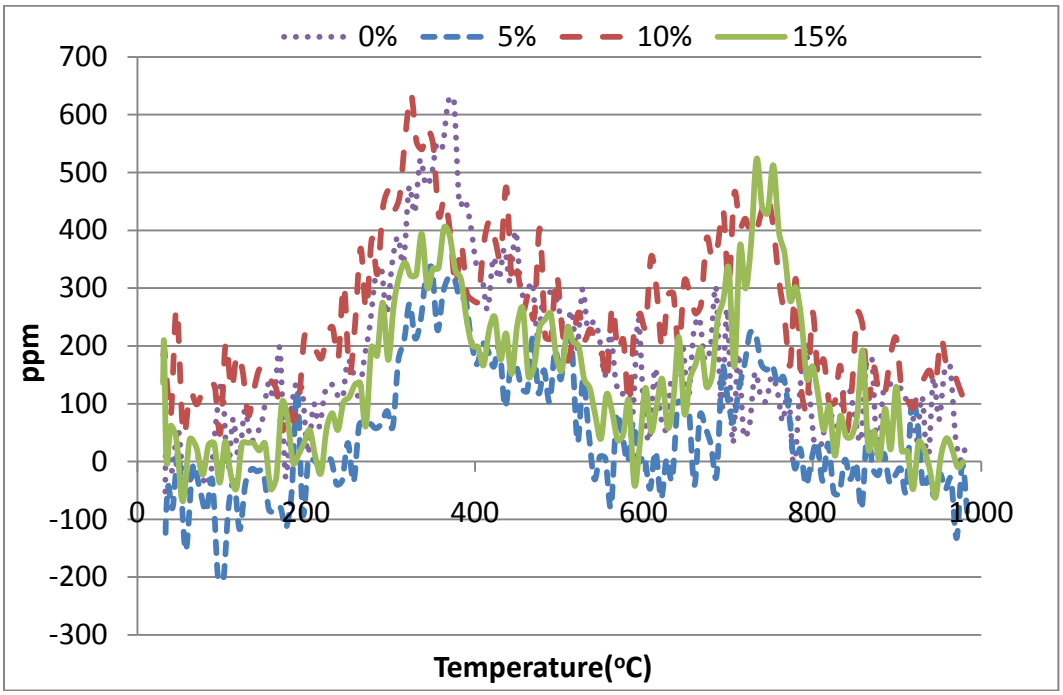

Figure 75. CO_2 concentration vs. temperature for mesquite fuel with dolomite catalyst

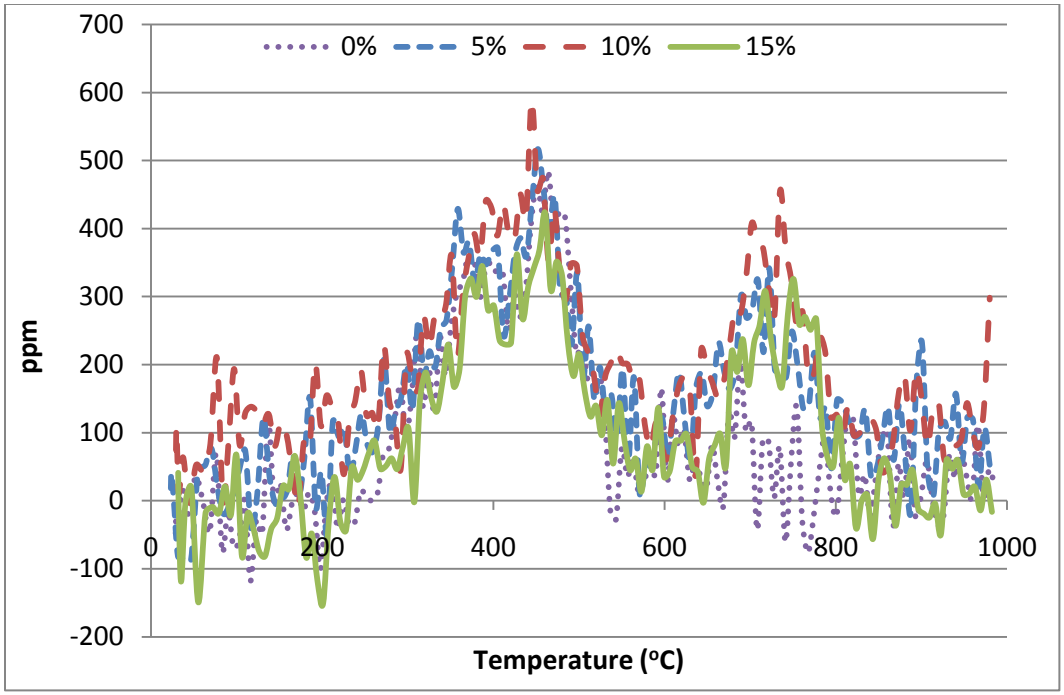

Figure 76. CO_2 concentration vs. temperature for juniper fuel with dolomite catalyst

Figure 77 and Figure 78 give the H_2O liberation from the two mixtures. Moisture started evaporating from the fuel when the fuel were heated up, and weight loss rate reached a peak value when the temperature went up to 100 ^oC. The moisture liberation went down with the further increase in temperature and the value of the moisture emission became 0 indicating there was not moisture liberated from the fuel. After temperature went up to 420 ^oC, a small amount of moisture started releasing from the fuel due to the cracking of the volatile matters.

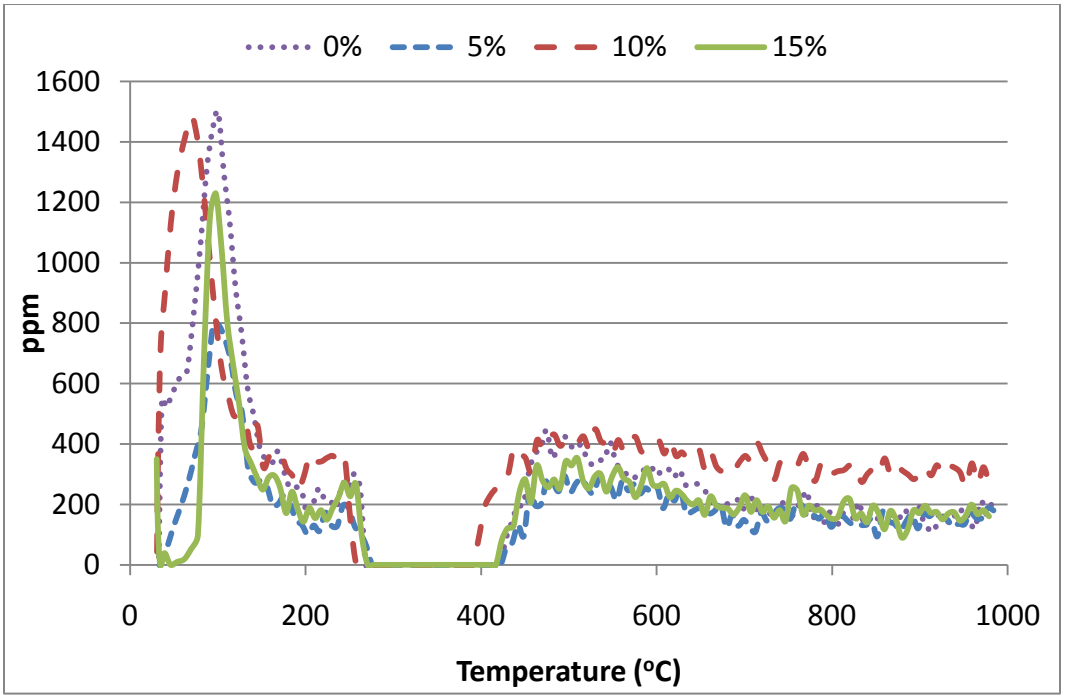

Figure 77. H_2O concentration vs. temperature for mesquite fuel with dolomite catalyst

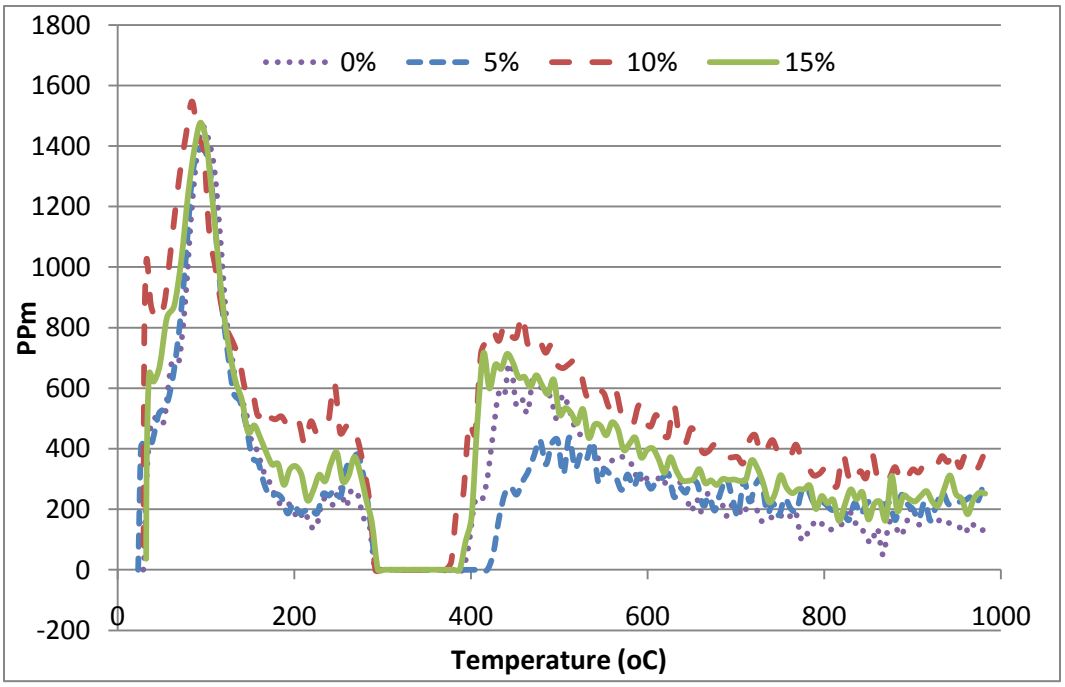

Figure 78. H_2O concentration vs. temperature for mesquite fuel with dolomite catalyst

Figure 79 and Figure 80 give the CH_4 concentration, the CH_4 started releasing from the fuel at the temperature of 300 ^oC and reached a maximum value (above 30 ppm) , and decreased with the temperature went up further. The temperature zone for CH_4 liberating mainly occurred between 300 ^oC and 700 ^oC.

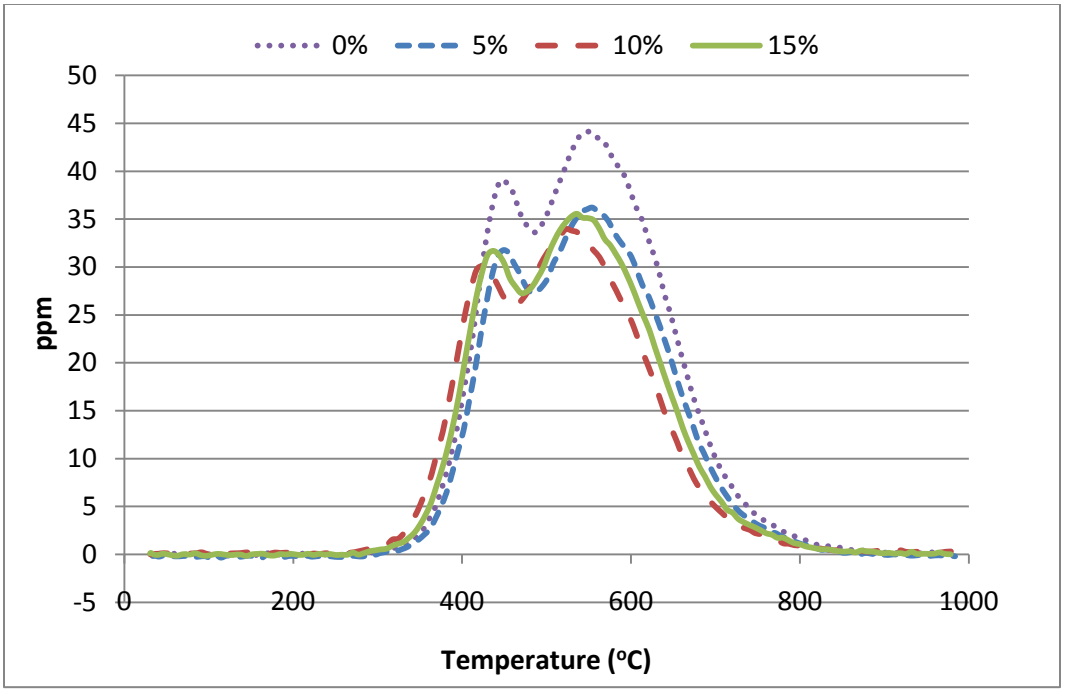

Figure 79. CH_4 concentration vs. temperature for mesquite fuel with dolomite catalyst

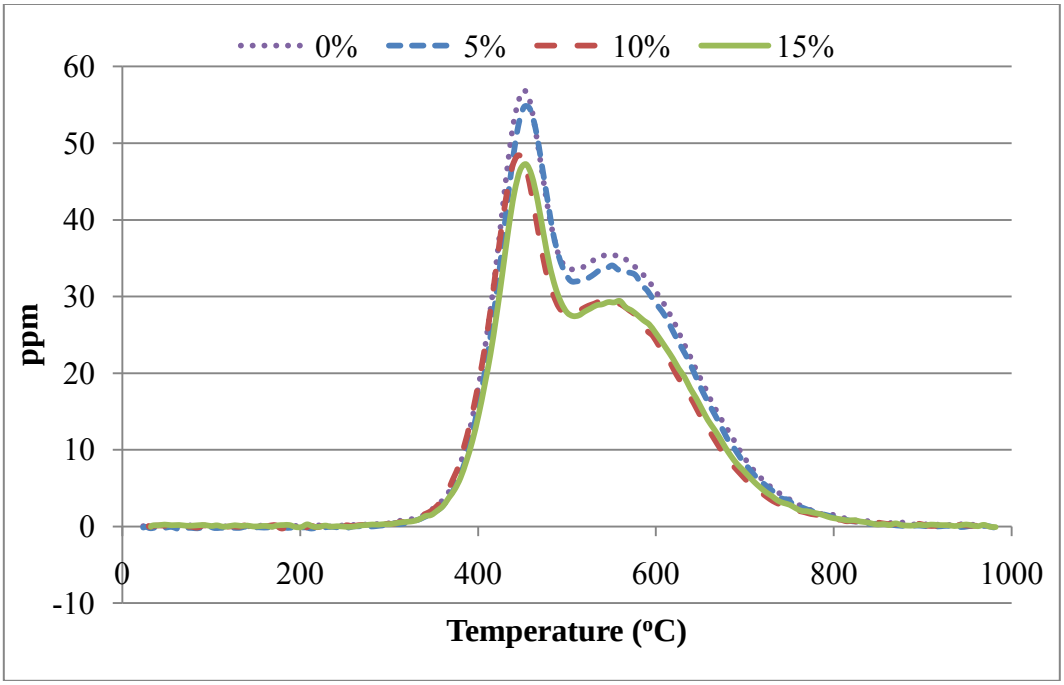

Figure 80. CH_4 concentration vs. temperature for juniper fuel with dolomite catalyst

Formaldehyde is a colorless gas with a characteristic pungent odor and it is an organic compound with the formula CH_2O[63]. From Figure 81 and Figure 82 it can been found that Formaldehyde releasing from two mixtures at temperature zone between 200-420 ^oC and mesquite: dolomite mixture released less formaldehyde than that of juniper: dolomite mixture.

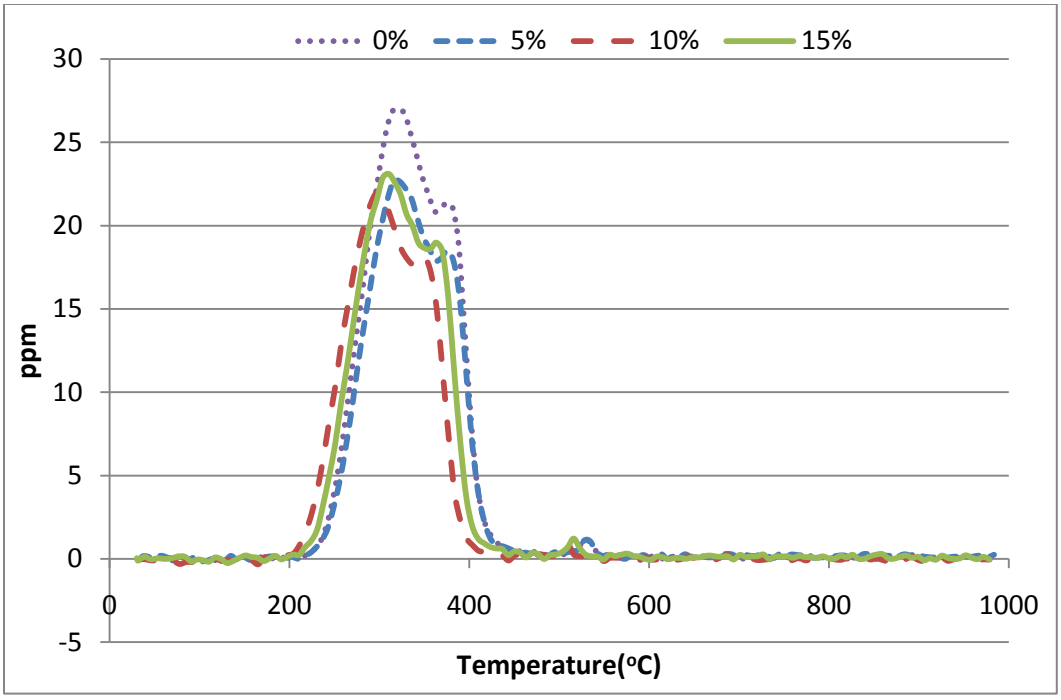

Figure 81.Formaldehyde concentration vs. temperature for mesquite fuel with dolomite Catalyst

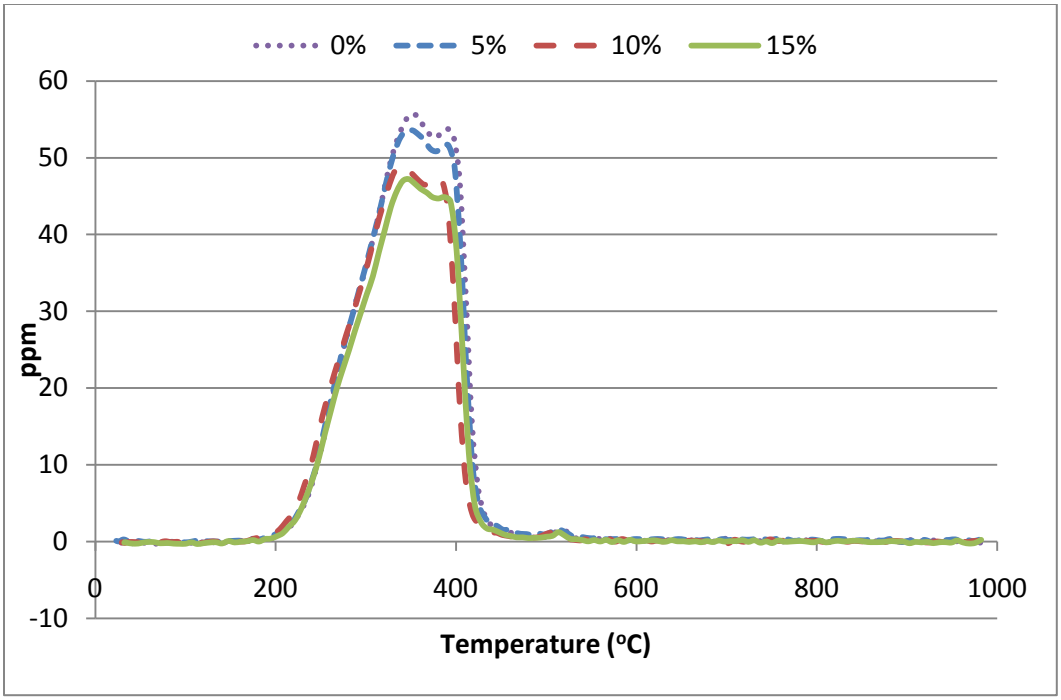

Figure 82. Formaldehyde concentration vs. temperature for juniper fuel with dolomite catalys

6.4 Gasification Experimental Results

The bed height is kept same for all cases at 24 cm (~8.5”), Table?? Presents an overview of experimental conditions and parametric studies performed

6.4.1 Overview of Experimental Conditions and Parametric studies Performed

i) Base air gasification case (mesquite)

- Bed height at 24 cm (~8.5”)
- Fuel: mesquite woody chips

- Particulate size, 2-6mm
- Fuel moisture content : 12%
- Fuel flow rate 1 kg h^{-1} (2.2046 lbm h^{-1})
- Air flow rate at 1.72 m^3h^{-1} (61 SCFH) at 298 K (536 R), 1.47 m^3h^{-1} (52 SCFH) at 298 K (536 R), 1.33 m^3h^{-1} (47 SCFH) at 298 K (536 R), 1.16 m^3h^{-1} (41 SCFH) at 298 K (536 R).
- Equivalence ratio (ER) at 2.7, 3.2, 3.7, and 4.2

ii) Base air gasification case (Juniper)

- Bed height at 24 cm (~8.5")
- Fuel: mesquite woody chips
- Particulate size, 2-6mm
- Fuel moisture content 12%
- Fuel flow rate 1 kg h^{-1} (2.2046 lbm h^{-1})
- Air flow rate at 1.73 m^3h^{-1} (61 SCFH) at 298 K (536 R), 1.47 m^3h^{-1} (52 SCFH) at 298 K (536 R), 1.33 m^3h^{-1} (47 SCFH) at 298 K (536 R), 1.16 m^3h^{-1} (41 SCFH) at 298 K (536 R).
- Equivalence ratio (ER) at 2.7, 3.2, 3.7, and 4.2

iii) Parametric cases (Mesquite)

- Fuel moisture content: 6%, 23%
- Air flow between 1.93 m^3h^{-1} (68 SCFH) at 298 K (536 R) and 0.99 m^3h^{-1} (35 SCFH)
- Steam to fuel ratio (S:F) between 0.3 and 0.6
- Equivalence ratio (ER) at 2.7, 3.2, 3.7, and 4.2
- Catalyst to Fuel ratio (C:F) between 0.052 and 0.111 (5% and 10% catalysis mixed with biomass)

iv) Parametric cases (Juniper)

- Fuel moisture content: 6%, 24%
- Air flow between 1.93 m^3h^{-1} (68 SCFH) at 298 K (536 R) and 1.04 m^3h^{-1} (36 SCFH)
- Steam to fuel ratio (S:F) between 0.3 and 0.6
- Equivalence ratio (ER) at 2.7, 3.2, 3.7, and 4.2

6.4.2 Temperature Profile for Air Gasification

Figure 84 to Figure 89 give the temperature profile for the mesquite and juniper fuel air gasification with moisture content of 6%, 12%, and 24% at ER of 2.7, 3.2, 3.7, and 4.2. It is found that all of the temperature profiles share the same trend for all the experiments: temperature increases first along the height of the gasifier, reaching a peak value at 3-6 cm above the grate. After that, the temperature decreased gradually and dropped significantly when the distance is 22 cm above the bed height. The peak

temperature (T_{peak}) occurred at few cm above the bottom of the gasifier since char oxidation occurred when there was an abundant supply of O_2. At the bottom of the bed, ash was accumulated and the temperature would be correspondingly low. Above the ash layer, char reacted with oxygen to produce CO and CO_2, as well as the heat for the gasification process. T_{peak} highly depended on the concentration of O_2, CO, and CO_2. T_{peak} in the combustion zone can rise above 1000 ^{o}C depending upon fuel HHV and oxygen concentration. Above the combustion zone, the O_2 concentration decreased and most of the reactions that occurred in this zone were endothermic processes which decreased the temperature. Once air was burn out completely, the pyrolysis zone follows the reduction zone in which organic materials were chemically decomposed by heat in the absence of oxygen. The lowest temperature occurred in the drying zone in which the moisture in the fuel was removed by extracting heat from the gases. Figure 83 gives a temperature profile and gasification zones for the mesquite fuel at a case of ER=3.2 and moisture content 24%. The T_{peak} in the combustion and reduction zones were slightly higher for juniper than for mesquite due to higher HHV of juniper.

Figure 83. Temperature profile along of the gasifier axis for a case ER=3.2 and moisture content 24%

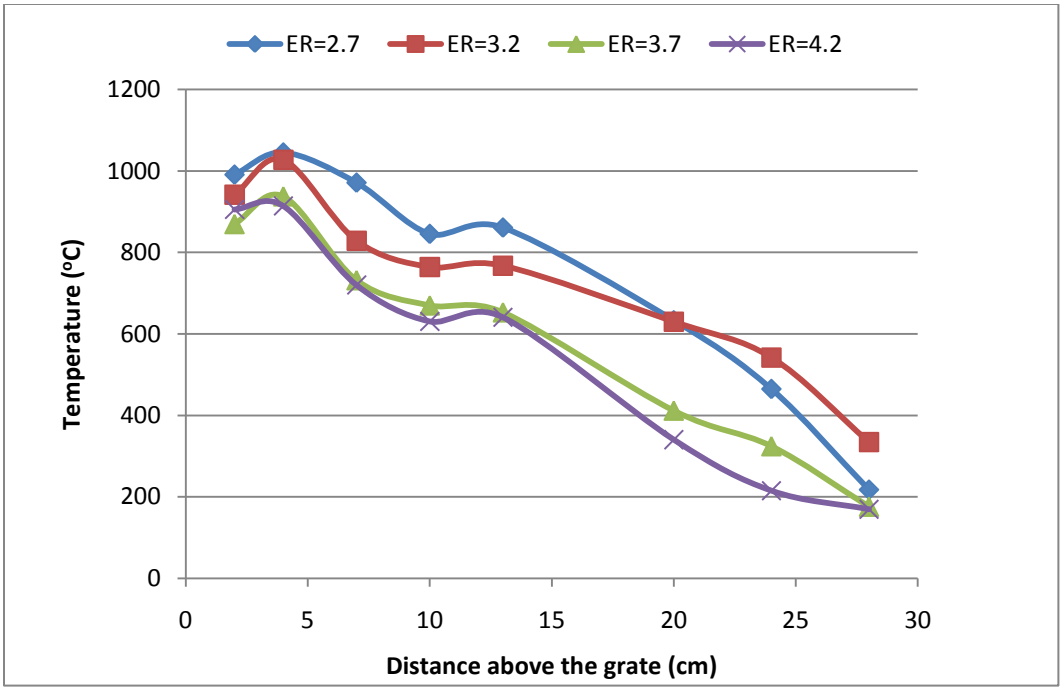

Figure 84. Temperature profile for mesquite fuel with moisture content 6%

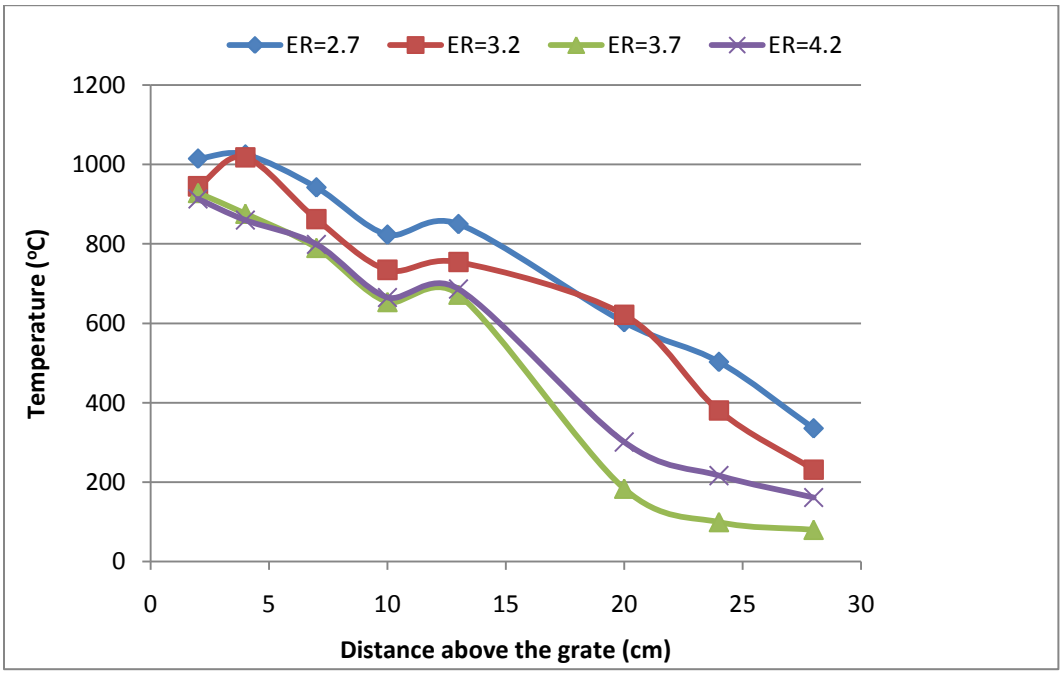

Figure 85. Temperature profile for mesquite fuel with moisture content 12%

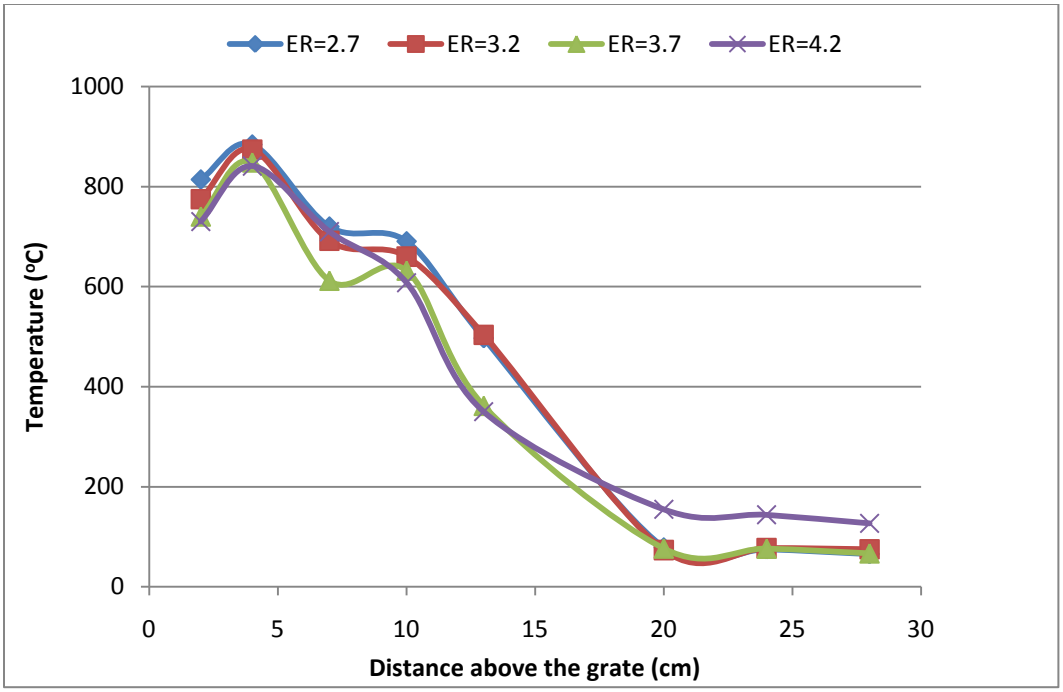

Figure 86. Temperature profile for mesquite fuel with moisture content 24%

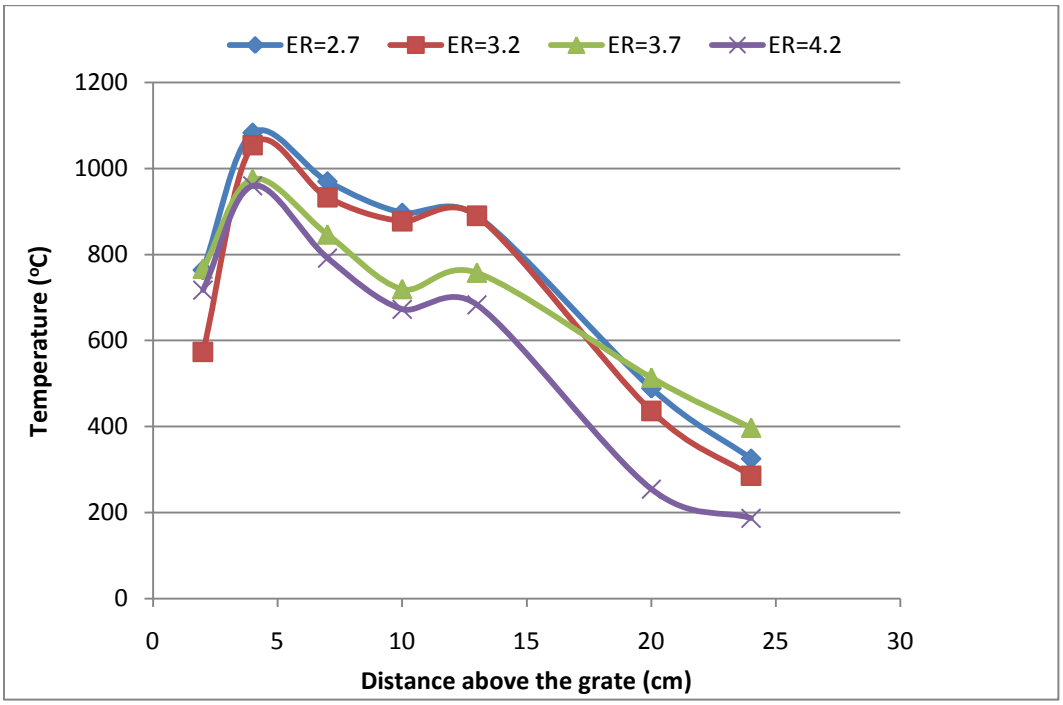

Figure 87. Temperature profile for juniper fuel with moisture content 6%

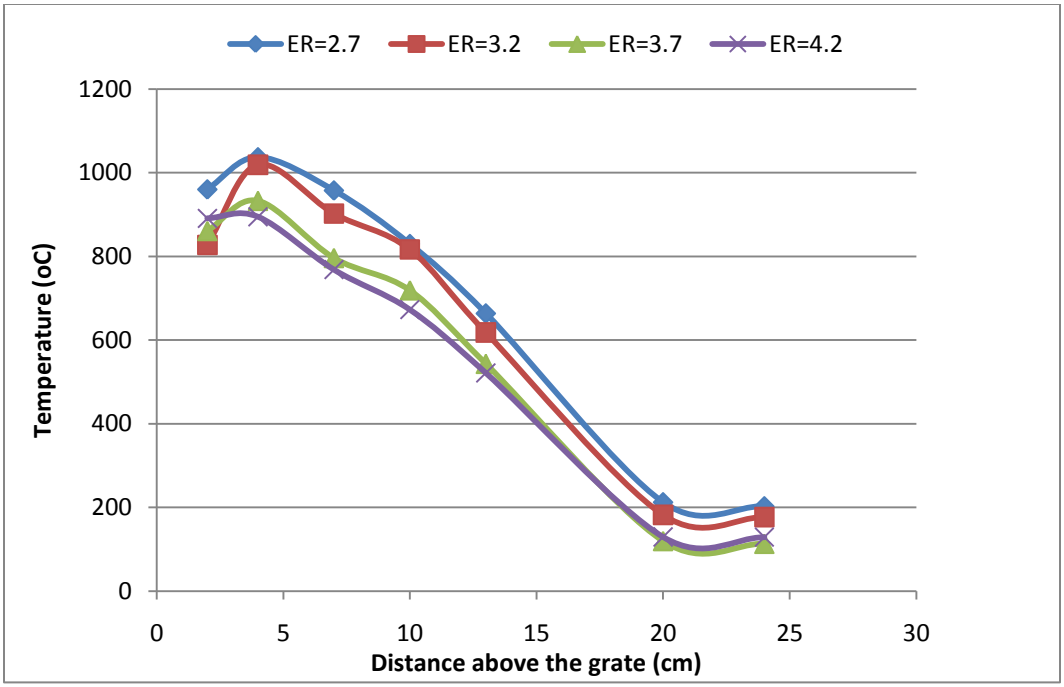

Figure 88. Temperature profile for juniper fuel with moisture content 12%

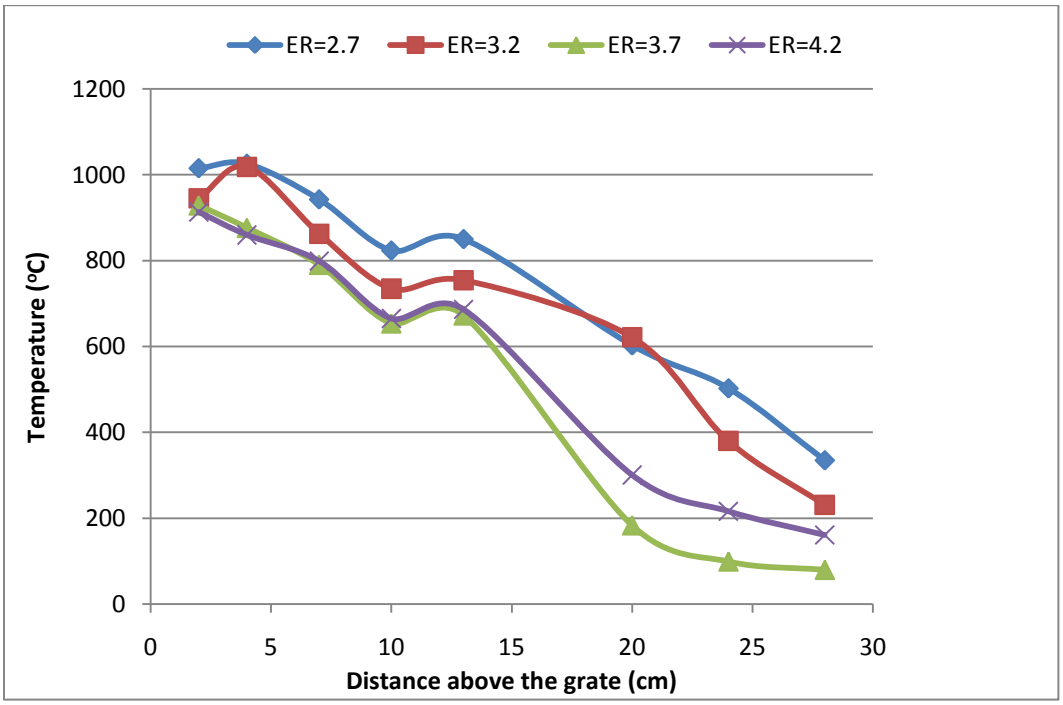

Figure 89. Temperature profile for juniper fuel with moisture content 24%

6.4.3 Peak Air Gasification Temperature (T_{peak})

Figure 90 and Figure 91 show the T_{peak} for mesquite and juniper fuels with different moisture contents under ER of 2.7, 3.2, 3.7, and 4.2, respectively. It was observed that the T_{peak} increased with the decrease in moisture content under the same ER and it decreased with the increase of ER for both samples since less air was available for oxidation of chat. T_{peak} decreased significantly when moisture content was above 24% for both fuels, especially for mesquite (T_{peak} < 900 ^{o}C) due to higher moisture content that effects both gas and tar yield.

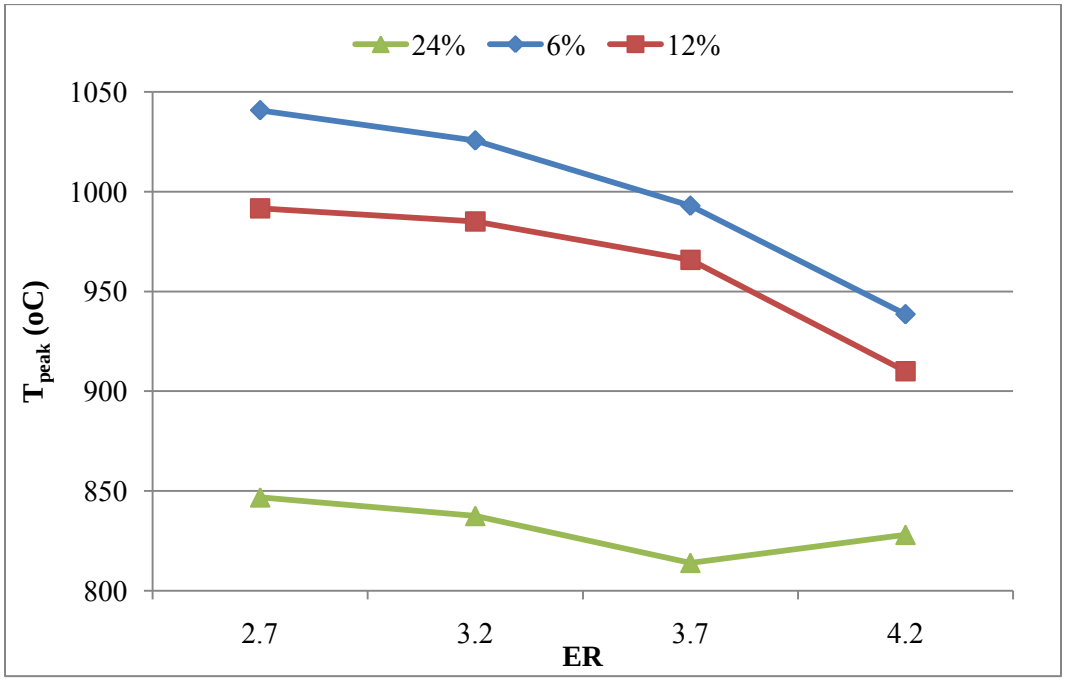

Figure 90. ER vs. T peak of mesquite fuel with different moisture

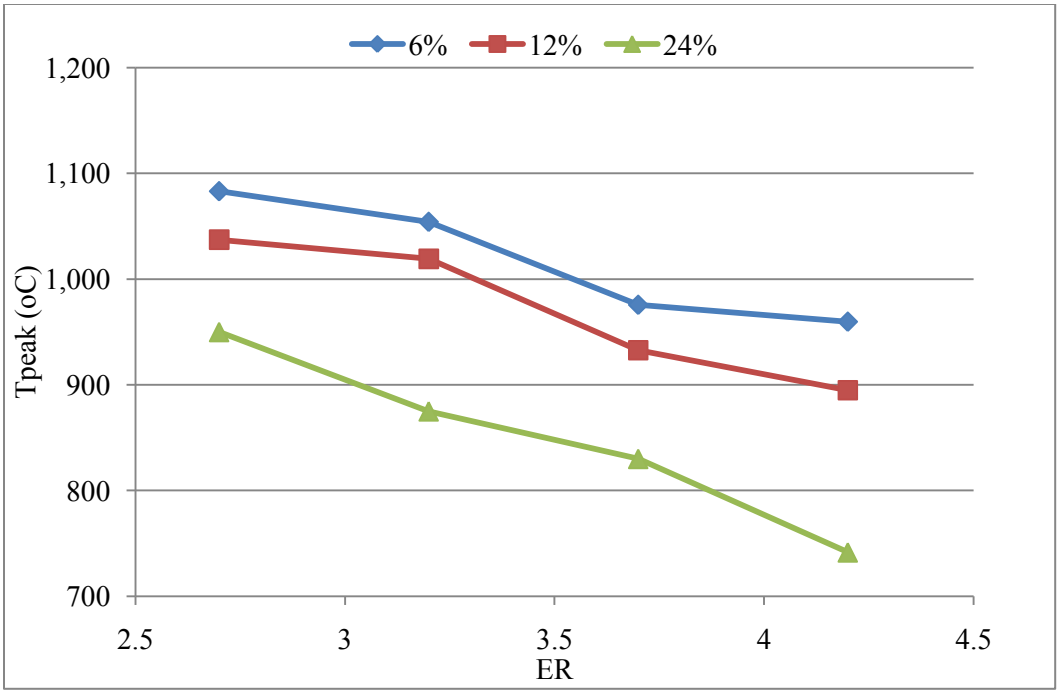

Figure 91. ER vs. T_{peak} of juniper fuel with different moisture

6.4.4 Temperature Profile of the Mesquite Fuel Air-Steam Gasification

Figure 92 to Figure 94 give the temperature profile for the mesquite steam gasification at S: F at 0.15, 0.3, and 0.45. The temperature profiles of the air-steam gasification shared the same trend with those of air gasification, but it was lower compared to that of air gasification. It was seen that most times the T_{peak} was below 1000 ^{o}C for most of the cases, which was lower than that of air gasification. For mesquite air gasification, the T_{peak} went up to 1050 ^{o}C when ER=2.7 while it was only 1010 ^{o}C for air-steam gasification at S:F=0.15. It is due to the following reasons: i) chemical effect: most of the steam gasification reactions are endothermic processes which resulted in lowering the gasification temperature; ii) physical effect: C_p of the

steam and air mixture is higher than that of compared to air[45]. Typically, the peak temperature inside the gasifier follows these inequalities:

$T_{ER=2.7}>T_{ER=3.2}>T=_{ER3.7}>T_{ER=4.7.}$

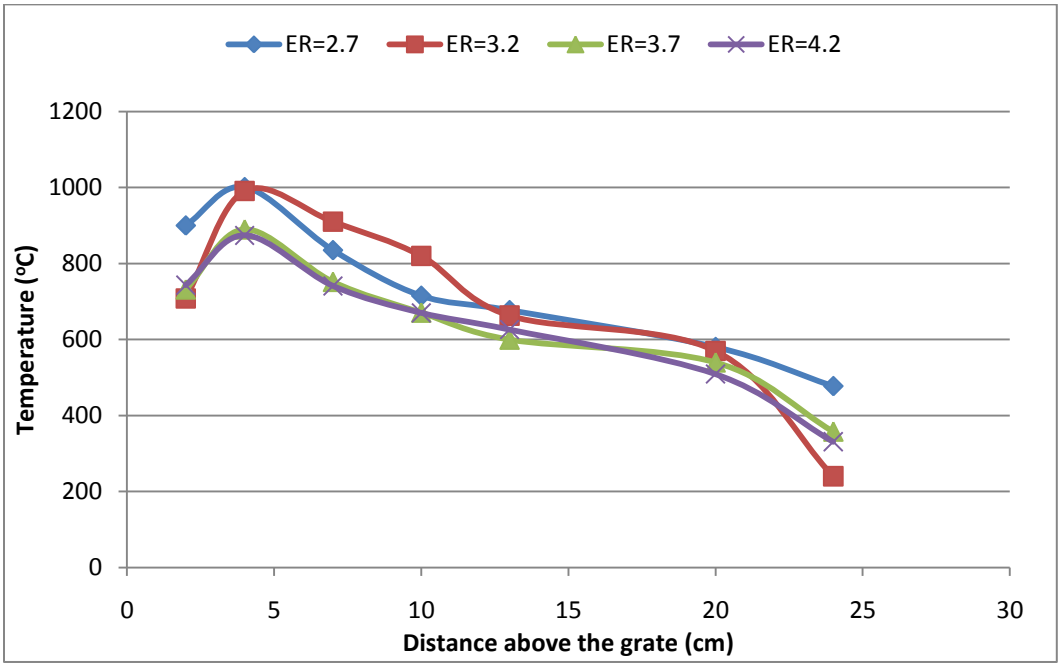

Figure 92. Temperature profile for mesquite fuel at S: F=0.15

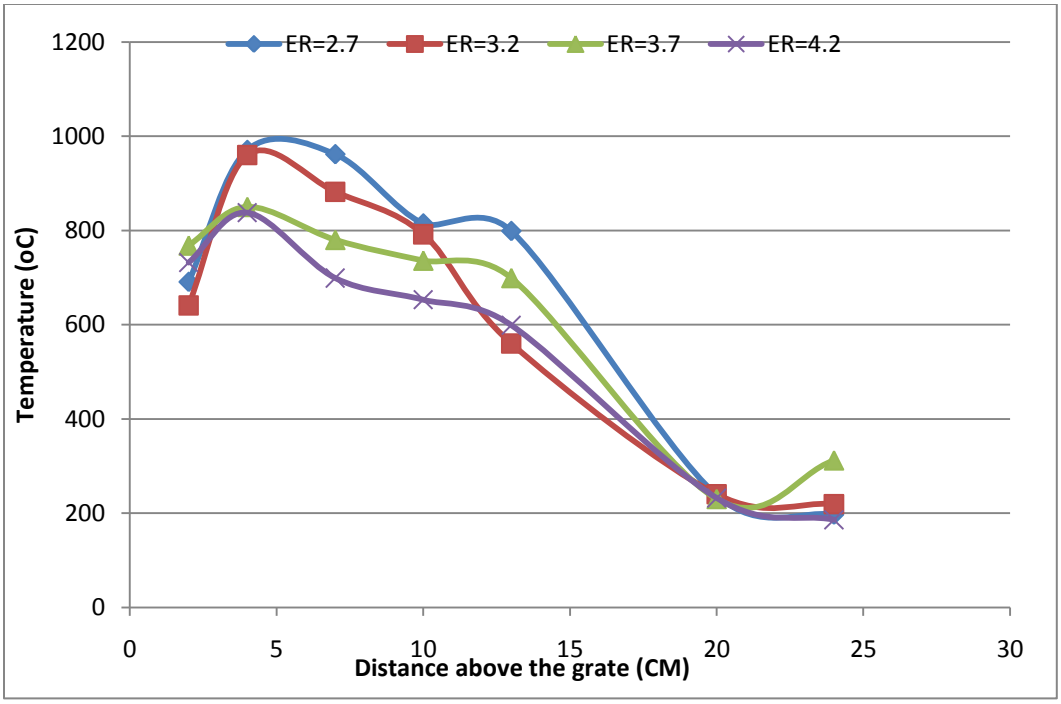

Figure 93. Temperature profile for mesquite fuel at S: F=0.3

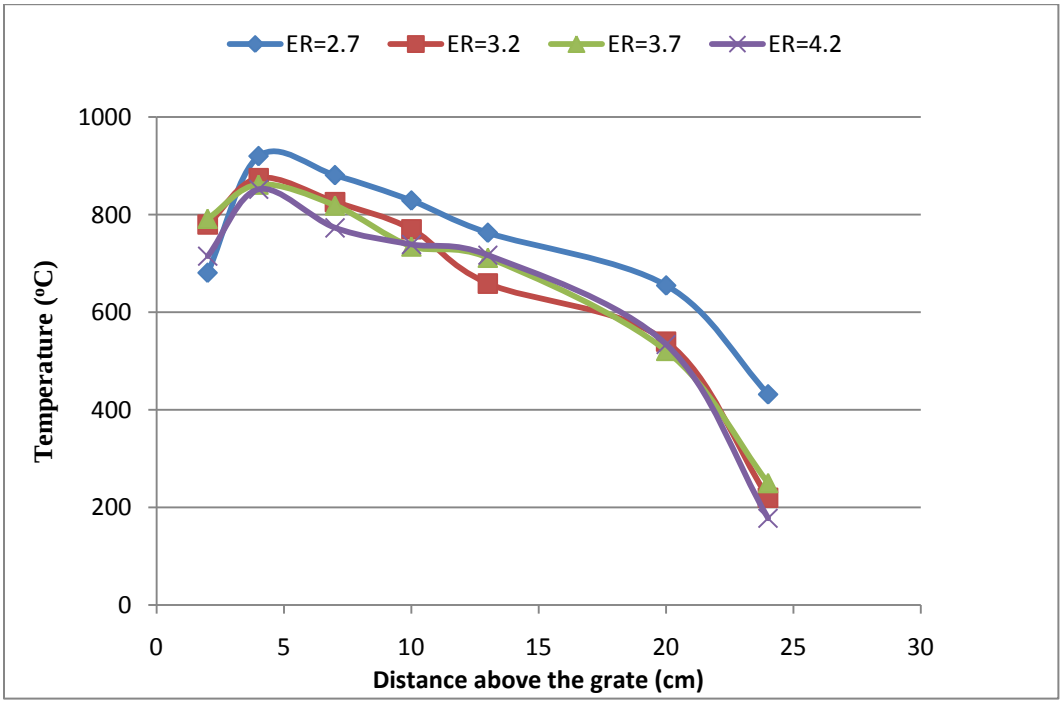

Figure 94. Temperature profile for mesquite fuel at S: F=0.45

Figure 95 gives the temperature profile for mesquite fuel at S: F ratio of 0, 0.15, 0.30 and 0.45 at ER=3.2. It was seen that the gasification temperature profiles is in the following order $T_0 > T_{0.15} > T_{0.30} > T_{0.45}$. Higher S: F ratio means more steam was sent into the gasifier and the endothermic reactions along with the increased C_p lowered the temperature inside the gasifier.

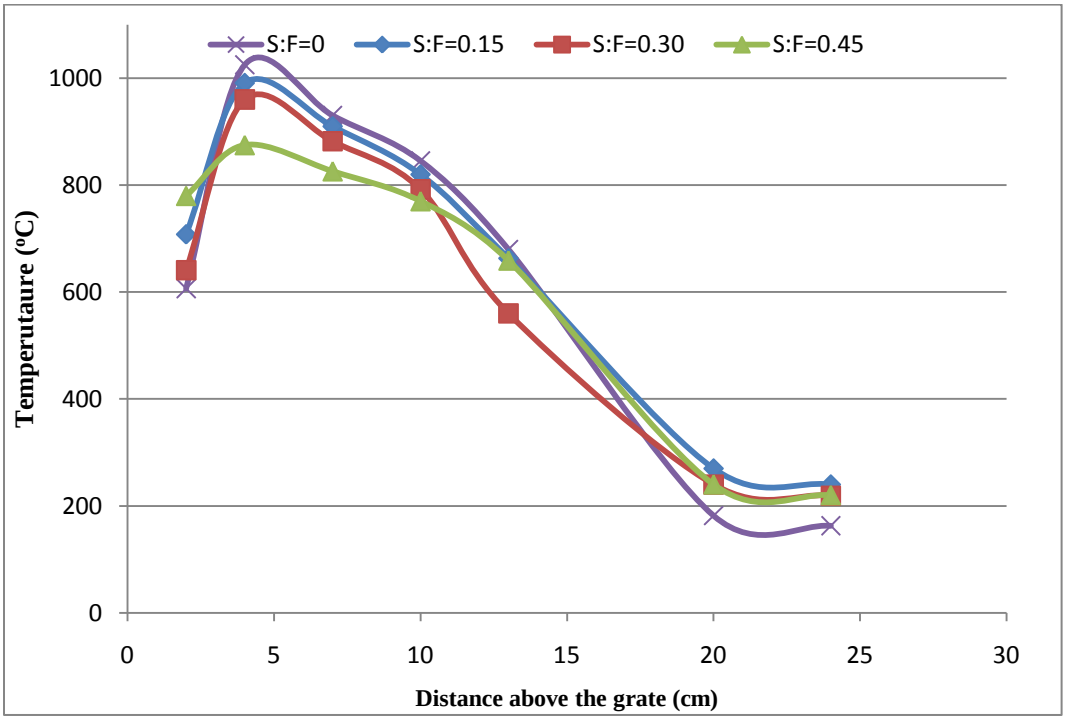

Figure 95. Temperature profile for mesquite fuel at ER=3.2 for several S:F ratio

6.4.5 Temperature Profile of the Mesquite and PRB Coal

Figure 96 and Figure 97 give the temperature profiles for the coal and mesquite mixtures with ratio of 10:90 and 20:80 at different ER.

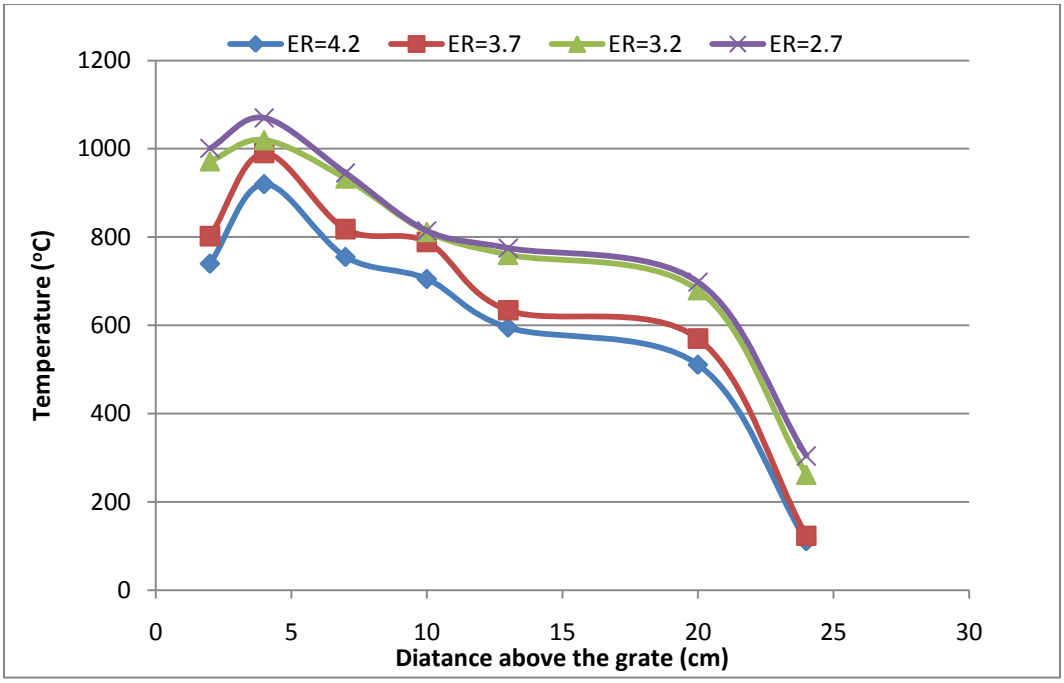

Figure 96. Temperature profile for coal: mesquite (10: 90) mixture

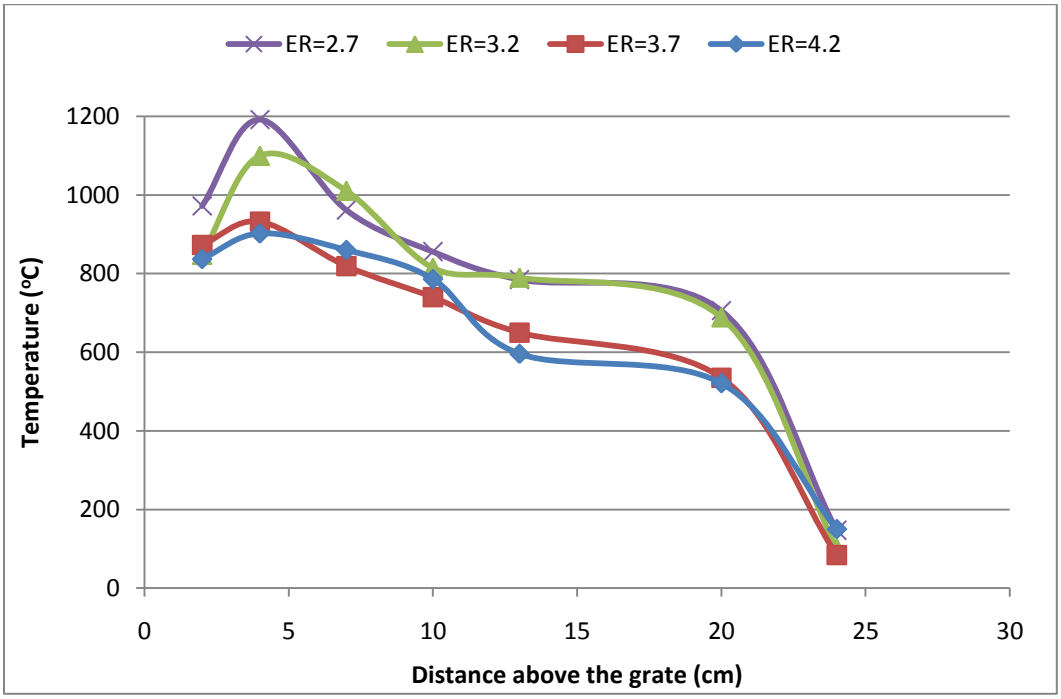

Figure 97. Temperature profile for coal: mesquite (20: 80) mixture

Figure 98 shows the T_{peak} for the coal and mesquite blend with ratios of 100: 0, 10:90, and 20:80. With the increase of the PRB coal percentage in the mixture, T_{peak} increased significantly. For example, T_{peak} went up to 1200 ^{o}C when the mixture with 20% coal while it dropped to 1070 ^{o}C when coal percentage decreased to 10% at ER=2.7. Since coal and VM from coal are of higher quality, more char is in the coal. Temperature is expected to be higher for mesquite and coal blend.

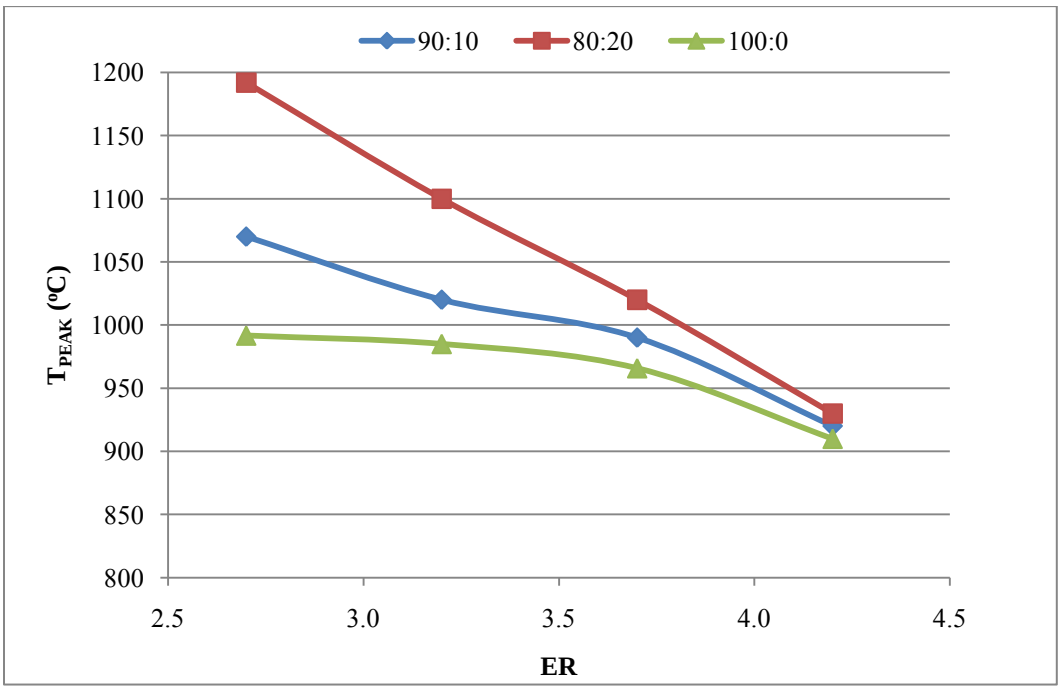

Figure 98. Peak temperature for the coal and mesquite blend ratio

6.4.6 Gas Composition from Air Gasification

The main gas species in the end product from the gasification process are: CO, CO_2, H_2, N_2, and a small amount of CH_4 and C_2H_6. Figure 99 and Figure 100 present the gas composition of the mesquite and juniper fuels at ER =2.7, 3.2, 3.7, 4.2, respectively. It was found that increasing ER (lower T_{ave}) resulted in an increase in CO_2 mole percentage, while CO and H_2 mole percentage decreased. These trends occurred because higher temperature shifts the equilibrium of the endothermic reaction (e.g. $CO_2 + H_2 \leftrightarrow CO + H_2O$) to the products and that of the exothermic reaction (e.g. $CO + H_2O \leftrightarrow CO_2 + H_2$) to the reactants. As a result, a series of biomass gasification endothermic and exothermic reactions could be used to explain the gasification mechanism[32] :

$$C(s) + H_2O \leftrightarrow CO + H_2 \qquad \Delta H = 131{,}160 \text{ kJ/kmol} \qquad (75)$$

$$CH_4 + H_2O \leftrightarrow CO + 3H_2 \qquad \Delta H = 206{,}000 \text{ kJ/kmol} \qquad (76)$$

$$C(s) + CO_2 \leftrightarrow 2CO \qquad \Delta H = 172{,}320 \text{ kJ/kmol} \qquad (77)$$

$$C(s) + O_2 \leftrightarrow CO_2 \qquad \Delta H = -393{,}180 \text{ kJ/kmol} \qquad (78)$$

$$CH_4 + 2H_2O \leftrightarrow CO_2 + 4H_2 \qquad \Delta H = 165{,}000 \text{ kJ/kmol} \qquad (79)$$

$$C(s) + 0.5O_2 \leftrightarrow CO \qquad \Delta H = -110{,}000 \text{ kJ/kmol} \qquad (80)$$

$$CO_2 + H_2 \leftrightarrow CO + H_2O \qquad \Delta H = -16180 \text{ kJ/kmol} \qquad (81)$$

Increasing the gasification temperature would result in equilibriums of reactions (75), (76), and (79) move forward favoring the formation of H_2 direction. Also, the endothermic reaction (75), (76), and (77) would prevail over the reaction (80) and thus result in increase of CO concentration [32]. Additionally, reaction (78) was favored at low temperature and thus more CO_2 was generated.

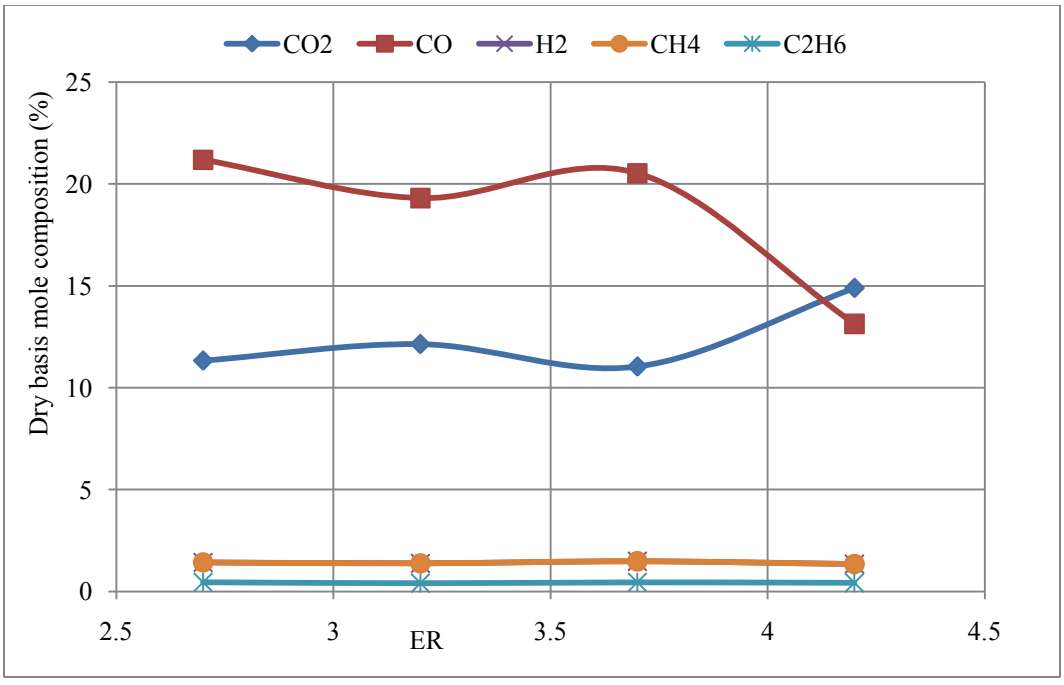

Figure 99. Mesquite (12.9%) gas composition (dry basis) vs. ER. Adapted from[63]

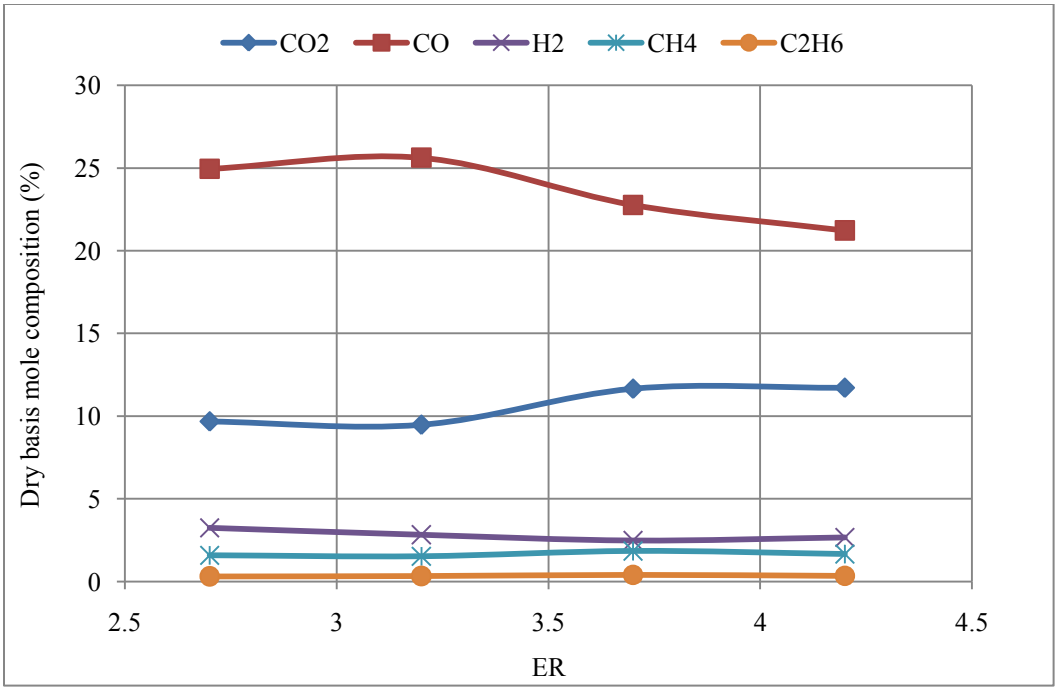

Figure 100. Juniper (13.2%) gas composition (dry basis) vs. ER. Adapted from[63].

Figure 101 to Figure 103 give the CO, CO_2 and H_2 concentration of juniper fuel with moisture content of 6%, 12%, and 24%, respectively. It was seen that the CO concentration increased with the decrease of the moisture content. For example, CO percentage was 30% at 6% moisture content while it dropped to 22% when moisture content increase to 24% at ER=2.7. On the other hand, CO_2 concentration increased slightly when moisture content increase from 6% to 12%, but its percentage decreased when moisture content went up to 24%. This is because higher moisture content fuel (20%) resulted in lowering gasification temperature, and thus the gasification rate decreased significantly and fewer gases were generated. From Figure 103, it was found that H_2 concentration increased when moisture content increased from 6% to 12%.

Similarly to CO and CO_2, its percentage decreased significantly when moisture content was of 24%.

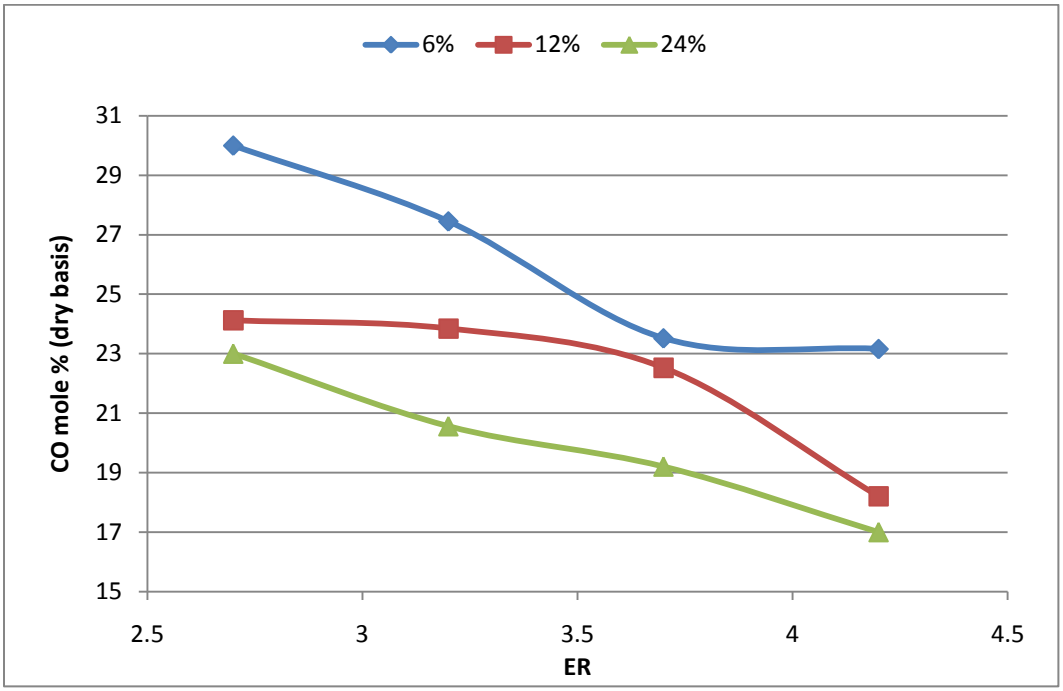

Figure 101. CO mole % for juniper fuel with different moisture content

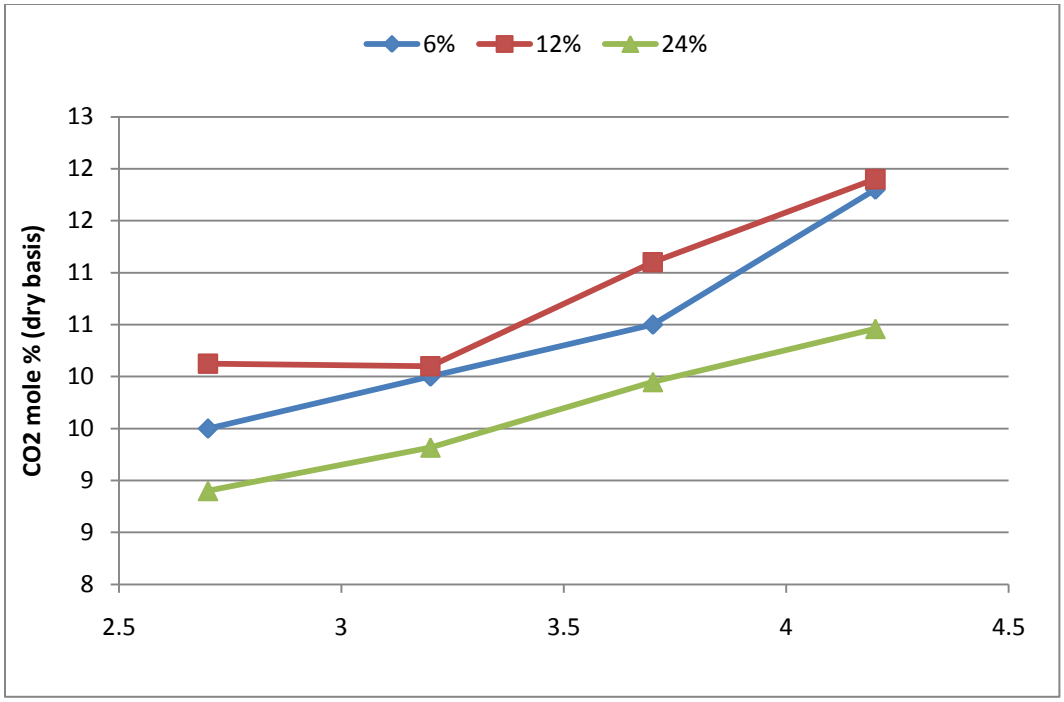

Figure 102. CO_2 mole % for juniper fuel with different moisture content

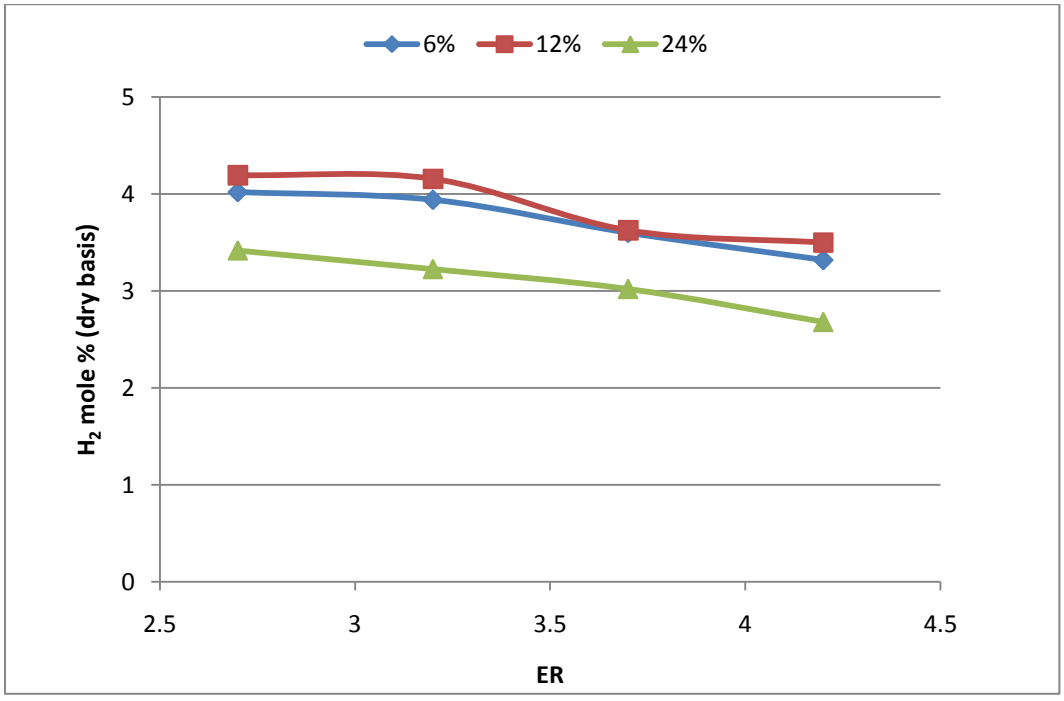

Figure 103. H_2 mole % for juniper fuel with different moisture content

6.4.7 Gas Composition of Mesquite from Air-Steam Gasification

Figure 104 gives gas compositions (CO, CO_2, H_2, CH_4) of mesquite fuel as a function of ER at S: F= 0.45. As discussed early, at a constant S: F increasing the ER would lower the CO concentration while increase the CO_2 percentage. Under the high steam environment, lower gasification temperature favors the formation of the CO_2 and H_2 while decrease CO. The CH_4 percentage did not vary much with the ER and its concentration remained almost constant at 1%-2%.

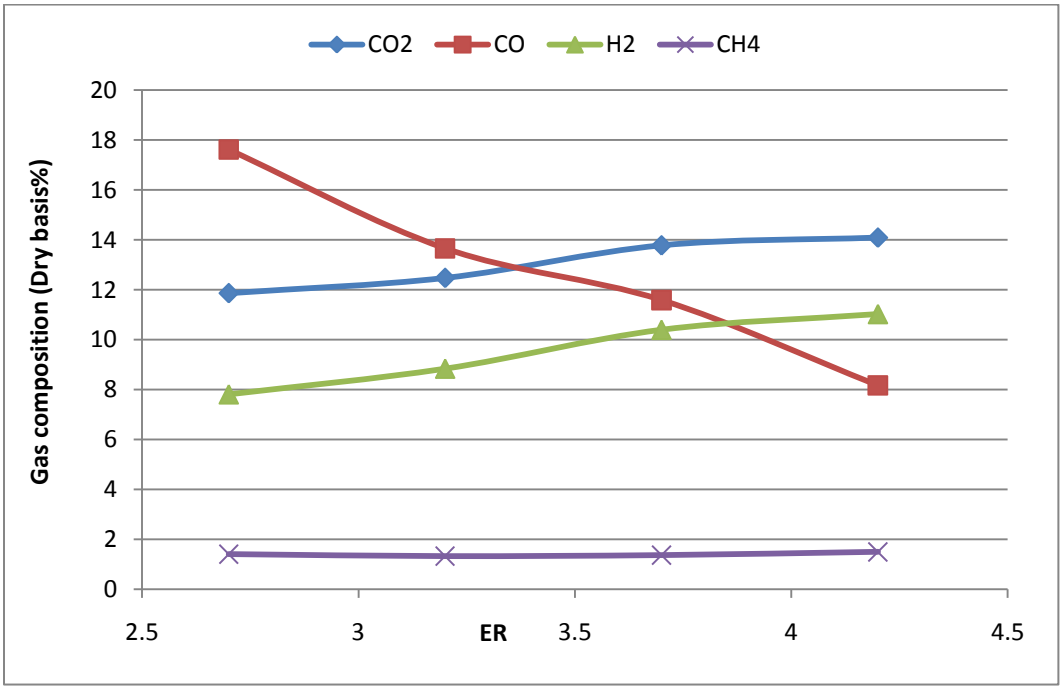

Figure 104. Gas composition for a typical experiment at S: F=0.45 for several ER

Figure 105 and Figure 106 give the CO_2 and CO concentration under different S: F ratio conditions. At a constant ER, the increasing of the S: F ratio led to the increase of the CO_2 concentration and decrease of the CO percentage. As discussed earlier, because the lower the gasification temperature and high steam rich concentration would shift the equilibrium of the reactions such as water-gas-shit reaction to the formation of CO_2 and H_2, CO_2 concentration increased.

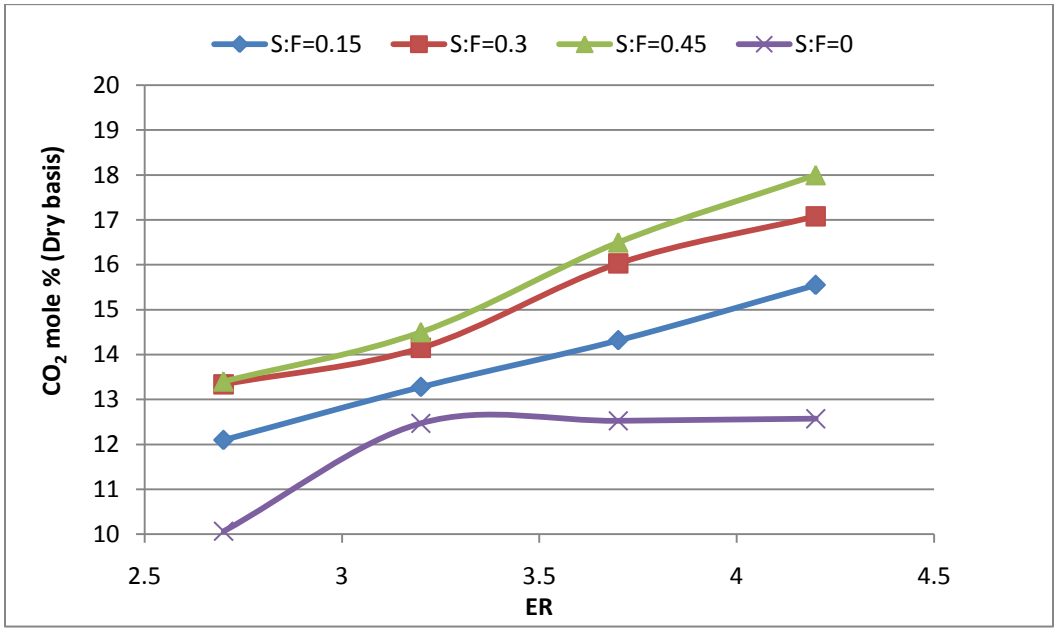

Figure 105. CO2 % vs. ER for different S: F ratios

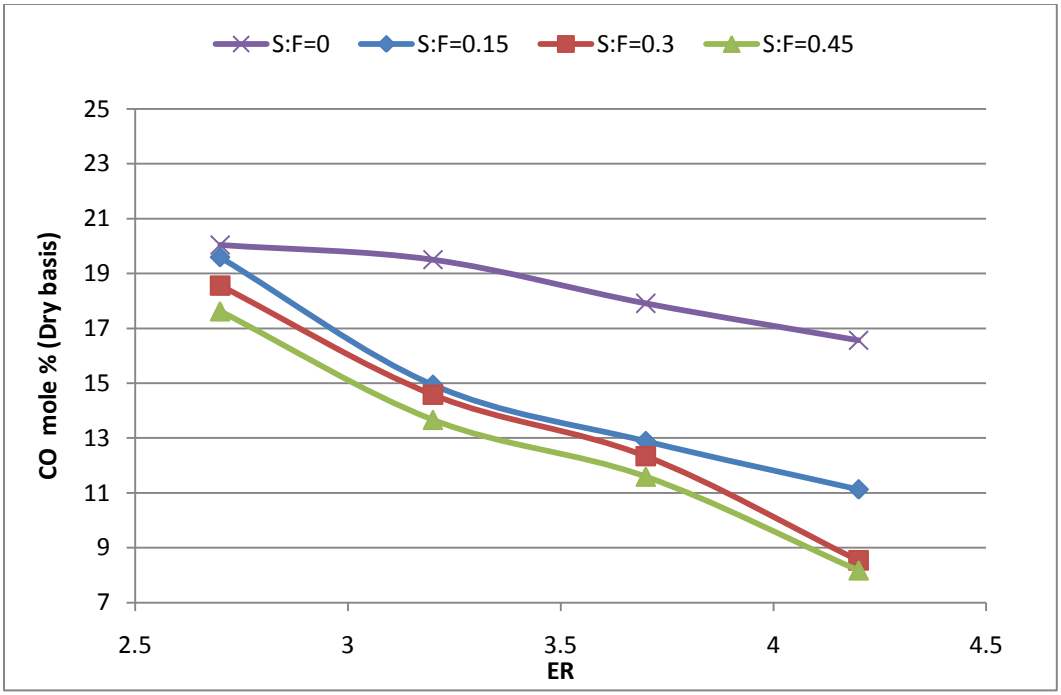

Figure 106. CO % vs. ER for different S:F ratios

Figure 107 shows the effect of ER and S: F ratio on the H_2 concentration. At a constant S: F, increase of the ER means increase of the S: A (steam to air ratio). The heterogeneous reaction of the char with steam could occur in the H_2O rich environment, produce more H_2[16]. In addition, the equilibrium of the water gas shit reaction shifted to the direction of formation of the H_2 in a H_2O rich environment[16]. At constant ER, increase of S: F ratio leads to more steam available to react with char to produce CO and H_2. For instance, H_2 concentration was less than 4% under pure air gasification (i.e. S: F=0); Its concentration increased to 4-7% when S: F increased to 0.15; furthermore, when S: F ratio went up to S: F=0.3, H_2 concentration increased to a range of 7-10.5%. The highest H_2 percentage was around 11% which occurred at S: F=0.45 and ER=4.2.

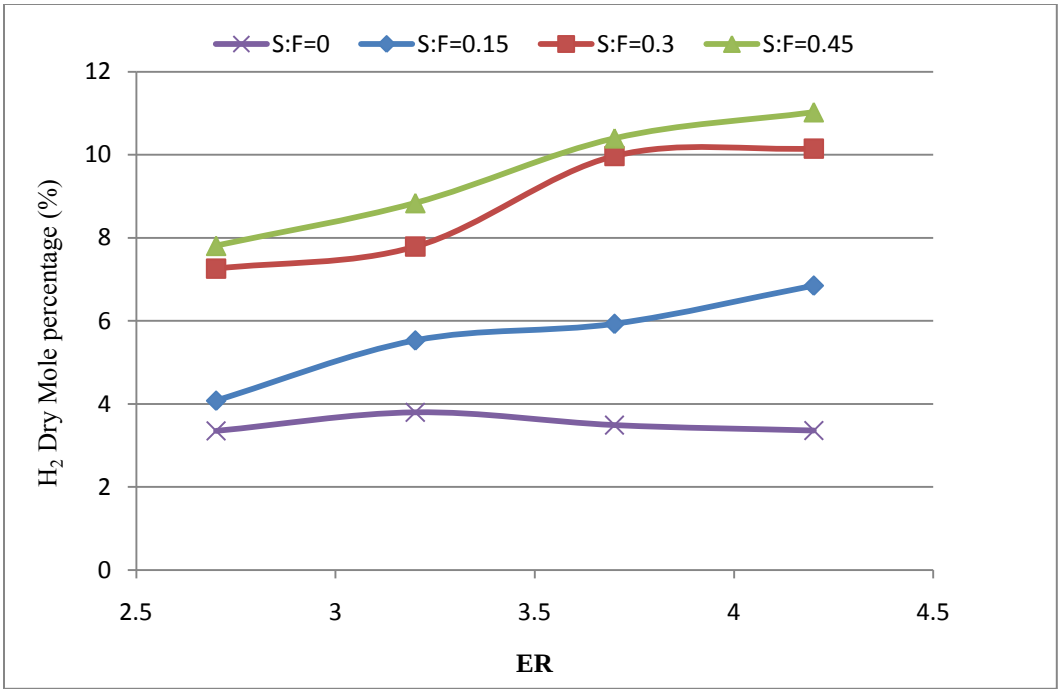

Figure 107. H_2% vs. ER for different S: F ratios

6.4.8 Gas Composition for the Co-gasification of Mesquite and Coal Blend

Figure 108 and Figure 109 present the CO_2 and CO concentration (dry basis) under different coal-biomass ratio. From Table 28, it was observed that the HHV of the PRB coal is much higher than that of the mesquite fuel; the peak temperature increased with the increase of PRB coal percentage in the blend. As a result, the CO_2 concentration decreased while CO concentration increased when the PRB: mesquite ratio increased. The CO_2 concentration and was between 6-18% and the CO percentage was between 14-23%.

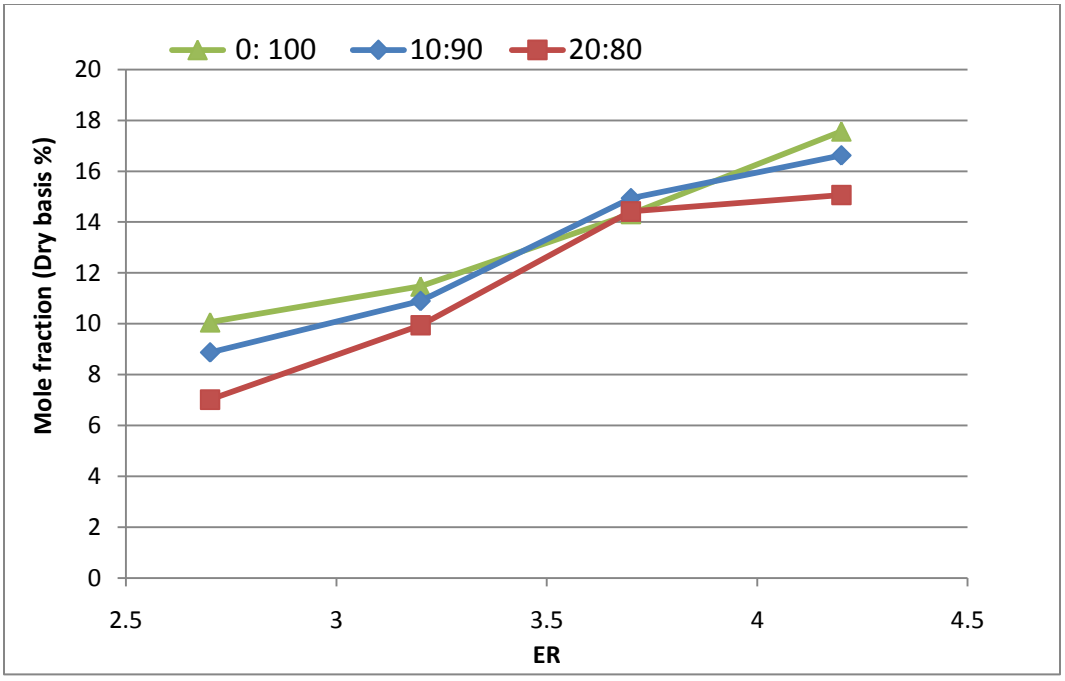

Figure 108. CO_2 concentration for different coal: mesquite fuel mixtures

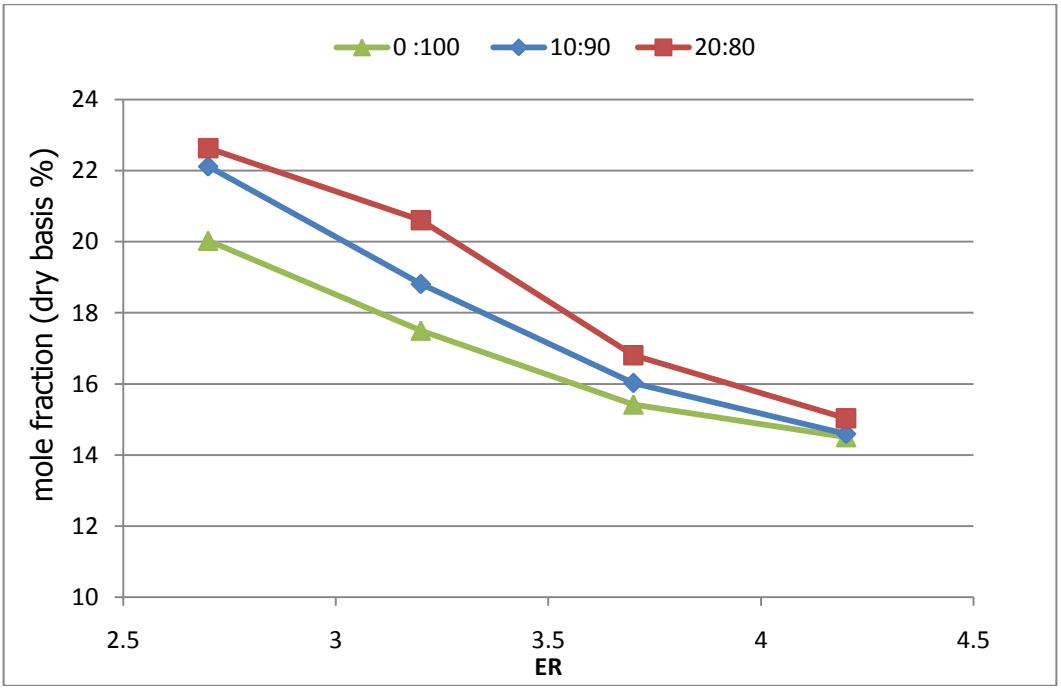

Figure 109. CO concentration for different coal: mesquite fuel mixtures

Figure 110 gives the H_2 and CH_4 concentration with blend ratio as a parameter. H_2 concentration was in a range of 2.5-4% and the CH_4 mole fraction was between1- 2% 。Increase of the coal ratio in the mixture resulted in slightly increases of the CH_4 concentration because more char was available to react with H_2

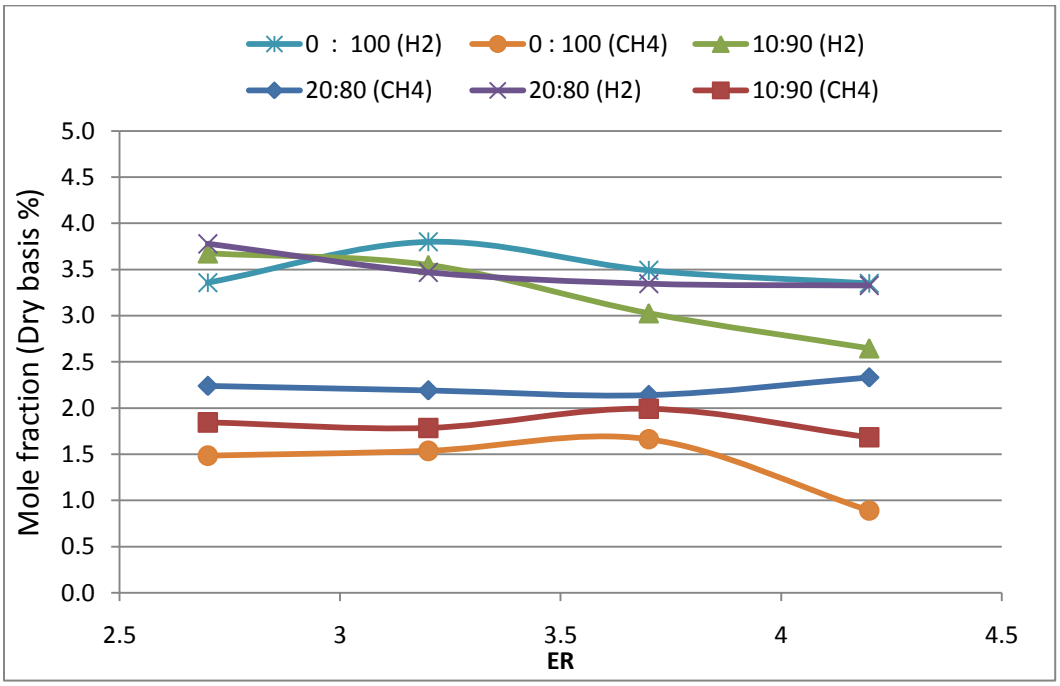

Figure 110. H_2 and CH_4 concentration for different coal: mesquite fuel mixtures

6.4.9 Gas HHV

When gas is used as a fuel in internal combustion engines or other applications, the optimal gasification performance conditions are those that yield the highest HHV and a more amount of combustible gases. In order to better understand the HHV of

synthesis gas, the concentration of each combustible gas species was converted to N_2 free basis in order to eliminate the dilution effect of N_2.

6.4.9.1 HHV of the Gas from Air Gasification

Figure 111 gives gas HHV of mesquite and juniper in kJ/kg and kJ/Nm^3 units as a function of ER. The gas produced from juniper generally yielded higher HHV in both N_2 and N_2-free conditions.

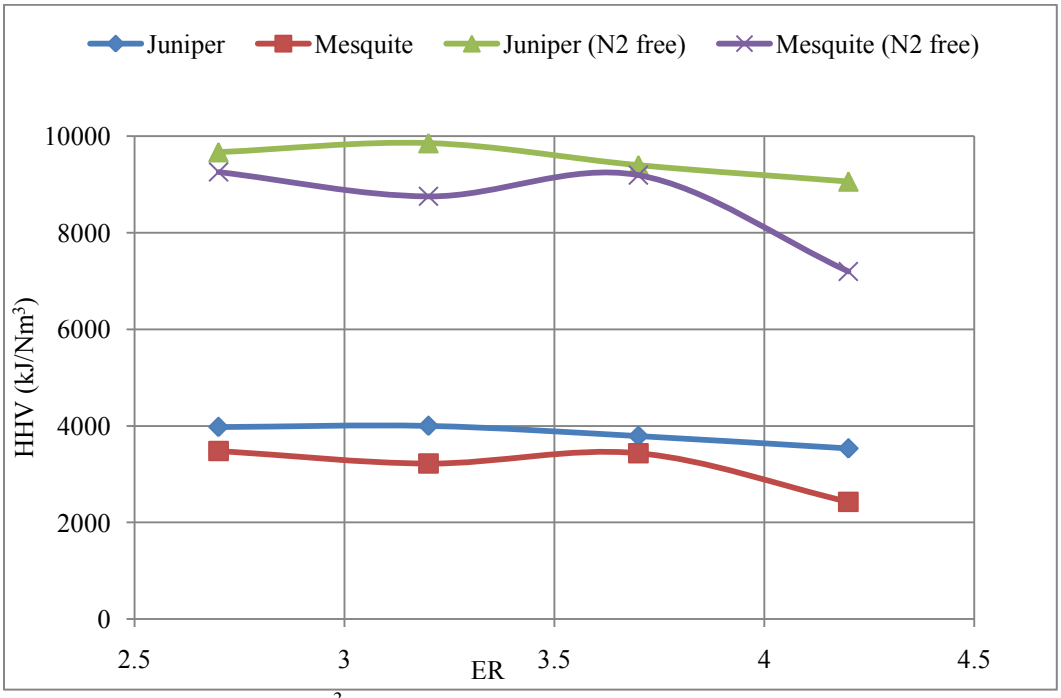

Figure 111. HHV (in kJ/Nm^3) of mesquite and juniper gas with moisture content 12.9% and 13.5%, respectively vs. ER. Adapted from[63].

As it is well known, CH_4 is a high quality fuel which almost "mimics" natural gas with HHV 55509 kJ/kg and is often used as reference for HHV. Figure 112 provides a comparison of HHV for syngas of mesquite and juniper fuel with moisture content between 12-13% and CH_4. The dry gas can reach almost 11% of HHV of CH_4 for juniper when ER is 2.7 when all the gas composition was included in the end product. Also, the HHV percentage decreased with the increase of ER for both mesquite and juniper. After removing the N_2, the heating value of gas increased to 27% of CH_4 HHV for juniper and 25.82% of CH_4 HHV for mesquite when the ER was set to 2.7, respectively. Increasing ER resulted in a decline in the heating value percentage.

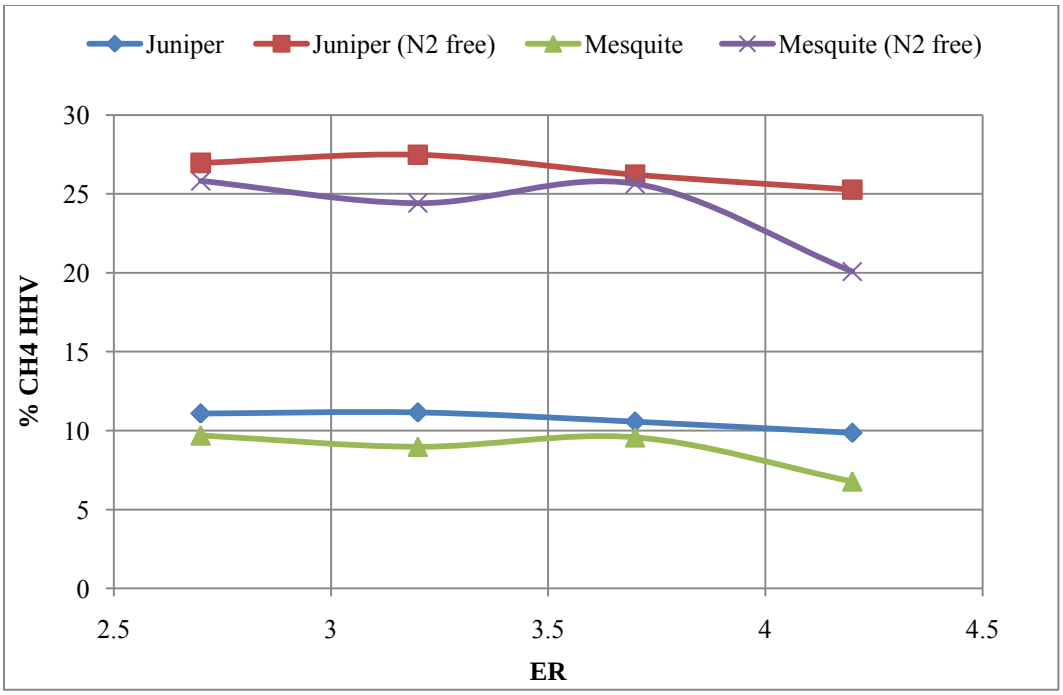

Figure 112. Percentage of CH_4 HHV vs. ER (kJ/kg basis). Adapted from [63]

6.4.9.2 Effect of the T_{peak}

Typically, the optimal gasification performance requires higher energy conversion efficiency along with high quality gases (i.e. higher heating value). Figure 113 and Figure 114 show the HHV of the producer gas from fuels with different moisture content. The HHV of mesquite gas was in a range of 2600 to 4100 kJ/Nm^3 and the HHV of juniper gas was between 2800 and 4600 kJ/Nm^3 when moisture content varied from 6% to 24%. Lower moisture content fuel produced higher quality gas. For instance , HHV of mesquite and juniper gases increased by 12% and 24% , respectively , when moisture content decreased from 12% to 6% at ER= 2.7. However, HHV of the gases produced from both the fuels decreased significantly when moisture content increased to 24% due to low gasification rate (i.e. low T_{peak}).

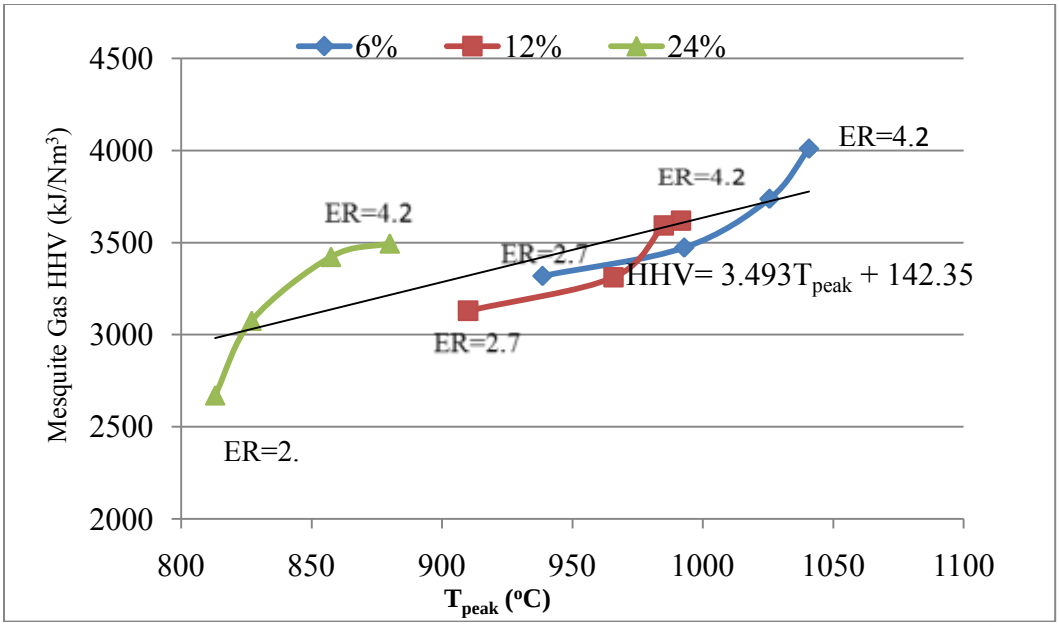

Figure 113 HHV of the mesquite gas with different moisture content (800 ^{o}C< T_{peak}<1100 ^{o}C)

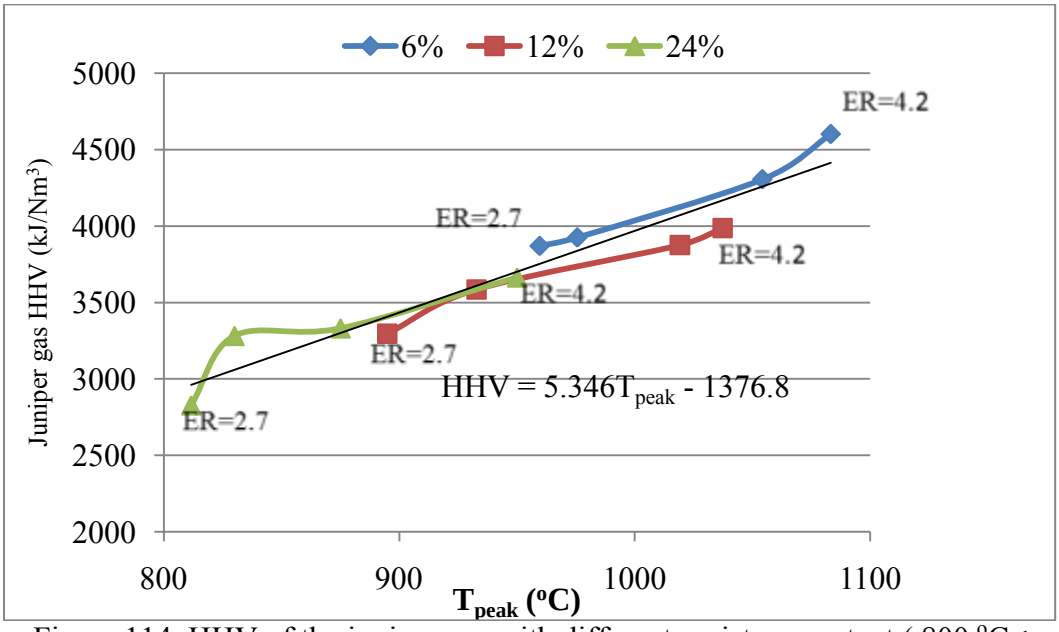

Figure 114. HHV of the juniper gas with different moisture content (800 ^{o}C< T_{peak}<1100 ^{o}C)

6.4.9.3 HHV of the Mesquite Steam Gasification Gas

Figure 115 shows the HHV of the mesquite fuel air-steam gasification gas under the S: F of 0, 0.15, 0.3, and 0.45 under dry tar free basis. It can be found that the HHV of the gas follow these inequalities $HHV_{0.45}<HHV_{0.15}\approx HHV_0 < HHV_{0.3}$. The HHV of the gas increased first when S: F ratio increased from 0.15 to 0.3 due to more H_2 was extracted from the steam. With the S: F ratio went up further (0.45), HHV of the gas decreased and its value was lower than that of gas obtained from S: F=0.15. This is because under high S:F condition, the lower gasification temperature resulted in generation of more noncombustible gas such as CO_2.

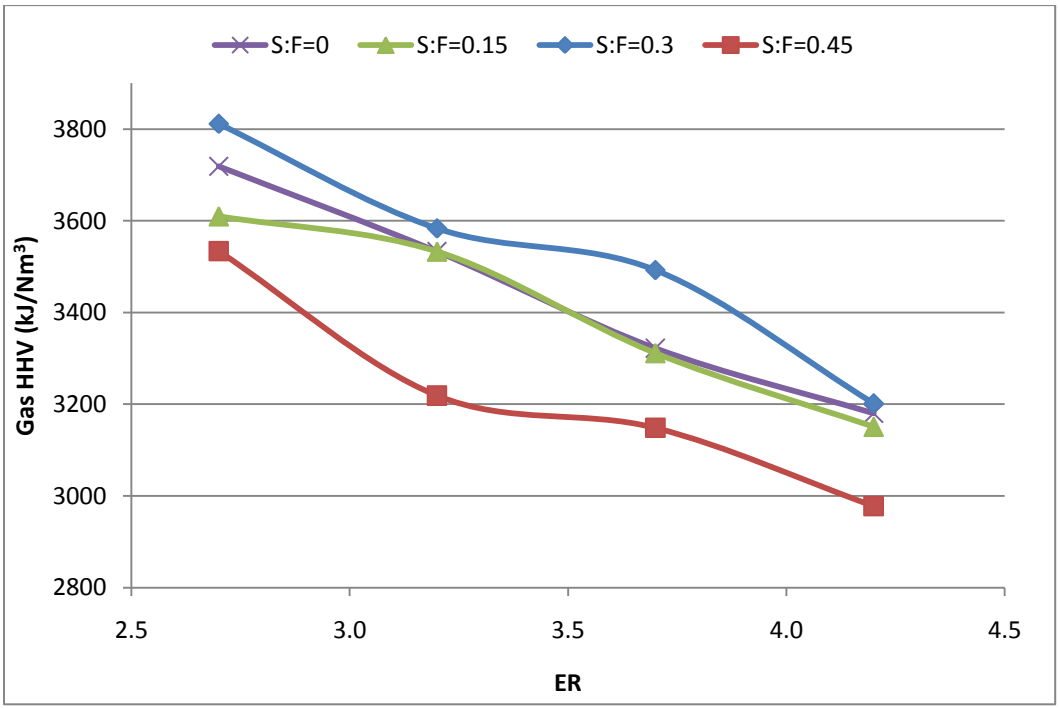

Figure 115. Gas HHV of steam gasification of mesquite biomass

6.4.9.4 HHV of Gas from Mesquite and PRB Coal Gasification

Figure 116 gives HHV of the gas from coal and mesquite mixture. It was found that HHV increased with the increase of the coal: mesquite ratio. From Figure 116, it was seen that HHV of the mesquite gas is between 2000 -3000 kJ/Nm^3; It increased to 2900 – 3600 kJ/Nm^3 with 10 % PRB coal in the mixture; HHV of gas can go up to 4000 kJ/m^3 at ER=2.7 PRB with 20% coal in the mixture.

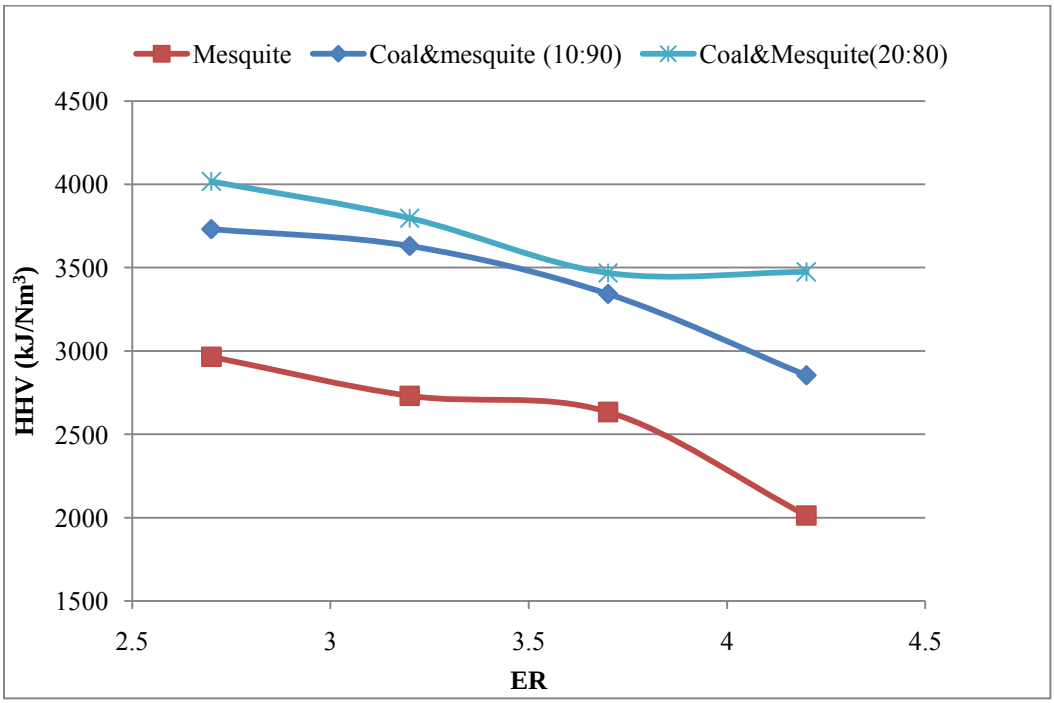

Figure 116. HHV for the PRB and mesquite mixture gas

6.5 Liquid Yield from the Gasification Process

6.5.1 Residence Time of the Mesquite and Juniper Gasification

The gas residence time is an important parameter in the tar formation. The gas residence time inside an updraft gasifier can be calculated by using the following equations:

$$\dot{m}_{total} = \dot{m}_{air} + \dot{m}_{f-g} \tag{81}$$

$$\dot{m}_{total} = \dot{m}_{air}\left(1 + \frac{\dot{m}_{f-g}}{\dot{m}_{air}}\right) \tag{82}$$

$$v = \frac{\dot{m}_{total}}{\rho \cdot A} \tag{83}$$

$$t = \frac{H}{v} \tag{84}$$

$\dot{m}_{total}$= totals gas mass flow rate

$\dot{m}_{air}$= Air mass flow rate

$\dot{m}_{f-g}$= Gas mass added to the gas stream assuming all the fuel except ash was converted into gas

V =gas velocity inside the gasifier

ρ =syngas density

A=gasifier chamber area

H=bed height in the gasifier

t=gas residence time

When calculation of syngas density, the temperature using average temperature inside the gasification chamber . The average temperature can be calculated as follow equation:

$$T_{avg} = \frac{\int_{X_{min}}^{X_{max}} T(x)dx}{X_{max} - X_{min}} \quad (85)$$

Where X_{min} presents the thickness ash layer and X_{max} is the bed height.

From equation (83) and (84), it can be found that the bed height, biomass flow rate, and air flow rate are the three main parameters that affect the gas residence time. In these experiments the bed height and the biomass feeding rate were kept constant during the experiments. Residence time can be altered by adjusting the air flow rate. Figure 117 and Figure 118 show the residence time of the mesquite and juniper fuel with different moisture content under different ER conditions. Higher air flow rate (low ER) led to less residence time. In addition, as the fuel moisture content increased from 6% to 24%, the residence time increased significantly. High moisture content fuel had very longer residence time due to low air flow rate and low gasification temperature inside the gasifier.

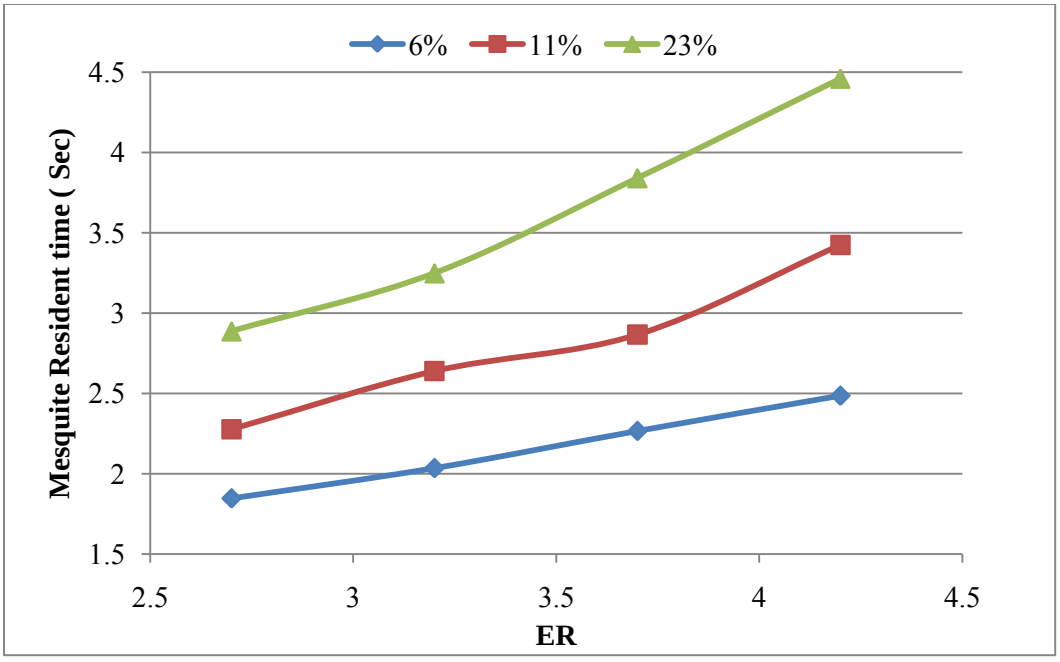

Figure 117. ER vs. the residence time of the mesquite fuel with different moisture content

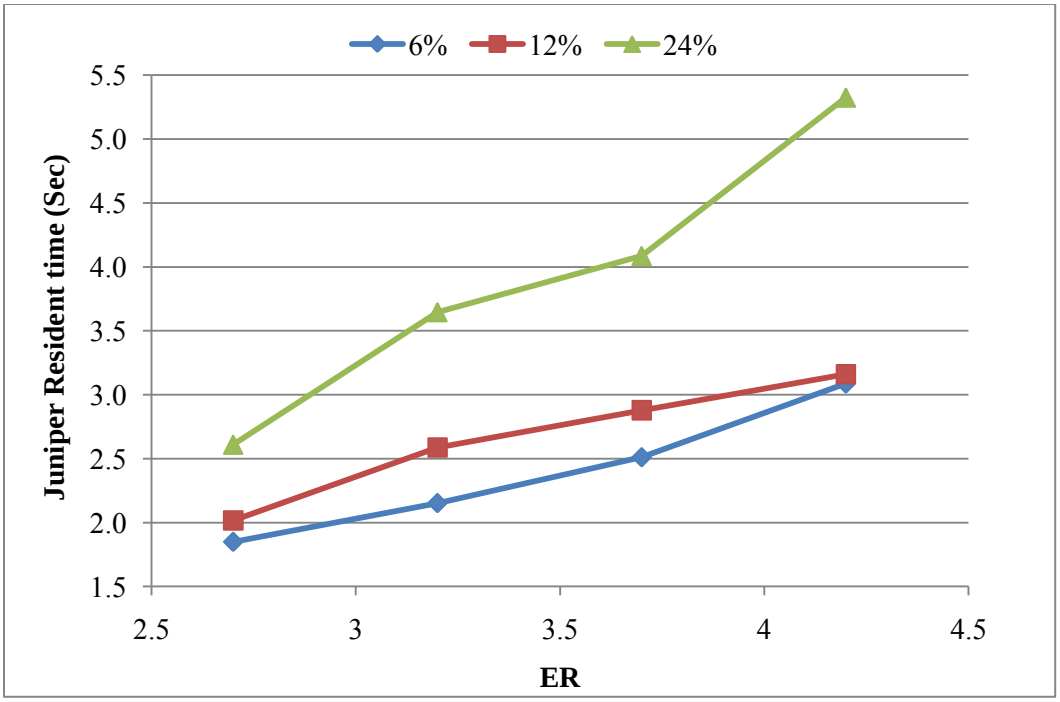

Figure 118. ER vs. the residence time of the juniper fuel with different moisture content

6.5.2 Specific Gas Yields

The specific yield gas (Nm^3 of gas per kg biomass as received) can be calculated by using the Nitrogen trace method. Figure 119 and Figure 120 show the total gas yield (CO_2+CO +H_2+ CH_4+C_2H_6) per unit mass biomass (Nm^3/ kg biomass). It was found that the total gas yield decreased with the increase of ER at constant moisture content (i.e. decrease in T_{peak}) and low moisture content biomass liberated more gas under the same ER. For instance, the total gas yield was 1.29 Nm^3/ kg biomass for juniper with moisture content 6% while only 0.79 Nm^3/ kg when biomass moisture content increased to 24% at ER=2.7. The reason of this would be discussed in the next section. Juniper released more gases when compared to mesquite under the same experimental condition due to its higher VM.

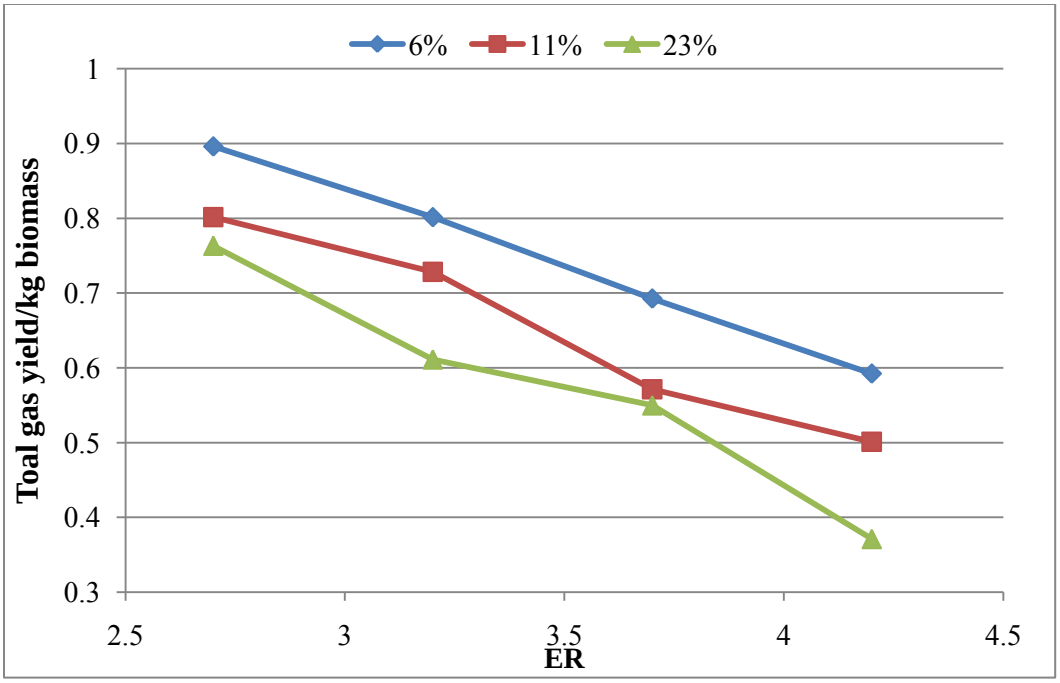

Figure 119. Volume of mesquite gas (CO_2+CO+H_2+CH_4+C_2H_6) from 1 kg biomass (Nm^3/kg)

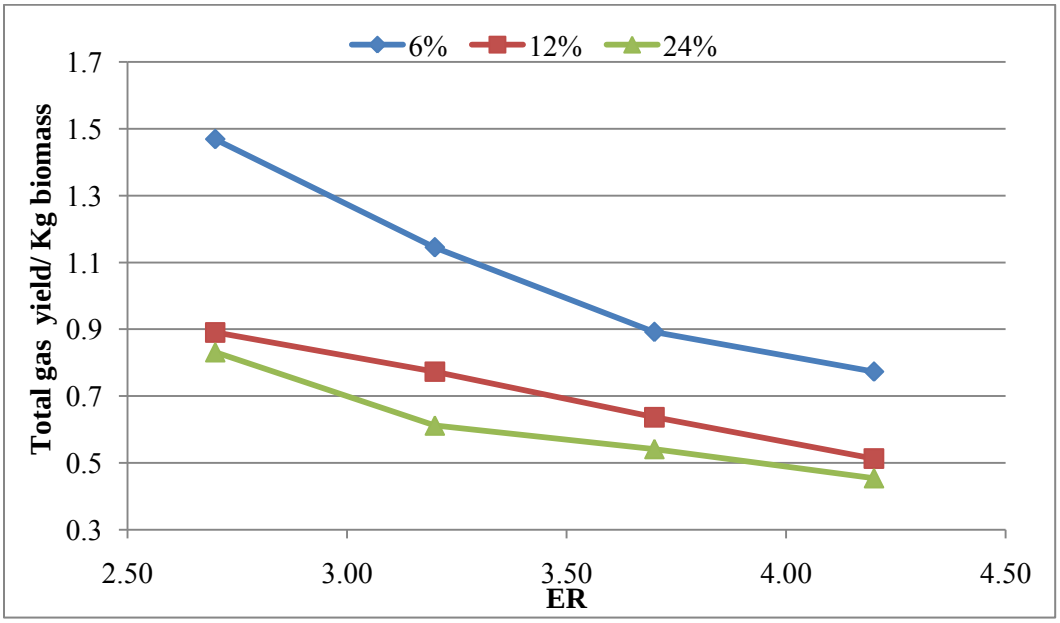

Figure 120. Volume of juniper gas (CO_2+CO+H_2+CH_4+C_2H_6) from 1 kg biomass (Nm^3/kg)

6.5.3 Tar Yield from the Mesquite and Juniper Gasification

It is well known that the updraft fixed bed gasifer produces a large amount tar since gas is leaving at colder temperature compared to downdraft gasifier. The conventional equivalence ratio and modified equivalence ratio are defined in equation (86) and (87):

Conventional Equivalence Ratio (ER):

$$ER = \frac{\text{stochiometric air moles}}{\text{actual air moles}} \tag{86}$$

Modified Equivalence Ratio (ER_M):

$$ER_M = \frac{\text{Stochiometric oxygen}}{\text{Actual oxygen through air and moisture}} \tag{87}$$

The tar yield as a function of ER and ER_m for both fuels was plotted from Figure 121 to Figure. 124. Figure 121 and Figure 122 present the tar yield for mesquite and juniper with moisture contents as a parameter. The tar content was above 100 g/ Nm^3 in the end product gas. As expected, tar yield increased with the increase in ER for all the moisture content levels and both fuels. Gasification temperature and residence time were two important parameters for the tar formation. Lower gasification temperature reduced the pyrolysis rate and tar cracking, and requires more residence time for the

particle to release the gases. On the other hand, the higher gasification temperature increased the pyrolysis rate and resulted in more long chain hydrogen-carbon tar cracking, then converting into gases. The high moisture content fuel was expected to produce more tar in the gasification process since the T_{peak} decreased with the increase in moisture content, and as well as more H_2O was condensed in tar. Fuel with moisture content of 12% generated more tar than that of 6% moisture content. However, the mesquite and juniper with moisture content of 24% produced less tar compared to those with moisture content 6% and 12%. This is because a large amount of moisture evaporation from the fuel resulted in very low gasification temperature and more combustibles loss in the ash. It was also found that unburned O_2% will increase in the product gases with higher moisture content. It was found that about 5 - 6% unused O_2 remained in the end product gas for high moisture content fuel (24%). For low moisture content fuel, the gasification temperature played a more important role than residence time in the tar formation in that the tar decreased even though the residence time was less for the low moisture fuel. The high moisture content fuel (24%) produced less tar in the end product gas. Furthermore, the gas HHV and yield as well as its gasification efficiency are reduced significantly.

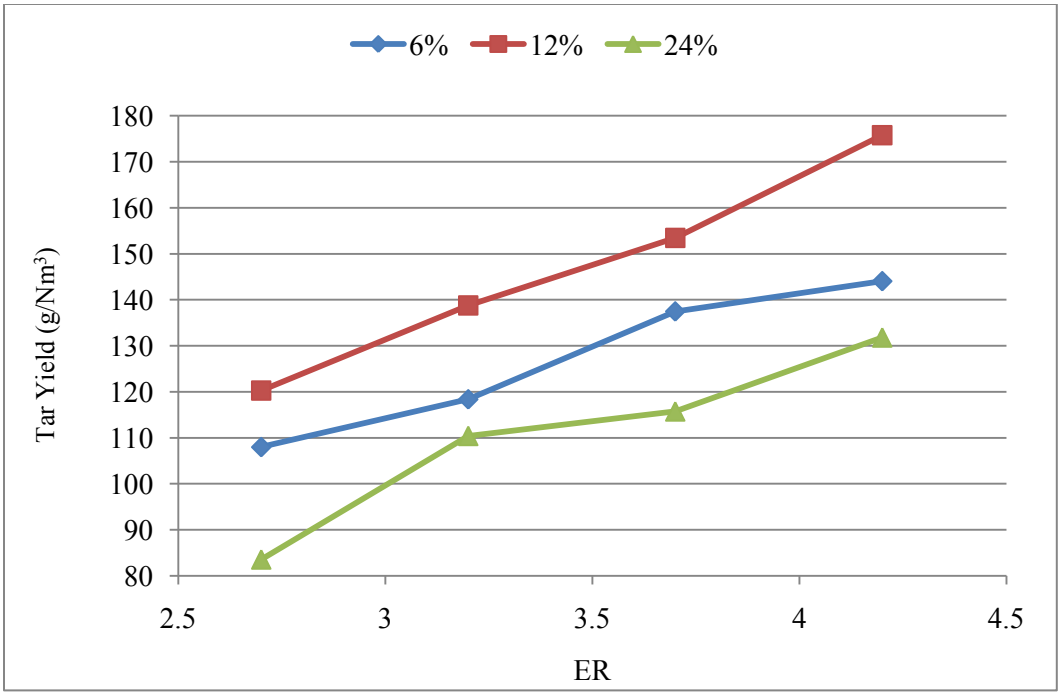

Figure 121.Tar yield for mesquite fuel with different moisture content

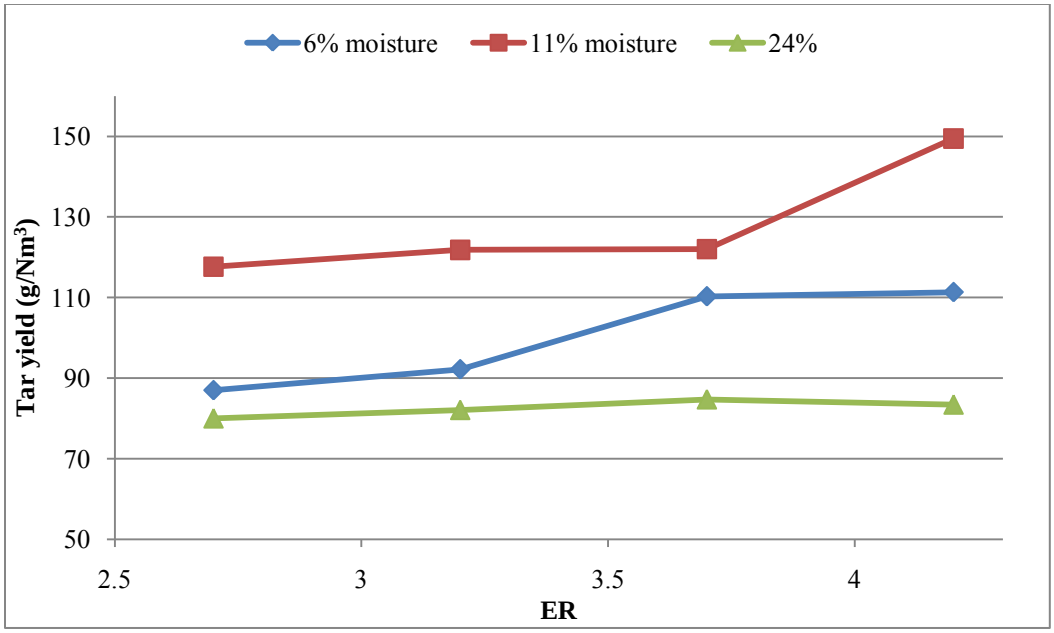

Figure 122. Tar yield for juniper fuel with different moisture content

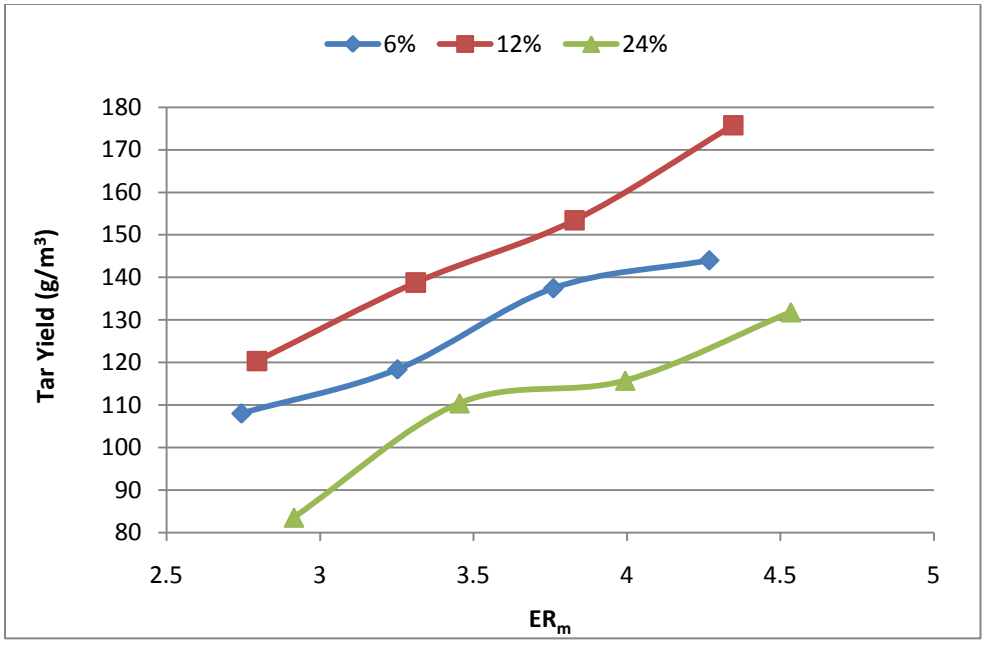

Figure 123. Tar yield vs. ER_m for mesquite fuel with different moisture content

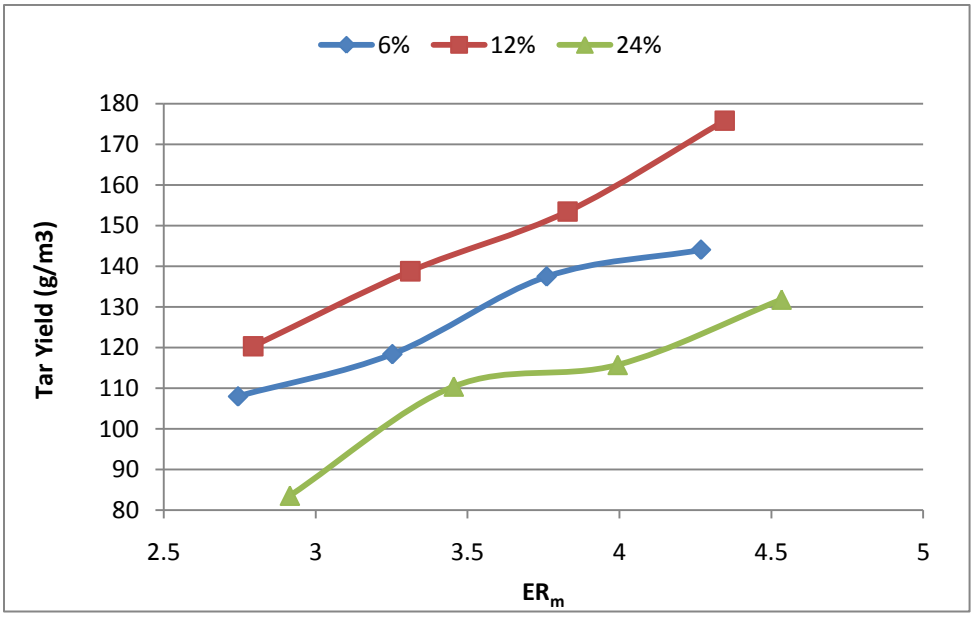

Figure. 124 Tar yield vs. ER_m for juniper fuel with different moisture content

6.5.4 Liquid and Gas Yield Percentages from Unit Biomass

Combustible gases, char, ash, and tar are the main products in the gasification process. Due to the small amount of ash (3%) yield for mesquite and juniper fuels, the weight of the ash was negligible. The weight of the tar was measured in the gasification process and the amount of the combustible gases was calculated by using the nitrogen trace method as mentioned before in the gas yield section. Carolyn Roots [64] summarized liquid, char, and gas yield from pyrolysis and gasification processes. It was found that the updraft gasifier produced 10% to 20% tar while char content in the ash from the updraft gasifier was low. Form Table 18 and Table 19, it was observed that with an increase in fuel moisture content the gas yield (f_{gas}) decreased while the yield of the tar (f_{tar}) increased slightly. F_{gas} and f_{tar} are defined as follow:

$$f_{gas} = \frac{m_{gas}}{m_{fuel} + m_{O2}} \tag{88}$$

$$f_{tar} = \frac{m_{tar}}{m_{fuel} + m_{O2}} \tag{89}$$

Where m_{tar} and m_{gas} are the mass of the tar and gas collected in the gasification process; M_{fuel} is the mass of fuel; m_{O2} is the mass of the O_2 in the air supplied to the gasifier.

When the fuel moisture increased to 24%, both the gas and tar yield decreased significantly. This is because under high moisture condition the less combustible content

was available for per unit biomass in feed and less air was sent into the gasifier to maintain the same equivalence ratio. The moisture evaporation required more energy which resulted in lowering the gasification temperature and thus the fuel oxidation rate reduced significantly.

In addition, at constant moisture content, increase of ER (with less air supplied into the gasifier) led to decrease of the gas yield. First, this may due to the fact that the higher ER (lower gasification temperature) resulted in less tar cracking and less gas generated. Also, with less air supplied into the gasifier, less carbon was oxidized into CO, CO_2, or CH_4 and more char left. The tar yield per unit fuel mass increased slightly when moisture content increased from 6% to 12% due to the longer residence time inside the gasifier for higher moisture content fuel. The tar yield was in a range of 13%-19% for mesquite and juniper.

Table 18. Gas and liquid yield in kg per unit mesquite biomass (as received)

	f_{gas}				f_{tar}			
Moisture \ ER	2.7	3.2	3.7	4.2	2.7	3.2	3.7	4.2
6%	0.52	0.49	0.42	0.36	0.13	0.15	0.17	0.18
12%	0.45	0.43	0.33	0.31	0.15	0.16	0.18	0.19
24%	0.41	0.38	0.34	0.25	0.12	0.14	0.14	0.12

Table 19. Gas and liquid yield in kg per unit juniper biomass (as received)

	f_{gas}				f_{tar}			
Moisture \ ER	2.7	3.2	3.7	4.2	2.7	3.2	3.7	4.2
6%	0.57	0.55	0.53	0.50	0.13	0.15	0.16	0.17
12%	0.52	0.44	0.35	0.32	0.15	0.17	0.17	0.19
24%	0.44	0.38	0.34	0.29	0.11	0.10	0.09	0.07

Table 20 and Table 21 show the sum of the gas and tar yield from per unit weight mesquite and juniper biomass. It was found that the sum of the tar and gas yield decreased with the increase of the ER. Also, with the increase of the moisture content, the sum of the tar and gas yield decreased.

Table 20. The sum of gas and tar yield from per unit mesquite in gasification process

Moisture content	6%				12%			
ER	2.7	3.2	3.7	4.2	2.7	3.2	3.7	4.2
Gas (f_{gas})	0.52	0.49	0.42	0.36	0.45	0.43	0.33	0.31
Tar (f_{tar})	0.13	0.15	0.17	0.18	0.15	0.16	0.18	0.19
Total	0.65	0.64	0.61	0.57	0.60	0.61	0.51	0.50

Table 21. The sum of gas and tar yield from per unit juniper in gasification process

Moisture content	6%				12%			
ER	2.7	3.2	3.7	4.2	2.7	3.2	3.7	4.2
Gas (f_{gas})	0.57	0.55	0.53	0.50	0.52	0.44	0.35	0.32
Tar (f_{gas})	0.13	0.15	0.16	0.17	0.15	0.17	0.17	0.19
Total	0.7	0.70	0.69	0.67	0.67	0.61	0.52	0.51

6.5.5 Energy Conversion Efficiency of Mesquite and Juniper Fuel

The gas and tar mass% yield do not indicate the quality of products from the gasification process since heat value per unit mass of gas and tar may change. On the other hand, the HHV gives the energy density of the gas; it does not provide the information on the fraction of the energy recaptured as gas from per unit fuel supplied to the gasifier [15]. This energy recuperated in the form of gas or the energy conversation efficiency (ECE) can be calculated in following equation

$$\eta_{Gas,E} = \frac{\mathrm{HHV}_{\mathrm{Gases}} \bullet \dot{m}_{gas}}{\dot{m}_{\mathrm{Fuel}} * \mathrm{HHV}_{\mathrm{Fuel}} + \dot{m}_{\mathrm{steam}} (\lambda + 4.18(373 - 298))} \tag{90}$$

where, $\dot{m}_{gas}$, $\dot{m}_{\mathrm{Fuel}}$ Fuel, and $\dot{m}_{\mathrm{steam}}$ correspond to the mass of fuel and steam supplied respectively to the gasifier in each normal m3 of dry product gases and λ is the latent heat of steam. HHV Fuel is the gross heat value (kJ/ kg of as received fuel) of the fuel and η Gas, E is the energy conversion efficiency, or energy recovery. In these experiments, only air was sent into the gasifier as gasification media. Setting $\dot{m}_{\mathrm{steam}}$=0, equation (90) can be simplified as:

$$\eta_{Gas,E} = \frac{\mathrm{HHV}_{\mathrm{Gases}} \bullet \dot{m}_{gas}}{\dot{m}_{\mathrm{Fuel}} * \mathrm{HHV}_{\mathrm{Fuel}}} = \frac{f_{gas} \bullet HHV_{gas}}{HHV_{fuel}} \tag{91}$$

Table 22 gives the ECE of the mesquite and juniper fuel. The energy recover efficiency was between 22.3-60% and 25-77% for mesquite and juniper, respectively. Juniper fuel has higher conversion efficiency than that of mesquite. This may due to the higher volatile content in the juniper (As Table 1) which releases more gas. It was observed from

Table 22 that ECE decreased with the increase of the ER. Also, with the increase of the moisture, the conversion efficiency decreased for both fuels. Higher ER and moisture content leads to decrease of ECE. Lower temperature resulted in decreasing of the amount of the combustible gas and more tar was generated. When ER=4.2 and moisture content =24% for mesquite, ECE went down to 22.3%. The gasification process tends to be almost pure pyrolysis process [15].

Table 22. Energy conversion efficiency of mesquite and juniper fuel

Moisture content	Mesquite				Juniper			
	ER							
	2.7	3.2	3.7	4.2	2.7	3.2	3.7	4.2
6%	60.45	49.62	38.41	33.70	76.82	56.08	43.04	36.41
12%	51.39	41.28	33.94	26.43	53.85	44.17	37.75	28.48
24%	44.84	39.59	31.02	22.30	48.19	40.61	33.71	25.66

7 SUMMARY AND CONCLUSIONS

The summary and conclusions of this study on TGA and gasification of mesquite and juniper fuels are presented in this section.

7.1 Fuel Properties and TGA Studies of the Mesquite and Juniper Fuel

1. The mesquite and juniper fuels harvested from the northern Texas areas have very low ash content (less 3%), high VM (80% as DAF), and HHV of 20,000 kJ/kg (as DAF).
2. In the TGA study, five different sized mesquite and juniper fuels (150-300 μm, 300-580 μm, 580-1190 μm, 1190-2000 μm, and 2000-2300 μm) were heated up in an inert environment to finial temperature of 1500 ^{o}C at a heating rate of 20 ^{o}C. The fuel particle size did not have significant effect on the pyrolysis process.
3. Juniper and mesquite began pyrolysis around 500 K and both fuels finished pyrolysis around 800 K. The rapid pyrolysis process occurred between 580 K and 700 K within which about 70% is volatile released from the fuel. The fuel weight loss as a function of temperature was recorded and the maximum weight rate and temperature at which it occurs can be found from the curves.
4. Both single and parallel reactions (SRM and PRM) were employed to simulate the pyrolysis process. The chemical kinetics such as activation energy and pre-exponential were obtained from these model.

a. Although the maximum volatile method (SRM-MVR) is based on a single point data, it is better than SRM-CA and results in less error. Due to its simplicity and accuracy around maximum volatile release rate (MVR), a program has been developed to automate the extraction of kinetics from TGA data on volatile yield vs. T (or time) data.

b. Juniper has higher activation energy than that of mesquite for all of the models. Typically activation energies for the three methods follow these inequalities $E_{SRM-CA} < E_{SRM-MVR} < E_{PRM}$.

c. The PRM seems to be the best model compared to SRM, and the SRM-CA seems to introduce largest error, generating 8% and 13 % standard deviation, respectively, for the whole domain to predict the juniper and mesquite mass loss.

d. Due to the low heating rate (20^{o}C/min), the particle size seems to have little influence on the activation energies and pre-exponential factors. The activation energies for mesquite and juniper were around 161,000 kJ/kmol and 157,000 kJ/kmol using PRM.

5. TGA studies of mesquite and juniper with dolomite catalyst blend were also performed

a. At low temperature 30 ^{o}C – 350 ^{o}C, catalyst did not have significantly effect on the fuel pyrolysis. When temperature was increased to 400 ^{o}C, more volatile matters were liberated from the fuel and the weight loss curves started deviating. With the temperature went up further (>700 ^{o}C), the dolomite catalyst started decomposed and the weight loss curves merged again.

b. For the weight loss rate of the dolomite and mesquite and juniper blend fuel, there are three weight loss peaks: the first peak was due to the moisture content released, the second peak due to the volatiles liberated from the hemicellulose and cellulose, and the third peak due to the decomposing of the dolomite catalyst.

c. CO, CO_2, NH_3, H_2O and CH_4 were the main gas species liberated from the pyrolysis of mesquite and juniper biomass fuels. The catalyst did not have significant effect on gas yield when the pyrolysis temperature. The CO concentration increased after temperature went up to 750 ^oC due to the dolomite decomposed, while the percentage of the CO_2, H_2O, CH_4 and Formaldehyde did not vary much with different wt % of dolomite

7.2 Modeling Studies

7.2.1 EES Model

EES was employed to simulate the mesquite and juniper gasification process according to the mass and energy conservation and thermodynamic equilibrium. The effect of the adiabatic temperature, moisture content, and ER on the gas composition and adiabatic temperature was investigated.

1. At constant moisture content, the CO and H_2 concentration decreased with the increase of the gasification adiabatic temperature. While the CO_2 increase with the increase of the adiabatic temperature.

2. At set adiabatic temperature of 1000 ^{o}C, the H_2 and CO_2 concentrations increase and the CO percentage decrease with the moisture content increase in the mesquite and juniper fuel. In addition, the H_2 and CO percentage increases with the decrease of the ER while the CO_2 increased with the increase of the ER.
3. The HHV of mesquite and juniper gases decreased with the increase of the adiabatic temperature from 800 K to 1100 K. It should be noticed that the equilibrium implies sufficient time to achieve. The HHV of the juniper is higher than that of mesquite

7.2.2 NASA Chemical Equilibrium with Applications (CEA) Model

In this model, both mesquite and juniper with 6%, 12%, and 24% moisture content were investigated under several modified ER of 2.7，3.2，3.7, and 4.2. The results are presented as follow:

1. The end product of juniper gases mainly contained 21%-31% H_2, 12-22% CO_2, 6-21% CO, 0-4% CH_4. The end product of mesquite gas mainly contained 22-31% H_2, 14-24%CO_2, 6-20% CO, and 0-4% CH_4.
2. H_2 percentage increased slightly with the increase of the ER. Fuel with high moisture content produced higher H_2 percentage in the end product.
3. With the increase of the ER, CO percentage increased while the CO_2 concentration decreased. Higher moisture content fuel produced more CO_2 while less CO under a constant ER.

4. CH_4 concentration in gas is very low compared to H_2, CO and CO_2. Under lower moisture content (6%) and ER (ER< 3.2), the CH_4 percentage can be neglected almost equal to 0. In addition, higher moisture content fuel produces more CH_4.
5. The adiabatic temperature for the mesquite and juniper fuel varied between 850 K and 1400 K. And the adiabatic temperature decreased with the increase of the ER. Fuel with lower moisture content has a higher an adiabatic temperature than that of the higher moisture content.

7.3 Gasification Results

Experiments on gasification using air, air-steam as media were carried out and the data on the gasification profile, gas composition, and HHV were obtained. In addition, the results of co-gasification of mesquite and PRB coal were presented.

7.3.1 Temperature Profile

1. The peak temperatures during combustion of both mesquite and juniper samples can went up to 1000 ^oC and occurred at a distance of about 3-6 cm above the grate in the gasifier. Temperature decreased along the axis of the gasifier in the reduction, pyrolysis, and drying zone due to the endothermic reactions. Increase of the ER resulted in decreasing of the gasification temperature due to less air was

supplied into the gasifier. In addition, as fuel moisture increased, T_{peak} decreased. The maximum T_{peak} occurred at ER=2.7 and moisture content=6%.

2. Both peak and average bed temperature decreased when used air-steam as gasification media compared to air gasification. In addition, increase of the S: F ratio and ER decreased the gasification temperature because char-steam reaction was endothermic.

3. When PRB coal was mixed with mesquite fuels at ratios of 10:90 and 20:80 for gasification experiment, T_{peak} increased significantly due to the higher HHV of the PRB coal. The peak temperature of blend of PRB coal and mesquite with a ratio 20:80 was 1200 ^{o}C at ER=2.7 while T_{peak} for pure mesquite is around 900 ^{o}C at ER=2.7.

7.3.2 Gas Composition

1. When ER decreased from 4.2 to 2.7, the mole composition of the end product gas for mesquite with moisture content 12.9% varied: 13-21% CO, 1.6-3% H2, 1-1.5% CH4, 0.4-0.6% C2H6, and 11-25% CO2. The mole composition of the end product gas for juniper with moisture content13.2% consisted of 21-25% CO, 2.5-3.5% H_2, 1.5-1.8% CH4, 0.3-0.5% C2H6, and 9-12% CO2. For both mesquite and juniper samples, increasing ER decreased the CO and H2 mole percentage and raised the CO2 and N2 mole percentage. With the moisture content increased, the CO

increased while CO2 and H2 increased. At high moisture content (24%), the gas yield decreased significantly due to the low gasification rate.

2. The main products for air-steam gasification are CO, CO_2, H_2, N_2, CH_4, and C_2H_6. Increasing of the S: F ratio from 0 to 0.45, the mole composition of the end product gas for juniper with moisture content 12% varied: 8-20% CO, 2-11% H_2, 1-3% CH_4, and 10-18% CO_2. Increase of the S: F ratio led to increase of the CO_2 and H_2 concentration and decrease of the CO percentage.
3. The T_{peak} increased with increase of the PRB coal percentage in the blend, CO_2 concentration decreased while CO and CH_4 percentage increased in the end product gases. When the coal % increased from 0 to 20%, the end product gases contained 14-23% CO, 6-18% CO2, 2.5-4% H_2, and 0.7-2.5% CH_4.

7.3.3 HHV of Gas

1. For air gasification, the HHV ranged from 2500 kJ/Nm^3 to 4100 kJ/Nm^3 for mesquite and from 2600 kJ/Nm^3 to 4600 kJ/Nm^3 for juniper when moisture content decreased from 24% to 6%. Lower moisture content fuels produced higher HHV gas due to the higher gasification temperature. Generally, the gas HHV increased with the increase of the gasification peak temperature.
2. The HHV of the mesquite gas increased at first when the S:F increased from 0.15 to 0.3, and then it decreased when the S:F was increased further from 0.3 to 0.45.

HHV of the gas ranged from 2800 to 3800 kJ/Nm^3 when moisture content increased from 0.15 to 0.45. The highest HHV of gas was obtained at S: F=0.3.

3. The HHV of the co-gasification gas from the mesquite and PRB coal blend increased with the PRB wt% in the mixture due to the high carbon content in the coal which resulted in more combustible gas released. The HHV increased by 20% when the coal percentage was increased from 0 to10 % in the blend.

7.3.4 **Liquid and Gas Yield from the Gasification Process**

1. Low moisture content fuel produced more gas ($CO+CO_2+H_2+CH_4+C_2H_6$) per unit weight biomass and the HHV of the producer gas was very high. Gasification temperature and residence time are two dominant parameters that affected the formation of liquid in the gasification process. Higher gasification temperature and longer residence times resulted in more tar cracking.
2. Mesquite and juniper samples with 12% moisture content generated more tar than fuels with 6% and 24% moisture. Fuel with 24% moisture produced the least tar. However, its oxidization rate, gas yield rate, and gas HHV reduced significantly.
3. The liquid yield from the mesquite and juniper gasification process included light tar (90%) and heavy tar (10%). The major component of the light tar was moisture and the heavy tar had very high volatile matter and lower ash content. The HHV of the heavy tar was more than 28,000 kJ/kg on a DAF basis.

Based on the gasification efficiency, the optimum moisture content was 6%, ER=2.7 since these conditions yield higher HHV gas, generated more gas, and yielded less tar.

REFERENCES

[1] "Climate Change 2007," *Synthesis Report,* vol. http://www.ipcc.ch/pdf/assessment-report/ar4/syr/ar4_syr_spm.pdf, 2007.

[2] U. S. E. I. Administration, "Complete international energy outlook " *http://www.eia.gov/oiaf/ieo/pdf/0484%282010%29.pdf,* 2010.

[3] L. Devi, K. J. Ptasinski, and F. J. J. G. Janssen, "A review of the primary measures for tar elimination in biomass gasification processes," *Biomass & Bioenergy,* vol. 24, pp. 125-140, 2003.

[4] R. Salzmann and T. Nussbaumer, "Fuel staging for NOx reduction in biomass combustion: experiments and modeling," *Energy & Fuels,* vol. 15, pp. 575-582, 2001.

[5] L. L. Tan and C. Z. Li, "Formation of NOx and SOx precursors during the pyrolysis of coal and biomass. Part I. Effects of reactor configuration on the determined yields of HCN and NH_3 during pyrolysis," *Fuel,* vol. 79, pp. 1883-1889, 2000.

[6] K.J.Ptasinki, A. Ues, and M.Jurascik,Chapter 4. Biowaste-to-biofuel routes via gasification, Biomass Gasification: Chemistry, Processes and Applications, Nova Publishers, 2009.

[7] F.Pinto , R.N.Andre, and I.Gulyurtlu, Chapter 2. Innivation on biomass waste utilization through gasification and co-gasification.Stage of development and needs for further R&D,Biomass Gasification: Chemistry, Processes and Applications, Nova Publishers, 2009.

[8] G. Gordillo, "Fixed Bed Counter Current Low Temperature Gasification of Dairy Biomass and Coal-dairy Biomass blends Using Air-Steam," Ph.D Dissertation,Texas A&M University, 2009.

[9] G. Morris, "The Value of the Benefits of U.S. Biomass Power," *Report for DOE,* 1999.

[10] B. Murray, R.Nicholson, M. Ross , T. Holloway , and S. Patil, "Biomass Energy Consumption in the Forest Products Industry," *Final Report for U.S. Department of Energy,* 2006.

[11] R.J.Ansley, M. Mirik, and M.J.Castellano, "Structural biomass partitioning in regrowth and undisturbed mesquite (Prosopis glandulosa): Implications for bioenergy uses," *Global Change Biology Bioenergy,* vol. 2, pp. 26-36, 2010.

[12] R. J. Ansley, H. T. Wiedemann, M. J. Castellano, and J. E. Slosser, "Herbaceous restoration of juniper dominated grasslands with chaining and fire," *Rangeland Ecology & Management,* vol. 59, pp. 171-178, Mar 2006.

[13] Y. Z. Tang, Y. B. Yang, M. Zhao, L. Yao, and Y. Li, "CoS-based QoS management framework for grid services," *Sixth International Conference on Grid and Cooperative Computing, Proceedings,* pp. 451-455, 2007.

[14] S .Priyadaran, K. Annamalai, J.M. Sweeten, S. MUkhtar, and M. T. holtzapple, "Fixed bed gasification of feedlot and poultry litter biomass," *Trans ASAE,* vol. 47, pp. 1689-1696, 2005.

[15] R. Warnecke, "Gasification of biomass: comparison of fixed bed and fluidized bed gasifier," *Biomass & Bioenergy,* vol. 18, pp. 489-497, 2000.

[16] G. Gordillo and K. Annamalai, "Adiabatic fixed bed gasification of dairy biomass with air and steam," *Fuel,* vol. 89, pp. 384-391, 2010.

[17] C.D.Blasi, G.G.Signorelli, and Portoricco, "Countercurrent fixed-bed gasification of biomass at laboratory scale," *Industrial & Engineering Chemistry Research,* vol. 38, pp. 2571-2581, 1999.

[18] N.A.Skov and M. L. Paperworth, "The Pegasus Unit," Pegasus Publishers, Olympia, *Washington*, 1974.

[19] C. Hoglund, "Agriculture residences as fuel for producer gas generation," Master thesis. Royal Institute of Technology, Sweden, 1981.

[20] "An investigation of the downdraft gasification characteristics of agriculture and forestry residues," *California Energy Commission. Interim Report,* 1979.

[21] K. P. Raman, W. P. Walawender, and L. T. Fan, "Gasification of Feedlot Manure in a Fluidized-Bed Reactor - the Effect of Temperature," *Industrial & Engineering Chemistry Process Design and Development,* vol. 19, pp. 623-629, 1980.

[22] L.Young and P.Pian, "High-temperature, air-blown gasification of dairy-farm wastes for energy production," *Energy,* vol. 28, pp. 655-672, 2003.

[23] M. J. Prins, K. J. Ptasinski, and F. J. J. G. Janssen, "Thermodynamics of gas-char reactions: first and second law analysis," *Chemical Engineering Science,* vol. 58, pp. 1003-1011, 2003.

[24] K. Annamalai and I. K.Puri, Combustion science and Engineering, Taylor&Francis Group, 2007.

[25] L.D. Smoot and P. J. Smith, "Coal combustion and gasification," Plenum Press, New York, 1985.

[26] S. S. Thrnapal, "Gasification of low ash partially composted dialy bioomass with enriched air mixture," Master Thesis, Texas A&M University, 2010.

[27] C.D. Blasi, "Modeling wood gasification in a countercurrent fixed-bed reactor," *Aiche Journal,* vol. 50, pp. 631-653, 2004.

[28] M. L. Hobbs, P. T. Radulovic, and L. D. Smoot, "Combustion and Gasification of Coals in Fixed-Beds," *Progress in Energy and Combustion Science,* vol. 19, pp. 505-586, 1993.

[29] K. Annamalai and W. Ryan, "Interactive Processes in Gasification and Combustion .2. Isolated Carbon, Coal and Porous Char Particles," *Progress in Energy and Combustion Science,* vol. 19, pp. 383-446, 1993.

[30] J. Bellettre, L. Gerun, M. Paraschiv, R. Vijeu, M. Tazerout, B. Gobel, and U. Henriksen, "Numerical investigation of the partial oxidation in a two-stage downdraft gasifier," *Fuel,* vol. 87, pp. 1383-1393, 2008.

[31] D.L.Giltrap and G. R. G. Barnes, "Modelling Fixed-bed Biomass Gasifiers: A Review," *Biomass Gasification : Chemistry, Processes and Applications,* 2009.

[32] L. A. Fryda, "Development of innovative systems of electricity production through biomass exploitation," PhD Dissertation, National Technical University of Athens, Greece, 2006.

[33] M. J.Antal and G.Varhegyi, "Cellulose Pyrolysis Kinetics - the Current State Knowledge," *Industrial & Engineering Chemistry Research,* vol. 34, pp. 703-717, 1995.

[34] H. Teng and Y. C. Wei, "Thermogravimetric studies on the kinetics of rice hull pyrolysis and the influence of water treatment," *Industrial & Engineering Chemistry Research,* vol. 37, pp. 3806-3811, 1998.

[35] L. Puigjaner, J. J. Manya, and E. Velo, "Kinetics of biomass pyrolysis: A reformulated three-parallel-reactions model," *Industrial & Engineering Chemistry Research,* vol. 42, pp. 434-441, 2003.

[36] J. J. M. Orfao, F. J. A. Antunes, and J. L. Figueiredo, "Pyrolysis kinetics of lignocellulosic materials - three independent reactions model," *Fuel,* vol. 78, pp. 349-358, 1999.

[37] C. Tangsathitkulchai, S. Junpirom, and M. Tangsathitkulchai, "Thermogravimetric analysis of longan seed biomass with a two-parallel reactions model," *Korean Journal of Chemical Engineering,* vol. 27, pp. 791-801, 2010.

[38] D.B. Anthony , H.C. Howard , H.C. Hottel , and H. P. Meissner, "Rapid devolatilization of pulverized coal," *Symposium (International) on Combustion,* vol. 15, pp. 1303-1317, 1974.

[39] A. J. Tsamba, W. H. Yang, and W. Blasiak, "Pyrolysis characteristics and global kinetics of coconut and cashew nut shells," *Fuel Processing Technology,* vol. 87, pp. 523-530, 2006.

[40] B. Martin and K. Annamalai, "Pyrolysis and ignition of behavior of coal, cattle biomass, and coal/cattle biomass blends,"Master thesis ,Texas A&M University, 2006.

[41] T. Hanaoka, S. Inoue, S. Uno, T. Ogi, and T. Minowa, "Effect of woody biomass components on air-steam gasification," *Biomass & Bioenergy,* vol. 28, pp. 69-76, 2005.

[42] S. Pipatmanomai and S. Kaewluan, "Potential of synthesis gas production from rubber wood chip gasification in a bubbling fluidised bed gasifier," *Energy Conversion and Management,* vol. 52, pp. 75-84, 2011.

[43] E. Kurkela, P. Stahlberg, P. Simell, and J. Leppalahti, "Updraft Gasification of Peat and Biomass," *Biomass,* vol. 19, pp. 37-46, 1989.

[44] J. Hightower, "Fluidized bed gasification of agriculture residues,," Master thesis, Chemical Engineering, Texas Tech University, 1979.

[45] S. S. Thanapal, K. Annamalai, J. Sweeten, and G. Gordillo, "Fixed Bed Gasification of Dairy Biomass with Enriched Air Mixture," *Applied Energy,* under eview, 2012.

[46] C. Lucas, D. Szewczyk, W. Blasiak, and S. Mochida, "High-temperature air and steam gasification of densified biofuels," *Biomass & Bioenergy,* vol. 27, pp. 563-575, 2004.

[47] A. Dutta and S. Jarungthammachote, "Thermodynamic equilibrium model and second law analysis of a downdraft waste gasifier," *Energy,* vol. 32, pp. 1660-1669, 2007.

[48] H. J. Huang and S. Ramaswamy, "Modeling Biomass Gasification Using Thermodynamic Equilibrium Approach," *Appl Biochem Biotechnol,* vol. 154, pp. 193–204, 2009.

[49] Z. A. Zainal, R. Ali, C. H. Lean, and K. N. Seetharamu, "Prediction of performance of a downdraft gasifier using equilibrium modeling for different biomass materials," *Energy Conversion and Management,* vol. 42, pp. 1499-1515, 2001.

[50] R.F. Probstein and R. E. Hicks, Synthetic Fuel. McGraw-Hill,New York, 1982.

[51] Y.A. Cengel and M. Boles, Thermodynamics: An engineering approach, McGraw-Hill,New York ,2002.

[52] D. M.L.Santos, "Solid fuels combustion and gasification: Modeling, simulation, and equipment operation". New York, Marcel Dekker, 2004.

[53] B. R. Martin, "Pyrolyisis and iginition behavior of coal ,cattle biomass, and coal/cattke biomass blends" Mater thesis,Texas A&M University, 2006.

[54] J. M. Sweeten, K. Heflin, K. Annamalai, B. W. Auvermann, F. T. McCollum, and D. B. Parker, "Combustion-fuel properties of manure or compost from paved vs. un-paved cattle feedlots," *ASBAE Annual International Meeting,* Portland, Oregon, 2006.

[55] W. H. Schlesinger, J. F. Reynolds, G. L. Cunningham, L. F. Huenneke, W. M. Jarrell, R. A. Virginia, and W. G. Whitford, "Biological Feedbacks in Global Desertification," *Science,* vol. 247, pp. 1043-1048, 1990.

[56] M. Abramovitz and I. Stegen, Handbook of mathermatical functions,Dover Publication, New York, 1974.

[57] D.B .Anthony, H.C. Howard, H.C. Hottel, and H.P. Meissner, "Rapid devolatilization of pulverized coal," *Symposium (International) on Combustion,* vol. 15, pp. 1303-1317, 1974.

[58] P. T. Williams and S. Besler, "The influence of temperature and heating rate on the pyrolysis of biomass," *Renewable Energy,* vol. 7, pp. 233-250, 1996.

[59] S. Patel, A. H. Vincent, S. R. Abel, C. M. Jacobs, S. R. Dunlop, and M. Seibert, "A Virtual Clean Room to Teach USP 797 Regulations for Intravenous Medications," *American Journal of Pharmaceutical Education,* vol. 75, 2011.

[60] C. I. Pearce, V. S. Coker, R. Cutting, R. A. D. Pattrick, J. R. Lloyd, and N. T. Prakash, "Bio-nano-engineering: From clean up to catalysis," *Geochimica Et Cosmochimica Acta,* vol. 72, pp. 730-730, 2008.

[61] M. J. Prins and K. J. Ptasinski, "Energy and exergy analyses of the oxidation and gasification of carbon," *Energy,* vol. 30, pp. 982-1002, 2005.

[62] C. Ngamcharussrivichai, W. Wiwatnimit, and S. Wangnoi, "Modified dolomites as catalysts for palm kernel oil transesterification," *Journal of Molecular Catalysis A-Chemical,* vol. 276, pp. 24-33, 17 2007.

[63] W Chen, K Annamalai, R. J Ansley, and M. Mirik, "Updraft fixed bed gasification of mesquite and juniper wood samples," *Energy & Fuels,* vol. 41, pp. 454-461, 2012.

[64] C. J. Roos, "Clean heat and power using biomass gasification for industrial and agricultural projects," *US DOE Report 2010,* 2010.

[65] T. M. Kegel, "Basic measurement uncertainty," *71st International School of Hydrocarbon Measurement,*Oklahoma City, OK. pp1-7, 1996.

APPENDIX A

Uncertainty Analysis

This analysis follows the example of Kegel[65] . The data of the temperature profile, equivalence ratio, and gas emission concentration would be analyzed for its uncertainty analysis. The temperature is measured using the thermocouples and thus thermocouples set the uncertainty interval. The equivalence ratio is the ratio of the stoichiometric air to provided air. All of the parameter are measured values and will have uncertainty. Gas emission concentration is tested using mass spectrometer and the measure values have some uncertainty. The mass spectrometer was calibrated using N_2 and mixture gas cylinder every 3 days of known composition for linearity, sensitivity and overlapping[8]. Table 23 and Table 24 give the gas uncertainty and temperature of the mesquite and juniper at ER=3.7 and moisture content 12%.

Table 23. Gas uncertainty analysis

	Juniper			Mesquite		
Gas	Maximum	Minimum	Average	Maximum	Minimum	Average
Carbon dioxide	24.9	0.422	8.1	11.62	0.141	3.15
carbon Monoxide	19.99	0.49	4.82	6.42	0.56	1.9
Hydrogen	15.2	0.31	5.26	6.82	0.19	3.81
Methane	20.91	0.11	6.31	22.5	0.61	6.74
Ethane	17.79	0.125	6.03	25.27	0.6	6.67
Nitrogen	13.37	0.1	3.42	3.1	0.141	1.44

Table 24. Uncertainty of mesquite (12 % moisture content) temperature profile at ER=3.7

	Mesquite			Juniper		
	Max	Min	average	Max	Min	average
2 cm above the grate	7.41	0.09	4.01	7.60	0.13	3.18
4 cm above the grate	5.16	0.07	2.43	2.64	0.01	1.33
7 cm above the grate	2.43	0.05	1.15	6.87	0.02	3.09
10 cm above the grate	2.36	0.02	1.03	11.00	0.08	4.47
13 cm above the grate	3.11	0.01	1.19	21.52	0.58	14.37
20 cm above the grate	26.78	0.14	5.58	23.51	1.36	22.97
24 cm above the grate	26.84	0.56	14.37	27.54	0.57	13.25
28 cm above the grate	15.77	0.42	2.48	25.15	0.55	16.15

Equivalence Ratio Uncertainty

Beginning with the definition of equivalence ratio:

$$\phi = \frac{A:F_{ST}}{A:F_{PROVIDED}} = \frac{\left(\frac{A}{F}\right)_{ST}}{\left(\frac{A}{F}\right)_{PROVIDED}} \tag{92}$$

Deleting the fuel flow rate because it is constant (1kg/h) for both A:F:

$$\phi = \frac{A_{ST}}{A_{PROVIDED}} \tag{93}$$

To determine the uncertainty, the partial derivative of equivalence ratio to each independent variable must be calculated:

$$\frac{\partial \phi}{\partial A_{ST}} = \frac{1}{A_{PROVIDED}} \tag{94}$$

$$\frac{\partial \phi}{\partial A_{PRO}} = -\frac{A_{ST}}{(A)^2_{PROVIDED}} \tag{95}$$

Table 25 presents the nominal values and pertinent uncertainty values for juniper sample calculation.

Table 25. Uncertainty of the ER for juniper fuel with moisture content of 12%

ER	2.7	3.2	3.7	4.2
Uncertainty	1.89	2.2	2.47	2.77

Table 26. Uncertainty of juniper at ER=2.7

Input Variable	Equivalence Ratio	Air Type	sxi=(δφ/δxi)*(xi/φ)	uxi	uxi*sxi	(uxi*sxi)2
X1	2.7	Primary Air, st	0.37037	0.00693	0.00257	6.586847E-06
X2	2.7	Air, pro	-1.00000	0.01871	-0.01871	3.500520E-04
					SUM	3.566389E-04
					Total (%)	1.89

Table 27. Uncertainty of juniper at ER=3.2

Input Variable	Equivalence Ratio	Air Type	sxi=(δφ/δxi)*(xi/φ)	uxi	uxi*sxi	(uxi*sxi)2
X1	3.2	Primary Air, st	0.31250	0.00684	0.00214	4.568402E-06
X2	3.2	Air, pro	-1.00000	0.02189	-0.02189	4.790317E-04
					SUM	4.836001E-04
					Total (%)	2.20

Table 28. Uncertainty of juniper at ER=3.7

Input Variable	Equivalence Ratio	Air Type	sxi=(δφ/δxi)*(xi/φ)	uxi	uxi*sxi	(uxi*sxi)2
X1	3.7	Primary Air, st	0.27027	0.00667	0.00180	3.250225E-06
X2	3.7	Air, pro	-1.00000	0.02468	-0.02468	6.091444E-04
					SUM	6.123946E-04
					Total (%)	2.47

Table 29.Uncertainty of juniper at ER=4.2

Input Variable	Equivalence Ratio	Air Type	sxi=(δφ/δxi)*(xi/φ)	uxi	uxi*sxi	(uxi*sxi)2
X1	4.2	Primary Air, st	0.23810	0.00658	0.00157	2.451434E-06
X2	4.2	Air, pro	-1.00000	0.02762	-0.02762	7.628118E-04
					SUM	7.652632E-04
					Total (%)	2.77

APPENDIX B

Principle of Operation for TGA

The TA Instruments Q600 thermogravimetric analyzer uses an accurate and highly reliable horizontal dual-balance mechanism that supports both DSC and TGA measurement. The sample balance monitors actual sample weight, while the reference balance is used to correct the TGA measurement for beam growth. The dual-beam design results in less drift compared to single-beam designs, improving accuracy and precision. During testing, the test sample is placed in an alumina sample pan, which in turn rests on the sample balance beam. A thin layer of alumina powder separates the sample pan from the thermocouples. A matched platinum/platinum rhodium thermocouple pair embedded in the ceramic beams provides sample, reference, and differential temperatures from ambient up to 1500 C. Temperatures are maintained by an ultra-reliable bifilar-wound furnace. The furnace is capable of heating rates up to 100 C/min, and software available for the Q600 allows the user to change the heating rate, hold at constant temperature, or any combination of the two. The Q600 also features a horizontal purge gas system with digital mass flow controllers and gas switching capability. Accurately metered gas flows through the furnace and directly across the sample and reference pans prior to exiting the analyzer. The exit port can also directly interface a mass spectrometer or FTIR [19].

APPENDIX C

Table 30. Juniper gas composition in the from the CEA model (%)

	Juniper			
	moisture content 6%			
CH_4	0.00	0.00	0.46	2.54
CO	10.76	16.05	19.94	20.81
CO_2	17.10	14.13	12.09	12.29
H_2	21.51	23.29	24.15	22.44
N_2	50.02	45.98	42.83	41.41
	moisture content 12%			
CH_4	0.00	1.30	1.30	3.47
CO	10.12	15.03	17.36	17.57
CO_2	17.97	15.25	14.38	15.08
H_2	24.14	26.00	25.90	24.10
N_2	47.20	43.19	40.66	39.29
	moisture content 24%			
CH_4	0	0	0.3	2.3
CO	7.6	10.23	10.4	11
CO_2	20.7	19.43	20	19.5
H_2	30.8	32	30.9	30.9
N_2	40	37.5	34.8	34.9

Table 31.Adiabatic temperature for juniper gasification

Moisture Content \ ER	2.7	3.2	3.7	4.2
6%	1382	1143	955	905
12%	1283	1048	920	887
24%	1081	936	898	868

Table 32. Mesquite gas composition in the from the CEA model (%)

Mesquite				
Gas composition	moisture content 6%			
CH_4	0	0	0.502	2.616
CO	10.428	15.769	19.566	20.363
CO_2	17.481	14.488	12.534	12.817
H_2	21.363	23.159	23.946	22.164
N_2	50.119	46.022	42.923	41.525
	moisture content 6%			
CH_4	0.00	0.02	1.21	3.45
CO	9.87	14.75	16.93	17.10
CO_2	18.30	15.62	14.85	15.59
H_2	24.03	25.88	25.71	23.91
N_2	47.23	43.22	40.80	39.46
	moisture content 24%			
CH_4	0	0	0	2.2
CO	6	6.5	6.9	7.06
CO_2	23	21.949	21.8	21
H_2	30	30.628	30.5	29.4
N_2	41	39	40.9	37.7

Table 33 Adiabatic temperature for mesquite gasification

Moisture \ ER	2.7	3.2	3.7	4.2
6%	1373	1135	950	902
12%	1275	1040	915	855
24%	957	874	856	841

Table 34. Mesquite gas composition at several S: F ratios

ER / Gas composition	2.70	3.20	3.70	4.20
		S:F=0.15		
CH_4	0.02	1.60	3.76	5.70
CO	7.37	8.50	8.20	7.40
CO_2	20.86	20.94	22.23	23.30
H_2	27.00	28.00	28.10	29.50
N_2	41.78	39.27	37.94	36.70
		S:f=0.3		
CH_4	0.00	1.47	4.20	4.78
CO	1.10	2.00	2.40	1.00
CO_2	25.31	25.83	26.80	28.21
H_2	32.00	33.88	33.90	34.00
N_2	39.01	39.33	35.08	33.52
		S:F=0.45		
CH_4	0.00	0.00	1.41	3.28
CO	0.00	0.00	0.00	0.00
CO_2	26.79	27.75	27.90	29.00
H_2	38.00	38.77	39.00	40.00
N_2	36.09	33.08	31.88	30.63

Table 35.Adiabatic temperature of the mesquite air-steam gasification

ER / S:F	2.7	3.2	3.7	4.2
0.15	985.15	871.59	843.79	824.43
0.30	911.50	806.30	769.04	726.90
0.45	764.64	724.80	616.70	603.20

Table 36. Gas composition for the juniper air steam gasification

Gas \ ER	2.7	3.2	3.7	4.2
S:F=0.15				
CH4	0.00	0.90	2.34	4.28
CO	8.96	12.02	11.95	11.55
CO2	18.00	18.40	19.04	20.01
H2	29.75	30.74	30.94	31.00
N2	41.10	37.50	36.29	34.96
S:F=0.3				
CH4	0	0.166	1.2	3.13
CO	2.68	5.75	5.9	5.17
CO2	22	22.86	23.22	24.5
H2	33.78	35.57	35.5	35.79
N2	38.78	35.27	33.73	31.97
S:F=0.45				
CH4	0	0	0	0
CO	0	0.3	1.2	0.8
CO2	26	26.84	26.64	27.48
H2	36.3	39.72	40.5	40.53
N2	36.65	32.77	30.8	29.17

Table 37. Adiabatic temperature of the juniper air-steam gasification

S:F \ ER	2.7	3.2	3.7	4.2
0.15	1093	913	883	863
0.3	1030	918	868	837
0.45	967	905	821	779